INVESTIGATING REPROGRAMMING FACTORS AND NEURAL CONDITIONS TO CONVERT HUMAN DENTAL PULP STEM CELLS INTO NEURAL STEM CELLS

Maria Roumenova Gancheva
BSc (Biomed), BHlthSc (Hons)

A thesis submitted to the University of Adelaide
For the degree of Doctor of Philosophy
December 2020



Discipline of Medicine
Adelaide Medical School
Faculty of Health and Medical Sciences
The University of Adelaide

TABLE OF CONTENTS

Declaration		VIII
Acknowledgments		IX
Abbreviations		XI
Publications		XIII
List of Figures		XIV
List of Tables		XVI
Abstract		XVII
CHAPTER 1: INTRODUCTION		1
1.1 Statement of Authorship		2
1.2 Review		3
1.3 Summary		20
1.3.1 Project Rationale		20
1.3.2 Hypothesis and Research Aims		20
CHAPTER 2: MATERIALS AND GENERAL METHODS		23
2.1 Reagents		24
2.2 General Methods		27
2.2.1 Cell Biology Techniques		27
2.2.1.1	Cell Culture	27
2.2.1.2	Cryopreservation and Thawing	28
2.2.1.3	Cell Counts: Trypan Blue Exclusion Assay	28
2.2.1.4	WST-1 Cell Proliferation Assay	28
2.2.1.5	Flow Cytometry	29
2.2.1.6	Fluorescence-Activated Cell Sorting	29
2.2.2 Molecular Biology Techniques		29
2.2.2.1	RNA Extraction	29
2.2.2.2	Reverse Transcription	30
2.2.2.3	Quantitative Polymerase Chain Reaction	30
2.2.2.4	Immunofluorescence Staining	31
2.2.2.5	Western Blot	32
	Protein Lysate Preparation	32
	Bradford Assay	32
	SDS-Polyacrylamide Gel Electrophoresis Gel Preparation	33
	SDS-PAGE	33
	Transfer	33

Staining 34
2.2.3 Cell Imaging 34
2.2.4 Statistical Analysis 34
CHAPTER 3: CHARACTERISATION OF HUMAN DENTAL PULP STEM CELLS 35
3.1 Introduction 36
3.2 Materials and Methods 37
3.2.1 Extraction of Human DPSC 37
3.2.2 Cell Surface Marker Staining 38
3.2.3 *In vitro* Cell Differentiation Assays 39
3.2.3.1 Osteogenic/odontogenic Differentiation and Alizarin Red S Staining 39
3.2.3.2 Chondrogenic Differentiation and DAPI/Saf-O Staining 40
3.2.3.3 Adipogenic Differentiation and Oil Red O Staining 41
3.2.3.4 Neurogenic Differentiation 42
(1) Method by Arthur et al. 2008 42
(2) Method by Kiraly et al. 2009 43
(3) Method by Gervois et al. 2015 43
3.2.4 Immunofluorescence Staining 44
3.3 Results 45
3.3.1 Human DPSC were plastic-adherent, grew as a monolayer and displayed a spindle-shaped morphology 45
3.3.2 Human DPSC had a high proliferation rate 46
3.3.3 Human DPSC expressed common MSC surface antigens 47
3.3.4 Human DPSC produced mineral under osteogenic/odontogenic differentiation conditions 51
3.3.5 Human DPSC differentiated into chondrocytes 52
3.3.6 Human DPSC differentiated into adipocytes 53
3.3.7 Human DPSC were able to differentiate into neuronal-like cells 56
3.4 Discussion 64
CHAPTER 4: CONSTRUCTION AND PREPARATION OF VIRAL VECTORS 70
4.1 Introduction 71
4.2 Materials and Methods 75
4.2.1 Cell Biology Techniques 75
4.2.1.1 Bacterial Culture 75
4.2.1.2 Making Chemically-competent Bacteria 75
4.2.2 Molecular Biology Techniques 76
4.2.2.1 Molecular Cloning 76

Heat-shock Transformation of Competent Bacteria 76
Plasmid Purification 76
Restriction Enzyme Digests 76
Agarose Gel Electrophoresis 76
Gel Extraction 77
Phosphatase Treatment 77
Ligation 77
Sanger Sequencing 77
4.2.2.2 Construction of Viral Vectors 78
Expression and Packaging Vectors 78
Construction of Retroviral Vectors 79
Construction of Lentiviral Vectors 79
4.2.2.3 Transfection 82
Viral Production 82
Retroviral Preparation 82
Lentiviral Preparation 82
4.2.2.4 Transduction 83
4.2.2.5 Lentiviral Titration 83
4.2.2.6 Quantitative PCR 84
4.2.2.7 Western Blot 84
4.3 Results 85
4.3.1 Base-line expression levels of OCT4, SOX2 and HES1 transcription factors in DPSC 85
4.3.2 HEK293T cells produced virus using the lentiviral system 86
4.3.3 The CMV promoter lentiviral vector was not silenced in human DPSC 88
4.3.4 Gene expression in HEK293T cells 91
4.3.5 Gene expression in human DPSC 93
4.4 Discussion 96
CHAPTER 5: NEURAL REPROGRAMMING OF HUMAN DENTAL PULP STEM CELLS 99
5.1 Introduction 100
5.2 Materials and Methods 101
5.2.1 Neural Reprogramming Methods 101
1) NSC Protocol 101
2) Multi-step Neural Induction Protocol 102
5.2.2 Neuronal Differentiation of Reprogrammed Human DPSC 104
5.2.3 Sphere Formation Assay 104

5.2.4 Surface antigen staining and FACS for CD146$^{-/+}$ DPSC 104
5.2.5 Quantitative PCR 105
5.2.6 Western Blot 105
5.2.7 Immunofluorescence Staining 106
5.2.8 Electrophysiology: Patch-clamping (Whole-cell Recording) 106
5.3 Results 107
5.3.1 Transduced human DPSC cultured using the NSC protocol 107
5.3.1.1 OCT4, SOX2, HES1 over-expressing DPSC cultured in standard DPSC conditions 107
5.3.1.2 OCT4 over-expressing DPSC cultured in NSC medium 111
5.3.1.3 OCT4 over-expression in DPSC 113
5.3.1.4 Changes in neural gene expression: effect of NSC medium 115
5.3.1.5 Changes in neural gene expression: effect of OCT4 over-expression 117
5.3.1.6 Protein expression supported gene expression 119
5.3.1.7 DPSC-OCT4 consisted of a greater number of stem/progenitor cells 121
5.3.1.8 Gene expression in monolayer versus suspension cultures 122
5.3.1.9 Neuronal differentiation following NSC protocol 126
5.3.2 Transduced human DPSC cultured using the multi-step neural induction protocol 130
5.3.2.1 DPSC morphology remained spindle-shaped throughout the multi-step neural induction protocol 130
5.3.2.2 DPSC displayed increased gene and protein expression of neural markers 132
5.3.2.3 Neural-induced DPSC differentiated along the neuronal lineage 136
5.3.2.4 OCT4 over-expressing DPSC underwent a morphological change 139
5.3.2.5 Transduced DPSC maintained their proliferation rate 142
5.3.2.6 OCT4 is over-expressed in DPSC throughout the multi-step neural induction protocol 146
5.3.2.7 Overall effect of genetic modification and neural inductive conditions 151
5.3.2.8 Effect of culture conditions: increased neural gene expression 155
5.3.2.9 Effect of lentiviral vector: increased *SOX1* and *SOX2* expression in neural conditions 159
5.3.2.10 Effect of OCT4: decreasing trend in *NEFM* 163
5.3.2.11 Protein expression confirmed gene expression 165
5.3.2.12 NANOG was not expressed under any conditions 168
5.3.2.13 DPSC-OCT4 formed more spheres than DPSC-EV 170
5.3.2.14 DPSC-OCT4 displayed enhanced neuronal differentiation capacity 172

5.3.2.15 Electrophysiology: preliminary patch-clamp analysis 181
5.3.2.16 CD146 DPSC sub-populations 183
5.4 Discussion 191
CHAPTER 6: TRANSCRIPTOMIC ANALYSIS OF OCT4 OVER-EXPRESSING, NEURAL-INDUCED HUMAN DENTAL PULP STEM CELLS 198
6.1 Introduction 199
6.2 Materials and Methods 199
6.2.1 Cells 199
6.2.2 RNA Extraction and Assessment 199
6.2.3 RNA-sequencing 199
6.2.4 Bioinformatics Analysis of RNA-sequencing Dataset 200
6.2.5 Functional Enrichment Analysis using GO and KEGG Pathway Databases 200
6.2.6 Quantitative PCR Validation 201
6.3 Results 202
6.3.1 Quantity and quality of RNA 202
6.3.2 RNA-sequencing 202
6.3.3 Alignment of sequencing reads 204
6.3.4 Sample groups displayed distinct transcriptional profiles 206
6.3.5 Differentially expressed genes 207
6.3.6 Quantitative PCR validation of RNA-sequencing data 210
6.3.7 Similarity with NSC 214
6.3.8 Functional enrichment analysis of the DEGs 216
6.4 Discussion 225
CHAPTER 7: RESPONSE OF OCT4 OVER-EXPRESSING, NEURAL-INDUCED HUMAN DENTAL PULP STEM CELLS IN A DEVEPMENTAL AVIAN MODEL 229
7.1 Introduction 230
7.2 Materials and Methods 233
7.2.1 DPSC Preparation 233
7.2.2 Chicken Embryo Staging and Preparation 233
7.2.3 Needle Preparation 234
7.2.4 DPSC Injections into Chicken Embryos 235
7.2.5 Removing the Tissue of Interest 235
7.2.6 Whole-mount Chicken Embryo Immunofluorescence Staining 236
7.2.7 Cell Imaging 237
7.2.8 Image Analysis 237

7.3 Results 240
7.3.1 Assay efficiency 240
7.3.2 Optimisation of immunofluorescence staining 243
7.3.3 Injected DPSC exhibited neuronal-like morphology and localised in the vicinity of established endogenous axonal processes 245
7.3.4 DPSC induced neuroplasticity 247
7.3.5 Survival of DPSC in chicken embryos 249
7.3.6 OCT4 over-expressing, neural-induced DPSC had greater expression of the neuronal marker β-III tubulin 250
7.4 Discussion 253
CHAPTER 8: GENERAL DISCUSSION AND CONCLUSION 257
8.1 Discussion 258
8.2 Recommendations for Future Work 263
8.2.1 *What is the mechanism that drives the change in transcriptional profile in OCT4 over-expressing, neural-induced human DPSC?* 263
8.2.2 *Do OCT4 over-expressing, neural-induced human DPSC differentiate into different types of neural cells in vivo?* 264
8.2.3 *Do OCT4 over-expressing, neural-induced human DPSC enhance functional recovery in a stroke model via cell replacement?* 264
8.3 Project Significance and Concluding Remarks 266
APPENDICES 267
A PRIMER DESIGN 268
B POSITIVE CONTROLS FOR ANTIBODIES 269
C HES1 VECTOR-TRANSDUCED HUMAN DENTAL PULP STEM CELLS 271
D RNA-SEQUENCING DATA ANALYSIS CODE 273
REFERENCES 282

DECLARATION

I certify that this work contains no material which has been accepted for the award of any other degree or diploma in my name, in any university or other tertiary institution and, to the best of my knowledge and belief, contains no material previously published or written by another person, except where due reference has been made in the text. In addition, I certify that no part of this work will, in the future, be used in a submission in my name, for any other degree or diploma in any university or other tertiary institution without the prior approval of the University of Adelaide and where applicable, any partner institution responsible for the joint-award of this degree.

I acknowledge that copyright of published works contained within this thesis resides with the copyright holder(s) of those works.

I also give permission for the digital version of my thesis to be made available on the web, via the University's digital research repository, the Library Search and also through web search engines, unless permission has been granted by the University to restrict access for a period of time.

I acknowledge the support I have received for my research through the provision of an Australian Government Research Training Program Scholarship.

I acknowledge the instruments and scientific and technical assistance of Microscopy Australia at Adelaide Microscopy, The University of Adelaide, a facility that is funded by the University, and State and Federal Governments.

Maria R. Gancheva

December 2020

ACKNOWLEDGMENTS

I have been supported by many people over the course of my PhD and I wish to duly acknowledge these individuals.

I would like to express my gratitude to my supervisors Professor Simon Koblar, Dr. Karlea Kremer, Professor Stan Gronthos and Professor Paul Thomas for their guidance, advice and support throughout this journey. This was a challenging but worthwhile experience, and I have not only developed skills that make me a better researcher but have also grown as a person. I count myself fortunate to have had a panel of supervisors that are experts in their field.

To my principle supervisor, Simon, thank you for giving me the opportunity to undertake my PhD studies on a topic that I was very passionate about, for helping me become a better researcher and pushing me outside of my comfort zone. To Karlea, thank you for not only being a wonderful supervisor and always being the first to read any draft, but also for your friendship and for always supporting me; I truly appreciate it. Stan, thank you for the dedication you have shown as my co-supervisor; your understanding, perspective, encouragement and counsel were most helpful and reassuring whenever I was feeling doubtful and overwhelmed. Paul, I am incredibly appreciative to have had you involved in my PhD. Thank you for your advice, ongoing encouragement and insightful ideas.

I would like to thank my fellow researchers, both past and present, at the Stroke Research Programme: Associate Professor Anne Hamilton-Bruce, Austin Milton, Dr. Fong Chan Choy, Dr. Anjali Nagpal, Dr. Joshua Winderlich, Associate Professor Erik Noschka, and Chelsea Graham; at the Mesenchymal Stem Cell Laboratory: Dr. Agnes Arthur, Sharon Paton, Dr. Dimitrios Cakouros, and Dr. Esther Camp-Dotlic; at the Gene Editing Laboratory: Dr. Stefka Tasheva; and at SAHMRI. Thank you all for your support and sharing your knowledge. Thank you to the SAHMRI and university students for their friendship; Chelsea, thanks for being my lab buddy, I'll miss our time together.

I would especially like to thank Agnes for her help, advice and guidance over the years; thank you for providing me with the knowledge and technical skills to perform the chicken embryo assay and for encouraging me when there were issues. I would also like to acknowledge the support and technical expertise provided by Mark van der Hoek for the RNA-sequencing, Dr. Jimmy Breen and Dr. Nader Aryamanesh for the bioinformatics analysis, Associate Professor Grigori Rychkov for the patch-clamp analysis, Dr. Randall Grose for training me on the flow cytometers, and Dr. Agatha Labrinidis from Adelaide Microscopy for training me to use the confocal microscope. Thank you all for your assistance.

To Anne, thank you for your support and encouragement, and for driving a long way to deliver my chicken eggs. Austin, thank you for always being supportive, and for doing last-minute editing of my thesis. Fong, thank you for your help in the early stage of my PhD. Thank you Sharon for always finding time when I needed something from the lab. I would also like to thank the Cell Signalling and Gene Regulation Group for their friendship and lending me lab reagents/equipment. Stef, thank you for your advice, lab help, positivity, friendship and coffee catch-ups; I'm grateful for our surprising encounter.

I would like to extend my gratitude to others from SAHMRI (Dr. Cedric Bardy, Dr. Mark van den Hurk, Julian Carosi, Kathryn Hattersley, Dr. Mari Ichinose), and our local (Dr. Mary-Louise Rogers) and interstate (Associate Professor Mirella Dottori and Rachael Chatterton) collaborators for providing me with cells and samples for my project. Thank you Dr. Paul Sambrook, it was a pleasure to collaborate with you. Thank you also to the post-graduate coordinators, Associate Professor Leonie Heilbronn and Professor Amanda Page, for their advice.

Last but definitely not least, I would like to thank my family and friends for their encouragement and understanding, and for always being there when I needed to complain. I would particularly like to thank my parents, sister and Roman, for their love, support and always believing in me. Thank you to my parents for their guidance and support throughout all my years. You instilled in me a desire to learn and achieve from a young age, and you built a foundation from which I have been provided many opportunities. Desi, thank you for being a supportive big sister, always proof-reading my 'science-y' things even when you didn't have time, and showing a genuine interest in my research; I'm proud of you for being able to explain it. Roman, thank you for making me happy and keeping me sane; navigating this PhD journey together has made it more memorable. Thank you for supporting me both in the lab with the science and outside the lab, reminding me to take a break and have fun.

Thank you everyone!

ABBREVIATIONS

αMEM	α-modification Eagle's Minimal Essential Medium
bFGF	Basic Fibroblast Growth Factor
bHLH	Basic Helix-Loop-Helix
BME	β-mercaptoethanol
BSA	Bovine Serum Albumin
cDNA	Complementary DNA
CMV	Cytomegalovirus
CNS	Central Nervous System
DAPI	4′,6-diamidino-2-phenylindole
dbcAMP	Dibutyryl Cyclic Adenosine Monophosphate
DEG	Differentially Expressed Gene
DMEM	Dulbecco's Modified Eagle Medium
DNA	Deoxyribonucleic Acid
DPSC	Dental Pulp Stem Cells
EDTA	Ethylenediaminetetraacetic Acid
EF-1α	Elongation Factor-1α
EGF	Epidermal Growth Factor
ESC	Embryonic Stem Cells
EV	Empty Vector
F12	Ham's F12 Nutrient Mixture
FACS	Fluorescence-Activated Cell Sorting
FBS	Foetal Bovine Serum
FDR	False Discovery Rate
GFAP	Glial Fibrillary Acidic Protein
GFP	Green Fluorescent Protein
GO	Gene Ontology
HEK293T	Human Embryonic Kidney 293T
HEPES	4-(2-hydroxyethyl)-1-piperazineethanesulfonic acid
HES1	Hairy and Enhancer of Split transcription factor-1
HIV	Human Immunodeficiency Virus
iPSC	Induced Pluripotent Stem Cells
IRES	Internal Ribosome Entry Site
KEGG	Kyoto Encyclopedia of Genes and Genomes
logFC	Log Fold Change
LTR	Long Terminal Repeat
MCS	Multiple Cloning Site

MEM	Minimum Essential Medium
MFI	Mean Fluorescence Intensity
MSC	Mesenchymal Stem/Stromal Cells
NF-M	Neurofilament-medium poly-peptide
NGFR	Nerve Growth Factor Receptor
NSC	Neural Stem Cells
OCT4	Octamer-binding transcription factor 4
PBS	Phosphate Buffered Saline
PLP	Proteolipid Protein
qPCR	Quantitative Polymerase Chain Reaction
RNA	Ribonucleic Acid
RT	Room Temperature
Saf-O	Safranin-O
SD	Standard Deviation
SDS	Sodium Dodecyl Sulfate
sGAG	Sulphated Glycosaminoglycan
SOX2	SRY (sex determining region Y)-box 2 transcription factor
VSV-G	Vesicular Stomatitis Virus-Glycoprotein

PUBLICATIONS

Gancheva, M. R., Kremer, K. L., Gronthos, S. and Koblar, S. A. (2019) Using Dental Pulp Stem Cells for Stroke Therapy. Frontiers in Neurology. 10:422. doi:10.3389/fneur.2019.00422.

LIST OF FIGURES

Figure 1.1 Stem cell lineage and reprogramming 5
Figure 1.2 Tooth anatomy and dental pulp stem cells 7
Figure 1.3 Sources of neural stem cells for transplantation in the stroke-affected brain and mechanisms of action 12
Figure 3.1 Human DPSC adhered to plastic and grew as a cell monolayer with a spindle-shaped morphology 45
Figure 3.2 Human DPSC proliferation *in vitro* 46
Figure 3.3 Expression of selected surface markers on human DPSC 48
Figure 3.4 Osteogenic/odontogenic differentiation of human DPSC 51
Figure 3.5 Chondrogenic differentiation of human DPSC 52
Figure 3.6 Adipogenic differentiation of human DPSC using adipogenic induction medium 1 53
Figure 3.7 Adipogenic differentiation of human DPSC using adipogenic induction medium 2 54
Figure 3.8 Adipogenic differentiation of human DPSC using adipogenic induction medium 3 55
Figure 3.9 Neurogenic differentiation of human DPSC using the method by Arthur *et al*. 2008 56
Figure 3.10 Neurogenic differentiation of human DPSC using the method by Kiraly *et al*. 2009 58
Figure 3.11 Neurogenic differentiation of human DPSC using the method by Gervois *et al*. 2015 60
Figure 3.12 Neurogenic differentiation of human DPSC 62
Figure 4.1 Transfer vectors 80
Figure 4.2 Expression levels of transcription factors selected for reprogramming, in human DPSC 85
Figure 4.3 Virus production in HEK293T cells 87
Figure 4.4 Human DPSC transduced by lentiviral vectors with different promoters 89
Figure 4.5 Viral titration 92
Figure 4.6 Transduction of human DPSC 94
Figure 5.1 Neural reprogramming methods 103
Figure 5.2 NSC protocol: single lentiviral transductions of DPSC 109
Figure 5.3 NSC protocol: proliferation rate of transduced DPSC 110
Figure 5.4 Transduced DPSC in NSC culture medium 112
Figure 5.5 NSC protocol: OCT4 over-expression in DPSC-OCT4 114
Figure 5.6 NSC protocol: effect of the NSC culture medium 116
Figure 5.7 NSC protocol: effect of OCT4 over-expression 118
Figure 5.8 NSC protocol: protein expression 120
Figure 5.9 NSC protocol: sphere formation 121
Figure 5.10 Comparison of monolayer and suspension cultures in NSC medium: effect of culture type 123
Figure 5.11 Comparison of monolayer and suspension cultures in NSC medium: effect of medium 124
Figure 5.12 Comparison of monolayer and suspension cultures in NSC medium: effect of OCT4 over-expression 125
Figure 5.13. NSC protocol: neuronal protein expression following neuronal differentiation 127
Figure 5.14 DPSC cultured using the multi-step neural induction protocol 131

Figure 5.15 Gene expression in DPSC cultured using the multi-step neural induction protocol 134
Figure 5.16 Protein expression in DPSC 135
Figure 5.17 Neuronal differentiation of DPSC cultured using the multi-step neural induction protocol 137
Figure 5.18 Multi-step neural induction protocol: single lentiviral transductions of DPSC 140
Figure 5.19 Multi-step neural induction protocol: proliferation rate of transduced DPSC 143
Figure 5.20 Multi-step neural induction protocol: OCT4 over-expression in DPSC-OCT4 147
Figure 5.21 Gene expression levels in DPSC-EV and DPSC-OCT4 cultured using the multi-step neural induction protocol 152
Figure 5.22 Multi-step neural induction protocol: effect of neural conditions 156
Figure 5.23 Multi-step neural induction protocol: effect of lentiviral vectors 160
Figure 5.24 Multi-step neural induction protocol: effect of OCT4 over-expression 164
Figure 5.25 Multi-step neural induction protocol: protein expression 166
Figure 5.26 NANOG detection in DPSC 169
Figure 5.27 Multi-step neural induction protocol: sphere formation 171
Figure 5.28 Multi-step neural induction protocol: terminal differentiation of reprogrammed DPSC 174
Figure 5.29 Multi-step neural induction protocol: protein expression following terminal differentiation 176
Figure 5.30 Membrane currents recorded in reprogrammed DPSC 182
Figure 5.31 $CD146^{-/+}$ DPSC sub-populations 185
Figure 6.1 Sample similarity 206
Figure 6.2 Hierarchical clustering heat map of all DEGs between samples and groups 208
Figure 6.3 Volcano plots of significant DEGs 209
Figure 6.4 Validation of selected genes 212
Figure 6.5 Gene expression levels in DPSC and NSC 215
Figure 6.6 Network diagram of enriched KEGG pathways by up-regulated DEGs in DPSC-OCT4 relative to DPSC 220
Figure 6.7 Genes involved in the neurotrophin signalling pathway 222
Figure 6.8 Genes involved in the notch signalling pathway 222
Figure 6.9 Genes involved in axon guidance 223
Figure 6.10 Genes involved in gated channel activity 224
Figure 7.1 Chicken embryo assay workflow 238
Figure 7.2 Chicken embryo assay efficiency 241
Figure 7.3 Whole-mount chicken embryo tissues stained for GFP and neuronal markers 244
Figure 7.4 DPSC transplanted into the chicken embryo localised with established axonal processes and displayed neuronal-like morphologies 246
Figure 7.5 DPSC transplanted into the chicken embryo induced neuroplasticity 248
Figure 7.6 DPSC survival in chicken embryos 249
Figure 7.7 Double-stained DPSC in chicken embryos 251
Figure 7.8 Mean intensity of β-III tubulin staining 252
Figure B Positive controls for antibodies used in protein expression analysis 270
Figure C HES1 over-expression in DPSC 272

LIST OF TABLES

Table 1.1 Neuronal induction protocols for human dental pulp stem cells with functional assessment 9
Table 1.2 Human dental pulp stem cells in stroke models 10
Table 2.1 Reagent list 24
Table 2.2 Standard DPSC culture medium 27
Table 2.3 Standard thermal cycling conditions for Power SYBR Green mastermix 31
Table 2.4 Fast thermal cycling conditions for PowerUp SYBR Green mastermix 31
Table 2.5 Components for 12.5% acrylamide gels for middle-sized proteins 33
Table 3.1 Antibodies used for human DPSC surface marker analysis by flow cytometry 38
Table 3.2 Osteogenic/odontogenic induction medium 39
Table 3.3 Chondrocyte induction medium 40
Table 3.4 Adipogenic induction media 41
Table 3.5 Neuronal differentiation media for the method by Arthur *et al*. 2008 42
Table 3.6 Neuronal differentiation media for the method by Kiraly *et al*. 2009 43
Table 3.7 Neuronal differentiation media for the method by Gervois *et al*. 2015 43
Table 3.8 Antibodies for immunofluorescence staining 44
Table 4.1 Sequencing primers 77
Table 4.2 Mammalian expression vectors 78
Table 4.3 Packaging plasmids 78
Table 4.4 Transfer constructs 82
Table 4.5 Primers for qPCR 84
Table 4.6 Antibodies for Western blots 84
Table 5.1 NSC protocol 101
Table 5.2 Multi-step neural induction protocol 102
Table 5.3 Media for neuronal, astroglial and oligodendroglial differentiation 104
Table 5.4 Primers for qPCR 105
Table 5.5 Antibodies for Western blots 105
Table 5.6 Antibodies for immunofluorescence staining 106
Table 5.7 Summary of NSC protocol results 129
Table 5.8 Summary of multi-step neural induction protocol results for non-transduced DPSC 138
Table 5.9 Summary of multi-step neural induction protocol results for transduced DPSC 190
Table 6.1 Primers for qPCR 201
Table 6.2 Raw reads for each sample 203
Table 6.3 Mapped reads for each sample 205
Table 6.4 DEGs between the three groups 207
Table 6.5 Genes selected for qPCR validation 211
Table 6.6 GO annotations of DEGs in DPSC-EV relative to DPSC 217
Table 6.7 GO annotations of DEGs in DPSC-OCT4 relative to DPSC 218
Table 6.8 GO annotations of DEGs in DPSC-OCT4 relative to DPSC-EV 219
Table 7.1 Antibodies for whole-mount immunofluorescence staining 236
Table A Parameters for primer design 268

ABSTRACT

Human dental pulp stem cells (DPSC), harvested from the pulp tissue of molar teeth, are a heterogeneous population of multipotent adult stem cells that possess neurogenic potential. They exert positive effects in the injured and diseased brain via multiple molecular and cellular mechanisms, and are potential candidates for cell-based therapies for treatment of neurological diseases, including stroke. Previous research of human DPSC in a stroke model demonstrated their ability to improve neurobehavioural function, which was mediated by paracrine effects but not cell replacement. In the adult brain, there are neurogenic niches in which reside neural stem cells (NSC). These NSC have a role in repairing the brain, however their capacity is limited under harsh conditions. Cellular reprogramming has been used to convert more accessible cell types, such as fibroblasts, into NSC for potential therapeutic use. Induced NSC have demonstrated positive outcomes in stroke models. DPSC may be a suitable cell type from which to obtain NSC, due to their neural crest origin. This may enhance their neurogenic capacity, including their ability to replace lost neural cells. The aim of this thesis was to investigate the ability to reprogram human DPSC into NSC.

Multiple transcription factors were selected for reprogramming and over-expressed via lentiviral transduction. Cells were cultured in neural conditions, and analysed for expression of neural markers and stem cell properties (self-renewal and multi-lineage differentiation). RNA-sequencing was performed to investigate the transcriptome-wide effects of reprogramming, and used to examine differentially expressed genes. *In vivo* analysis was performed in a developmental avian model to examine the ability of the cells to respond to endogenous signals and differentiate.

DPSC over-expressing the transcription factor OCT4 when cultured using a multi-step neural inductive protocol, underwent morphological changes, displaying a neural-like phenotype. They showed increased expression levels of neural markers in response to the environmental conditions and decreased levels of the mature neuronal marker in response to the transcription factor, suggesting that the cells were directed to an early neural state. The reprogrammed cells had a greater capacity for sphere formation, which indicated a greater number of stem cells present. They also displayed enhanced neuronal differentiation but not glial differentiation. Transcriptomic analysis showed significant differences to the controls, with an increased expression in genes associated with neural and neuronal function and components, and similarities with NSC. *In vivo* analysis showed the cells' ability to survive in the developing

central nervous system, localising to established endogenous axonal processes and differentiating into neuronal-like cells, as well as their capacity to induce neuroplasticity.

These results suggest that DPSC may be reprogrammed along the neural lineage. Enhanced neural properties were observed in the OCT4 over-expressing, neural induced human DPSC, with data suggesting they resemble neuronal progenitor cells. Future research with these cells will aim to examine their response in a stroke model, to determine if they enhance functional recovery and whether cell replacement is a mechanism of action. An efficient and reliable reprogramming method could provide an alternative source of NSC for use in cell-based therapies for neurological diseases.

CHAPTER 1

INTRODUCTION

1.1 | Statement of Authorship

Title of Paper	Using Dental Pulp Stem Cells for Stroke Therapy
Publication Status	☑ Published ☐ Accepted for Publication ☐ Submitted for Publication ☐ Unpublished and Unsubmitted work written in manuscript style
Publication Details	Gancheva, M.R., Kremer, K.L., Gronthos, S., Koblar, S.A. (2019) Using Dental Pulp Stem Cells for Stroke Therapy. Frontiers in Neurology 10: 422. *doi: 10.3389/fneur.2019.00422.*

Principal Author

Name of Principal Author (Candidate)	Maria Gancheva		
Contribution to the Paper	Conception and design, research, manuscript writing and preparation, editing.		
Overall percentage (%)	80		
Certification	This paper reports on original research I conducted during the period of my Higher Degree by Research candidature and is not subject to any obligations or contractual agreements with a third party that would constrain its inclusion in this thesis. I am the primary author of this paper.		
Signature		Date	21/11/2020

Co-Author Contributions

By signing the Statement of Authorship, each author certifies that:

i. the candidate's stated contribution to the publication is accurate (as detailed above);
ii. permission is granted for the candidate to include the publication in the thesis; and
iii. the sum of all co-author contributions is equal to 100% less the candidate's stated contribution.

Name of Co-Author	Karlea Kremer		
Contribution to the Paper	Critical revision of manuscript.		
Signature		Date	30/11/2020

Name of Co-Author	Stan Gronthos		
Contribution to the Paper	Critical revision of manuscript.		
Signature		Date	30/11/2020

Name of Co-Author	Simon Koblar		
Contribution to the Paper	Conception, supervision, revision and final approval of manuscript, funding.		
Signature		Date	29/11/20

frontiers in Neurology

REVIEW
published: 29 April 2019
doi: 10.3389/fneur.2019.00422

Using Dental Pulp Stem Cells for Stroke Therapy

Maria R. Gancheva[1*], *Karlea L. Kremer*[1], *Stan Gronthos*[2,3] *and Simon A. Koblar*[1,3,4]

[1] *Stroke Research Programme Laboratory, Adelaide Medical School, Faculty of Health and Medical Sciences, University of Adelaide, Adelaide, SA, Australia,* [2] *Mesenchymal Stem Cell Laboratory, Adelaide Medical School, Faculty of Health and Medical Sciences, University of Adelaide, Adelaide, SA, Australia,* [3] *South Australian Health and Medical Research Institute, Adelaide, SA, Australia,* [4] *Central Adelaide Local Health Network, Adelaide, SA, Australia*

Stroke is a leading cause of permanent disability world-wide, but aside from rehabilitation, there is currently no clinically-proven pharmaceutical or biological agent to improve neurological disability. Cell-based therapies using stem cells, such as dental pulp stem cells, are a promising alternative for treatment of neurological diseases, including stroke. The ischaemic environment in stroke affects multiple cell populations, thus stem cells, which act through cellular and molecular mechanisms, are promising candidates. The most common stem cell population studied in the neurological setting has been mesenchymal stem cells due to their accessibility. However, it is believed that neural stem cells, the resident stem cell of the adult brain, would be most appropriate for brain repair. Using reprogramming strategies, alternative sources of neural stem and progenitor cells have been explored. We postulate that a cell of closer origin to the neural lineage would be a promising candidate for reprogramming and modification towards a neural stem or progenitor cell. One such candidate population is dental pulp stem cells, which reside in the root canal of teeth. This review will focus on the neural potential of dental pulp stem cells and their investigations in the stroke setting to date, and include an overview on the use of different sources of neural stem cells in preclinical studies and clinical trials of stroke.

Keywords: cell-based therapy, ischaemic stroke, dental pulp stem cells, neural stem cells, multipotent, reprogramming, differentiation, neural crest

OPEN ACCESS

Edited by:
Andrew N. Clarkson,
University of Otago, New Zealand

Reviewed by:
Henry Ma,
Monash University, Australia
Bronwen Connor,
The University of Auckland, New Zealand

***Correspondence:**
Maria R. Gancheva
maria.gancheva@adelaide.edu.au

Specialty section:
This article was submitted to Stroke, a section of the journal Frontiers in Neurology

Received: *20 December 2018*
Accepted: *08 April 2019*
Published: *29 April 2019*

Citation:
Gancheva MR, Kremer KL, Gronthos S and Koblar SA (2019) Using Dental Pulp Stem Cells for Stroke Therapy. Front. Neurol. 10:422. doi: 10.3389/fneur.2019.00422

INTRODUCTION

The central nervous system (CNS) functions through complex molecular and cellular interactions, and disruption by severe injury or disease leads to irreversible neuronal loss and associated functional deficits. This results in highly debilitating pathologies associated with significant health and economic burden for patients, their families, carers, and the health systems.

Stroke is a global health care problem and a leading cause of acquired adult neurological disability (1). With an aging population, the incidence and prevalence of stroke is predicted to rise. A stroke is characterised by reduced and insufficient blood supply to part of the brain. Inadequate oxygen and nutrients lead to tissue infarction, resulting in disability due to loss-of-function associated with the damaged area of the brain.

Abbreviations: BBB, blood-brain barrier; bFGF, basic fibroblast growth factor; BMSC, bone marrow stromal/stem cell(s); CNS, central nervous system; DPSC, dental pulp stem cell(s); EGF, epidermal growth factor; ESC, embryonic stem cell(s); MSC, mesenchymal stem cell(s); NSC, neural stem cell(s); OCT4, octamer-binding transcription factor 4; PSC, pluripotent stem cell(s); SDF1α, stromal cell-derived factor 1-alpha; SOX2, SRY (sex determining region Y)-box 2; VEGF, vascular endothelial growth factor.

There are two main types of stroke; haemorrhagic and ischaemic. Haemorrhagic strokes, accounting for 13 percent of strokes (1), result from bleeding when a blood vessel is ruptured. Ischaemic stroke is the most common presentation of stroke at 87 percent of all cases (1), and is due to an obstruction in the blood supply, which could be formed locally (thrombosis) or formed elsewhere in the body (embolism).

During an ischaemic stroke, a complex chain of events takes place at the molecular and cellular levels, which results in cell necrosis at the site of the vascular insult (the ischaemic core), while the region surrounding the core (the ischaemic penumbra) remains viable for some time due to collateral blood supply and can thus be salvaged. A strong inflammatory response is initiated within hours of stroke onset, characterised by reactive astrogliosis, microglial activation, disruption to the blood-brain barrier (BBB), and infiltration of neutrophils and monocytes/macrophages (2). Growth factors and inflammatory mediators, from local glial and inflammatory cells, alter the reaction of endogenous neural stem and progenitor cells. Over time, reorganisation of the neural network around the core takes place. If untreated, the penumbra will transform into ischaemic tissue, expanding the irreversibly damaged area of brain. There is an opportunity to save the penumbral tissue via acute recanalisation therapies.

The currently available therapeutic interventions, such as thrombectomy and thrombolysis, are limited to a narrow therapeutic window and eligibility criteria, and though they have a significant impact on stroke outcome, disability remains after any intervention. Thrombectomy refers to the mechanical removal of a blood clot, which has been effective when performed within 24 h post-stroke (3). The more common intervention is thrombolysis by intravenously administered recombinant tissue plasminogen activator, to breakdown the clot. This is currently the only approved pharmacological agent that shows significant benefits in acute ischaemic stroke, but is only applicable within a short time frame of 4.5 h from symptomatic onset (4). Unfortunately, many patients are ineligible for these reperfusion therapies. In addition, poor patient outcomes can still be observed. Once a stroke patient is stabilised, rehabilitation interventions are relied upon to promote neuroplasticity, as patients adapt to residual disability. Improvements are most significant in the first several months following a stroke (5). There is currently no therapy that can restore damaged neural tissue and its associated functions.

Cell-based therapies have the potential to promote functional recovery in patients affected by stroke and other neurological diseases. Stem cells are promising candidates, as they can act through multiple cellular and molecular mechanisms to provide support for endogenous cells, stimulate endogenous processes, and act as a source of cell replacement. Neural stem cells (NSC), which reside in specific areas of the CNS, are the most appropriate stem cells for brain repair. Research is focused on two therapeutic paradigms; enhancing and manipulating endogenous NSC, and implanting exogenous NSC. Reprogramming strategies are being applied to develop NSC from more easily accessible and abundant cell types (6). Dental pulp stem cells (DPSC) are adult stem cells obtained from the dental pulp tissue in the tooth chamber (7). These cells are easily sourced and have neurogenic potential. They are being investigated as an alternative source of neural cells and in preclinical models of neurological diseases, including stroke. This review will focus on the potential use of human DPSC for stroke therapy and will include an overview of different types of NSC being studied.

TYPES OF STEM CELLS

Stem cells are unique cells that have the ability to differentiate into a variety of cell types while maintaining the pool of unspecialised stem cells through their self-renewal capacity. They can be classified based on their differentiation potential. Totipotent stem cells can give rise to all the cells needed for embryonic development including the extra-embryonic tissues, while pluripotent stem cells are able to differentiate into cells of all three germinal lineages (ectoderm, mesoderm, endoderm) and hence any cell of the body (**Figure 1**). Multipotent stem cells are more restricted as they can differentiate into the cells of the tissue they reside in, whereas unipotent stem cells maintain the population of one cell type within their tissue. There are two broad types of stem cells; pluripotent embryonic stem cells and multipotent post-natal adult or somatic stem cells.

Embryonic stem cells (ESC) are derived from the early embryo, more specifically the inner cell mass of the blastocyst (**Figure 1**). They were first isolated from the mouse blastocyst in the 1980s (8, 9), then from human embryos in 1998 (10). They can be propagated indefinitely and are cultured as embryoid bodies or as a monolayer using feeder layers. Due to their pluripotent nature, ESC give rise to teratomas *in vivo*, which are tumours derived from multiple germ layers and consist of a mixture of differentiated cells (11). By applying specific molecules, ESC can be induced along the neural lineage, making them safer for transplantation (11, 12). However, ESC-derived cells are subject to ethical controversy as culturing ESC involves the destruction of embryos.

Adult stem cells are found in tissues throughout the developed body where they function to maintain homeostasis and repair by giving rise to tissue-specific specialised cells. Examples of multipotent adult stem cells are bone marrow-derived mesenchymal stem or stromal cells (BMSC) and haematopoietic stem cells. Adult stem cells are not subjected to the same ethical considerations as ESC, nor do they possess the same tumorigenic potential. They also allow for autologous cell therapy, to prevent immunocompatibility issues.

It was believed that lineage specification and terminal differentiation into specialised cells was an irreversible process. However, this classic notion that cellular identity is stable has been challenged in the past few decades by evidence of nuclear transfer, dedifferentiation, epigenetic modifications, and ectopic gene expression, suggesting that cells are plastic (13). We now know that somatic cells, such as fibroblasts, can be genetically reprogrammed to stem cells that resemble ESC, termed induced pluripotent stem cells (induced PSC) (14, 15) (**Figure 1**). Breakthrough research conducted by Yamanaka and colleagues more than a decade ago, demonstrated the underlying molecular mechanism permitting this plasticity (14, 15). Yamanaka's reprogramming method involves the use of specific transcription factors that activate/deactivate genes and modify signalling

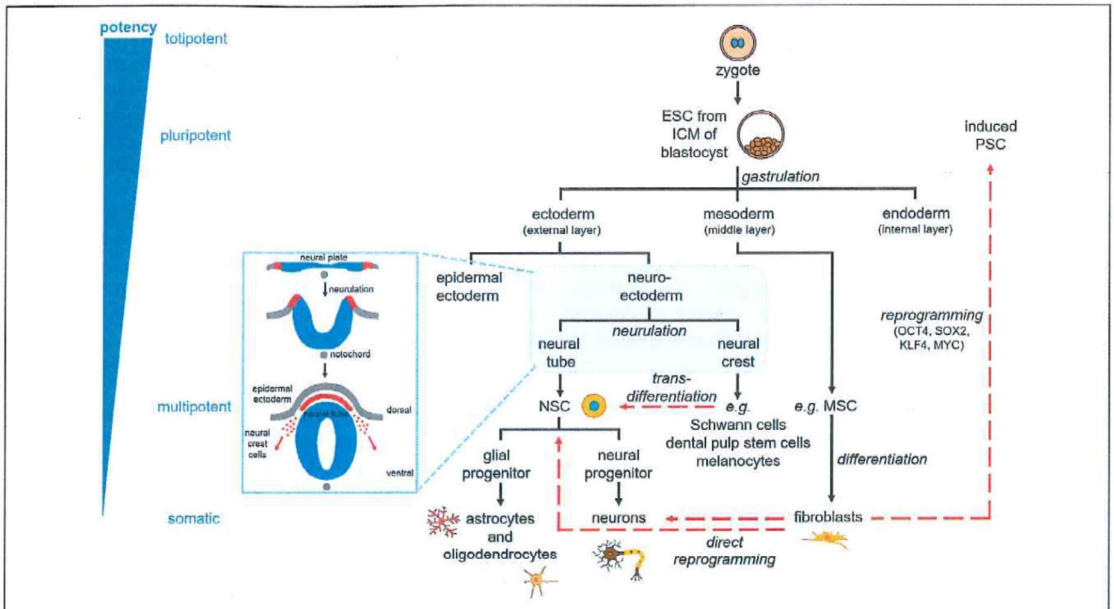

FIGURE 1 | Stem cell lineage and reprogramming. Pluripotent embryonic stem cells (ESC) are derived from the inner cell mass (ICM) of the blastocyst. The three germinal layers (ectoderm, mesoderm, endoderm) are specified through the process of gastrulation. The ectoderm gives rise to the skin and nervous system; the mesoderm gives rise to muscle, bone, blood, and fat; the endoderm gives rise to the respiratory, gastrointestinal, and urogenital tracts. The ectoderm consists of epidermal ectoderm forming the skin, and neuroectoderm, which forms the neural plate and undergoes neurulation to form the neural tube and neural crest cells. The neural tube gives rise to the central nervous system via neural stem cells (NSC), which give rise to neural and glial progenitors, and subsequently neurons, astrocytes, and oligodendrocytes. The neural crest cells migrate and contribute to tissues throughout the body, including the peripheral nervous system (e.g., Schwann cells), ectomesenchymal tissues of the head (e.g., dental pulp stem cells), and the pigmented cells of the skin known as melanocytes. Somatic cells, such as fibroblasts, can be reprogrammed to induced pluripotent stem cells (PSC) through the ectopic expression of four specific transcription factors. These cells can then be differentiated similar to ESC. Somatic cells can also be directly reprogrammed into neurons and NSC. Transdifferentiation is direct reprogramming of cells within the same germinal lineage, such as dental pulp stem cells into neural cells.

pathways. In this case, the transcription factors used consist of the pluripotency-associated factors; octamer-binding transcription factor 4 (OCT4), SRY (sex determining region Y)-box 2 (SOX2), KLF4, and MYC. These induced PSC resemble ESC with respect to their morphology, growth properties, gene/protein expression profiles, differentiation potential, teratoma formation *in vivo*, and potential to generate chimeras when injected into blastocysts to demonstrate germline transmission (14, 15). Induced PSC present a cell population with the same level of pluripotency as ESC but circumvent ethical issues, while also providing a source of cells for autologous cell therapies like adult stem cells. However, induced PSC too have a greater risk of tumorigenesis, thus giving adult stem cells, despite their more limited potential, an advantage in terms of safety and timing to the market. Nevertheless, this breakthrough technology has expanded the stem cell research field and helped enhance the progress of cell therapies by providing a cell source with unlimited proliferation and differentiation potentials, and more importantly, a strategy for manipulating cells across all cell lineages.

Within a few years of discovery, the focus on cellular reprogramming turned to a direct strategy. The concept was to bypass the pluripotent state and reprogram cells directly to the desired cell type, thus providing an accelerated reprogramming pathway with a biologically safer product. This direct reprogramming pathway is sometimes referred to as transdifferentiation. In theory, transdifferentiation occurs within the same germinal lineage (**Figure 1**) (13), thereby requiring fewer epigenetic modifications and decreasing the risk of accumulating mutations and leading to tumorigenesis. Nevertheless, some studies have claimed that inter-lineage transdifferentiation is possible via various transient intermediates (16). Direct strategies therefore increase safety and efficiency, and result in terminally differentiated cells or multipotent stem/progenitor cells with limited proliferation and differentiation capacity (**Figure 1**). This strategy has been applied to different cell sources to induce cells along the neural lineage (6, 13).

NEURAL STEM CELLS

The CNS has an inherent, albeit limited capacity for repair. Neural stem cells, capable of self-renewal and differentiation

into neurons, astrocytes, and oligodendrocytes, reside in specific regions called neurogenic niches. The formation of the CNS is a series of complex developmental processes initiated early in embryonic development, following the specification of the three germ layers, the ectoderm, mesoderm and endoderm. The neuroectoderm is induced by the underlying mesoderm, through the inhibition of signals that specify epidermal ectoderm. Neurulation is then initiated when the neural plate folds in to form the neural tube, which is composed of neuroepithelial cells (**Figure 1**). These cells give rise to bipolar NSC called radial glia, which initially span the neural tube, multiply and act as scaffolds for migrating cells. They give rise to cells that respond to gradients of morphogens and mitogens, resulting in the patterning of the neural tube and ultimately giving rise to all the neurons and glia of the CNS (17).

The adult mammalian brain has two main neurogenic niches that contain NSC; the sub-ventricular zone of the lateral ventricles and the sub-granular layer of the dentate gyrus in the hippocampus (17). Neural stem cells give rise to intermediate glial and neural progenitors. Subsequently neuroblasts arise from neural progenitors, and migrate and differentiate into various neuronal sub-types that may integrate within the existing network. Under normal physiological conditions, neuroblasts in the sub-ventricular zone migrate to the olfactory bulb via the rostral migratory stream after which they migrate radially and differentiate into interneurons (granule cells and periglomerular cells), while those in the sub-granular layer migrate into the inner granule cell layer and differentiate into granule cells (17). Adult neurogenesis has been proposed to be involved in maintenance and repair of the neural network, memory formation, and olfaction (17).

Neural stem cells are mostly quiescent under normal physiological conditions but are induced to proliferate and migrate to the affected site in response to injury and disease, such as stroke (17). It has been shown that stroke induction stimulates NSC proliferation and neuroblasts are recruited to the ischaemic striatum (18, 19). This migratory response is mediated by molecules, such as the chemokine stromal cell-derived factor 1-alpha (SDF1α), secreted by glial, immune and endothelial cells (20–22). However, due to the hostile microenvironment, cell survival is low, thereby limiting the intrinsic repair potential (17).

Neural stem cells were described and isolated from the adult mouse brain in the late 1980s (23) and early 1990s (24), though there was evidence of mitogenic cells in the rodent brain from as early as the 1960s (25). In the presence of growth factors, including basic fibroblast growth factor (bFGF) and epidermal growth factor (EGF), these cells proliferated and formed cell clusters termed neurospheres, which could be passaged following single-cell dissociation to generate second, third and further generation neurospheres, or differentiate into neurons and glial cells (24). They were also capable of surviving, proliferating and differentiating when transplanted into the CNS (26, 27). In the late 1990s, analysis of post-mortem tissue confirmed the presence of NSC in the adult human brain (28, 29) and a few years later, NSC were isolated from the adult human olfactory bulb from patients undergoing invasive neurosurgery (30). They are rarely accessible from the living adult human brain and only through extremely invasive surgery, therefore NSC from rodents have been studied as well as human foetal brain-derived NSC (31, 32).

It is presumed that the optimum brain repair mechanism resides within the brain mediated by the local stem cells. Age is a risk factor for neurological diseases including stroke, but aging also attenuates brain repair potential, thus increasing susceptibility to disease. Neural stem cell proliferation rate, viability, and migration capacity can thus be restricted (17). For this reason, exogenous sources of NSC are being studied, including ESC-derived, foetal brain-derived, or reprogrammed from somatic cells either indirectly via the production of induced PSC or directly bypassing the pluripotent stage (6). Ethical and practical considerations limit the application of NSC from ESC and brain tissue, leaving reprogramming as an appealing alternative to provide a source of NSC for cellular therapy.

To be applicable for regenerative medicine, a cell source needs to be easily accessible, expandable under good manufacturing practices to provide sufficient cell numbers, and able to be differentiated/reprogrammed using an efficient and reproducible protocol with defined media. In this regard, stem cells have been investigated, and promising candidates include neural crest-derived DPSC (7, 33).

DENTAL STEM CELLS

The tooth is an ectomesenchymal tissue that contains, along with the supporting tissues, multiple stem cell niches. Several dental stem cell populations have been identified, which include; DPSC from the dental pulp tissue of permanent teeth (**Figure 2**) (7), stem cells from the dental pulp tissue of exfoliated deciduous teeth (34), stem cells from apical papilla isolated from the root canal of immature permanent teeth (35), and stem cells from tooth germs (36). Other stem cell populations from the supporting tissues in the oral cavity include; periodontal ligament stem cells (37), alveolar bone-derived MSC (38), gingival MSC (39), and dental follicle stem cells from the surrounding connective tissue of the tooth germ (40).

Dental stem cells follow the criteria that define multipotent mesenchymal stem/stromal cells (MSC), as described by the International Society for Cellular Therapy in 2006 (41). These criteria include; plastic adherence under standard culture conditions; ability to differentiate along the adipogenic, chondrogenic, and osteogenic lineages when cultured in appropriate inductive media; expression of the common MSC-associated markers CD73, CD90, CD105; and lack of expression of haematopoietic markers CD14, CD34, CD45, CD19, and HLA-DR. These dental stem cells are isolated similarly to MSC-like populations from other tissues, such as bone marrow and adipose tissue, and display a spindle-shaped morphology. This review will focus on DPSC, which were the first dental stem cells to be identified.

DENTAL PULP STEM CELLS

Human DPSC isolated from third molars, were first described by Gronthos et al. (7). They are a heterogeneous multipotent

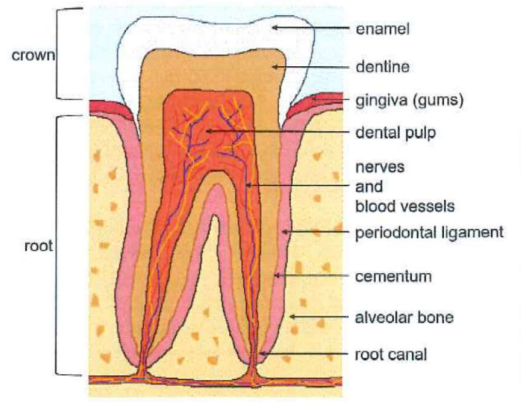

FIGURE 2 | Tooth anatomy and dental pulp stem cells. There are two anatomical parts of the tooth; the crown exposed to the oral cavity and the root embedded in the gum. The crown is composed of enamel on the outside, the underlying dentine, and pulp tissue, which contains nerves, blood vessels, and lymphatics. The root, covered with the bone-like tissue cementum, contains dentine and the root canal. The tooth is supported by the periodontal ligament, connecting it to the alveolar bone. Dental pulp stem cells reside in the perivascular niches of the dental pulp tissue of permanent teeth.

adult stem cell population that reside in the perivascular niche of the dental pulp (**Figure 2**) (42). The role of the dental pulp is to maintain tooth homeostasis and repair. The dental pulp cell population consists of dentine-generating odontoblasts on the outer side of the tissue, fibroblasts, immune cells, nerve and glial cells, and stem and progenitor cells in the perivasculature. It was demonstrated early on that DPSC can regenerate tooth structures, as they were capable of forming a dentin-pulp complex when transplanted into immunocompromised mice, which suggested the presence of stem and progenitor cells (7).

Dental pulp stem cells possess high proliferative and clonogenic capacity, and it is for this reason that they have attracted attention with regard to therapeutic applications (7). Limited cell proliferation and tendency to undergo senescence when cultured *ex vivo*, is a challenge that needs to be overcome if cells are to be used in the clinic. In comparison to some cell populations, such as BMSC, DPSC display a higher frequency of colony formation and greater proliferation potential, which is maintained throughout culture (7, 43).

Their multilineage differentiation potential has been demonstrated under *in vitro* inductive conditions and following implantation *in vivo*, along multiple lineages including the odontogenic, osteogenic, chondrogenic, adipogenic, neurogenic, and myogenic lineages (44, 45). This extensive array of lineages is an advantage over other stem cell populations, such as haematopoietic stem cells, which have a more limited differentiation capacity.

There is no known unique marker to identify and isolate DPSC. Extensive immunophenotyping of *ex vivo* expanded DPSC has demonstrated their expression of markers associated with; MSC-like populations; bone and dentine; and perivascular cells, including CD146 (7). Dental pulp stem cells may also express neural lineage markers, including low-affinity nerve growth factor receptor known as p75, the intermediate filament nestin, and glial fibrillary acidic protein, as well as more mature neuronal lineage markers, such as β-III tubulin and neuronal nuclear antigen (45). This immunophenotype reflects their origin and high level of heterogeneity.

Dental pulp stem cells originate from the embryonic neural crest. In vertebrate embryogenesis, during the formation of the neural tube, a transient population of multipotent cells arises at the junction between the neural tube and the epidermal ectoderm, termed the neural crest (**Figure 1**). These neural crest cells migrate from the dorsal margins of the neural tube, undergoing an epithelial to mesenchymal transition, and give rise to multiple neural and non-neural cell types throughout the body, including all of the neurons and glia of the peripheral nervous system, the ectomesenchymal derivatives of the craniofacial area and melanocytes of the skin (**Figure 1**). It is the migrating cranial neural crest cells that contribute to the dental pulp tissue, established using genetic lineage tracing (46–48). In addition, a more recent study demonstrated that a significant subpopulation of cells extracted from the dental pulp originates from peripheral nerve-associated glia during tooth development, homeostasis and regeneration (49). Thus, neural crest-derived stem and progenitor cells persist in adult tissues, and some, such as the glial Schwann cells lining peripheral nerves and melanocytes in the skin, are able to dedifferentiate into stem/progenitor-like cells (13).

It is therefore not surprising that DPSC express markers of the neural lineage, which substantiate their neural predisposition. However, they are heterogeneous and this quality can impact the differentiation efficiency (7). Analysis of individual colonies also demonstrated the different proliferation rates, suggesting that the more highly proliferating cells will dominate a multi-colony population, altering the composition (33).

Most studies have focused on using the whole DPSC population extracted from the dental pulp (50, 51). However, it may be beneficial to select subpopulations, using fluorescence- or magnetic-activated cell sorting, based on markers that may be associated with increased neurogenic potential. Using a more homogenous cell population could increase the differentiation efficiency. For example, stromal precursor cell surface marker STRO-1, known as an early marker of multiple MSC-like populations, has been used to purify DPSC (42). However, STRO-1 is downregulated very early during *ex vivo* expansion, creating a problem in obtaining sufficient cell numbers (42). The neural crest marker p75, co-expressed with STRO-1 on BMSC (52), may be suitable as $p75^+$ DPSC express higher levels of neural stem cell markers (53). It is however expressed by <10 percent of the overall DPSC population (53). Isolation methods may also make a difference. The common isolation method is to enzymatically release the cells from the dental pulp tissue using collagenase and dispase (7). Alternatively, cells can be allowed to migrate out using the explant method, which may select for specific subpopulations (54).

Dental pulp stem cells have also been shown to express the pluripotency-associated markers OCT4, SOX2 and MYC (55), which is uncommon to MSC. However, unlike ESC and induced PSC that express these markers, transplanted DPSC have not resulted in tumour formation (33). Additionally, both spontaneously and induced immortalised DPSC did not form tumours when transplanted into immunocompromised mice (56). Embryonic stem cells and induced PSC require complete differentiation prior to implantation due to tumorigenic risk.

These properties make DPSC promising candidates for stem cell therapy, in particular for neurological diseases due to their neurogenic predisposition. Most importantly, dental pulp presents an easily-accessible non-invasive source of adult stem cells with high proliferation potential. They are isolated from routinely extracted teeth that would otherwise be discarded as clinical waste, unlike the invasive aspiration of bone marrow required to obtain BMSC.

NEURONAL DIFFERENTIATION OF HUMAN DENTAL PULP STEM CELLS

Under defined neuronal inductive conditions, human DPSC are able to differentiate into functionally active neuronal cells. They acquire a neuronal morphology, displaying a rounded cell body with cytoplasmic extensions, and show an immunophenotype consisting of neuronal-associated markers (e.g., β-III tubulin, neuronal nuclear antigen) (50, 51). As outlined in **Table 1**, there have been multiple neuronal differentiation protocols applied to human DPSC, varying in media composition, use of supplements, growth factors, and small molecules, as well as seeding density, growth surfaces, number of stages, and duration. However, few studies have conducted functional analysis of their neuronally differentiated DPSC (**Table 1**), such as electrophysiological analysis for the presence of voltage-gated ion channels (Na^+, K^+, Ca^{2+}), which are required for the generation and propagation of action potentials in functionally mature neurons.

One of the earlier methods for neuronal induction of human DPSC, and the first to examine their functionality, resulted in neurons that displayed voltage-gated sodium channels, important for initiation of action potentials (50). A subpopulation of DPSC has been shown to display sodium currents in their normal state (57). These cells may have a role in sensory transduction within teeth. If this subpopulation differentiates into neuronal-like cells, enhanced electrophysiological properties would be expected. It is however uncertain, which subpopulations neuronally differentiate, and whether they initially display any voltage-dependent ion currents. A modified version of this neuronal differentiation protocol resulted in cells expressing both sodium and potassium currents (58).

Subsequently, a shorter, 2-week neuronal differentiation protocol for DPSC was developed, resulting in neurons displaying both voltage-dependent sodium and potassium currents and were sensitive to respective inhibitors (51). This method had a pre-induction step exposing the cells to the demethylating agent 5-azacytidine, thus modifying the epigenome to increase the ability of the cells to go down the specified lineage. These neuronally differentiated human DPSC localised to the neurogenic niches in the rodent brain and were detected in the lesioned cortex following injury (59). This demonstrated that the DPSC-derived neuronal cells survived and responded to the environmental signals, similar to results obtained in an avian embryo model using undifferentiated human DPSC (60).

Other groups have been interested in directing DPSC into specific neuronal types, including dopaminergic and spiral ganglion neurons (61–63). However, the investigations are few at the current time and more research is needed. Furthermore, xeno- and serum-free conditions from initial culture to neuronal differentiation have also been investigated (64). Removing animal-derived products and creating defined media is a critical step towards establishing a safe and consistent cell source for therapeutic purposes.

More recently, studies have begun to use neurosphere generation for neural induction of human DPSC (65). Neurospheres are a commonly used culture system for NSC, where cells are grown in conditions lacking adherent substrates and in the presence of growth factors, most commonly bFGF and EGF. They are heterogeneous, containing cells at different stages of differentiation and maturation, thus identifying the presence neural stem cells. Recent studies have incorporated this culture system in the neuronal differentiation of DPSC (65, 66). The cells were differentiated to functional neurons *in vitro*, through a two-step protocol, firstly by stimulating neurosphere formation, then going through a neuronal maturation stage. Patch-clamp analysis and calcium imaging were used to confirm the presence of functional properties. One research group observed that the cells not only expressed functional voltage-gated sodium and potassium channels but a subset of cells also generated single action potentials (65). Repeated action potentials were not observed nor were spontaneous action potentials, which would indicate fully functional neurons. The initial neurosphere culture step was further analysed by Pisciotta et al. (67), who demonstrated the prolonged expansion of the DPSC-derived spheres throughout which they maintained their neural crest properties.

These *in vitro* differentiation studies demonstrated that DPSC respond to local environmental cues, which is also true for the *in vivo* setting. When injected into an embryonic model at a time of active neurogenesis, DPSC followed the migratory pathway of endogenous cranial neural crest cells, reiterating their origin, and underwent neuronal differentiation (60).

HUMAN DENTAL PULP STEM CELLS IN STROKE MODELS

Despite the extensive *in vitro* research examining the neurogenic properties of DPSC, there have only been a hand-full of studies that have examined the efficacy of human DPSC-based therapies *in vivo* to treat stroke. **Table 2** summarises the use of human DPSC in animal stroke models, based on rodent models of focal

TABLE 1 | Neuronal induction protocols for human dental pulp stem cells with functional assessment.

Cells	Growth conditions					Functional assessment	References
	Basal media	Use of spheres	Coating	Growth factors	Duration		
$CD34^+$/$cKit^+$/ $STRO\text{-}1^+$ DPSC	DMEM/F12	Yes	Poly-L-lysine	bFGF EGF BDNF NGF	>3 weeks	Patch-clamp analysis of Na^+ and K^+ currents.	Pisciotta et al. (67)
DPSC	DMEM/F12	Yes	Poly-L-ornithine, laminin	bFGF EGF BDNF GDNF NT-3	19–23 days	Fluorescent detection of Ca^{2+} influx following stimulation.	Gonmanee et al. (63)
DPSC	Neuro-basal	No		bFGF EGF BDNF	12 days	Fluorescent detection of Ca^{2+} influx following stimulation.	Singh et al. (62)
DPSC	DMEM/F12	No	Type I and IV collagen, laminin, fibronectin	bFGF EGF BDNF GDNF IGF-I	>3 weeks	Transplantation into neonatal rat brain and spinal cord injury rat model.	Jung et al. (64)
DPSC	Neuro-basal A	No	Geltrex	bFGF EGF	3 weeks	Patch-clamp analysis of Na^+ and K^+ currents.	Ullah et al. (58)
DPSC	DMEM/F12, Neuro-basal	Yes	Poly-L-ornithine, laminin	bFGF EGF NT-3	5 weeks	Patch-clamp analysis of Na^+ and K^+ currents, and action potential production.	Gervois et al. (65)
DPSC	Neuro-basal	No		bFGF FGF8 BDNF	9 days	Fluorescence detection of Ca^{2+} influx, and measurement of dopamine release with/without stimulation.	Kanafi et al. (61)
DPSC	Neuro-basal	Yes	Type IV collagen	bFGF EGF	2 weeks	Fluorescent detection of Ca^{2+} influx following stimulation.	Osathanon et al. (66)
DPSC	DMEM/F12, Neuro-basal A	No	Poly-L-lysine	bFGF NGF NT-3	9–13 days	Patch-clamp analysis of Na^+ and K^+ currents, transplantation into the cerebrospinal fluid of neonatal rats, transplantation into rats with lesions to the forelimb motor cortex.	Kiraly et al. (51, 59)
DPSC	Neuro-basal A	No	Poly-ornithine, laminin	bFGF EGF	3 weeks	Patch-clamp analysis of Na^+ currents.	Arthur et al. (50)

BDNF, brain-derived neurotrophic factor; bFGF, basic fibroblast growth factor; DMEM, Dulbecco's Modified Eagle's Medium; DPSC, dental pulp stem cell(s); EGF, epidermal growth factor; F12, Ham's F12 nutrient mixture; FGF8, fibroblast growth factor 8; GDNF, glial cell-derived neurotrophic factor; IGF-I, insulin-like growth factor I; NGF, nerve growth factor; NT-3, neurotrophin-3.

cerebral ischaemia via the transient occlusion of the middle cerebral artery.

The first study to investigate DPSC in an animal model of stroke used a mechanical extraction method to obtain cells from human wisdom teeth (68). These cells expressed the nuclear receptor related 1 protein, which is essential for the dopaminergic system of the brain. Although the study involved a small sample size, it provided preliminary data for the therapeutic potential of dental pulp cells for stroke. Functional recovery was exhibited and cells were detected in the penumbra, however potential mechanisms were not investigated.

A subsequent study provided the first preclinical support for use of human DPSC in acute ischaemic stroke (69). Dental pulp stem cells were intracerebrally transplanted into the rat brain 24 h post-stroke, at two injection sites; in the cortex and in the striatum. At 4 weeks, significant neurobehavioural improvement was observed, however only 2.3 percent of engrafted cells were detected. These results suggest that the improvement was not mediated by a cell replacement mechanism rather through a DPSC-dependent paracrine effect, involving the many growth factors secreted by DPSC, such as nerve growth factor, brain-derived neurotrophic

TABLE 2 | Human dental pulp stem cells in stroke models.

Cells	Experimental model	Delivery method	Cell number	Timing	Outcome	References
DPSC	Rat Transient Middle Cerebral Artery occlusion (MCAo)	IV	1×10^6	Cells injected at 0 or 3 h post-stroke, analysis performed up to 14 days post-stroke.	Cells reversed motor deficits and reduced infarct volume by inhibiting microglial activation, pro-inflammatory cytokine production, and neuronal degeneration.	Nito et al. (71)
DPSC over-expressing hepatocyte growth factor		IV	1×10^6	Cells injected at 0 h post-stroke, analysis performed up to 14 days post-stroke.	Cells improved motor function and decreased infarct size via immunomodulation, enhanced angiogenesis, suppression of neuronal degeneration, and maintenance of blood-brain barrier integrity.	Sowa et al. (76)
$CD34^+/c\text{-}Kit^+/STRO\text{-}1^+$ DPSC		IV	4×10^6	Cells injected 24 h post-stroke, analysis performed up to 28 days.	Cells stimulated functional recovery and decreased infarct volume via autocrine/paracrine mechanisms.	Song et al. (75)
DPSC		IC	6×10^5	Cells injected 24 hours post-stroke, analysis performed up to 28 days.	DPSC enhanced post-stroke forelimb sensorimotor recovery via DPSC-dependent Paracrine effects.	Leong et al. (69)
Dental pulp-derived nuclear receptor related 1 $protein^+$ stem cells		IC	$1–2 \times 10^5$	Analysis performed up to 28 days.	Transplanted cells survived and promoted functional recovery, due to hypo-immunogenic properties and immunomodulation ability.	Yang et al. (68)

DPSC, dental pulp stem cell(s); IC, intracerebral; IV, intravenous.

factor, glial-derived neurotrophic factor, and ciliary neurotrophic factor (70, 71). The low survival rate observed in this preclinical model may indicate a specific subpopulation of DPSC have greater neurogenic potential and ability to survive and differentiate, with the $p75^+$ subpopulation being a candidate. The DPSC displayed targeted migration towards the infarct, and differentiated into astrocytes within the vicinity of the infarct and neurons further from the infarct site. The targeted migration of the transplanted cells towards the ischaemic border zone is likely mediated by the SDF1 gradient produced by endogenous cells following stroke (20). This chemokine is upregulated for at least a month post-stroke (72). Furthermore, it was previously shown in an avian embryo model that DPSC induce endogenous axon guidance of host trigeminal ganglion axons via the production of SDF1 (60). In this preclinical study, a reduction in post-stroke corpus callosum atrophy was also observed, again indicating to the ability of DPSC to influence host axonal remodelling. These results demonstrate the role of SDF1 signalling in DPSC migration and neuroplasticity properties.

Of note, both of these studies used an intracerebral route of administration, which is a highly invasive procedure. Subsequent studies used an intravascular route, which may be clinically safer in the acute stroke setting (73). It has been shown that stem cells administered through this route can be detected in the brain but involves the transmigration of the BBB. This could be a result of the disrupted BBB post-stroke, however cellular trafficking occurs even after the period of increased BBB permeability (74), implicating other mechanisms at play.

In these DPSC studies, administration via the tail vein resulted in cells transmigrating the BBB and migrating towards the infarct (71, 75, 76), with a lack of detection in systemic organs (75). Winderlich et al. previously demonstrated that human DPSC stimulate BBB permeability via the production of the soluble factor vascular endothelial growth factor-alpha (VEGFα) (73), which is known to be produced following stroke and is secreted by stem cells, including DPSC (77). DPSC mediate their angiogenic effect via VEGFα (75, 76). In addition to its role in angiogenesis, VEGFα is involved in vascular permeability, and has been shown to decrease tight junction proteins thus increasing permeability (78). Interestingly, Sowa et al. showed that the integrity of the BBB was maintained via the DPSC attenuation of the decrease in tight junction proteins that results from stroke (76). This was observed with unmodified DPSC, but also with DPSC overexpressing the pleiotropic cytokine hepatocyte growth

factor, which showed an even greater effect. This factor may have a role in inhibiting BBB disruption (79). Hence, DPSC not only produce factors like VEGFα that allow them to transmigrate the BBB but they also have the counteracting potential to maintain BBB integrity. There are likely other factors involved in regulating BBB permeability and with more research, the complex mechanisms used by stem cells can be uncovered.

Dental pulp stem cells have been shown to modulate the immune response in several ways. They inhibit microglial activation, as evidenced by the decrease in cells expressing ionised calcium-binding adaptor molecule 1, a marker specifically expressed in the brain by activated microglial cells (71, 76). Analysis of DPSC-conditioned medium has shown their expression of various cytokines, including interleukin 10, which decreases pro-inflammatory cytokine production (71). Additionally, decreased levels of the pro-inflammatory cytokines tumour necrosis factor-alpha and interleukin 1-beta are observed in brain tissue and serum from DPSC-treated stroke animals (71, 76).

The BBB has a role in maintaining the immune privileged status of the CNS. It appears that DPSC are not entirely rejected, as these studies have not employed the use of immunosuppressive drugs (71, 75, 76). This could be mediated by the DPSC expression of the Fas ligand, which induces the apoptosis of T cells, and is also one of the mechanisms used to maintain immune privilege of certain tissues. Fas ligand is known to be expressed by stem cells including DPCS, even with prolonged culture and particularly using the neurosphere culture system (67). Thus, DPSC have the potential to evade the immune system, transmigrate the BBB, migrate towards the infarct and modulate the inflammatory response. The ability of DPSC to exert these therapeutic effects in the acute phase when inflammation occurs, demonstrates their high level of potency (71).

Dental pulp stem cells are also able to inhibit reactive astrogliosis (75), which leads to glial scar formation as a protective mechanism but impedes axonal regrowth. Attenuation of neuronal degeneration by DPSC is also evidenced by decreased numbers of degenerating neurons (71, 76). This neuroprotective effect is likely mediated by the array of neurotrophic factors produced by DPSC, such as nerve growth factor, brain-derived neurotrophic factor, glial-derived neurotrophic factor (70). Additionally, DPSC express the cytokine interleukin 3 (IL-3) (71), which promotes proliferation and differentiation of stem cells, suggesting that DPSC may have capacity to stimulate endogenous cells, though this mechanism has not been investigated in these studies.

These *in vivo* studies observed functional recovery and decreased infarct volumes (**Table 2**). Evidence from all preclinical studies suggest that the therapeutic effects of DPSC are most likely mediated through paracrine mechanisms and less so of a neural cell replacement mechanism. Dental pulp stem cells secrete growth factors, neurotrophins and cytokines, which promote angiogenesis, modulate the immune response, provide neuroprotection, and enhance neuroplasticity (**Figure 3**).

Even though cell survival and differentiation to astrocytes and neurons is observed, neural tissue replacement is unlikely to play a big part. Cell survival may be increased through the addition of neurotrophic factors, such as brain-derived neurotrophic factor (80). Alternatively, the culture method may be important, with a better outcome observed with DPSC-derived neurospheres, possibly due to greater amounts of neural progenitor cells (81). As previously mentioned, certain DPSC subpopulations may have greater neurogenic potential and survival. The perivascular cell marker CD146 is used to purify MSC-like populations from different tissues. However, it may actually select cells that are more committed to non-neural lineages, as $CD146^+$ cells demonstrate greater regeneration of the dentin-pulp complex than $CD146^-$ cells (82). The $CD146^-$ subpopulation may instead contain cells that are of neural crest origin, and may explain why it displayed positive outcomes in an ischaemic model (83). Another investigated subpopulation is $CD34^+$ DPSC, which despite their slower proliferation and loss of "stemness," have greater commitment to the neural lineage and express the neural markers p75 and nestin, compared to $CD34^-$ DPSC (75, 84). Although CD34 is believed to be a distinct marker for cells of haematopoietic origin and endothelial cells, this subpopulation improved functional recovery via the aforementioned mechanisms but also exhibited superior neuroprotective properties in comparison to BMSC (75).

There is strong experimental evidence that stem cell therapy can improve neurological function through a variety of cellular and molecular mechanisms, with growing evidence to support DPSC as an attractive source. These cells are appealing for use in autologous and allogeneic therapies of stroke. Stroke is more widely regarded as an aging disease, and improved healthcare suggests that a greater proportion of the older population retain their teeth. Nevertheless, to reach all stroke patients irrespective of having their own teeth, an allogeneic strategy may be required, and the immunosuppressive properties of DPSC make them attractive for this type of clinical application (85).

While promising, the efficacy of DPSC to deliver therapeutic outcomes based on their capacity to differentiate into functional neural cell populations remains the subject of intense research. The limitation in using undifferentiated and unselected DPSC is that they may differentiate along multiple lineages or only a small fraction would differentiate to neural cells, thereby decreasing the clinical efficacy. A neural cell population would be more suited to the environment and have greater potential to replace lost and damaged neural tissue. For example, neuronally pre-differentiated human DPSC responded well to the normal and injured *in vivo* environment (59). However, since neuronal cells lack the ability to self-renew, the number of cells that can actually mediate positive outcomes will be fewer than initially transplanted due to cell loss. Furthermore, in a disease like stroke where the ischaemic milieu affects multiple neural cell populations, administering neuronal cells would be targeting the replacement of only one affected population. Neural stem or progenitor cell populations would be a better alternative, allowing

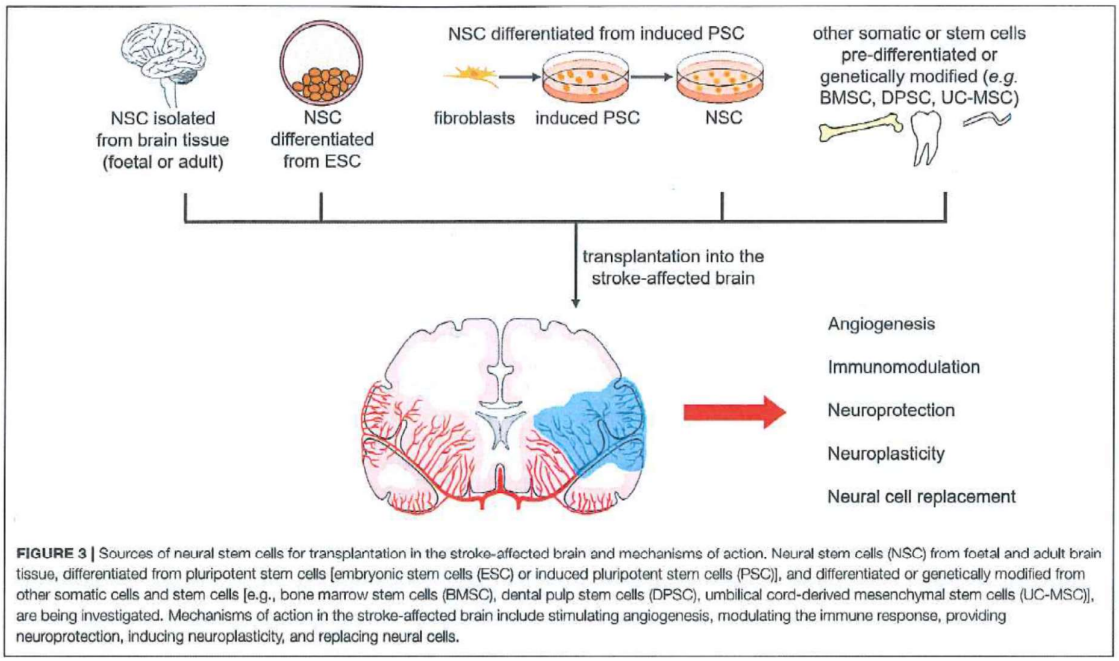

FIGURE 3 | Sources of neural stem cells for transplantation in the stroke-affected brain and mechanisms of action. Neural stem cells (NSC) from foetal and adult brain tissue, differentiated from pluripotent stem cells [embryonic stem cells (ESC) or induced pluripotent stem cells (PSC)], and differentiated or genetically modified from other somatic cells and stem cells [e.g., bone marrow stem cells (BMSC), dental pulp stem cells (DPSC), umbilical cord-derived mesenchymal stem cells (UC-MSC)], are being investigated. Mechanisms of action in the stroke-affected brain include stimulating angiogenesis, modulating the immune response, providing neuroprotection, inducing neuroplasticity, and replacing neural cells.

expansion to provide sufficient cell numbers and differentiation into various cells based on the endogenous environment.

REPROGRAMMING DENTAL PULP STEM CELLS

Finding an alternative source of NSC has been a major research focus for some years now, with much of the research investigating cellular reprogramming strategies. In this regard, DPSC might be a promising cell source. Due to their neural crest origin, they may require less manipulation or display greater efficiency than other cell types. As previously mentioned, cells can be directed along the neural lineage either indirectly, using induced PSC production, or directly to the desired cell type.

Dental pulp stem cells have successfully been reprogrammed to induced PSC (86, 87), even in the absence of the oncogenic MYC, and subsequently directed along the neural lineage (88). Dental pulp can thus provide an alternative cell source for establishing induced PSC banks for regenerative medicine. There has been little investigation in the area of converting DPSC into NSC, other than by the use of neurosphere culture methods, usually as a transient step in the pathway to neuronal differentiation (65). While there has been some evidence of the neurosphere culture system maintaining prolonged culture of DPSC-derived spheres (67), these spheres are not clonal nor consisting of only stem cells. Since DPSC are of neural crest origin, it may be more efficient to use a direct reprogramming strategy to convert them to NSC, in comparison to cells of a different germinal lineage. Transdifferentiation should be possible between these cell types, which share a common tissue of origin. Similar methods that have been applied to other somatic cell types to induce NSC can be applied to DPSC (89–92).

DIRECT REPROGRAMMING OF CELLS ALONG THE NEURAL LINEAGE

Direct reprogramming along the neural lineage was first investigated by Wernig et al. who demonstrated the production of induced neurons from mouse fibroblasts using the neural-specific transcription factors, ASCL1, BRN2 and MYT1L (93), and from human fibroblasts with the addition of the NEUROD1 transcription factor (94). Since fibroblasts are from a heterogeneous mesenchymal cell population potentially containing cells of neural crest origin, they further applied this transcription factor combination to a homogeneous non-neural-derived cell population (95). This demonstrated that reprogramming is not restricted to cells of the same germinal lineage. Thereafter, they established that the pro-neural factor ASCL1 alone was capable of reprogramming fibroblasts to neuronal cells (96); thus this gene may be viewed as a pioneer transcription factor (97). Reprogramming is associated with epigenetic modifications of the DNA. Pioneer transcription factors are first to occupy chromatin sites, leading to remodelling of the chromatin configuration at lineage-specific genes and subsequent recruitment of other transcription factors, demonstrating the hierarchical mechanisms in lineage

reprogramming. The achievement of generating induced neurons is of clinical importance with regard to addressing the safety issues associated with induced PSC. However, the post-mitotic nature of neurons may not be ideal for all applications.

Subsequent studies applied a direct reprogramming strategy to obtain expandable neural stem and progenitor cells, using pluripotency-associated and/or neural-specific transcription factors. The first study to derive induced neural stem or progenitor cells, applied transient expression of the Yamanaka factors (OCT4, SOX2, KLF4, MYC) in fibroblasts. However, these induced cells occurred at a low frequency of <1 percent, were expandable *ex vivo* for only three to five passages, giving rise to neurons and astrocytes but not oligodendrocytes (16). A similar study used the same factors but limited OCT4 expression to the first 5 days of reprogramming, resulting in tripotent NSC that could be stably expanded for more than 50 passages and exhibited a transcriptional profile similar to brain-derived NSC (92). These studies claimed to transdifferentiate the fibroblasts to the neural lineage using the same factors for induced pluripotency but under neural conditions, thus bypassing the pluripotent state. However, genetic lineage tracing studies demonstrated that these methods actually involved cells passing through a transient pluripotent state, before differentiating along the lineage specified by their environment (98, 99). This suggests that the pluripotent state is a requisite when reprogramming cells between different germinal lineages, although transcription factor combinations may also influence this.

Different research groups instead used neural-specific transcription factor combinations, including SOX2, which has a role in embryonic development and neural induction (89, 100). One combination included BRN2, a transcription factor in the same family as OCT4, which was necessary for tripotency, while SOX2 was essential for development of mature neurons (89). In another study, the Yamanaka factors were used but OCT4 was replaced with BRN4, again in the same family (90). These fibroblast-derived NSC survived in the mouse brain for up to 6 months and differentiated along the three neural lineages (101). More recently, the same group compared the transcriptome of these induced NSC with forebrain-derived NSC and ESC-derived NSC (102). They showed that all three groups of NSC were distinct from one another, but that induced NSC and forebrain-derived NSC had a greater similarity with each other than with ESC-derived NSC. Moreover, this transcription factor combination resulted in NSC that possessed mostly a caudal identity, while forebrain-derived NSC had a rostral identity and ESC-derived NSC had a less defined regional identity indicating their more immature state. This suggests that different transcription factor combinations could yield NSC suitable for different areas of the brain.

From these studies, it appears that members of the POU domain family of transcription factors, like OCT4, have a critical role in lineage conversion (103). This factor is a fundamental transcriptional regulator of pluripotency. The OCT4 and SOX2 transcription factors heterodimerise; SOX2 binds weakly to DNA while OCT4 contains the POU DNA-binding domain. Together, they govern the activation of genes for pluripotency and concurrently the suppression of genes for differentiation. It has been proposed that OCT4 acts as a pioneer transcription factor to induce plasticity of cells, with subsequent factors and environmental conditions directing the lineage differentiation (103, 104). Indeed OCT4 alone has been used to reprogram fibroblasts (105) and blood cells (106, 107) to NSC, which under neural conditions do not display hallmarks of induced pluripotency (104).

Other groups have demonstrated the production of induced neural cells from fibroblasts using only SOX2 (91), and from blood cells using SOX2 and MYC (108, 109). Like OCT4, SOX2 is a key regulator of pluripotency but is further involved in maintenance of multiple stem cell populations, including NSC, and may be crucial for reprogramming (110). The role of the proto-oncogene MYC in the reprogramming process may involve chromatin remodelling. This factor aids the reprogramming process since removal of MYC lowers the efficiency of induced PSC generation (14, 15).

Cellular reprogramming is a rather inefficient process, requiring ongoing investigations to better understand the process and methods to optimise it. Low efficiency may reflect the stoichiometry of the transcription factors or the need for integration of the transgenes in specific loci (14, 15). Furthermore, the process is stochastic; reprogramming occurs randomly so cells in the population can be at different stages of differentiation and maturity, while incomplete reprogramming may also occur, whereby cells retain epigenetic memory of the donor cells (111). The heterogeneity of the initial cell populations and the molecular state of the cells likely contribute to this process.

Rather than inducing the ectopic expression of transcription factors, microRNAs (112) and small molecules (113, 114) have been applied, which in effect target the enzymes for epigenetic modifications and/or transcription factors and other elements of their signalling pathways to result in similar cellular outcomes as transcription factor-mediated reprogramming. For example, the microRNA miR-124 has a role in regulating the epigenome as well as multiple neuronal differentiation genes (6, 112). Chemical cocktails for reprogramming usually include epigenetic modulators that improve efficiency, such as the histone deacetylase inhibitor valproic acid, and DNA and histone methyltransferase inhibitors (113, 114). Other modulators are used to activate or deactivate specific signalling pathways, such as the Wnt, MAPK/ERK, TGFβ, and hedgehog signalling pathways, to activate appropriate neural genes, promote self-renewal, enhance mesenchymal to epithelial transition, improve viability, decrease cell senescence, and increase efficiency (6, 113, 114). This suggests that multiple signalling pathways have important roles in the reprogramming process and a variety of small molecules can be used to achieve this.

With regard to DPSC, little research exists on transcription factor-mediated reprogramming. Induced overexpression of OCT4A, the OCT4 isoform thought to be the key regulator of pluripotency, enhanced expression of other pluripotency regulators and multilineage differentiation in human DPSC (115). However, the effect on differentiation along the neural lineage was not investigated. Overexpression of SOX2 in DPSC

was also investigated, focusing on proliferation, migration, and adhesion, but the effect on multilineage differentiation is unknown (116).

NEURAL STEM CELL THERAPY FOR ISCHAEMIC STROKE: PRECLINICAL STUDIES

Neural stem cells are a promising cell source for establishment of functional neuronal networks following disruption by neurological injury or disease. They would be an appropriate stem cell source for stroke treatment, where the ischaemic environment affects multiple cell types, with additional heterogeneity seen among patients. Preclinical studies using NSC in rodent models of ischaemic stroke have utilised human and rodent NSC derived from ESC, brain tissue, induced PSC and more recently via somatic cell transdifferentiation (**Figure 3**) (117–120). They have been shown to survive, migrate towards the lesion, differentiate into neurons and astrocytes, decrease infarct volume, integrate, induce neuroplasticity, and stimulate functional improvements via paracrine effects (117, 118, 121–125). Transplanted NSC also induce endogenous NSC to proliferate (119, 120, 126, 127).

Even though beneficial effects have been observed, similar to other stem cells, research is still focused on how to better improve survival of the engrafted cells. Neural stem cells are expected to be better suited for the neural environment, and as such, survival of transplanted human foetal NSC has been shown to be >30 percent at 1 month after transplantation (121, 123), in comparison to the survival of human DPSC at only 2.3 percent (69). Cell survival decreased as time of transplantation post-stroke increased, i.e., hours vs. weeks, however it was still more than 10 times greater than that of DPSC (128), demonstrating their ability to survive in the harsh acute stage. Interestingly, a study that examined the difference of foetal and adult mouse NSC showed that even though both showed therapeutic effects, foetal NSC had a higher survival rate (129), indicating that the adult NSC were mediating their effects through mechanisms other than cell replacement similar to observations with other adult stem cells, such as DPSC. This suggests that there is a difference in foetal and adult stem cells that governs their mechanisms of action.

Multiple studies have shown that survival of transplanted NSC is enhanced when modified to express neurotrophic factors, including nerve growth factor (130), VEGF (131), neurotrophin-3 (132, 133), glial-derived neurotrophic factor (134), brain-derived neurotrophic factor (135, 136), and bFGF (137), or when pre-treated prior to transplantation (138).

Ischaemia produces a harsh environment containing reactive oxygen species, which damage macromolecules in the cells. Some studies have demonstrated that hypoxic preconditioning of cells increases viability (139). The hypoxia-inducible factor 1-alpha (HIF1α) transcription factor is expressed under hypoxic conditions, and one of its downstream targets is VEGF, leading to increased angiogenesis. Alternatively, NSC were modified to express HIF1α to aid their survival (140). In another study, NSC that were modified to overexpress an anti-oxidant enzyme to eliminate reactive oxygen species, showed greater survival following transplantation (141). Thus, NSC may be better primed using mechanisms that activate pathways addressing survival under hypoxic conditions.

Interestingly, in addition to the role in angiogenesis, VEGF has been shown to be involved in transdifferentiation of astrocytes into mature neurons (142). This suggests that an additional beneficial effect of reactive astrogliosis, which has a role in neuroprotection following stroke, is neuronal cell replacement. Furthermore, studies often see differentiation of transplanted stem cells into neurons and astrocytes. Timing of transplantation post-stroke has also been shown to affect differentiation, with earlier time point leading to astrocyte differentiation while later time point leads to neuronal differentiation (143). Thus, astrocytes appear to have a crucial role in the acute stage. Overall, NSC exhibit therapeutic effects but there are multiple ways they can be modified, as well as transplantation parameters, which can alter their survivability and differentiation outcome.

NEURAL STEM CELL THERAPY FOR ISCHAEMIC STROKE: CLINICAL TRIALS

There have been few clinical trials for ischaemic stroke using human neural stem or progenitor cells, and no trials utilising DPSC to date.

The first clinical trial of cell therapy for chronic stroke in patients with fixed motor deficits was conducted using the NTERA2 human teratocarcinoma cell line as a source of neurons. When treated with retinoic acid, these cells that resemble neuroepithelial cells differentiate into post-mitotic neurons that are indistinguishable from ESC-derived neurons. Following the phase I trial consisting of 12 patients and demonstrating the feasibility, a phase II trial was carried out with 18 patients (50 percent ischaemic stroke) who participated in a subsequent stroke rehabilitation program. The safety and feasibility of using these neurons was demonstrated, and although functional improvements were observed, they did not appear to have an overall significant effect on motor function (144, 145).

Several clinical trials have examined multiple cell combination therapy, including neural stem/progenitor cells.

Rabinovich et al. used cells from human foetal nervous and hemopoietic tissues (146). The clinical trial consisted of 10 patients, 5 male and 5 female, aged between 35 to 56 years, with haemorrhagic or ischaemic stroke (70 percent ischaemic stroke) and stable disability 4 to 24 months post-stroke. All patients had received rehabilitation therapy but showed no improvement. Cells were administered in the subarachnoidal space through spinal puncture. There were no serious complications and positive outcomes were observed in all patients, with significant improvements at 6 months compared to the control group. Positive shifts in neurological status became apparent at 2–3 weeks and progressed in the subsequent 30–50 days.

Between 2003 and 2011, a pilot study using combinations of human foetal tissue olfactory ensheathing cells, neural progenitor cells, umbilical cord mesenchymal cells, and Schwann cells was

conducted. This trial consisted of 10 stroke patients (60 percent ischaemic stroke), 6 male and 4 female, aged between 42 to 87 years, 6 months to 20 years post-stroke. Cells were administered via several routes; intracranial parenchymal implantation, intrathecal implantation, or intravenous administration. Follow up was carried out 6 months to 2 years post-transplantation. The study demonstrated the clinical safety of this combination therapy, and every patient achieved improved neurological function (147).

In another clinical trial for ischaemic stroke patients, human foetal brain-derived neural stem/progenitor cells, and umbilical cord-derived MSC were intravenously administered (148). Neurological function and daily living abilities were improved, and no tumorigenesis was detected at 2 years. The study was small, but further provided evidence of safety and feasibility for cell combination therapy.

The first clinical trial to use NSC for chronic ischaemic stroke began in 2010, called the Pilot Investigation of Stem Cells in Stroke (PISCES) (149). This trial used a clonal cell line (ReNeuron's CTX0E03) of allogeneic human foetal brain-derived NSC genetically modified to express the immortalising gene, MYC. The expression is conditional and activated by tamoxifen, so proliferation and differentiation can be controlled. The phase I trial evaluated the safety of this cell line. Recruited patients were male, over the age of 60, 6 months to 5 years post-stroke, and with stable moderate to severe disability. They received a single dose of either 2, 5, 10, or 20 million cells in a single site (ipsilateral putamen), and data was collected over 2 years. No cell-related adverse events were observed up to the highest dose, and improved neurological function was exhibited. The trial involved a small number of patients, however it provided evidence of safety using this cell line and promising signs of efficacy. A phase II trial has now been started to assess safety and efficacy, and examine functional recovery of upper-limb movement. Patients enrolled include male and female, aged 40 and over, 3 months to 1 year post-stroke, with stable upper-limb disability. The dose of 20 million cells will be administered in a minimum cohort of 21 patients.

CONCLUSION AND FUTURE PERSPECTIVES

Stem cell-based therapy is a promising alternative for stroke treatment. While stem cells from different sources, including induced PSC, ESC, MSC, and NSC, have been investigated, using NSC and enhancing the natural mechanisms is most appropriate for brain repair. In preclinical models of stroke, stem cell transplantation has led to positive outcomes through a variety of cellular and molecular mechanisms, many being mediated by the array of beneficial factors produced by the cells. Recent advances in cellular reprogramming have provided alternative sources of NSC to be investigated, allowing for safer and more efficient induction of NSC. More closely related cells, such as DPSC, are potential candidates for manipulation along the neural lineage. They have provided encouraging outcomes in stroke models and their neural replacement potential may be enhanced if resembling NSC. With more research, the limitations of cellular reprogramming can be overcome, and efficient, safe and reproducible methods for NSC induction can be developed.

AUTHOR CONTRIBUTIONS

MG: research and writing of manuscript. KK, SG, and SK: critical revision of manuscript for important intellectual content.

FUNDING

MG is supported by an Australian Government Research Training Program Scholarship.

REFERENCES

1. Benjamin EJ, Virani SS, Callaway CW, Chamberlain AM, Chang AR, Cheng S, et al. Heart disease and stroke statistics - 2018 update: a report from the american heart association. *Circulation.* (2018) 137:e67–e492. doi: 10.1161/CIR.0000000000000558. [Epub ahead of print].
2. Barthels D, Das H. Current advances in ischemic stroke research and therapies. *Biochim Biophys Acta.* (2018). doi: 10.1016/j.bbadis.2018.09.012. [Epub ahead of print].
3. Nogueira RG, Jadhav AP, Haussen DC, Bonafe A, Budzik RF, Bhuva P, et al. Thrombectomy 6 to 24 hours after stroke with a mismatch between deficit and infarct. *N Engl J Med.* (2018) 378:11–21. doi: 10.1056/NEJMoa1706442
4. Lansberg MG, Bluhmki E, Thijs VN. Efficacy and safety of tissue plasminogen activator 3 to 4.5 hours after acute ischemic stroke: a metaanalysis. *Stroke.* (2009) 40:2438–41. doi: 10.1161/STROKEAHA.109.552547
5. Kelly-Hayes M, Wolf PA, Kase CS, Gresham GE, Kannel WB, D'Agostino RB. Time course of functional recovery after stroke: the Framingham study. *J Neuro Rehab.* (1989) 3:65–70. doi: 10.1177/136140968900300202
6. Mertens J, Marchetto MC, Bardy C, Gage FH. Evaluating cell reprogramming, differentiation and conversion technologies in neuroscience. *Nat Rev Neurosci.* (2016) 17:424–37. doi: 10.1038/nrn.2016.46
7. Gronthos S, Mankani M, Brahim J, Robey PG, Shi S. Postnatal human dental pulp stem cells (DPSCs) *in vitro* and *in vivo*. *Proc Natl Acad Sci USA.* (2000) 97:13625–30. doi: 10.1073/pnas.240309797
8. Martin GR. Isolation of a pluripotent cell line from early mouse embryos cultured in medium conditioned by teratocarcinoma stem cells. *Proc Natl Acad Sci USA.* (1981) 78:7634–8. doi: 10.1073/pnas.78.12.7634
9. Evans MJ, Kaufman MH. Establishment in culture of pluripotent cells from mouse embryos. *Nature.* (1981) 292:154–6. doi: 10.1038/292154a0
10. Thomson JA, Itskovitz-Eldor J, Shapiro SS, Waknitz MA, Swiergiel JJ, Marshall VS, et al. Embryonic stem cell lines derived from human blastocysts. *Science.* (1998) 282:1145–7. doi: 10.1126/science.282.5391.1145
11. Reubinoff BE, Pera MF, Fong CY, Trounson A, Bongso A. Embryonic stem cell lines from human blastocysts: somatic differentiation *in vitro*. *Nat Biotechnol.* (2000) 18:399–404. doi: 10.1038/74447
12. Zhang SC, Wernig M, Duncan ID, Brustle O, Thomson JA. *In vitro* differentiation of transplantable neural precursors from human embryonic stem cells. *Nat Biotechnol.* (2001) 19:1129–33. doi: 10.1038/nbt1201-1129
13. Jopling C, Boue S, Izpisua Belmonte JC. Dedifferentiation, transdifferentiation and reprogramming: three routes to regeneration. *Nat Rev Mol Cell Biol.* (2011) 12:79–89. doi: 10.1038/nrm3043
14. Takahashi K, Yamanaka S. Induction of pluripotent stem cells from mouse embryonic and adult fibroblast cultures by defined factors. *Cell.* (2006) 126:663–76. doi: 10.1016/j.cell.2006.07.024

15. Takahashi K, Tanabe K, Ohnuki M, Narita M, Ichisaka T, Tomoda K, et al. Induction of pluripotent stem cells from adult human fibroblasts by defined factors. *Cell.* (2007) 131:861–72. doi: 10.1016/j.cell.2007.11.019
16. Kim J, Efe JA, Zhu S, Talantova M, Yuan X, Wang S, et al. Direct reprogramming of mouse fibroblasts to neural progenitors. *Proc Natl Acad Sci USA.* (2011) 108:7838–43. doi: 10.1073/pnas.1103113108
17. Ming GL, Song H. Adult neurogenesis in the mammalian brain: significant answers and significant questions. *Neuron.* (2011) 70:687–702. doi: 10.1016/j.neuron.2011.05.001
18. Arvidsson A, Collin T, Kirik D, Kokaia Z, Lindvall O. Neuronal replacement from endogenous precursors in the adult brain after stroke. *Nat Med.* (2002) 8:963–70. doi: 10.1038/nm747
19. Jin K, Wang X, Xie L, Mao XO, Zhu W, Wang Y, et al. Evidence for stroke-induced neurogenesis in the human brain. *Proc Natl Acad Sci USA.* (2006) 103:13198–202. doi: 10.1073/pnas.0603512103
20. Imitola J, Raddassi K, Park KI, Mueller FJ, Nieto M, Teng YD, et al. Directed migration of neural stem cells to sites of CNS injury by the stromal cell-derived factor 1alpha/CXC chemokine receptor 4 pathway. *Proc Natl Acad Sci USA.* (2004) 101:18117–22. doi: 10.1073/pnas.0408258102
21. Kojima T, Hirota Y, Ema M, Takahashi S, Miyoshi I, Okano H, et al. Subventricular zone-derived neural progenitor cells migrate along a blood vessel scaffold toward the post-stroke striatum. *Stem Cells.* (2010) 28:545–54. doi: 10.1002/stem.306
22. Thored P, Arvidsson A, Cacci E, Ahlenius H, Kallur T, Darsalia V, et al. Persistent production of neurons from adult brain stem cells during recovery after stroke. *Stem Cells.* (2006) 24:739–47. doi: 10.1634/stemcells.2005-0281
23. Temple S. Division and differentiation of isolated CNS blast cells in microculture. *Nature.* (1989) 340:471–3. doi: 10.1038/340471a0
24. Reynolds BA, Weiss S. Generation of neurons and astrocytes from isolated cells of the adult mammalian central nervous system. *Science.* (1992) 255:1707–10. doi: 10.1126/science.1553558
25. Altman J, Das GD. Autoradiographic and histological evidence of postnatal hippocampal neurogenesis in rats. *J Compar Neurol.* (1965) 124:319–36. doi: 10.1002/cne.901240303
26. Gage FH, Coates PW, Palmer TD, Kuhn HG, Fisher LJ, Suhonen JO, et al. Survival and differentiation of adult neuronal progenitor cells transplanted to the adult brain. *Proc Natl Acad Sci USA.* (1995) 92:11879–83. doi: 10.1073/pnas.92.25.11879
27. Snyder EY, Deitcher DL, Walsh C, Arnold-Aldea S, Hartwieg EA, Cepko CL. Multipotent neural cell lines can engraft and participate in development of mouse cerebellum. *Cell.* (1992) 68:33–51. doi: 10.1016/0092-8674(92)90204-P
28. Eriksson PS, Perfilieva E, Bjork-Eriksson T, Alborn A, Nordborg C, Peterson DA, et al. Neurogenesis in the adult human hippocampus. *Nat Med.* (1998) 4:1313–7. doi: 10.1038/3305
29. Schwartz PH, Bryant PJ, Fuja TJ, Su H, O'Dowd DK, Klassen H. Isolation and characterization of neural progenitor cells from post-mortem human cortex. *J Neurosci Res.* (2003) 74:838–51. doi: 10.1002/jnr.10854
30. Pagano SF, Impagnatiello F, Girelli M, Cova L, Grioni E, Onofri M, et al. Isolation and characterization of neural stem cells from the adult human olfactory bulb. *Stem Cells.* (2000) 18:295–300. doi: 10.1634/stemcells.18-4-295
31. Carpenter MK, Cui X, Hu Z, Jackson J, Sherman S, Seiger A, et al. *In vitro* expansion of a multipotent population of human neural progenitor cells. *Exp Neurol.* (1999) 158:265–78. doi: 10.1006/exnr.1999.7098
32. Uchida N, Buck DW, He D, Reitsma MJ, Masek M, Phan TV, et al. Direct isolation of human central nervous system stem cells. *PNAS.* (2000) 97:14720–5. doi: 10.1073/pnas.97.26.14720
33. Gronthos S, Brahim J, Li W, Fisher LW, Cherman N, Boyde A, et al. Stem cell properties of human dental pulp stem cells. *J Dent Res.* (2002) 81:531–5. doi: 10.1177/154405910208100806
34. Miura M, Gronthos S, Zhao M, Lu B, Fisher LW, Robey PG, et al. SHED: stem cells from human exfoliated deciduous teeth. *Proc Natl Acad Sci USA.* (2003) 100:5807–12. doi: 10.1073/pnas.0937635100
35. Sonoyama W, Liu Y, Yamaza T, Tuan RS, Wang S, Shi S, et al. Characterization of the apical papilla and its residing stem cells from human immature permanent teeth: a pilot study. *J Endod.* (2008) 34:166–71. doi: 10.1016/j.joen.2007.11.021
36. Yalvac ME, Ramazanoglu M, Rizvanov AA, Sahin F, Bayrak OF, Salli U, et al. Isolation and characterization of stem cells derived from human third molar tooth germs of young adults: implications in neo-vascularization, osteo-, adipo- and neurogenesis. *Pharmacogenomics J.* (2010) 10:105–13. doi: 10.1038/tpj.2009.40
37. Seo BM, Miura M, Gronthos S, Bartold PM, Batouli S, Brahim J, et al. Investigation of multipotent postnatal stem cells from human periodontal ligament. *Lancet.* (2004) 364:149–55. doi: 10.1016/S0140-6736(04)16627-0
38. Park JC, Kim JC, Kim YT, Choi SH, Cho KS, Im GI, et al. Acquisition of human alveolar bone-derived stromal cells using minimally irrigated implant osteotomy: *in vitro* and *in vivo* evaluations. *J Clin Periodontol.* (2012) 39:495–505. doi: 10.1111/j.1600-051X.2012.01865.x
39. Tang L, Li N, Xie H, Jin Y. Characterization of mesenchymal stem cells from human normal and hyperplastic gingiva. *J Cell Physiol.* (2011) 226:832–42. doi: 10.1002/jcp.22405
40. Morsczeck C, Gotz W, Schierholz J, Zeilhofer F, Kuhn U, Mohl C, et al. Isolation of precursor cells (PCs) from human dental follicle of wisdom teeth. *Matrix Biol.* (2005) 24:155–65. doi: 10.1016/j.matbio.2004.12.004
41. Dominici M, Le Blanc K, Mueller I, Slaper-Cortenbach I, Marini FC, Krause D, et al. Minimal criteria for defining multipotent mesenchymal stromal cells. The International Society for Cellular Therapy position statement. *Cytotherapy.* (2006) 8:315–7. doi: 10.1080/14653240600855905
42. Shi S, Gronthos S. Perivascular niche of postnatal mesenchymal stem cells in human bone marrow and dental pulp. *J Bone Miner Res.* (2003) 18:696–704. doi: 10.1359/jbmr.2003.18.4.696
43. Shi S, Robey PG, Gronthos S. Comparison of human dental pulp and done marrow stromal stem cells by cDNA microarray analysis. *Bone.* (2001) 29:532–9. doi: 10.1016/S8756-3282(01)00612-3
44. Zhang W, Walboomers XF, Van Kuppevelt TH, Daamen WF, Van Damme PA, Bian Z, et al. *In vivo* evaluation of human dental pulp stem cells differentiated towards multiple lineages. *J Tissue Eng Regen Med.* (2008) 2:117–25. doi: 10.1002/term.71
45. Govindasamy V, Abdullah AN, Ronald VS, Musa S, Ab Aziz ZA, Zain RB, et al. Inherent differential propensity of dental pulp stem cells derived from human deciduous and permanent teeth. *J Endod.* (2010) 36:1504–15. doi: 10.1016/j.joen.2010.05.006
46. Janebodin K, Horst OV, Ieronimakis N, Balasundaram G, Reesukumal K, Pratumvinit B, et al. Isolation and characterization of neural crest-derived stem cells from dental pulp of neonatal mice. *PLoS ONE.* (2011) 6:e27526. doi: 10.1371/journal.pone.0027526
47. Chai Y, Jiang X, Ito Y, Bringas P, Han J, Rowitch DH, et al. Fate of the mammalian cranial neural crest during tooth and mandibular morphogenesis. *Development.* (2000) 127:1671–9.
48. Yamazaki H, Tsuneto M, Yoshino M, Yamamura K, Hayashi S. Potential of dental mesenchymal cells in developing teeth. *Stem Cells.* (2007) 25:78–87. doi: 10.1634/stemcells.2006-0360
49. Kaukua N, Shahidi MK, Konstantinidou C, Dyachuk V, Kaucka M, Furlan A, et al. Glial origin of mesenchymal stem cells in a tooth model system. *Nature.* (2014) 513:551–4. doi: 10.1038/nature13536
50. Arthur A, Rychkov G, Shi S, Koblar SA, Gronthos S. Adult human dental pulp stem cells differentiate toward functionally active neurons under appropriate environmental cues. *Stem Cells.* (2008) 26:1787–95. doi: 10.1634/stemcells.2007-0979
51. Kiraly M, Porcsalmy B, Pataki A, Kadar K, Jelitai M, Molnar B, et al. Simultaneous PKC and cAMP activation induces differentiation of human dental pulp stem cells into functionally active neurons. *Neurochem Int.* (2009) 55:323–32. doi: 10.1016/j.neuint.2009.03.017
52. Gronthos S, Simmons PJ. The growth factor requirements of STRO-1-positive human bone marrow stromal precursors under serum-deprived conditions *in vitro*. *Blood.* (1995) 85:929–40.
53. Pan W, Kremer KL, Kaidonis X, Ludlow VE, Rogers ML, Xie J, et al. Characterization of p75 neurotrophin receptor expression in human dental pulp stem cells. *Int J Dev Neurosci.* (2016) 53:90–8. doi: 10.1016/j.ijdevneu.2016.07.007
54. Hilkens P, Gervois P, Fanton Y, Vanormelingen J, Martens W, Struys T, et al. Effect of isolation methodology on stem cell properties and multilineage differentiation potential of hDPSCs. *Cell Tissue Res.* (2013) 353:65–78. doi: 10.1007/s00441-013-1630-x

55. Liu L, Wei X, Ling J, Wu L, Xiao Y. Expression pattern of Oct-4, Sox2, and c-Myc in the primary culture of human dental pulp derived cells. *J Endod.* (2011) 37:466–72. doi: 10.1016/j.joen.2010.12.012
56. Wilson R, Urraca N, Skobowiat C, Hope KA, Miravalle L, Chamberlin R, et al. Assessment of the tumorigenic potential of spontaneously immortalized and hTERT-immortalized cultured dental pulp stem cells. *Stem Cells Transl Med.* (2015) 4:905–12. doi: 10.5966/sctm.2014-0196
57. Davidson RM. Neural form of voltage-dependent sodium current in human cultured dental pulp cells. *Archs Oral Biology.* (1994) 39:613–20. doi: 10.1016/0003-9969(94)90137-6
58. Ullah I, Subbarao RB, Kim EJ, Bharti D, Jang SJ, Park JS, et al. *In vitro* comparative analysis of human dental stem cells from a single donor and its neuronal differentiation potential evaluated by electrophysiology. *Life Sci.* (2016) 154:39–51. doi: 10.1016/j.lfs.2016.04.026
59. Kiraly M, Kadar K, Horvathy DB, Nardai P, Racz GZ, Lacza Z, et al. Integration of neuronally predifferentiated human dental pulp stem cells into rat brain *in vivo*. *Neurochem Int.* (2011) 59:371–81. doi: 10.1016/j.neuint.2011.01.006
60. Arthur A, Shi S, Zannettino AC, Fujii N, Gronthos S, Koblar SA. Implanted adult human dental pulp stem cells induce endogenous axon guidance. *Stem Cells.* (2009) 27:2229–37. doi: 10.1002/stem.138
61. Kanafi M, Majumdar D, Bhonde R, Gupta P, Datta I. Midbrain cues dictate differentiation of human dental pulp stem cells towards functional dopaminergic neurons. *J Cell Physiol.* (2014) 229:1369–77. doi: 10.1002/jcp.24570
62. Singh M, Kakkar A, Sharma R, Kharbanda OP, Monga N, Kumar M, et al. Synergistic effect of BDNF and FGF2 in efficient generation of functional dopaminergic neurons from human mesenchymal stem cells. *Sci Rep.* (2017) 7:10378. doi: 10.1038/s41598-017-11028-z
63. Gonmanee T, Thonabulsombat C, Vongsavan K, Sritanaudomchai H. Differentiation of stem cells from human deciduous and permanent teeth into spiral ganglion neuron-like cells. *Arch Oral Biol.* (2018) 88:34–41. doi: 10.1016/j.archoralbio.2018.01.011
64. Jung J, Kim JW, Moon HJ, Hong JY, Hyun JK. Characterization of neurogenic potential of dental pulp stem cells cultured in xeno/serum-free condition: *in vitro* and *in vivo* assessment. *Stem Cells Int.* (2016) 2016:6921097. doi: 10.1155/2016/6921097
65. Gervois P, Struys T, Hilkens P, Bronckaers A, Ratajczak J, Politis C, et al. Neurogenic maturation of human dental pulp stem cells following neurosphere generation induces morphological and electrophysiological characteristics of functional neurons. *Stem Cells Dev.* (2015) 24:296–311. doi: 10.1089/scd.2014.0117
66. Osathanon T, Sawangmake C, Nowwarote N, Pavasant P. Neurogenic differentiation of human dental pulp stem cells using different induction protocols. *Oral Dis.* (2014) 20:352–8. doi: 10.1111/odi.12119
67. Pisciotta A, Bertoni L, Riccio M, Mapelli J, Bigiani A, La Noce M, et al. Use of a 3D floating sphere culture system to maintain the neural crest-related properties of human dental pulp stem cells. *Front Physiol.* (2018) 9:547. doi: 10.3389/fphys.2018.00547
68. Yang KL, Chen MF, Liao CH, Pang CY, Lin PY. A simple and efficient method for generating Nurr1-positive neuronal stem cells from human wisdom teeth (tNSC) and the potential of tNSC for stroke therapy. *Cytotherapy.* (2009) 11:606–17. doi: 10.1080/14653240902806994
69. Leong WK, Henshall TL, Arthur A, Kremer KL, Lewis MD, Helps SC, et al. Human adult dental pulp stem cells enhance poststroke functional recovery through non-neural replacement mechanisms. *Stem Cells Transl Med.* (2012) 1:177–87. doi: 10.5966/sctm.2011-0039
70. Nosrat IV, Smith CA, Mullally P, Olson L, Nosrat CA. Dental pulp cells provide neurotrophic support for dopaminergic neurons and differentiate into neurons *in vitro*; implications for tissue engineering and repair in the nervous system. *Eur J Neurosci.* (2004) 19:2388–98. doi: 10.1111/j.0953-816X.2004.03314.x
71. Nito C, Sowa K, Nakajima M, Sakamoto Y, Suda S, Nishiyama Y, et al. Transplantation of human dental pulp stem cells ameliorates brain damage following acute cerebral ischemia. *Biomed Pharmacother.* (2018) 108:1005–14. doi: 10.1016/j.biopha.2018.09.084
72. Hill WD, Hess DC, Martin-Studdard A, Carothers JJ, Zheng J, Hale D, et al. SDF-1 (CXCL12) is upregulated in the ischemic penumbra following stroke association with bone marrow cell homing to injury. *J Neuropathol Exp Neurol.* (2004) 63:84–96. doi: 10.1093/jnen/63.1.84
73. Winderlich JN, Kremer KL, Koblar SA. Adult human dental pulp stem cells promote blood-brain barrier permeability through vascular endothelial growth factor-a expression. *J Cereb Blood Flow Metab.* (2016) 36:1087–97. doi: 10.1177/0271678X15608392
74. Shen LH, Li Y, Chen J, Zacharek A, Gao Q, Kapke A, et al. Therapeutic benefit of bone marrow stromal cells administered 1 month after stroke. *J Cereb Blood Flow Metab.* (2007) 27:6–13. doi: 10.1038/sj.jcbfm.9600311
75. Song M, Lee JH, Bae J, Bu Y, Kim EC. Human dental pulp stem cells are more effective than human bone marrow-derived mesenchymal stem cells in cerebral ischemic injury. *Cell Transplant.* (2017) 26:1001–16. doi: 10.3727/096368916X694391
76. Sowa K, Nito C, Nakajima M, Suda S, Nishiyama Y, Sakamoto Y, et al. Impact of dental pulp stem cells overexpressing hepatocyte growth factor after cerebral ischemia/reperfusion in rats. *Mol Ther Methods Clin Dev.* (2018) 10:281–90. doi: 10.1016/j.omtm.2018.07.009
77. Bronckaers A, Hilkens P, Fanton Y, Struys T, Gervois P, Politis C, et al. Angiogenic properties of human dental pulp stem cells. *PLoS ONE.* (2013) 8:e71104. doi: 10.1371/journal.pone.0071104
78. Argaw AT, Gurfein BT, Zhang Y, Zameer A, John GR. VEGF-mediated disruption of endothelial CLN-5 promotes blood-brain barrier breakdown. *Proc Natl Acad Sci USA.* (2009) 106:1977–82. doi: 10.1073/pnas.0808698106
79. Shimamura M, Sato N, Oshima K, Aoki M, Kurinami H, Waguri S, et al. Novel therapeutic strategy to treat brain ischemia: overexpression of hepatocyte growth factor gene reduced ischemic injury without cerebral edema in rat model. *Circulation.* (2004) 109:424–31. doi: 10.1161/01.CIR.0000109496.82683.49
80. Zhang X, Zhou Y, Li H, Wang R, Yang D, Li B, et al. Intravenous administration of DPSCs and BDNF improves neurological performance in rats with focal cerebral ischemia. *Int J Mol Med.* (2018) 41:3185–94. doi: 10.3892/ijmm.2018.3517
81. Kumasaka A, Kanazawa K, Ohke H, Miura I, Miura Y. Post-ischemic intravenous administration of allogeneic dental pulp-derived neurosphere cells ameliorated outcomes of severe forebrain ischemia in rats. *Neurocrit Care.* (2017) 26:133–42. doi: 10.1007/s12028-016-0304-4
82. Matsui M, Kobayashi T, Tsutsui TW. CD146 positive human dental pulp stem cells promote regeneration of dentin/pulp-like structures. *Hum Cell.* (2018) 31:127–38. doi: 10.1007/s13577-017-0198-2
83. Sugiyama M, Iohara K, Wakita H, Hattori H, Ueda M, Matsushita K, et al. Dental pulp-derived CD31-/CD146- side population stem/progenitor cells enhance recovery of focal cerebral ischemia in rats.pdf>. *Tissue Eng A.* (2011) 17:1303–11. doi: 10.1089/ten.tea.2010.0306
84. Pisciotta A, Carnevale G, Meloni S, Riccio M, De Biasi S, Gibellini L, et al. Human dental pulp stem cells (hDPSCs): isolation, enrichment and comparative differentiation of two sub-populations. *BMC Dev Biol.* (2015) 15:14. doi: 10.1186/s12861-015-0065-x
85. Wada N, Menicanin D, Shi S, Bartold PM, Gronthos S. Immunomodulatory properties of human periodontal ligament stem cells. *J Cell Physiol.* (2009) 219:667–76. doi: 10.1002/jcp.21710
86. Tamaoki N, Takahashi K, Tanaka T, Ichisaka T, Aoki H, Takeda-Kawaguchi T, et al. Dental pulp cells for induced pluripotent stem cell banking. *J Dent Res.* (2010) 89:773–8. doi: 10.1177/0022034510366846
87. Yan X, Qin H, Qu C, Tuan RS, Shi S, Huang GT. iPS cells reprogrammed from human mesenchymal-like stem/progenitor cells of dental tissue origin. *Stem Cells Dev.* (2010) 19:469–80. doi: 10.1089/scd.2009.0314
88. Chang YC, Li WC, Twu NF, Li HY, Lo WL, Chang YL, et al. Induction of dental pulp-derived induced pluripotent stem cells in the absence of c-Myc for differentiation into neuron-like cells. *J Chin Med Assoc.* (2014) 77:618–25. doi: 10.1016/j.jcma.2014.08.009
89. Lujan E, Chanda S, Ahlenius H, Sudhof TC, Wernig M. Direct conversion of mouse fibroblasts to self-renewing, tripotent neural precursor cells. *Proc Natl Acad Sci USA.* (2012) 109:2527–32. doi: 10.1073/pnas.1121003109
90. Han DW, Tapia N, Hermann A, Hemmer K, Hoing S, Arauzo-Bravo MJ, et al. Direct reprogramming of fibroblasts into neural stem cells by defined factors. *Cell Stem Cell.* (2012) 10:465–72. doi: 10.1016/j.stem.2012.02.021
91. Ring KL, Tong LM, Balestra ME, Javier R, Andrews-Zwilling Y, Li G, et al. Direct reprogramming of mouse and human fibroblasts into multipotent

neural stem cells with a single factor. *Cell Stem Cell.* (2012) 11:100–9. doi: 10.1016/j.stem.2012.05.018
92. Thier M, Worsdorfer P, Lakes YB, Gorris R, Herms S, Opitz T, et al. Direct conversion of fibroblasts into stably expandable neural stem cells. *Cell Stem Cell.* (2012) 10:473–9. doi: 10.1016/j.stem.2012.03.003
93. Vierbuchen T, Ostermeier A, Pang ZP, Kokubu Y, Sudhof TC, Wernig M. Direct conversion of fibroblasts to functional neurons by defined factors. *Nature.* (2010) 463:1035–41. doi: 10.1038/nature08797
94. Pang ZP, Yang N, Vierbuchen T, Ostermeier A, Fuentes DR, Yang TQ, et al. Induction of human neuronal cells by defined transcription factors. *Nature.* (2011) 476:220–3. doi: 10.1038/nature10202
95. Marro S, Pang ZP, Yang N, Tsai MC, Qu K, Chang HY, et al. Direct lineage conversion of terminally differentiated hepatocytes to functional neurons. *Cell Stem Cell.* (2011) 9:374–82. doi: 10.1016/j.stem.2011.09.002
96. Chanda S, Ang CE, Davila J, Pak C, Mall M, Lee QY, et al. Generation of induced neuronal cells by the single reprogramming factor ASCL1. *Stem Cell Rep.* (2014) 3:282–96. doi: 10.1016/j.stemcr.2014.05.020
97. Wapinski OL, Vierbuchen T, Qu K, Lee QY, Chanda S, Fuentes DR, et al. Hierarchical mechanisms for direct reprogramming of fibroblasts to neurons. *Cell.* (2013) 155:621–35. doi: 10.1016/j.cell.2013.09.028
98. Bar-Nur O, Verheul C, Sommer AG, Brumbaugh J, Schwarz BA, Lipchina I, et al. Lineage conversion induced by pluripotency factors involves transient passage through an iPSC stage. *Nat Biotechnol.* (2015) 33:761–8. doi: 10.1038/nbt.3247
99. Maza I, Caspi I, Zviran A, Chomsky E, Rais Y, Viukov S, et al. Transient acquisition of pluripotency during somatic cell transdifferentiation with iPSC reprogramming factors. *Nat Biotechnol.* (2015) 33:769–74. doi: 10.1038/nbt.3270
100. Maucksch C, Firmin E, Butler-Munro C, Montgomery JM, Dottori M, Connor B. Non-viral generation of neural precursor-like cells from adult human fibroblasts. *J Stem Cells Regenerat Med.* (2012) 8:162–70.
101. Hemmer K, Zhang M, van Wullen T, Sakalem M, Tapia N, Baumuratov A, et al. Induced neural stem cells achieve long-term survival and functional integration in the adult mouse brain. *Stem Cell Reports.* (2014) 3:423–31. doi: 10.1016/j.stemcr.2014.06.017
102. Hallmann AL, Arauzo-Bravo MJ, Zerfass C, Senner V, Ehrlich M, Psathaki OE, et al. Comparative transcriptome analysis in induced neural stem cells reveals defined neural cell identities *in vitro* and after transplantation into the adult rodent brain. *Stem Cell Res.* (2016) 16:776–81. doi: 10.1016/j.scr.2016.04.015
103. Sterneckert J, Hoing S, Scholer HR. Concise review: Oct4 and more: the reprogramming expressway. *Stem Cells.* (2012) 30:15–21. doi: 10.1002/stem.765
104. Mitchell R, Szabo E, Shapovalova Z, Aslostovar L, Makondo K, Bhatia M. Molecular evidence for OCT4-induced plasticity in adult human fibroblasts required for direct cell fate conversion to lineage specific progenitors. *Stem Cells.* (2014) 32:2178–87. doi: 10.1002/stem.1721
105. Mitchell RR, Szabo E, Benoit YD, Case DT, Mechael R, Alamilla J, et al. Activation of neural cell fate programs toward direct conversion of adult human fibroblasts into tri-potent neural progenitors using OCT-4. *Stem Cells Dev.* (2014) 23:1937–46. doi: 10.1089/scd.2014.0023
106. Liao W, Huang N, Yu J, Jares A, Yang J, Zieve G, et al. Direct conversion of cord blood CD34+ cells into neural stem cells by OCT4. *Stem Cells Transl Med.* (2015) 4:755–63. doi: 10.5966/sctm.2014-0289
107. Lee JH, Mitchell RR, McNicol JD, Shapovalova Z, Laronde S, Tanasijevic B, et al. Single transcription factor conversion of human blood fate to NPCs with CNS and PNS developmental capacity. *Cell Rep.* (2015) 11:1367–76. doi: 10.1016/j.celrep.2015.04.056
108. Giorgetti A, Marchetto MCN, Li M, Yu D, Fazzina R, Mu Y, et al. Cord blood-derived neuronal cells by ectopic expression of Sox2 and cMyc. *PNAS.* (2012) 109:12556–61. doi: 10.1073/pnas.1209523109
109. Castano J, Menendez P, Bruzos-Cidon C, Straccia M, Sousa A, Zabaleta L, et al. Fast and efficient neural conversion of human hematopoietic cells. *Stem Cell Rep.* (2014) 3:1118–31. doi: 10.1016/j.stemcr.2014.10.008
110. Maucksch C, Jones KS, Connor B. Concise review: the involvement of SOX2 in direct reprogramming of induced neural stem/precursor cells. *Stem Cells Transl Med.* (2013) 2:579–83. doi: 10.5966/sctm.2012-0179
111. Hanna J, Saha K, Pando B, van Zon J, Lengner CJ, Creyghton MP, et al. Direct cell reprogramming is a stochastic process amenable to acceleration. *Nature.* (2009) 462:595–601. doi: 10.1038/nature08592
112. Yoo AS, Sun AX, Li L, Shcheglovitov A, Portmann T, Li Y, et al. MicroRNA-mediated conversion of human fibroblasts to neurons. *Nature.* (2011) 476:228–31. doi: 10.1038/nature10323
113. Han YC, Lim Y, Duffieldl MD, Li H, Liu J, Abdul Manaph NP, et al. Direct reprogramming of mouse fibroblasts to neural stem cells by small molecules. *Stem Cells Int.* (2016) 2016:4304916. doi: 10.1155/2016/4304916
114. Zheng J, Choi KA, Kang PJ, Hyeon S, Kwon S, Moon JH, et al. A combination of small molecules directly reprograms mouse fibroblasts into neural stem cells. *Biochem Biophys Res Commun.* (2016) 476:42–8. doi: 10.1016/j.bbrc.2016.05.080
115. Liu L, Wu L, Wei X, Ling J. Induced overexpression of Oct4A in human dental pulp cells enhances pluripotency and multilineage differentiation capability. *Stem Cells Dev.* (2015) 24:962–72. doi: 10.1089/scd.2014.0388
116. Liu P, Cai J, Dong D, Chen Y, Liu X, Wang Y, et al. Effects of SOX2 on proliferation, migration and adhesion of human dental pulp stem cells. *PLoS ONE.* (2015) 10:e0141346. doi: 10.1371/journal.pone.0141346
117. Yao H, Gao M, Ma J, Zhang M, Li S, Wu B, et al. Transdifferentiation-induced neural stem cells promote recovery of middle cerebral artery stroke rats. *PLoS ONE.* (2015) 10:e0137211. doi: 10.1371/journal.pone.0137211
118. Yuan T, Liao W, Feng N-H, Lou Y-L, Niu X, Zhang A-J, et al. Human induced pluripotent stem cell-derived neural stem cells survive, migrate, differentiate, and improve neurologic function in a rat model of middle cerebral artery occlusion. *Stem Cell Res Ther.* (2013) 4:1–10. doi: 10.1186/scrt224
119. Jin K, Xie L, Mao X, Greenberg MB, Moore A, Peng B, et al. Effect of human neural precursor cell transplantation on endogenous neurogenesis after focal cerebral ischemia in the rat. *Brain Res.* (2011) 1374:56–62. doi: 10.1016/j.brainres.2010.12.037
120. Mine Y, Tatarishvili J, Oki K, Monni E, Kokaia Z, Lindvall O. Grafted human neural stem cells enhance several steps of endogenous neurogenesis and improve behavioral recovery after middle cerebral artery occlusion in rats. *Neurobiol Dis.* (2013) 52:191–203. doi: 10.1016/j.nbd.2012.12.006
121. Kelly S, Bliss TM, Shah AK, Sun GH, Ma M, Foo WC, et al. Transplanted human fetal neural stem cells survive, migrate, and differentiate in ischemic rat cerebral cortex. *Proc Natl Acad Sci USA.* (2004) 101:11839–44. doi: 10.1073/pnas.0404474101
122. Chu K, Kim M, Park KI, Jeong SW, Park HK, Jung KH, et al. Human neural stem cells improve sensorimotor deficits in the adult rat brain with experimental focal ischemia. *Brain Res.* (2004) 1016:145–53. doi: 10.1016/j.brainres.2004.04.038
123. Darsalia V, Kallur T, Kokaia Z. Survival, migration and neuronal differentiation of human fetal striatal and cortical neural stem cells grafted in stroke-damaged rat striatum. *Eur J Neurosci.* (2007) 26:605–14. doi: 10.1111/j.1460-9568.2007.05702.x
124. Andres RH, Horie N, Slikker W, Keren-Gill H, Zhan K, Sun G, et al. Human neural stem cells enhance structural plasticity and axonal transport in the ischaemic brain. *Brain.* (2011) 134(Pt 6):1777–89. doi: 10.1093/brain/awr094
125. de la Rosa-Prieto C, Laterza C, Gonzalez-Ramos A, Wattananit S, Ge R, Lindvall O, et al. Stroke alters behavior of human skin-derived neural progenitors after transplantation adjacent to neurogenic area in rat brain. *Stem Cell Res Ther.* (2017) 8:59. doi: 10.1186/s13287-017-0513-6
126. Zhang P, Li J, Liu Y, Chen X, Lu H, Kang Q, et al. Human embryonic neural stem cell transplantation increases subventricular zone cell proliferation and promotes peri-infarct angiogenesis after focal cerebral ischemia. *Neuropathology.* (2011) 31:384–91. doi: 10.1111/j.1440-1789.2010.01182.x
127. Ryu S, Lee SH, Kim SU, Yoon BW. Human neural stem cells promote proliferation of endogenous neural stem cells and enhance angiogenesis in ischemic rat brain. *Neural Regen Res.* (2016) 11:298–304. doi: 10.4103/1673-5374.177739
128. Darsalia V, Allison SJ, Cusulin C, Monni E, Kuzdas D, Kallur T, et al. Cell number and timing of transplantation determine survival of human neural stem cell grafts in stroke-damaged rat brain. *J Cereb Blood Flow Metab.* (2011) 31:235–42. doi: 10.1038/jcbfm.2010.81
129. Takahashi K, Yasuhara T, Shingo T, Muraoka K, Kameda M, Takeuchi A, et al. Embryonic neural stem cells transplanted in middle cerebral artery occlusion model of rats demonstrated potent therapeutic effects,

compared to adult neural stem cells. *Brain Res.* (2008) 1234:172–82. doi: 10.1016/j.brainres.2008.07.086

130. Andsberg G, Kokaia Z, Bjorklund A, Lindvall O, Martinez-Serrano A. Amelioration of ischaemia-induced neuronal death in the rat striatum by NGF-secreting neural stem cells. *Eur J Neurosci.* (1998) 10:2026–36. doi: 10.1046/j.1460-9568.1998.00214.x
131. Zhu W, Mao Y, Zhao Y, Zhou LF, Wang Y, Zhu JH, et al. Transplantation of vascular endothelial growth factor-transfected neural stem cells into the rat brain provides neuroprotection after transient focal cerebral ischemia. *Neurosurgery.* (2005) 57:325–33. doi: 10.1227/01.NEU.0000166682.50272.BC
132. Park KI, Himes BT, Stieg PE, Tessler A, Fischer I, Snyder EY. Neural stem cells may be uniquely suited for combined gene therapy and cell replacement: evidence from engraftment of Neurotrophin-3-expressing stem cells in hypoxic-ischemic brain injury. *Exp Neurol.* (2006) 199:179–90. doi: 10.1016/j.expneurol.2006.03.016
133. Zhang ZH, Wang RZ, Wang RZ, Li GL, Wei JJ, Li ZJ, et al. Transplantation of neural stem cells modified by human neurotrophin-3 promotes functional recovery after transient focal cerebral ischemia in rats. *Neurosci Lett.* (2008) 444:227–30. doi: 10.1016/j.neulet.2008.08.049
134. Chen B, Gao XQ, Yang CX, Tan SK, Sun ZL, Yan NH, et al. Neuroprotective effect of grafting GDNF gene-modified neural stem cells on cerebral ischemia in rats. *Brain Res.* (2009) 1284:1–11. doi: 10.1016/j.brainres.2009.05.100
135. Zhu JM, Zhao YY, Chen SD, Zhang WH, Lou L, Jin X. Functional recovery after transplantation of neural stem cells modified by brain-derived neurotrophic factor in rats with cerebral ischaemia. *J Int Med Res.* (2011) 39:488–98. doi: 10.1177/147323001103900216
136. Chang DJ, Lee N, Choi C, Jeon I, Oh SH, Shin DA, et al. Therapeutic effect of BDNF-overexpressing human neural stem cells (HB1.F3.BDNF) in a rodent model of middle cerebral artery occlusion. *Cell Transplant.* (2013) 22:1441–52. doi: 10.3727/096368912X657323
137. Zhang J-J, Zhu J-J, Hu Y-B, Xiang G-H, Deng L-C, Wu F-Z, et al. Transplantation of bFGF-expressing neural stem cells promotes cell migration and functional recovery in rat brain after transient ischemic stroke. *Oncotarget.* (2017) 8:102067–77. doi: 10.18632/oncotarget.22155
138. Rosenblum S, Smith TN, Wang N, Chua JY, Westbroek E, Wang K, et al. BDNF pretreatment of human embryonic-derived neural stem cells improves cell survival and functional recovery after transplantation in hypoxic-ischemic stroke. *Cell Transplant.* (2015) 24:2449–61. doi: 10.3727/096368914X679354
139. Theus MH, Wei L, Cui L, Francis K, Hu X, Keogh C, et al. *In vitro* hypoxic preconditioning of embryonic stem cells as a strategy of promoting cell survival and functional benefits after transplantation into the ischemic rat brain. *Exp Neurol.* (2008) 210:656–70. doi: 10.1016/j.expneurol.2007.12.020
140. Wu W, Chen X, Hu C, Li J, Yu Z, Cai W. Transplantation of neural stem cells expressing hypoxia-inducible factor-1alpha (HIF-1alpha) improves behavioral recovery in a rat stroke model. *J Clin Neurosci.* (2010) 17:92–5. doi: 10.1016/j.jocn.2009.03.039
141. Sakata H, Niizuma K, Wakai T, Narasimhan P, Maier CM, Chan PH. Neural stem cells genetically modified to overexpress cu/zn-superoxide dismutase enhance amelioration of ischemic stroke in mice. *Stroke.* (2012) 43:2423–9. doi: 10.1161/STROKEAHA.112.656900
142. Shen SW, Duan CL, Chen XH, Wang YQ, Sun X, Zhang QW, et al. Neurogenic effect of VEGF is related to increase of astrocytes transdifferentiation into new mature neurons in rat brains after stroke. *Neuropharmacology.* (2016) 108:451–61. doi: 10.1016/j.neuropharm.2015.11.012
143. Rosenblum S, Wang N, Smith TN, Pendharkar AV, Chua JY, Birk H, et al. Timing of intra-arterial neural stem cell transplantation after hypoxia-ischemia influences cell engraftment, survival, and differentiation. *Stroke.* (2012) 43:1624–31. doi: 10.1161/STROKEAHA.111.637884
144. Kondziolka D, Wechsler L, Goldstein S, Meltzer C, Thulborn KR, Gebel J, et al. Transplantation of cultured human neuronal cells for patients with stroke. *Neurology.* (2000) 55:565–9. doi: 10.1212/WNL.55.4.565
145. Kondziolka D, Steinberg GK, Wechsler L, Meltzer CC, Elder E, Gebel J, et al. Neurotransplantation for patients with subcortical motor stroke: a phase 2 randomized trial. *J Neurosurg.* (2005) 103:38–45. doi: 10.3171/jns.2005.103.1.0038
146. Rabinovich SS, Seledtsov VI, Banul NV, Poveshchenko OV, Senyukov VV, Astrakov SV, et al. Cell therapy of brain stroke. *Cell Technol Biol Med.* (2005) 1:126–8. doi: 10.1007/s10517-005-0229-y
147. Chen L, Xi H, Huang H, Zhang F, Liu Y, Chen D, et al. Multiple cell transplantation based on an intraparenchymal approach for patients with chronic phase stroke. *Cell Transplant.* (2013) 22(Suppl. 1):S83–91. doi: 10.3727/096368913X672154
148. Qiao LY, Huang FJ, Zhao M, Xie JH, Shi J, Wang J, et al. A two-year follow-up study of cotransplantation with neural stem/progenitor cells and mesenchymal stromal cells in ischemic stroke patients. *Cell Transplant.* (2014) 23:65–72. doi: 10.3727/096368914X684961
149. Kalladka D, Sinden J, Pollock K, Haig C, McLean J, Smith W, et al. Human neural stem cells in patients with chronic ischaemic stroke (PISCES): a phase 1, first-in-man study. *Lancet.* (2016) 2016:1–10. doi: 10.1016/S0140-6736(16)30513-X

Conflict of Interest Statement: The authors declare that the research was conducted in the absence of any commercial or financial relationships that could be construed as a potential conflict of interest.

Copyright © 2019 Gancheva, Kremer, Gronthos and Koblar. This is an open-access article distributed under the terms of the Creative Commons Attribution License (CC BY). The use, distribution or reproduction in other forums is permitted, provided the original author(s) and the copyright owner(s) are credited and that the original publication in this journal is cited, in accordance with accepted academic practice. No use, distribution or reproduction is permitted which does not comply with these terms.

1.3 | Summary

1.3.1 Project Rationale

Dental pulp stem cells (DPSC) have been identified as promising candidates for cell-based therapies of neurological diseases, such as stroke. Research has demonstrated that DPSC exhibit neurogenic properties under specific environmental conditions, both *in vitro* and *in vivo* (1-3). This is believed to be attributed to their mesoectodermal origin, with a sub-population of DPSC deriving from the cranial neural crest stem cells during embryonic development (4-7). Whilst DPSC have led to positive neurobehavioural outcomes in stroke models, this has been mediated mostly through paracrine effects (8, 9). In order to enhance their neural potential, including their ability to replace cells, they may need to become more neural. As such, we aimed to convert human DPSC into neural stem cells (NSC) using cellular reprogramming techniques. It is believed that since DPSC are of closer origin to the desired cell type, they may require less manipulation or may be more efficiently converted than cells that are further in origin. Additionally, DPSC are clinically easily obtained and they have a high proliferation rate giving them further advantages for such applications. Developing a method to convert human DPSC into NSC would enhance the DPSC neural potential, to better survive, differentiate and influence the local environment *in vivo*, and hence provide greater improvement in neurobehavioural function when applied in cell-based therapy for stroke.

1.3.2 Hypothesis and Research Aims

The hypothesis is that human DPSC can be reprogrammed into NSC using specific transcription factors under defined neural culture conditions.

To address the hypothesis, three research aims were developed:

1) To investigate the ability to reprogram human DPSC into NSC using selected transcription factors in neural culture conditions.

2) To characterise the reprogrammed DPSC using transcriptome-wide analysis of differentially expressed genes, using RNA-sequencing.

3) To investigate the response of the reprogrammed DPSC *in vivo*, using a developmental assay (chicken embryo).

For the scope of this PhD, three transcription factors were selected for initial analysis in human DPSC. These transcription factors were selected based on previously published research in the cellular reprogramming field and their known developmental roles. The selected transcription factors were OCT4, SOX2 and HES1.

OCT4 (octamer-binding transcription factor 4), encoded by the *POU5F1* (POU (Pit-Oct-Unc) domain, class 5, transcription factor 1) gene, is a key transcriptional regulator of pluripotency. It is a transcription factor of the POU family of DNA-binding proteins, and binds an octameric DNA sequence in the promoter and enhancer regions of target genes. OCT4 is highly expressed in embryonic stem cells (ESC) and is crucial for early embryonic development (10). Without OCT4, the lack of pluripotent stem cells at the inner cell mass stage leads to death of the embryo (10). OCT4 is decreased during differentiation of ESC, however the level of OCT4 expression is important in determining the fate of the stem cells (10). It has been proposed that OCT4 induces plasticity, allowing other transcription factors and conditions to guide the cells down the desired lineage (11, 12). Using only OCT4, reprogramming of fibroblasts and blood cells into NSC has been achieved (12-15). In DPSC, OCT4 over-expression enhanced multi-lineage differentiation potential, however the neural lineage remains to be investigated (16). Forced expression of OCT4 may revert the cells to an earlier developmental stage, making them receptive to signalling pathways, via molecules such as basic fibroblast growth factor (bFGF) and epidermal growth factor (EGF) present in neural cultures, for differentiation along the neural lineage. These signalling pathways may lead to expression of more neural-specific transcription factors. OCT4 itself could implicate factors directly, such as SOX2 (10).

The SOX2 (SRY (sex determining region Y)-box 2) transcription factor, encoded by the *SOX2* gene, is also a key regulator of pluripotency. It is a member of the SOX family of transcription factors, containing a highly conserved high-mobility-group DNA binding domain, which have important roles in development. Together SOX2, OCT4 and NANOG regulate many genes for self-renewal and pluripotency, as well as their own expression (17). SOX2 heterodimerises with OCT4 on some target genes (18). OCT4 also binds genes that regulate SOX2 expression (17). Like OCT4, the expression level of SOX2 is tightly regulated. It has a role in maintaining multiple stem cell populations, including ESC and NSC (17, 18). Early in embryonic development, removal of SOX2 is lethal. SOX2 is expressed during brain development in the neural tube and subsequently in neural stem and progenitor cells of the adult brain. Whilst SOX2 is expressed in stem and progenitor cells, it also has a role in ensuring proper neuronal differentiation (17, 18). SOX2 has been used individually to reprogram fibroblasts into NSC (19). In DPSC, SOX2 has been over-expressed but the effect on multi-lineage differentiation and specifically the neural lineage has not been investigated (20). Due to the known roles in neural development and expression in neural stem and progenitor cells, SOX2 was selected to be investigated.

HES1 (HES (hairy and enhancer of split) family, transcription factor 1), a transcription factor encoded by the *HES1* gene, belongs to the basic helix-loop-helix (bHLH) family of transcription factors, which have roles in critical developmental processes. It is one member of the HES family, with several of them having roles in the central nervous system (CNS) (21). It is a transcriptional repressor of genes that require a bHLH transcriptional activator. In the context of neural development, the main target of HES factors are bHLH proneural transcription factors, responsible for neuronal determination (22). HES1 can inhibit proneural transcriptional activators, such as ASCL1 and NEUROG2, by direct transcriptional repression as a homodimer or heterodimer with other repressors, such as HEY1 (23). It can also inhibit them indirectly by physical interaction with the activators themselves, thereby preventing them from binding to DNA (23). HES1 regulates its own expression via a negative feedback loop (21, 23). During development, HES1 is expressed in NSC, which include neuroepithelial cells and radial glial cells. In the adult brain, it is expressed in the neurogenic niches (22). HES1 regulates cell proliferation and differentiation in the CNS, and acts through the Notch signalling pathway (23). When HES1 is inactivated, along with the other HES genes so there is no compensation, proneural gene expression is increased and neurogenesis proceeds while the NSC pool is depleted (22). When HES1 is over-expressed, neurogenesis is inhibited while the NSC population is maintained (23). HES1 has been included in a panel of reprogramming factors to convert cells of mesodermal origin into NSC (24). Due to its importance in maintaining NSC populations, it was selected to be investigated in DPSC.

CHAPTER 2

MATERIALS AND GENERAL METHODS

2.1 | Reagents

Table 2.1 Reagent list.

Reagent	Company	Catalogue Number
α-modification Eagle's Minimal Essential Medium	Sigma-Aldrich	M4526
β-glycerophosphate	Sigma-Aldrich	G9422
β-mercaptoethanol	Sigma-Aldrich	M3148
1kb DNA Ladder	New England Biolabs	N3232S
3-isobutyl-1-methylxanthine	Sigma-Aldrich	I5879
5-azacytidine	Sigma-Aldrich	A2385
Accutase, StemPro Cell Dissociation Reagent	Gibco	A1110501
Acetic Acid, Glacial	Merck Millipore	1000632511
Acrylamide, 40%	Bio-Rad	1610140
Agar	Sigma-Aldrich	A5306
Agarose, Ultra Pure	Life Technologies	16500500
Alizarin Red S	Sigma-Aldrich	A5533
Ammonium Persulfate	Sigma-Aldrich	A3678
Ampicillin	Sigma-Aldrich	A0155
B27 Supplement, 50x	Gibco	17504044
*Bam*HI-High Fidelity Restriction Enzyme	New England Biolabs	R3136S
Basic Fibroblast Growth Factor, Human Recombinant	Prospec	CYT-218
Bisacrylamide Solution	Sigma-Aldrich	M1533
Bovine Serum Albumin	Sigma-Aldrich	A9647
Brain-derived neurotrophic factor, recombinant	Merck Millipore	GF029
Bromophenol Blue	Sigma-Aldrich	B0126
Calcium Chloride, Dihydrate	Ajax Finechem	AJA127
Chloroform	Sigma-Aldrich	C7559
Collagenase, Type IV	Life Technologies	17104019
CutSmart Buffer, 10x	New England Biolabs	B7200
DAPI	Sigma-Aldrich	D9542
Deoxynucleotide Mix, 10mM	Sigma-Aldrich	D7295
Dexamethasone	Sigma-Aldrich	D4902
D-Glucose	Sigma-Aldrich	G8270
Dibutyryl Cyclic Adenosine Monophosphate	Sigma-Aldrich	D0627
Dimethyl Sulfoxide	Sigma-Aldrich	D2650
Dispase	Sigma-Aldrich	D4693
Dithiothreitol, 0.1M	Invitrogen	18080544
DNase I Reaction Buffer	New England Biolabs	B0303S
DNase I, RNase-free	New England Biolabs	M0303S
Dulbecco's Modified Eagle Medium (high glucose)	Gibco	11995065
Dulbecco's Modified Eagle Medium (no glucose)	Gibco	11966025
*Eco*RI-High Fidelity Restriction Enzyme	New England Biolabs	R3101S
EDTA, Disodium Salt Dihydrate	Amresco	0105
Egtazic Acid	Sigma-Aldrich	E3889
Epidermal Growth Factor, Human Recombinant	Prospec	CYT-217
Ethanol, Absolute	Ajax Finechem	AJA214
Ethidium Bromide	Sigma-Aldrich	E7637
Fast Green FCF Dye	Sigma-Aldrich	F7252
Foetal Bovine Serum	CellSera Australia	AU-FBS/PG

Formalin Solution, Neutral Buffered, 10%	Sigma-Aldrich	HT501128
Forskolin	Sigma-Aldrich	F6886
Gelatin	Sigma-Aldrich	G2500
GelRed Nucleic Acid Gel Stain, 10,000x	Biotium	41003
GeneJET Gel Extraction Kit	Thermo Scientific	K0691
GeneJET Plasmid Miniprep Kit	Thermo Scientific	K0503
GlutaMAX Supplement, 100x	Gibco	35050061
Glycerol	Sigma-Aldrich	G5546
Glycine	Amresco	0167
Haematoxylin	SAHMRI	N/A
Ham's F12 Nutrient Mix	Gibco	11765054
Heparin	Sigma-Aldrich	H3149
HEPES, 1M	Gibco	15630080
Hydrochloric Acid	Sigma-Aldrich	H1758
Hydrocortisone	Sigma-Aldrich	H0888
Indian Ink, Black	Winsor and Newton	N/A
Indomethacin	Sigma-Aldrich	I7378
Insulin	Sigma-Aldrich	I2643
Insulin-Transferrin-Sodium Selenite Media Supplement	Sigma-Aldrich	I1884
Isopropanol	Merck Millipore	1096342511
KnockOut DMEM/F12	Gibco	12660012
KnockOut Serum Replacement	Gibco	10828010
Laminin, Mouse Protein	Gibco	23017015
L-ascorbate 2-phosphate	Alpha Laboratories	013-19641
L-glutamine, 200mM	Gibco	25030-081
Lipofectamine 2000 Reagent	Invitrogen	11668019
Magnesium Chloride, Anhydrous	Sigma-Aldrich	M8266
Methanol	Merck Millipore	1060092500
Mycoalert Mycoplasma Test Kit	Lonza	LT07-318
N2 Supplement, 100x	Gibco	17502048
Nerve Growth Factor-β, Human	Sigma-Aldrich	N1408
Neurobasal A Medium	Gibco	10888022
Neurobasal Medium	Gibco	21103049
Neurotrophin-3, Human Recombinant	Prospec	CYT-257
Non-Essential Amino Acids, MEM, 100x	Gibco	11140076
Normal Horse Serum	SA Pathology	N/A
*Not*I-High Fidelity Restriction Enzyme	New England Biolabs	R3189S
NP-40 (IGEPAL CA-630)	Sigma-Aldrich	I8896
Oil Red O	Sigma-Aldrich	O0625
Oligo(dT)15 Primers, 500ng/µL	Promega	C1101
Opti-MEM I Reduced Serum Medium	Gibco	31985062
Orange G	Sigma-Aldrich	O3756
Paraformaldehyde	Sigma-Aldrich	P6148
Penicillin-Streptomycin, 10,000U/mL-10,000µg/mL	Gibco	15140122
Phosphate Buffered Saline Tabs, pH 7.4	Astral scientific	09-2051-100
Platelet-Derived Growth Factor-AA, Human Recombinant	ImmunoTools	11343683
Polybrene	Sigma-Aldrich	H9268
Poly-D-Lysine	Sigma-Aldrich	P6407
Poly-L-Lysine	Sigma-Aldrich	P4707
Poly-L-Ornithine	Sigma-Aldrich	P4957
Potassium Chloride	Ajax Finechem	AJA383

Potassium Gluconate	Sigma-Aldrich	P1847
Potassium Hydroxide	Sigma-Aldrich	P5958
Potassium Phosphate Monobasic	Sigma Aldrich	P5655
Power SYBR Green PCR Master Mix, 2x	Applied Biosystems	4368702
PowerUp SYBR Green Master Mix, 2x	Applied Biosystems	A25777
Precision Plus Protein Dual Color Standards	Bio-Rad	1610374
ProLong Gold Antifade Mountant with DAPI	Life Techologies	P36935
Protease Inhibitor Cocktail, cOmplete EDTA-free	Roche	05056489001
Protein Assay Dye Reagent Concentrate, 5x	Bio-Rad	5000006
PureLink RNA Mini Kit	Invitrogen	12183018A
QIAfilter Plasmid Midi Kit	Qiagen	12143
qPCR Lentivirus Titration (Titer) Kit	Applied Biological Materials	LV900
Random Primers, 500ng/µL	Promega	C1181
Retinoic Acid, all-trans	Sigma-Aldrich	R2625
RNAlater Stabilisation Solution	Invitrogen	AM7020
RNaseOut, Recombinant RNase Inhibitor, 40U/µL	Invitrogen	10777019
Safranin-O Stain	Sigma-Aldrich	S8884
Shrimp Alkaline Phosphatase, Recombinant	New England Biolabs	M0371S
Skim Milk	Generic Brand	N/A
Sodium Azide	Sigma-Aldrich	S2002
Sodium Chloride	Ajax Finechem	AJA465
Sodium Deoxycholate	Sigma-Aldrich	D6750
Sodium Dodecyl Sulfate	Sigma-Aldrich	L4509
Sodium Fluoride	Sigma-Aldrich	201154
Sodium Hydroxide	Sigma-Aldrich	221465
Sodium Orthovanadate	Sigma-Aldrich	450243
Sodium Phosphate Dibasic	Sigma Aldrich	S9763
Sodium Pyrophosphate Dibasic	Sigma-Aldrich	P8135
Sodium Pyruvate, 100mM	Gibco	11360070
StemPro Neural Stem Cells	Gibco	A15655
StemPro Neural Supplement	Gibco	A10508-01
Sucrose	Sigma-Aldrich	S9378
SuperScript IV Reverse Transcriptase Buffer, 5x	Invitrogen	18090050B
SuperScript IV Reverse Transcriptase, 10,000U	Invitrogen	18090050
T4 DNA Ligase	New England Biolabs	M0202S
T4 DNA Ligase Reaction Buffer, 10x	New England Biolabs	B0202
TEMED	Sigma-Aldrich	T9281
TPA (PMA)	Sigma-Aldrich	P1585
Transforming Growth Factor-β3, Human	Sigma-Aldrich	SRP3171
Triiodothyronine	Sigma-Aldrich	T6397
TriReagent	Sigma-Aldrich	T9424
Tris Base, Ultra Pure Grade	Amresco	0497
Triton X-100	Sigma-Aldrich	X100
Trypan Blue Solution, 0.4%	Sigma-Aldrich	T8154
Trypsin-EDTA, 0.5%, no phenol red	Gibco	15400054
Tryptone, Bacto	BD Biosciences	211705
Tween-20	Sigma-Aldrich	P2287
WST-1 Premix, Cell Proliferation Assay System	Scientifix	MK400
*Xba*I Restriction Enzyme	New England Biolabs	R0145S
*Xho*I Restriction Enzyme	New England Biolabs	R0146S
Yeast Extract	BD Biosciences	211929

2.2 | General Methods

This section contains common methods used throughout the thesis. Specific methods are included in the relevant chapters.

2.2.1 Cell Biology Techniques

2.2.1.1 Cell Culture

Cells were cultured in tissue culture-treated vented flasks (25cm^2, 75cm^2, 175cm^2), dishes (100mm, 60mm) or plates (6-, 24-, 96-well) (Corning Inc., NY, USA) under standard cell culture conditions of 37°C in a humidified 5% CO_2 incubator (Binder GmbH, Tuttlingen, Germany; Thermo Scientific HERAcell, MA, USA; New Brunswick Scientific Galaxy S, NJ, USA). Media were changed every 3-4 days, unless stated otherwise. Table 2.2 indicates the components in standard DPSC culture medium. Cells were maintained as sub-confluent monolayer cultures, unless otherwise indicated. To passage, harvest or cryopreserve, cells were washed in phosphate buffered saline (PBS) and dissociated with 0.05% (w/v) Trypsin-EDTA for 3-5 minutes at 37°C. Foetal bovine serum (FBS)-supplemented media was added to neutralise the trypsin solution. Centrifugation was performed at 200 x *g* for 5 minutes in 15mL or 50mL tubes (Corning Inc., NY, USA). Cells were passaged at 80-90% confluence, typically at a ratio of 1 in 4 for maintenance. For experiments, cell pellets were resuspended and cell counts performed. Routine mycoplasma testing was performed using MycoAlert Mycoplasma Test Kit, according to the product protocol with half-volumes (Lonza, Basel, Switzerland).

Table 2.2 Standard DPSC culture medium.

Component	Concentration
αMEM	
FBS	10% (v/v)
Penicillin, Streptomycin	100units/mL, 100µg/mL
L-glutamine	2mM
L-ascorbate 2-phosphate	100µM
Sodium pyruvate	1mM

The neuroblastoma cell line SH-SY5Y, kindly provided by the Hopwood Centre for Neuroscience (SAHMRI, SA, Australia), was used as a positive control for evaluation of antibodies against neural proteins. The cells were cultured in DMEM (high glucose) medium supplemented with 10% (v/v) FBS, 100units/mL penicillin, 100µg/mL streptomycin and 2mM L-glutamine. The cells were differentiated in firstly DMEM medium as above but with 5% (v/v) FBS and 10µM all-trans retinoic acid for 3 days, and then Neurobasal A medium supplemented

with 100units/mL penicillin, 100µg/mL streptomycin, 2mM L-glutamine, 1% N2 and 50ng/mL brain-derived neurotrophic factor for 3 days (25).

HEK293T Lenti-X cells, kindly gifted by the Hopwood Centre for Neuroscience, (SAHMRI, SA, Australia) were cultured in DMEM (high glucose) medium supplemented with 10% (v/v) FBS, 100units/mL penicillin and 100µg/mL streptomycin.

2.2.1.2 Cryopreservation and Thawing of Cells

All cells were cryopreserved by resuspending cell pellets in FBS with 10% (v/v) dimethyl sulfoxide, with 1mL/cryotube (Corning Inc., NY, USA). The cells were cooled at 1°C/minute (Nalgene Mr. Frosty; Nalge Nunc International, NY, USA) before being stored at -80°C for short-term storage (to be used for experiments) or liquid nitrogen for long-term storage (SAHMRI, SA, Australia). Cells were thawed quickly at 37°C, with 1mL warm culture medium subsequently added in a drop-wise manner. The cell suspension was centrifuged, washed with PBS, and then resuspended in fresh warm culture medium and plated at an appropriate density.

2.2.1.3 Cell Counts: Trypan Blue Exclusion Assay

Cell viability was determined using a haemocytometer and the Trypan Blue exclusion method. The cell pellet was resuspended in medium, and a small volume was then diluted with Trypan Blue (using dilution factor between 2 to 10). From this cell/dye suspension, 10µL was loaded into each chamber of the haemocytometer. Trypan blue distinguishes live and dead cells as it passes through the cell membranes of dead cells only. The live cells (white) were counted in the four large corner squares of each chamber, and averaged. The concentration of viable cells/mL was calculated using the formula; average number of cells x dilution factor x 10,000.

2.2.1.4 WST-1 Cell Proliferation Assay

The colorimetric WST-1 premix reagent was used to measure cell proliferation based on its measure of metabolic activity. Cells were seeded at $1x10^4$ cells/well in triplicate in two 96-well plates; one plate for ‘0 hour’ time point and one plate for ‘24 hour’ time point. Medium-only controls were included. The ‘24 hour’ plate was incubated. WST-1 premix was added to each well of the ‘0 hour’ plate at a 1 in 10 dilution for a total volume of 100µL, and incubated for 4 hours. Absorbance was measured using the GloMax Discover plate reader (Promega, WIS, United States) at a test wavelength of 490nm and reference wavelength of 650nm. This was repeated for the ‘24 hour’ plate the following day. Absorbance was corrected by removing background absorbance (medium-only controls). Proliferation rate was defined as the fold-change in absorbance at 24 hours compared to baseline (0 hour).

2.2.1.5 Flow Cytometry

Cells stained for surface markers with fluorescent antibodies or expressing fluorescent proteins were resuspended in fixation buffer (10% formalin solution with 2% (v/v) glucose and 0.02% (v/v) sodium azide) in 5mL Falcon polypropylene, round-bottom tubes (BD Biosciences Australia, NSW, Australia). Samples were stored at 4°C until analysed on the BD FACSCanto II Cell Analyser using the BD FACSDiva 8.0 software (Becton Dickinson, NJ, USA), at the Australian Cancer Research Foundation Flow and Laser Scanning Cytometry Facility (SAHMRI, SA, Australia). Single cells were gated (threshold set at 10,000 events) and the negative control cells (no fluorescence) were used to determine the gating for positive staining.

2.2.1.6 Fluorescence-Activated Cell Sorting (FACS)

When cells expressing fluorescent proteins or stained for surface markers with fluorescent antibodies reached approximately 90% confluency, they were harvested and resuspended in 1% (v/v) FBS in PBS in 5mL polypropylene, round-bottom tubes. Cells were sorted for purity on the FACSMelody cell sorter using FACSChorus software (Becton Dickinson, NJ, USA), at the Australian Cancer Research Foundation Flow and Laser Scanning Cytometry Facility (SAHMRI, SA, Australia). Events were gated for single events and then for fluorescent cells based on the negative control. The brighter cells in the positive fraction were selected to be sorted into tubes. The sorted cells were cultured in standard DPSC culture medium to recover and expand.

2.2.2 Molecular Biology Techniques

2.2.2.1 RNA Extraction

Total RNA was isolated using the TriReagent method, according to the manufacturer's protocol (Sigma-Aldrich, MO, USA). Cells were washed 1x with PBS. An appropriate amount of TriReagent was added to the cells (e.g. 1mL/10cm^2), and the cells were left to lyse at room temperature (RT) for 5 minutes. The solution was transferred to a 1.5mL microcentrifuge tube (Thermo Scientific, MA, USA), and 0.2mL chloroform was added per 1mL of TriReagent used. The tube was shaken vigorously and allowed to stand for 5 minutes at RT. The sample was then centrifuged at 12,000 x *g* for 15 minutes at 4°C. The colourless aqueous upper phase was transferred to a new 1.5mL microcentrifuge tube and 0.5mL isopropanol was added per 1mL of TriReagent used. The sample was inverted to mix evenly and allowed to stand at RT for 5-10 minutes prior to centrifugation at 12,000 x *g* for 10 minutes at 4°C. The RNA precipitate formed a pellet on the side and bottom of the tube. The supernatant was discarded and the RNA pellet was washed with 1mL 75% ethanol per 1mL of TriReagent used. The sample was

vortexed and centrifuged at 7500 x *g* for 5 minutes at 4°C. The ethanol was carefully removed and the RNA pellet was left to air-dry for approximately 10 minutes. The pellet was then resuspended in 20-30µL RNase-free water. The concentration and quality of RNA samples was determined using the NanoDrop 8000 spectrophotometer (Thermo Scientific, MA, USA).

2.2.2.2 Reverse Transcription

Reverse transcription reactions to create cDNA were performed using Superscript IV Reverse Transcriptase, according to the manufacturer's instructions (Invitrogen, CA, USA). Reactions were performed in 20µL volumes in 0.2mL tubes (Thermo Scientific, MA, USA). Each reaction contained 500ng RNA in nuclease-free water, 2.5µM random hexamers and oligo(dT) primers, 0.5mM deoxynucleotide mix, 10U/µL reverse transcriptase, 4µL 5x enzyme buffer, 5mM dithiothreitol and 2U/µL RNase Out. The RNA, random hexamers, oligo(dT) primers and deoxynucleotides were first combined, and incubated in a thermocycler (Bio-Rad Laboratories Inc., CA, USA) at 65°C for 5 minutes, then placed on ice for at least one minute. The remaining reagents were then added, the contents of the tubes mixed and briefly centrifuged. The tubes were placed into the thermocycler and reverse transcription was performed with the following program: 23°C for 10 minutes, 50-55°C for 10 minutes, 80°C for 10 minutes (inactivation), and held at 4°C. The cDNA samples were then diluted 1:10 with ddH_2O.

2.2.2.3 Quantitative Polymerase Chain Reaction (qPCR)

Real-time qPCR reactions were performed using Power and PowerUp SYBR Green master mixes, according to the product protocol (Applied Biosystems, CA, USA), on a CFX Connect real-time PCR instrument (Bio-Rad Laboratories Inc., CA, USA). Reactions were performed in 20µL volumes in qPCR 96-well optical plates (Bio-Rad Laboratories Inc., CA, USA). Each reaction contained 2µL diluted cDNA (10% of reaction), 300nM forward and reverse primers, 10µL of the 2x mastermix, and nuclease-free water. Primers (Thermo Scientific, MA, USA and Sigma-Aldrich, NSW, Australia) used are indicated in the relevant chapter methods. For primer design, see Appendix A. The plates were sealed with optical adhesive covers (Bio-Rad Laboratories Inc., CA, USA). The thermal cycling conditions were as indicated in Tables 2.3 (Power SYBR Green master mix) and 2.4 (PowerUp SYBR Green master mix), followed by a default dissociation step to generate a melting curve. Reactions for each sample were performed in triplicate. The endogenous control gene was *ACTB*. Negative controls were included, which were a no template (water) control and no reverse transcriptase control.

Relative gene expression analysis was performed using the ΔΔCt method (26). For a given sample, the Ct value of the endogenous control gene was subtracted from the Ct value of the

gene-of-interest to calculate ΔCt. The reference/calibrator sample (e.g. matched untreated sample, highest Ct value sample, or control average) was selected and the ΔCt was subtracted from the ΔCt of the experimental/treated sample to calculate the ΔΔCt. The fold change was calculated, and log (base 2) transformed.

Table 2.3 Standard thermal cycling conditions for Power SYBR Green mastermix.

Step	Temperature (°C)	Duration	Cycles
Activation	95	10 minutes	Hold
Denature	95	15 seconds	40
Anneal/Extend	60	1 minute	

Table 2.4 Fast thermal cycling conditions for PowerUp SYBR Green mastermix.

Step	Temperature (°C)	Duration	Cycles
UDG Activation	50	2 minutes	Hold
Dual-Lock DNA Polymerase	95	2 minutes	Hold
Denature	95	3 seconds	40
Anneal/Extend	60	30 seconds	

2.2.2.4 Immunofluorescence Staining

Cells cultured on glass coverslips (ProSciTech, QLD, Australia) were washed with PBS, fixed with cold 10% formalin for 15-20 minutes at RT, and then washed 3x for 5 minutes with ice-cold PBS. The cells were then permeabilised with 0.3% Triton X-100 in PBS for 10 minutes at RT, and then washed 3x for 5 minutes with 0.1% Tween-20 in PBS (PBS-T). The cells were blocked in 10% normal horse serum in 0.1% Triton X-100 in PBS for 1 hour at RT. Primary antibodies were diluted in blocking solution and cells were incubated at 4°C overnight with gentle agitation. The primary antibody solution was removed and the cells were washed 3x for 5 minutes with PBS-T. The cells were then incubated with secondary antibodies diluted in blocking solution for 2.5 hours at 4°C with gentle agitation in the dark. The secondary antibody solution was removed and the cells were washed 3x for 5 minutes with PBS-T. The coverslips were mounted on microscope slides (Thermo Scientific, MA, USA) with ProLong Gold Antifade Mountant with DAPI. The microscope slides were allowed to dry and the edges were sealed with clear nail polish. Antibodies used are indicated in the relevant chapter methods. Negative secondary antibody (omission of primary antibody) and isotype controls (primary antibodies substituted with isotype-specific antibodies) were included to control for non-specific binding and background staining, and determine the optimal exposure time to eliminate non-specific/background staining. See Appendix B for positive controls. The cells were imaged using a fluorescence microscope with appropriate filters.

2.2.2.5 Western Blot

Protein Lysate Preparation

Cells grown in 6-well culture plates were washed with PBS and placed on ice. RIPA lysis buffer (50mM Tris-HCl pH 7.5, 150mM sodium chloride, 1mM EDTA, 1mM Egtazic acid, 50mM β-glycerolphosphate, 10mM sodium fluoride, 2.5mM sodium pyrophosphate, 1% sodium deoxycholate, 1% NP-40, 0.1% sodium dodecyl sulphate (SDS), 14.3mM β-mercaptoethanol, 2mM sodium orthovanadate, 1x protease inhibitor cocktail) was added to the cells. Using a cell scraper (Corning Inc., NY, USA), the cells were removed and the solution transferred to a 1.5mL microcentrifuge tube. The lysates were left on ice for 30 minutes, then centrifuged at 16,000 x *g* at 4°C for 10 minutes. The supernatant (protein lysate) was collected into a new 1.5mL microcentrifuge tube, leaving behind the cell debris pellet. The concentration of the lysate was determined using the Bradford assay, and the lysates were stored at -20°C.

To confirm that the antibodies were detecting the proteins of interest, lysates from cells known to express these proteins were used. These included SH-SY5Y, human ESC and mouse NSC. The human ESC were kindly provided by the Laboratory for Human Neurophysiology, Genetics and Stem Cells (SAHMRI, SA, Australia), and the mouse NSC by Mari Suzuki Ichinose from the Gastrointestinal Cancer Biology Group (SAHMRI, SA, Australia).

Bradford Assay

The total protein concentration of the lysates was determined using a standard curve of bovine serum albumin (BSA). The 5x Protein Dye Reagent Concentrate was diluted to 1x using ddH_2O and warmed to ambient temperature. Protein standards (4, 2, 1, 0.5, 0.25, 0.125, 0.0625 mg/mL) were made using BSA diluted in RIPA lysis buffer. The standards and lysates were diluted in ddH_2O; 9µL of ddH_2O was added to wells of a 96-well plate followed by 1µL of standards or lysates. A 'blank' control of lysis buffer was included. All samples were assayed in duplicate. To each sample, 250µL of the 1x dye reagent was added and allowed to stand at RT for 5 minutes. The absorbance was measured using the GloMax Discover plate reader (Promega, WIS, USA) at 600nm, with agitation prior to reading. Duplicate values within 0.05 of each other were used, and averaged. The background absorbance ('blank' control) was subtracted from the samples. The standards were used to generate a standard curve. The concentrations of the lysates were then extrapolated from the standard curve.

SDS-Polyacrylamide Gel Electrophoresis (PAGE) Gel Preparation

Gels were prepared using the Bio-Rad mini-PAGE system (Bio-Rad Laboratories Inc., CA, USA), using 1.5mm spacers and 15-well combs. Table 2.5 lists the gel components for 12.5% acrylamide gels suitable for analysing middle-sized proteins.

Table 2.5 Components for 12.5% acrylamide gels for middle-sized proteins.

Components	12.5%	
	Running Gel	Stacking Gel
ddH_2O	5.6mL	4mL
40% acrylamide	5.3mL	0.75mL
2% bis-acrylamide	1.7mL	0.4mL
1.5M Tris-HCl (pH 8.8)	4.25mL	N/A
1.5M Tris-HCl (pH 6.8)	N/A	0.75mL
20% SDS	85µL	30µL
10% ammonium persulfate	85µL	30µL
TEMED	17µL	6µL

SDS-PAGE

SDS-PAGE gels were secured in a Bio-Rad running tank (Bio-Rad Laboratories Inc., CA, USA) filled with running buffer (10x running buffer; 25mM Tris base, 192mM glycine, 0.1% (w/v) SDS, pH 8.3, dilute to 1x with ddH_2O). Protein samples were prepared to the desired concentration and volume using RIPA lysis buffer and 5x sample buffer (0.25M Tris-HCl pH 6.8, 10% (w/v) SDS, 20% (v/v) glycerol, 0.02% (w/v) Bromophenol Blue, 5% β-mercaptoethanol, in ddH_2O,) adjusted to 1x concentration. Samples were boiled at 100°C for 3 minutes, briefly centrifuged, before loading into wells at 20-40µg per lane (depending on sample availability, kept consistent for each Western blot). Precision Plus Protein Dual Colour Standards were used as the protein ladder; 1µL was added to 1x sample buffer. Gel electrophoresis was run at 100V for 10 minutes until the samples passed through the stacking gel and into the running gel, followed by 1 hour at 180V till the dye ran off.

Transfer

Western blot "sandwiches" were prepared in a tray filled with transfer buffer (10x; 25mM Tris base, 192mM glycine, 20% (v/v) methanol, 0.02% (v/v) SDS, pH 8.3, dilute to 1x with ddH_2O), soaking sponges, Whatman paper (Whatman plc, Maidstone, UK), gels, and nitrocellulose membranes (Bio-Rad Laboratories Inc., CA, USA) . The 'sandwich' was arranged on a plastic cassette with the gel on the negative side and membrane on the positive side, and then closed with a clasp. Air bubbles were removed using a roller as each component of the 'sandwich' was put into place. The cassettes were inserted into the chamber of a Bio-Rad wet tank transfer

system (Bio-Rad Laboratories Inc., CA, USA), the tank was filled with transfer buffer, and the transfer was run for 100V for 1 hour on ice.

Staining

Following the transfer, the nitrocellulose membrane was rinsed with reverse osmosis (RO) water, followed by a wash in 0.1% (v/v) Tween-20 in PBS (PBS-T), and then blocked in 5% (w/v) skim milk in PBS for 30-60 minutes at RT on an orbital shaker. The membrane was rinsed with RO water and washed 3x for 5 minutes in PBS-T, and then incubated with primary antibody solution (antibody in 5% (w/v) BSA in PBS-T) at 4°C overnight on a roller. The membrane was rinsed with RO water and washed 3x for 5 minutes in PBS-T, and then incubated with secondary antibody solution (antibody in PBS-T) in the dark at RT for 1-2 hours on an orbital shaker. After rinsing with RO water and washing 3x for 5 minutes in PBS-T, the membrane was scanned on the Odyssey CLx Infrared Imaging System with the 700 and 800 nm wavelength channels using Image Studio software (LI-COR Biosciences, NE, USA). Exported images were then viewed and densitometry analysis performed using Image Studio Lite v 5.2. Antibodies used are indicated in the relevant chapter methods. See Appendix B for positive controls.

2.2.3 Cell Imaging

Bright-field images of cell cultures were acquired with a Nikon Eclipse TS100 inverted light microscope using NIS Elements F3.0 software (Nikon, Tokyo, Japan). Bright-field and fluorescence images of cell cultures with colour micrographs (multi-lineage differentiation assays, green fluorescent protein (GFP) expression) were captured on the Zeiss Axiovert 200 microscope using ZEN software (Carl Zeiss AG, Oberkochen, Germany). Fluorescence images were captured with the Nikon Ni-Eclipse fluorescence microscope using NIS Elements BR4.40 software (Nikon, Tokyo, Japan). Digital images if processed, were all modified equally for only brightness and/or contrast. The image processing program ImageJ (National Institutes of Health, MD, USA), as part of the Fiji package (27), was used where necessary for colour correction, distance measurements, and mean fluorescence intensity (MFI) measurements.

2.2.4 Statistical Analysis

Statistical analysis was performed using the GraphPad Prism 8 software (GraphPad Software Inc., CA, USA). Data was presented as mean±SD with the appropriate statistical test and multiple comparisons test performed (two-tailed) as indicated in figure legends. The sample size (n) is indicated in figure legends. An alpha value of $p<0.05$ was considered statistically significant.

CHAPTER 3

CHARACTERISATION OF HUMAN DENTAL PULP STEM CELLS

3.1 | Introduction

Dental pulp stem cells (DPSC) are a heterogeneous population of multipotent adult stem cells, isolated from the dental pulp tissue of molar teeth (28). They are of ectomesenchymal origin, and are characterised similarly to mesenchymal stem/stromal cells (MSC) (4, 29). Criteria for MSC characterisation include; plastic adherence under standard culture conditions; expression of the surface markers CD73, CD90 and CD105, while lacking expression of haematopoietic markers, such as CD45 and CD34; and differentiation along the osteogenic, chondrogenic and adipogenic lineages under standard *in vitro* differentiation conditions (30).

The DPSC are extracted enzymatically, using collagenase and dispase to break down proteins of the extracellular matrix (28). In more recent years, an explant method has been investigated that allows cells to migrate out of the tissue, however this is a more time consuming approach (31). Both methods have been successful in obtaining DPSC, with no significant difference in stem cell properties between methods (31).

Human DPSC are typically grown as monolayer cultures in standard plastic tissue culture-treated vessels and in standard stromal cell growth medium (28). They have been reported to express surface antigens including CD44, CD73, CD90, CD105, CD146, stromal precursor cell surface marker STRO-1, and the neural crest marker nerve growth factor receptor (NGFR). Additionally, DPSC are positive for MHC Class I antigen or HLA-ABC, found on all nucleated cells, while they are negative for MHC Class II antigen or HLA-DR, typically found on antigen presenting cells or following immune stimulation. Importantly, DPSC lack expression of the pan-leukocyte marker, CD45, and haematopoietic stem cell marker, CD34. Co-expression of STRO-1, CD146 and NGFR, have also been used as markers for bone marrow MSC (32-35).

The DPSC are also assessed for multi-lineage differentiation capacity *in vitro*, which includes differentiation along the adipogenic, osteogenic/odontogenic and chondrogenic lineages. In addition to these lineages, DPSC have the capacity to differentiate into neuronal-like cells, believed to be due to their neural crest origin (4). Various *in vitro* neuronal differentiation methods for DPSC have been published (36), with immunofluorescence used to detect the expression of neuronal proteins, indicating successful differentiation into neuronal-like cells, in addition to the ability to develop an action potential (1-3).

This chapter characterises the stem cell properties of human DPSC that are used in subsequent chapters investigating reprogramming.

3.2 | Materials and Methods

3.2.1 Extraction of Human DPSC

Human DPSC were isolated as described by Gronthos *et al.* (28). Briefly, impacted third molars were collected with informed consent from patients (approximately 18-40 years of age, male and female) undergoing routine extractions, under approved guidelines set by the University of Adelaide Human Ethics Research Committee (H-2015-253). Teeth were cleaned and opened to reveal the pulp chamber. The dental pulp tissue was separated from the crown and root, minced and digested in a solution of 3mg/mL collagenase type I and 4mg/mL dispase for 1-2 hours at 37°C. After centrifugation, the supernatant was removed and the pellet resuspended in fresh medium. Cultures from individual teeth were established by seeding the cell suspension into 25cm^2 tissue culture-treated flasks in standard DPSC culture medium, then passaged a week later into 75cm^2 tissue culture-treated flasks, and subsequently expanded for experiments. Contaminated samples were not used; this included bacterial and fungal contaminants. Experiments were set up with cells between passages 3 to 6. Cells were cultured and maintained as outlined in Chapter 2, section 2.2.1.1, pg. 27.

3.2.2 Cell Surface Marker Staining

Flow cytometry (Chapter 2, section 2.2.1.5, pg. 29) was used to analyse DPSC for a panel of surface markers. Briefly, for each antibody to be tested (Table 3.1), $1.5x10^5$ cells were used. Antibody solution was added to the cells in a 1.5mL microcentrifuge tube in PBS with 1% (v/v) FBS, and incubated at 4°C for 1 hour in the dark with agitation. Unstained cells were included as a negative control. Unconjugated antibodies were incubated for 30 minutes, followed by centrifugation and 3x PBS washes, and then 30 minute incubation with secondary antibody solution. Following incubation with antibodies, samples were centrifuged and washed 3x with PBS.

Table 3.1 Antibodies used for human DPSC surface marker analysis by flow cytometry.

Antigen	Source	Conjugate	Dilution	Manufacturer	Catalogue Number
HLA-ABC	Mouse	PE	1:5	BD Biosciences	555553
HLA-DR	Mouse	PE	1:5	BD Biosciences	555812
CD45	Mouse	PE	1:10	BD Biosciences	555483
CD44	Mouse	PE	1:10	BD Biosciences	550989
CD73	Mouse	PE	1:10	BD Biosciences	550257
CD90	Mouse	PE	1:400	BD Biosciences	555596
CD105	Mouse	PE	1:10	BD Biosciences	560839
CD146	Mouse	PE	1:10	BD Biosciences	550315
STRO-1	Mouse	N/A *	1:10	R&D Systems	MAB1038
NGFR	Mouse	N/A *	4µg/mL	**	
			1:10 (stock=100µg/mL)	***	

Abbreviations: PE=phycoerythrin.

* Secondary antibody used; donkey anti-mouse IgG DyLight 488, 1:400 dilution (Jackson Immunoresearch, catalogue number 718485187).

** Kindly gifted by Dr. Mary-Louise Rogers (Flinders University, SA, Australia).

*** Kindly provided by Mesenchymal Stem Cell Laboratory research group (University of Adelaide and SAHMRI, SA, Australia).

3.2.3 *In vitro* Cell Differentiation Assays

3.2.3.1 Osteogenic/odontogenic Differentiation and Alizarin Red S Staining

Human DPSC were plated in triplicate at $1x10^4$ cells/well in a 96-well tissue culture-treated plate in standard DPSC culture medium. Once cells had reached 80-90% confluency, medium was changed to osteogenic induction medium (Table 3.2) (37, 38), and subsequently changed every 3-4 days for four weeks. Control cells were maintained in standard DPSC culture medium. To detect mineral deposition, Alizarin Red S staining was performed. Alizarin Red S is a water-soluble sodium salt of Alizarin sulfonic acid, which binds to calcium to form a pigment that is orange/red in colour. Cells were fixed in 10% phosphate buffered formalin for 1 hour at RT, washed with water, then stained with Alizarin Red S (2% (w/v) aqueous solution, pH 4.1-4.3, 0.2µm filtered) overnight at 4°C with gentle agitation. After washing and removing water, samples were imaged. For quantification, the Alizarin Red S precipitates were solubilised (39). Briefly, 50µL of 10% acetic acid was added to each well and incubated at RT for 30 minutes with agitation. The supernatant was collected and transferred to a 1.5mL microcentrifuge tube. Supernatants were heated at 85°C for 10 minutes, then cooled on ice for 5 minutes, and centrifuged at 15,000*g* for 15 minutes. After centrifugation, the supernatant was transferred to an opaque-walled, transparent-bottomed 96-well plate (Corning Inc., NY, USA), and the absorbance was read at 405nm using the GloMax Discover microplate reader (Promega, WIS, United States).

Table 3.2 Osteogenic/odontogenic induction medium.

Component	**Concentration**
αMEM	
FBS	5% (v/v)
L-glutamine	2mM
L-ascorbate 2-phosphate	100µM
Sodium pyruvate	1mM
Penicillin, Streptomycin	100units/mL, 100µg/mL
HEPES	10mM
Dexamethasone	100nM
Potassium dihydrogen phosphate	2.64mM

3.2.3.2 Chondrogenic Differentiation and DAPI/Safranin-O Staining

A glycosaminoglycan assay was used, with this version of the method optimised by the Mesenchymal Stem Cell Laboratory research group (University of Adelaide and SAHMRI, SA, Australia) (40). Human DPSC were plated in triplicate at $4x10^3$ cells/well in a 96-well tissue culture-treated plate in standard DPSC culture medium. Once cells had reached 80-90% confluency, medium was changed to chondrocyte induction medium (Table 3.3) and control medium (DMEM-high glucose, 5% FCS, L-glutamine, L-ascorbate 2-phosphate, penicillin, streptomycin), and subsequently changed at day 3 or 4, and cultured till day 7. Chondrogenic differentiation was analysed using DAPI staining for DNA and Safranin-O (Saf-O) staining for sulphated glycosaminoglycans (sGAGs). Following fixation with 4% paraformaldehyde at RT for 15 minutes, cells were washed and stained with DAPI at RT for 15 minutes in the dark. After washing with PBS, 170µl PBS was added (including blank wells) and the fluorescence was read using the FLUOstar Omega microplate reader (BMG LabTech GmbH, Offenburg, Germany) at 340nM excitation / 460nM emission. Cells were then washed with 1% (v/v) acetic acid for 1 minute, then 0.1% (w/v) Saf-O was added for 5 minutes at RT with agitation. After 5x PBS washes, images were taken. The bound Saf-O was then released by adding 170µl of 75% ethanol (include blank well) for 5 minutes at RT with agitation. Fluorescence was read at 530nM excitation / 570nM emission. The background reading (blanks) was subtracted, and the mean fluorescence ratio was calculated as normalised sGAG values.

Table 3.3 Chondrocyte induction medium.

Component	**Concentration**
DMEM-high glucose	
L-glutamine	2mM
L-ascorbate 2-phosphate	100µM
Penicillin, Streptomycin	50units/mL, 50µg/mL
Insulin-Transferrin-Sodium Selenite	1x
Dexamethasone	0.1mM
BSA	0.125% (w/v)
Transforming Growth Factor-β3	10ng/mL (add fresh)

3.2.3.3 Adipogenic Differentiation and Oil Red O Staining

Human DPSC were plated in triplicate at $1x10^4$ cells/well in a 96-well tissue culture-treated plate in standard DPSC culture medium. Once cells had reached 80-90% confluency, medium was changed to adipogenic induction medium (Table 3.4), and subsequently changed every 3-4 days for 6 weeks. Adipogenic differentiation was evaluated using Oil Red O staining, which shows the presence of lipid droplets. Cells were fixed in 10% phosphate buffered formalin for 15 minutes at RT. After washing with PBS, cells were stained with Oil Red O (working solution was prepared by adding 6mL of stock solution (0.5g Oil Red O in 100mL isopropanol) to 4mL ddH_2O, filtered through Whatman paper (Whatman, Maidstone, UK), and 0.2µm filtered immediately before use) for at least 2 hours at RT. After washing with water, cells were counterstained with haematoxylin for 5 minutes and washed, then imaged. For quantification, the Oil Red O dye was extracted (41). The water was aspirated and cells allowed to dry, then 100µL/well of 100% isopropanol was added and incubated at RT for 10 minutes. The supernatant was transferred to a 96-well plate and absorbance at 490nm was measured using the GloMax Discover microplate reader (Promega, WIS, United States).

Table 3.4 Adipogenic induction media.

Component	**Concentration**		
	Medium 1*	**Medium 2****	**Medium 3*****
αMEM			
FBS	10% (v/v)	10% (v/v)	10% (v/v)
L-glutamine	2mM	2mM	2mM
L-ascorbate 2-phosphate	100µM	100µM	100µM
Sodium pyruvate	1mM	1mM	1mM
Penicillin, Streptomycin	100units/mL, 100µg/mL	100units/mL, 100µg/mL	100units/mL, 100µg/mL
HEPES	10mM		
Dexamethasone	100nM	250nM	
Indomethacin	60µM	60µM	60µM
3-isobutyl-1-methylxanthine		0.5mM	0.5mM
Insulin		5µg/mL	
Hydrocortisone			0.5µM

* Medium 3 optimised by Mesenchymal Stem Cell Laboratory and Myeloma Research Laboratory research groups (University of Adelaide and SAHMRI, SA, Australia), using human bone explant cultures.

** Jenna Rich, 2010 Honours thesis, Stroke Research Programme research group (University of Adelaide, SA, Australia), replaced 1µM rosiglitazone with indomethacin.

*** As published by Gimble 1998. (42).

3.2.3.4 Neurogenic Differentiation

Three published protocols for neuronal differentiation of human DPSC were used here.

(1) Method by Arthur *et al.* 2008 (1)

Tissue culture-treated plates and glass coverslips were coated with 0.01% poly-L-lysine (overnight at RT, washed with ddH_2O) and 5µg/mL laminin (in PBS, overnight at 37°C, washed with PBS and then culture medium). Human DPSC were seeded at a density of $1.5x10^4$ cells/cm^2 in a 24-well plate in standard DPSC culture medium and cultured for 3 days, before changing to the neuronal differentiation medium A for 1 week, then medium B for 1 week, and medium C for 1 week. Neuronal differentiation media (Table 3.5) were made fresh and changed every 3-4 days. Cells were washed with PBS between different media.

Table 3.5 Neuronal differentiation media for the method by Arthur *et al*. 2008. (1)

Medium A (7 days)	**Medium B (7 days)**	**Medium C (7 days)**
Neurobasal A	1:1 DMEM/F12	1:1 DMEM/F12
100U/mL penicillin, 100µg/mL streptomycin	100U/mL penicillin, 100µg/mL streptomycin	100U/mL penicillin, 100µg/mL streptomycin
2% (v/v) B27	1x Insulin-Transferrin-Sodium Selenite	1x Insulin-Transferrin-Sodium Selenite
40ng/mL bFGF	40ng/mL bFGF	40ng/mL bFGF
20ng/mL EGF		0.5µM retinoic acid

(2) Method by Kiraly *et al.* 2009 (2)

Tissue culture-treated plates and glass coverslips were coated with 0.01% poly-L-lysine. Human DPSC were seeded at a density of $2x10^4$ cells/cm^2 in 24-well plates in standard DPSC culture medium and cultured overnight. The cells were then cultured in neuronal induction medium for 24 hours, then epigenetic reprogramming medium for 48 hours, followed by neural differentiation medium for 3 days, and finally neuronal maturation medium for 1 week with a medium change half-way through. Neuronal differentiation media (Table 3.6) were made fresh. Cells were washed with PBS between different media.

Table 3.6 Neuronal differentiation media for the method by Kiraly *et al*. 2009. (2)

Neuronal Induction (24 hours)	Epigenetic Reprogramming (48 hours)	Neural Differentiation (3 days)	Neuronal Maturation (3-7 days)
1:1 DMEM/F12	1:1 DMEM/F12	1:1 DMEM/F12	Neurobasal A
100U/mL penicillin	2.5% (v/v) FBS	250µM 3-isobutyl-1-methylxanthine	1% (v/v) B27
100µg/mL streptomycin	10µM 5-azacytidine	50µM forskolin	1% (v/v) N2
2.5% (v/v) FBS	10ng/mL bFGF	200nM TPA	1mM dbcAMP
		1mM dbcAMP	30ng/mL neurotrophin-3
		10ng/mL bFGF	
		10ng/mL nerve growth factor	
		30ng/mL neurotrophin-3	
		1x Insulin-Transferrin-Sodium Selenite	

(3) Method by Gervois *et al.* 2015 (3)

Human DPSC were seeded at a density of $7.5x10^3$ cells/cm^2 in Costar Ultra-Low Attachment Well plates and standard plates (Corning Inc., NY, USA) in neural induction medium for 1 week, with medium changed half-way through. Spheres were monitored to not exceed a diameter of 250µm. Cells/spheres were then harvested, dissociated with Accutase, and washed in PBS. Cells were seeded in tissue culture-treated plates and glass coverslips, previously coated with 0.01% poly-L-lysine and 2µg/mL laminin, in neuronal maturation medium and cultured for 4 weeks. Neuronal differentiation media (Table 3.7) were made fresh.

Table 3.7 Neuronal differentiation media for the method by Gervois *et al*. 2015. (3)

Neuronal Induction (1 week)	Neuronal Maturation (4 weeks)
1:1 DMEM/F12	Neurobasal
100U/mL penicillin, 100µg/mL streptomycin	100U/mL penicillin, 100µg/mL streptomycin
2% (v/v) B27	2mM L-glutamine
20ng/mL bFGF	2% (v/v) B27
20ng/mL EGF	1% (v/v) N2
	1mM dbcAMP
	30ng/mL neurotrophin-3

3.2.4 Immunofluorescence Staining

Immunofluorescence staining of DPSC undergoing neuronal differentiation was carried out at the completion of each protocol. See Chapter 2, section 2.2.2.4, pg. 31 for method, using antibodies in Table 3.8. ImageJ software was used to measure the MFI. For each image, measurements were made as triplicates. The background was averaged and subtracted from the signal, and the signal averaged.

Table 3.8 Antibodies for immunofluorescence staining.

Antibody	Species	Stock Concentration	Dilution	Manufacturer	Catalogue Number
Primary Antibodies					
Anti-Nestin	Mouse	0.5mg/mL	1:250	Abcam	ab6320
Anti-Nestin	Rabbit	Not disclosed	1:250	Abcam	ab105389
Anti-β-III tubulin	Mouse	Not disclosed	1:250	Merck Millipore	MAB1637
Anti-NF-M	Mouse	0.5mg/mL	1:250	Invitrogen	13-0700
Isotype Control Antibodies					
Anti-mouse IgG	N/A	1mg/mL	1:250	*	
Anti-rabbit IgG	N/A	5mg/mL	1:250	*	
Secondary Antibodies					
Anti-mouse IgG Cyanin3	Donkey	1mg/mL	1:500	Merck Millipore	AP192C
Anti-rabbit IgG Alexa Fluor 488	Goat	2mg/mL	1:500	Invitrogen	A-11008

* Kindly provided by Mesenchymal Stem Cell Laboratory research group (University of Adelaide and SAHMRI, SA, Australia).

3.3 | Results

3.3.1 Human DPSC were plastic-adherent, grew as a monolayer and displayed a spindle-shaped morphology

Human DPSC were cultured in standard DPSC culture medium consisting of 10% FBS. They were grown in standard plastic tissue culture-treated flasks as cell monolayers, at 37°C in a humidified 5% CO_2 incubator. Under these conditions, they demonstrated plastic adherence and displayed a spindle-shaped morphology (Figure 3.1).

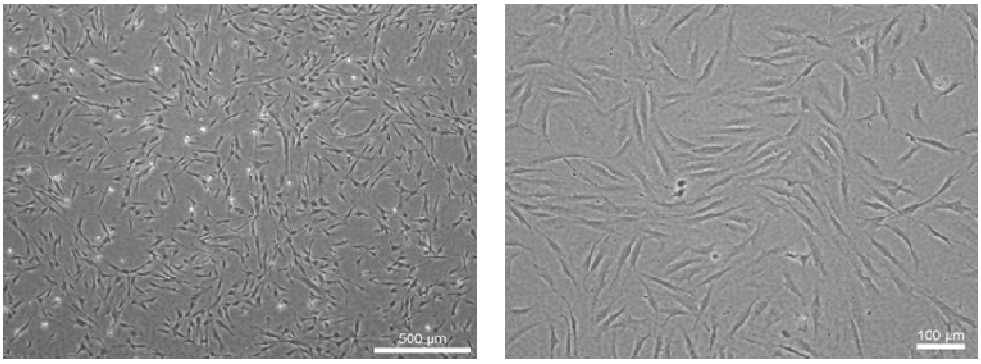

Figure 3.1 Human DPSC adhered to plastic and grew as a cell monolayer with a spindle-shaped morphology. Representative images, n=15, scale bar= 500µm (left) and 100µm (right).

3.3.2 Human DPSC had a high proliferation rate

Human DPSC proliferation was assessed by WST-1 assay. The WST-1, a tetrazolium salt (4-[3-(4-Iodophenyl)-2-(4-nitro-phenyl)-2H-5-tetrazolio]-1,3-benzene sulfonate), is cleaved by mitochondrial dehydrogenases in viable cells. This produces formazan, a dye that can be quantified by measuring the absorbance at 490nm. The amount of absorbance is proportional to cell number. Here, the absorbance at 24 hours (1.10±0.37) was more than double than at the baseline at zero hours (0.39±0.15), with statistical significance of $p<0.0001$ (Figure 3.2A). The average proliferation rate was 2.96±0.58, meaning that over 24 hours the cell number tripled (Figure 3.2C). The absorbance values and proliferation rates of the individual DPSC samples were graphed (Figure 3.2 B and D), demonstrating that all the DPSC samples had a proliferation rate of at least two-fold over 24 hours.

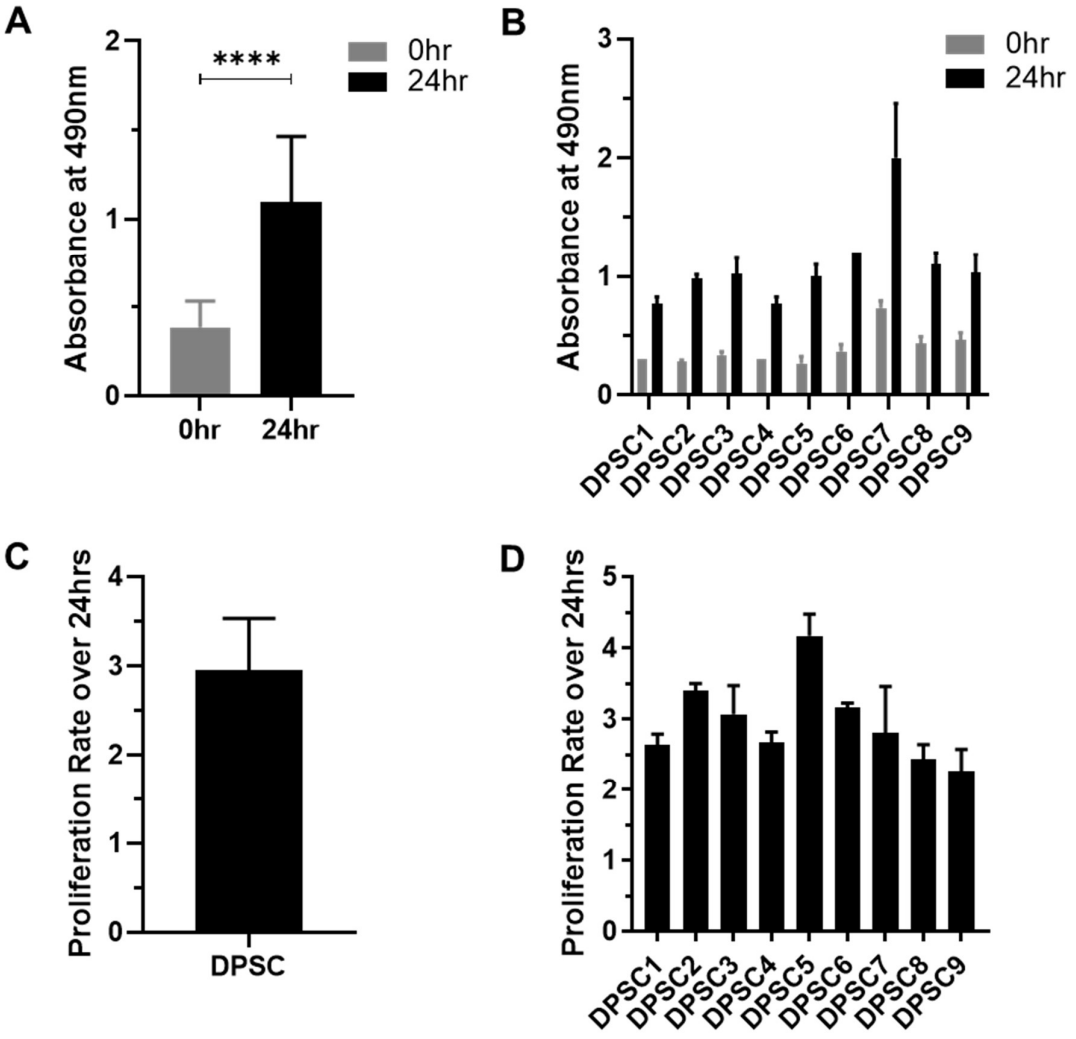

Figure 3.2 Human DPSC proliferation *in vitro*. A WST-1 cell proliferation assay was used to examine the proliferation rate over 24 hours. The **(A)** average and **(B)** individual absorbance values measured at 0 and 24 hours. The **(C)** average and **(D)** individual proliferation rates over 24 hours. Data represents mean±SD, Mann-Whitney test, n=9, ****$p<0.0001$.

3.3.3 Human DPSC expressed common MSC surface antigens

A panel of surface markers were assessed via flow cytometry (Figure 3.3). The DPSC were positive for HLA-ABC at >90% (96.75±4.97). Positive expression was expected as this molecule is found on all nucleated cells, and is involved in presenting peptides from within the cell to help identify foreign antigens. DPSC were negative for HLA-DR at <1% (0.20±0.44), which was also expected as this molecule is expressed by antigen presenting cells, such as macrophages, or following immune stimulation by interferon-γ. The DPSC were negative for the leukocyte antigen CD45 at <1% (0.10±0.14), and were >95% positive for the MSC markers CD44 (99.85±0.21), CD73 (99.66±0.37), CD90 (97.69 ±2.75) and CD105 (98.14±2.22). The expression of CD146 was more varied between the DPSC samples (65.79±13.53). It is a marker used for cells of the endothelial lineage and is also used as a MSC marker. The expression of the MSC marker STRO-1 (1.10±1.76) and the neural crest marker NGFR (0.40±0.42) were negative.

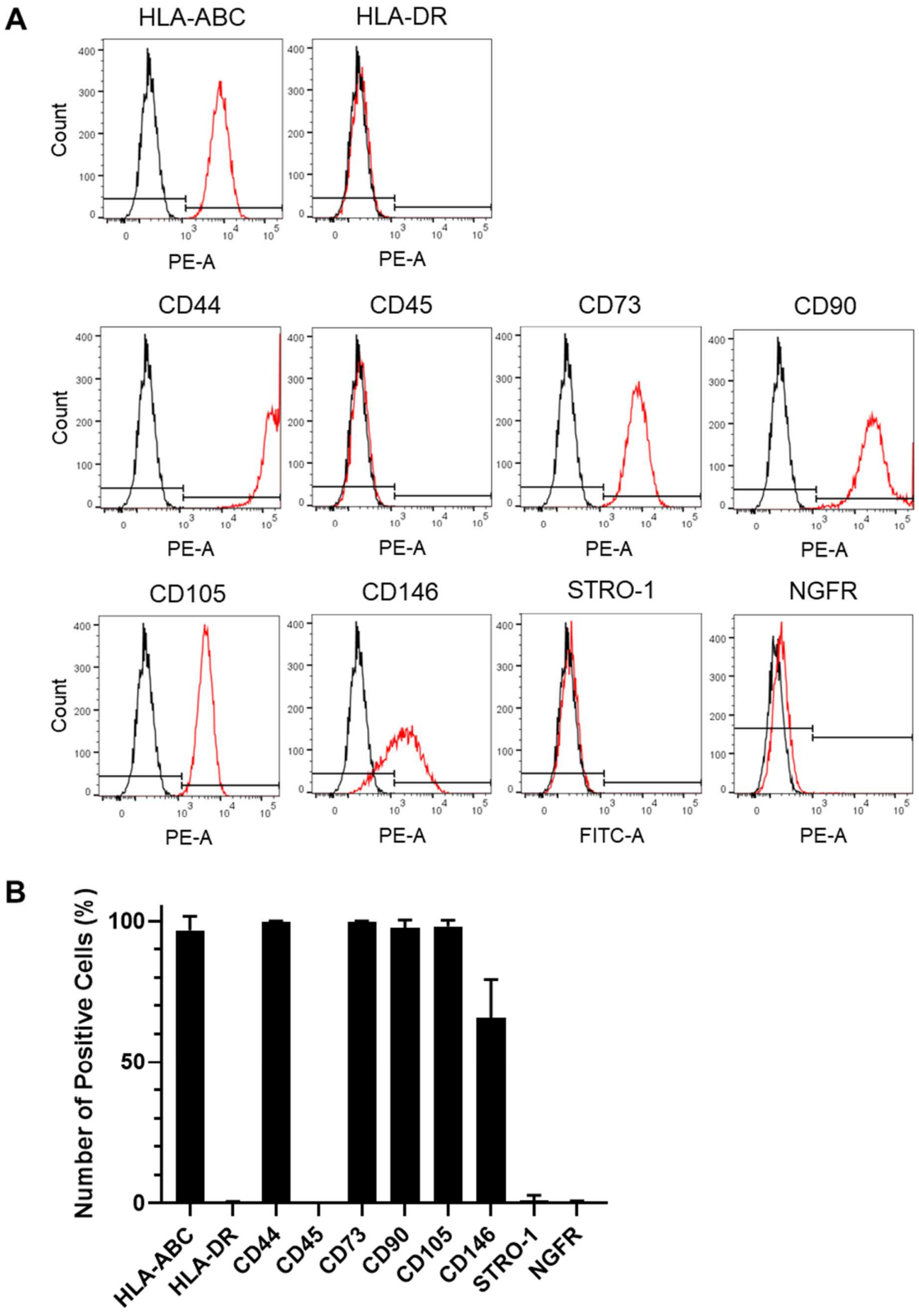
A
HLA-ABC
HLA-DR
CD44
CD45
CD73
CD90
CD105
CD146
STRO-1
NGFR
Count
PE-A
FITC-A
B
Number of Positive Cells (%)
100
50
0
HLA-ABC
HLA-DR
CD44
CD45
CD73
CD90
CD105
CD146
STRO-1
NGFR

C

Protein	Expression (% of single cell population)											
	DPSC1 (p5)	DPSC2 (p3)	DPSC3 (p3)	DPSC4 (p5)	DPSC5 (p4)	DPSC6 (p6)	DPSC8 (p5)	DPSC9 (p5)	DPSC10 (p4)	DPSC11 (p3)	DPSC12 (p3)	Mean±SD
HLA-ABC	99.5	83.1	95.6	99.6	98.8	97.3	99.9	99.7	100.0	93.6	97.2	96.8±5.0
HLA-DR	1.5	0.0	0.1	0.0	0.1	0.2	0.0	0.2	0.1	0.0	0.0	0.2±0.4
CD44	99.7	99.9	99.8	99.9	99.8	99.3	100.0	100.0	100.0	99.9	100.0	99.8±0.2
CD45	0.1	0.0	0.3	0.0	0.0	0.2	0.0	0.4	0.1	0.0	0.0	0.1±0.1
CD73	99.8	99.6	99.8	99.9	99.8	99.4	100.0	100.0	99.9	99.3	98.8	99.7±0.4
CD90	99.7	97.8	92.0	100.0	99.9	94.5	99.9	99.4	99.7	95.9	95.8	97.7±2.7
CD105	97.3	93.3	99.4	99.6	99.7	95.0	99.9	99.4	99.9	97.2	98.8	98.1±2.2
CD146	67.9	58.9	64.5	77.0	85.8	78.8	41.0	56.0	75.5	49.4	68.9	65.8±13.5
STRO-1	3.9	0.4	0.5	0.6	0.3	5.3	0.1	0.3	0.1	0.3	0.3	1.1±1.8
NGFR	0.4	0.0	0.0	0.1	1.0	0.6	0.4	0.9	1.0	0.0	0.0	0.4±0.4

Figure 3.3 Expression of selected surface markers on human DPSC. **(A)** Graphs show the negative control in black and the expression of the surface markers in red. **(B)** The average percentage of cells expressing the surface markers. **(C)** The expression of every surface marker for each DPSC sample. Representative images, data represents mean±SD, n=11.

3.3.4 Human DPSC produced mineral under osteogenic/odontogenic differentiation conditions

Human DPSC were cultured in osteogenic/odontogenic differentiation medium for four weeks, and then stained with Alizarin Red S for calcium deposition. The controls, cultured in standard DPSC medium for the same duration, did not show any staining for calcium deposits (Figure 3.4A), while the differentiated cells stained for calcium deposits as seen by the orange/red colour (Figure 3.4B). Though the cells were cultured for four weeks, mineral deposition could be observed from earlier in the differentiation process. The dye was released and absorbance was measured at 405nm. The absorbance was significantly greater ($p<0.01$) in the differentiated cells (2.99±1.48) than the control cells (0.03±0.004) (Figure 3.4C). Figure 3.4D shows the absorbance of the individual DPSC samples.

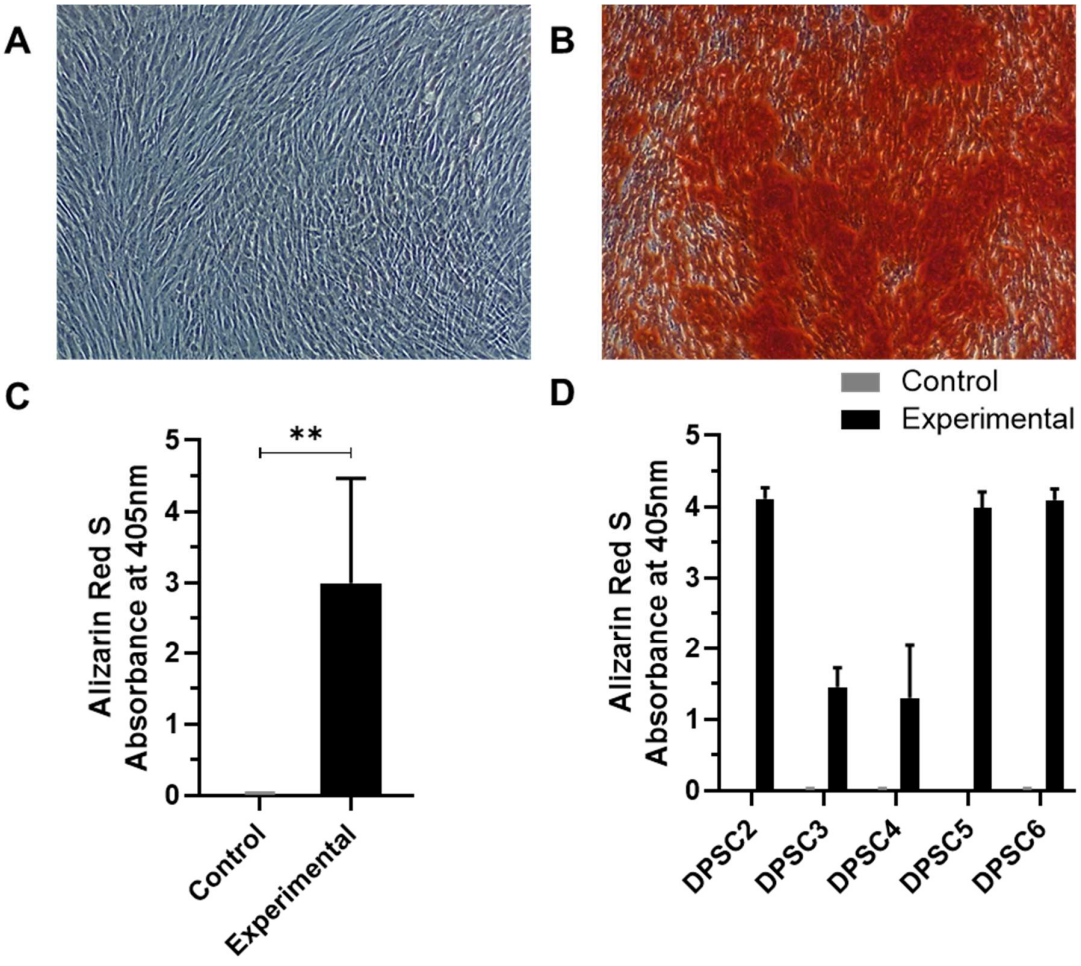

Figure 3.4 Osteogenic/odontogenic differentiation of human DPSC. Cells were cultured in control and differentiation media for 4 weeks. Alizarin Red S staining for calcium deposition was performed. DPSC in **(A)** control and **(B)** osteogenic/odontogenic differentiation conditions. The stain was released and absorbance measured; **(C)** average and **(D)** individual. Representative images taken at 100x magnification (n=13), data represents mean±SD, Mann-Whitney test, n=5, **$p<0.01$.

3.3.5 Human DPSC differentiated into chondrocytes

Human DPSC were cultured in serum-free chondrogenic differentiation medium for one week, and then stained with Saf-O for sGAGs (e.g. chondroitin sulphate), which are commonly used to detect the presence of chondrocytes *in vitro*. This assay was based on the fluorescent staining of DNA with DAPI and sGAGs with Saf-O, and allows for qualitative and quantitative results. The differentiated cells (Figure 3.5B) showed more orange/pink stain than the control cells (Figure 3.5A). The mean fluorescence ratio was calculated. It was significantly greater ($p<0.01$) in the differentiated cells (63.67±15.97) than the control cells (27.83±6.88) (Figure 3.5C). The individual DPSC sample ratios are shown in Figure 3.5D, with DPSC3 showing a smaller difference between the control and differentiated cells.

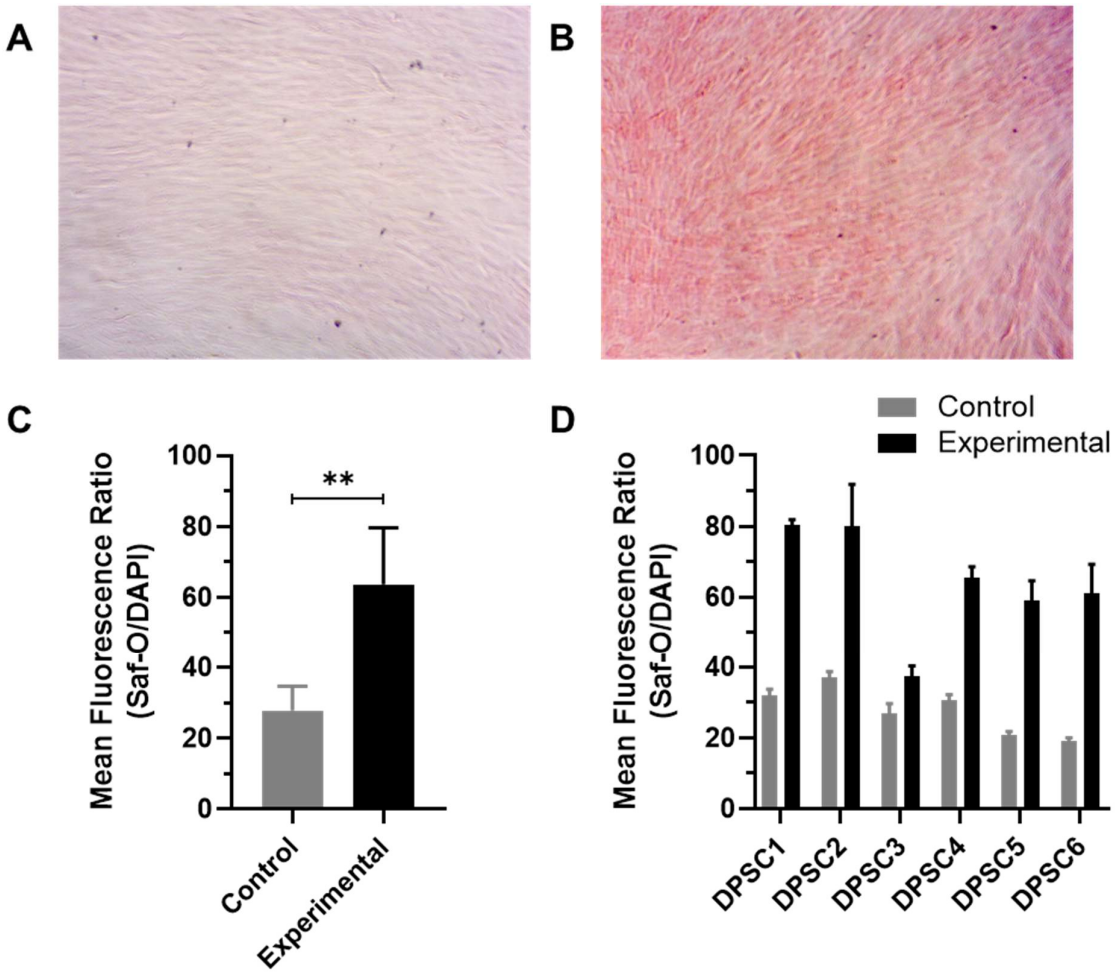

Figure 3.5 Chondrogenic differentiation of human DPSC. Cells were cultured in control and differentiation media for 1 week. Saf-O staining for sGAG expression was performed. DPSC in **(A)** control and **(B)** chondrogenic differentiation conditions. Mean fluorescence ratio; **(C)** average and **(D)** individual. Representative images taken at 100x magnification, data represents mean±SD, Mann-Whitney test, n=6, **$p<0.01$.

3.3.6 Human DPSC differentiated into adipocytes

Human DPSC were cultured in adipogenic differentiation media for six weeks, and then stained with Oil Red O for lipid droplets. The first medium tested appeared unsuccessful, as no difference was observed in staining for lipid droplets between the control and differentiated cells (Figure 3.6). Haematoxylin staining (not shown) highlighted the unhealthy state of the cells, suggesting that this method affected their survival and hence differentiation was not occurring. This method was based on one published by Gimble in 1998 (42), and optimised using human bone explant cultures. This optimisation involved the removal of 3-isobutyl-1-methylxanthine, as well as the replacement of hydrocortisone with dexamethasone at a lower dose. This optimised method had not been tested for MSC from other sources. Due to lack of staining and poor culture viability, quantification was not performed.

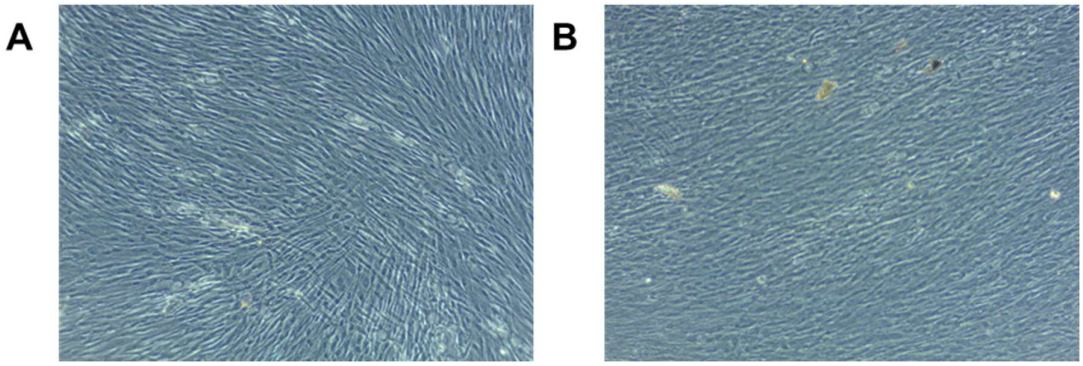

Figure 3.6 Adipogenic differentiation of human DPSC using adipogenic induction medium 1. Cells were cultured in control and adipogenic differentiation media for 6 weeks. Oil Red O staining for lipid droplets was performed. DPSC in **(A)** control and **(B)** adipogenic differentiation conditions. Representative images taken at 100x magnification, n=3.

The second medium had previously been used by our research group with DPSC. Here, rosiglitazone was replaced with indomethacin. Based on the images, it was unclear whether there was a difference between the control (Figure 3.7A) and differentiated (Figure 3.7B) cells. The Oil Red O dye was solubilised and the absorbance measured. There was no significant difference between the control (0.07±0.01) and differentiated (0.06±0.01) cells (Figure 3.7C). The individual DPSC samples are shown in Figure 3.7D.

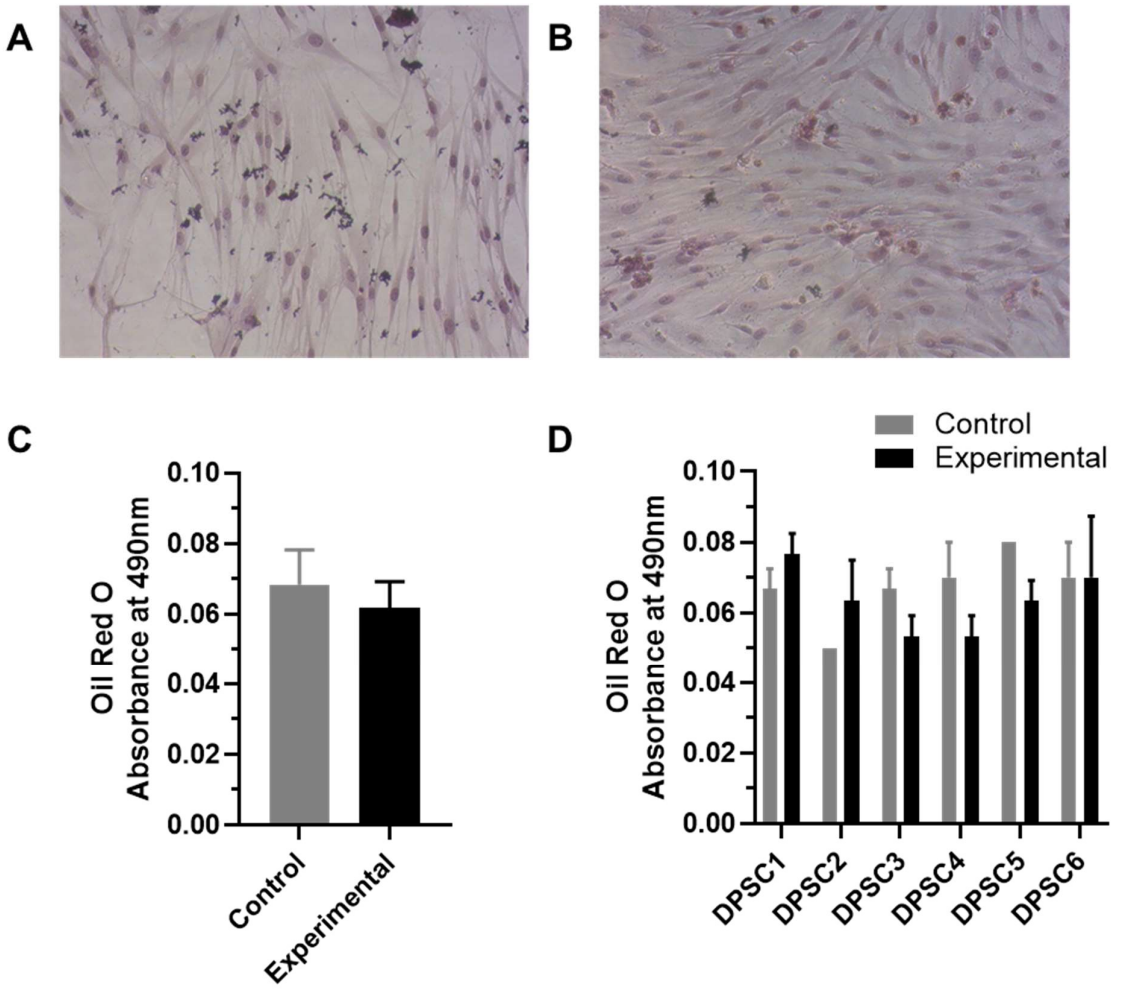

Figure 3.7 Adipogenic differentiation of human DPSC using adipogenic induction medium 2. Cells were cultured in control and adipogenic differentiation media for 6 weeks. Oil Red O staining for lipid droplets was performed. DPSC in **(A)** control and **(B)** adipogenic differentiation conditions. The stain was released and absorbance measured; **(C)** average and **(D)** individual. Representative images taken at 200x magnification, data represents mean±SD, Mann-Whitney test, n=6.

The third medium was as published by Gimble in 1998 (42). Unlike the control cells (Figure 3.8A), stained lipid droplets were observed in all of the differentiated cells (Figure 3.8 B and C). Quantification of Oil Red O showed greater absorbance ($p<0.05$) in the differentiated cells (0.14±0.09) when compared to the control cells (0.08±0.01) (Figure 3.8D). Figure 3.8E shows the individual DPSC samples, where five of the six samples showed a small increase in absorbance in the differentiation cells and one showed a more than two-fold increase (DPSC2). Exclusion of this sample did not remove significance.

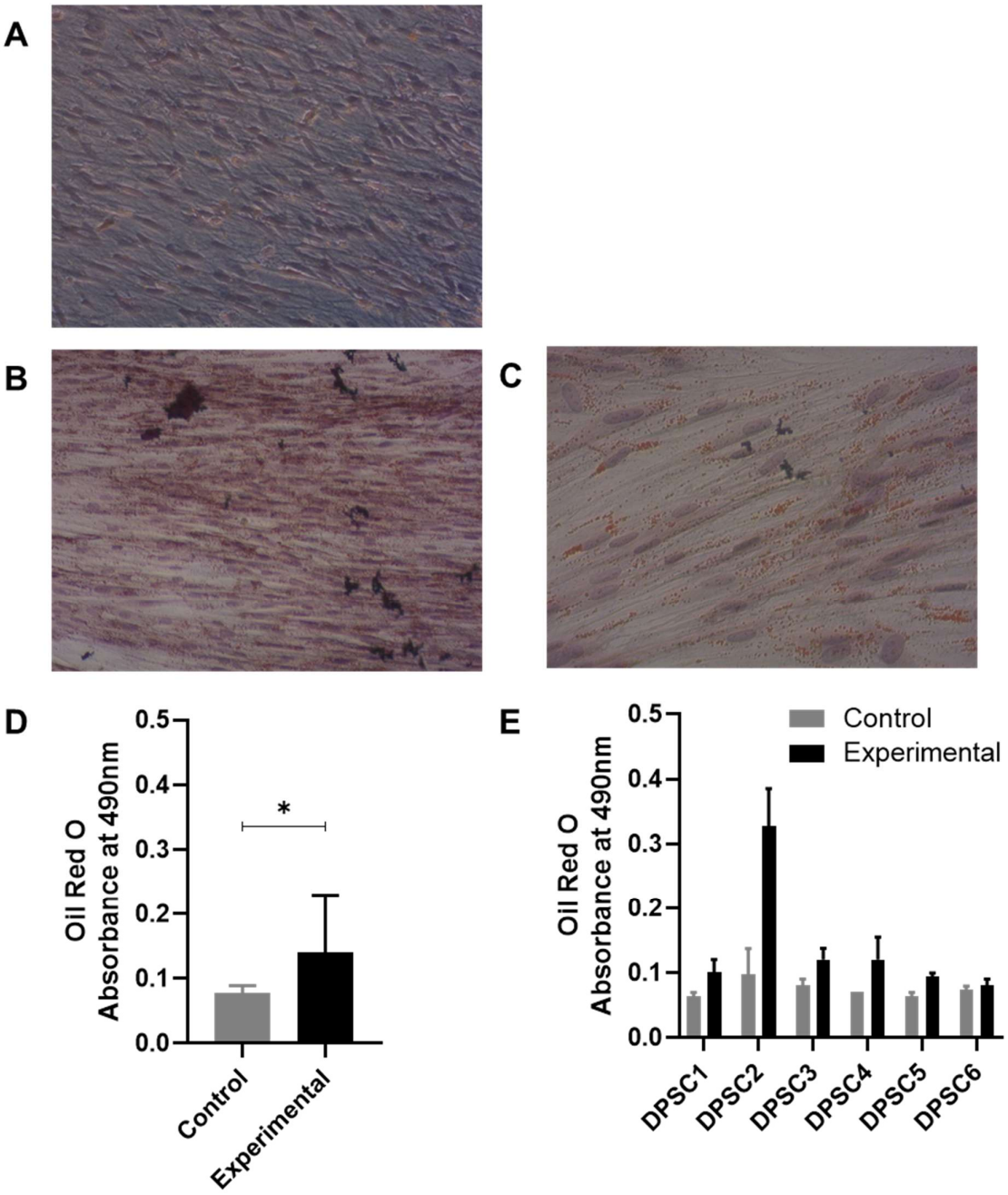

Figure 3.8 Adipogenic differentiation of human DPSC using adipogenic induction medium 3. Cells were cultured in control and adipogenic differentiation media for 6 weeks. Oil Red O staining for lipid droplets was performed. DPSC in **(A)** control and **(B, C)** adipogenic differentiation conditions. The stain was released and absorbance measured; **(D)** average and **(E)** individual. Representative images taken at 200x (A, B) and 400x (C) magnification, data represents mean±SD, Mann-Whitney test, n=6, *p<0.05.

3.3.7 Human DPSC were able to differentiate into neuronal-like cells

Three published neuronal differentiation protocols for human DPSC were tested. At the completion of each protocol, the samples were immunostained for the early neuronal protein nestin (acronym; neuroectodermal stem cell marker), intermediate neuronal protein tubulin β-III chain (referred to as β-III tubulin) and mature neuronal protein neurofilament-medium poly-peptide (NF-M).

The first protocol, published by Arthur *et al*. in 2008 (1), involved culturing the DPSC in three types of media sequentially for one week in each media. There was no obvious morphological change after medium A (Figure 3.9A). The cells appeared to display a bipolar morphology and were less flat following medium B (Figure 3.9A). They appeared morphologically similar after medium C, but flatter and formed clusters (Figure 3.9A). Staining was clearly evident for nestin but weak for β-III tubulin and NF-M, with a lack of extensive processes (Figure 3.9B).

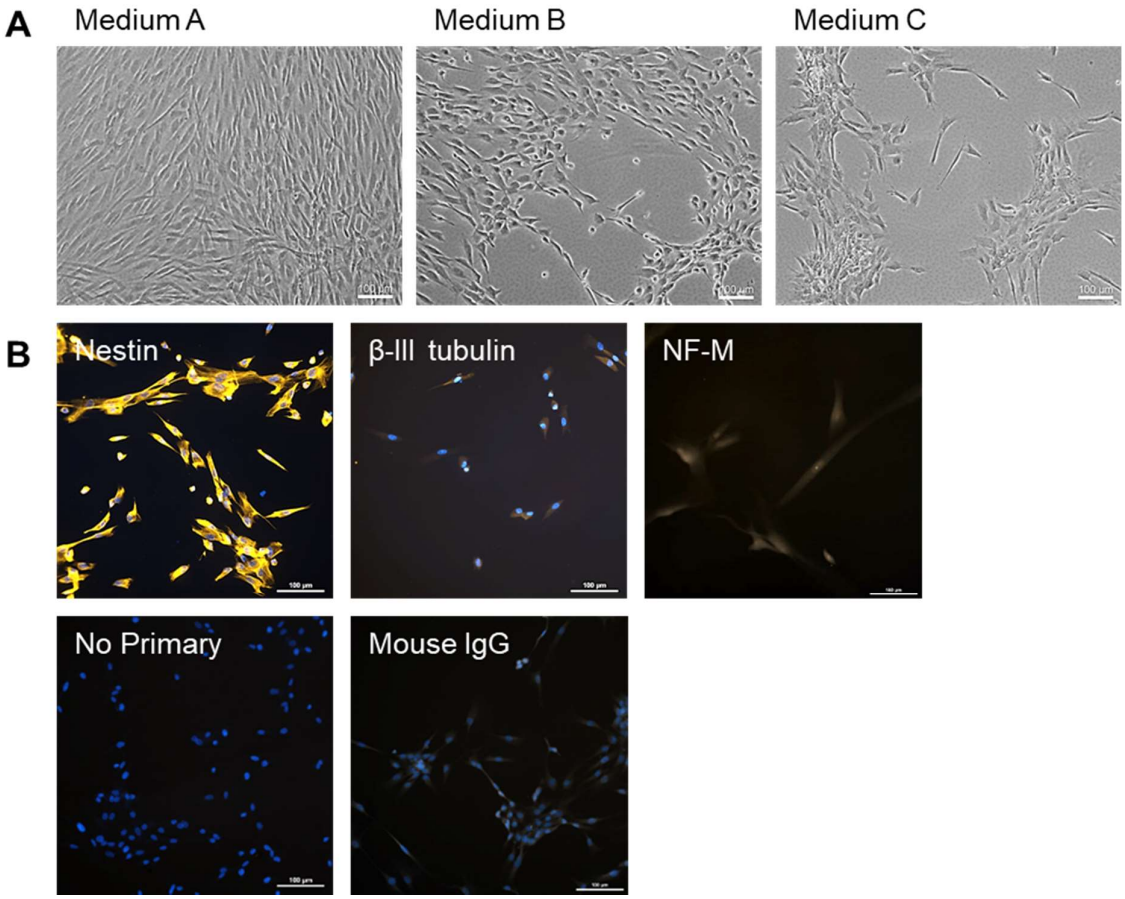

Figure 3.9 Neurogenic differentiation of human DPSC using the method by Arthur *et al*. 2008. **(A)** The cells at the completion of each step of the method: 1 week in medium A, 1 week in medium B and 1 week in medium C. **(B)** Expression of the neuronal proteins: nestin, β-III tubulin and NF-M, upon completion of the protocol. Negative immunostaining controls shown. Representative images, n=2, scale bar=100µm.

The second protocol, published by Kiraly *et al*. in 2009 (2) and routinely used within our laboratory (43), used four types of media with a two-week duration. The cells were firstly cultured in neuronal induction medium for 24 hours, during which no apparent physical change was observed (Figure 3.10A). They were next cultured in epigenetic reprogramming medium for 48 hours. The DPSC were subsequently cultured in neural differentiation medium for three days. Morphologically, the cells appeared larger and rounder, and some multipolar cells were present (indicated by red arrow). The final step was in neuronal maturation medium for one week, in which more cell extensions were observed. After two weeks, nestin-positive staining was observed in all the cell samples, whereas β-III tubulin staining was not present, while some NF-M staining was observed (Figure 3.10B).

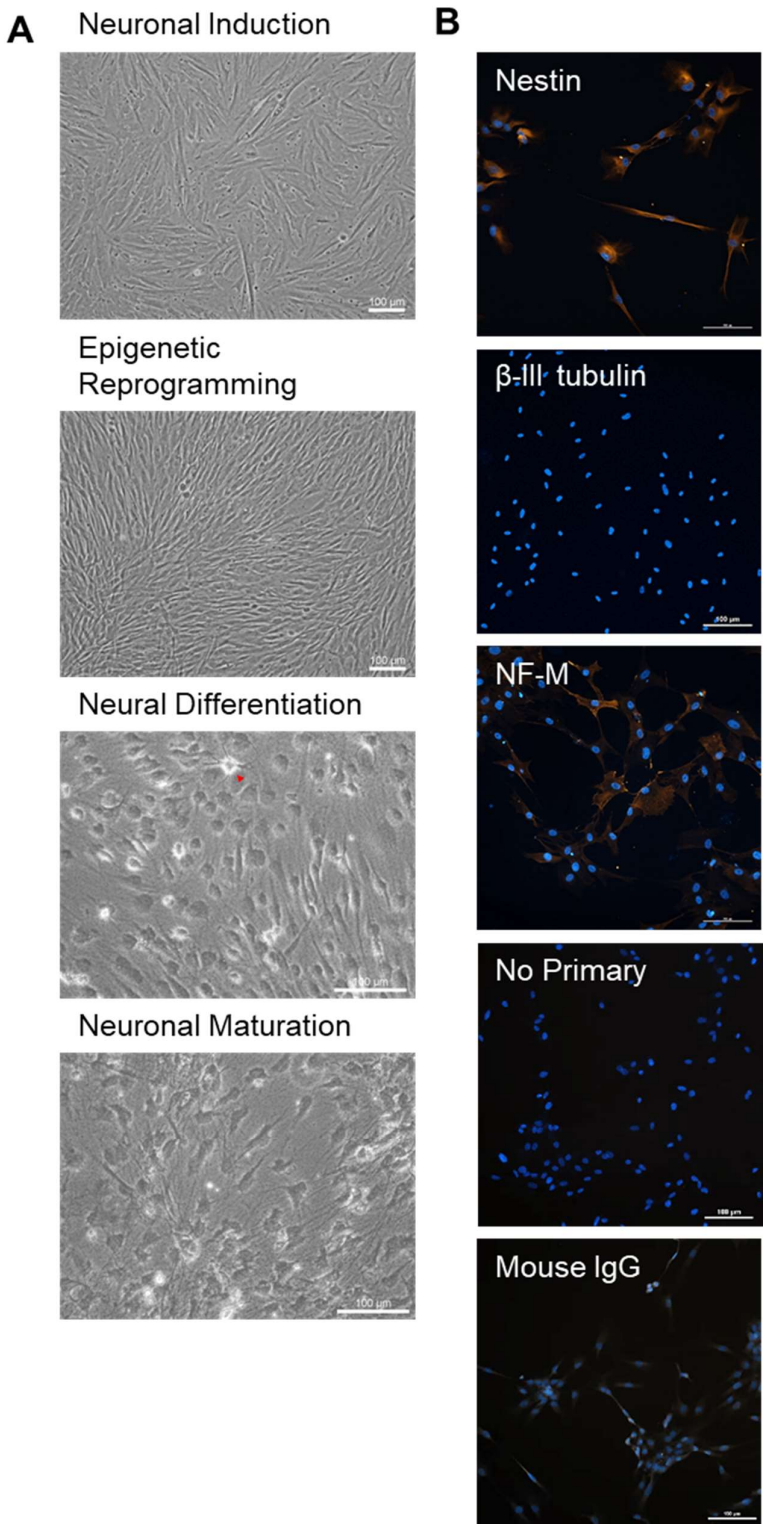

Figure 3.10 Neurogenic differentiation of human DPSC using the method by Kiraly *et al*. 2009. **(A)** Cells at the completion of each step of the method: 24 hours neuronal induction, 48 hours epigenetic reprogramming, 3 days neural differentiation, and 7 days neuronal maturation. Red arrow indicates a multipolar cell. **(B)** Expression of the neuronal proteins: nestin, β-III tubulin and NF-M, upon completion of the protocol. Negative immunostaining controls shown. Representative images, n=6, scale bar=100µm.

The third protocol, based on the method published by Gervois *et al*. in 2015 (3), involved a one week neuronal induction step (suspension culture) followed by four weeks of neuronal maturation. In the neuronal induction step, while both monolayer and suspension cultures were achieved (Figure 3.11A), there was difficulty dissociating the spheres with viable cells remaining, therefore the monolayer cultures were used to proceed with the neuronal maturation step. Following neuronal induction, the cells were seeded in neuronal maturation medium and grown as a monolayer on poly-L-lysine and laminin coated surfaces. In Figure 3.11A, the morphology of the cells from two weeks in neuronal maturation medium is shown, up until five weeks. Within two weeks the cells began to exhibit neuronal-like morphologies. Unlike the previous methods, the majority of the cells displayed large spherical cell bodies with long extensions reaching out to make connections with other cells. Both bipolar and multipolar cells were present. The cells appeared in clusters with some bipolar cells making connections towards other cell clusters. Upon completion of the protocol, these cells stained for all three neuronal markers, with NF-M highlighting the extensions and connections between cells (Figure 3.11B). Patch-clamp analysis was performed by Dr. Grigori Rychkov (University of Adelaide and SAHMRI, SA, Australia) on several of these samples, however no voltage-dependent ion currents were detected (data not shown).

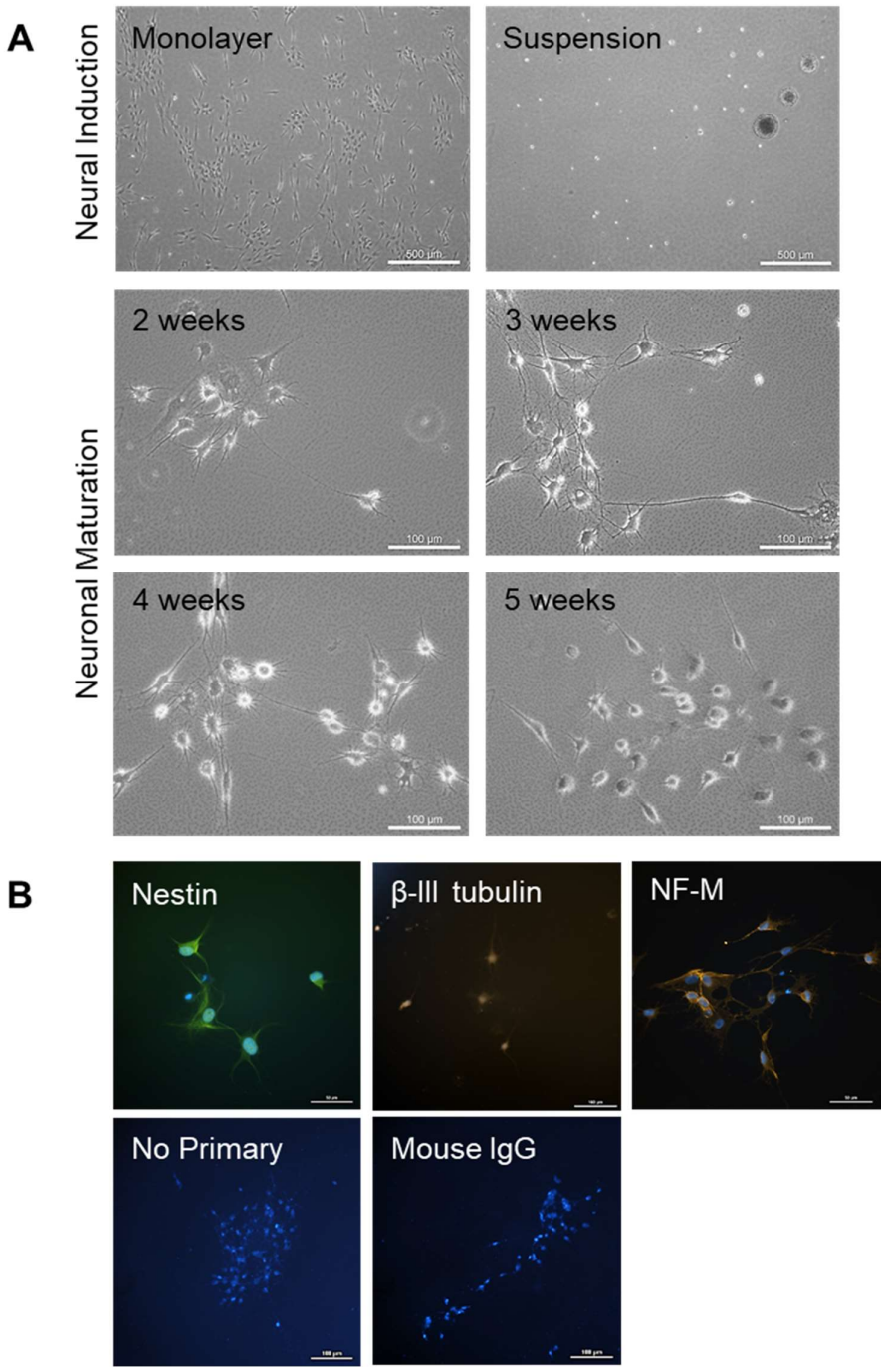

Figure 3.11 Neurogenic differentiation of human DPSC using the method published by Gervois *et al*. 2015. **(A)** Cells after 1 week neural induction (monolayer and suspension cultures), and at 2-5 weeks neuronal maturation. **(B)** Expression of neuronal proteins: nestin, β-III tubulin and NF-M, upon completion of the protocol. Negative immunostaining controls shown. Representative images, n=3, scale bar=500µm (A; neural induction), 100µm (A; neuronal maturation, B; β-III tubulin and controls), 50µm (B; nestin and NF-M).

The third neuronal differentiation protocol was applied to the DPSC samples that would be used for subsequent reprogramming experiments. Upon differentiation, all of the DPSC samples stained for the three neuronal markers (Figure 3.12A). Nestin staining was least intense, however β-III tubulin and NF-M appeared highly expressed (Figure 3.12 A and B). In this experiment, poly-L-lysine was substituted by poly-D-lysine, as cells displayed better adherence (Figure 3.12C).

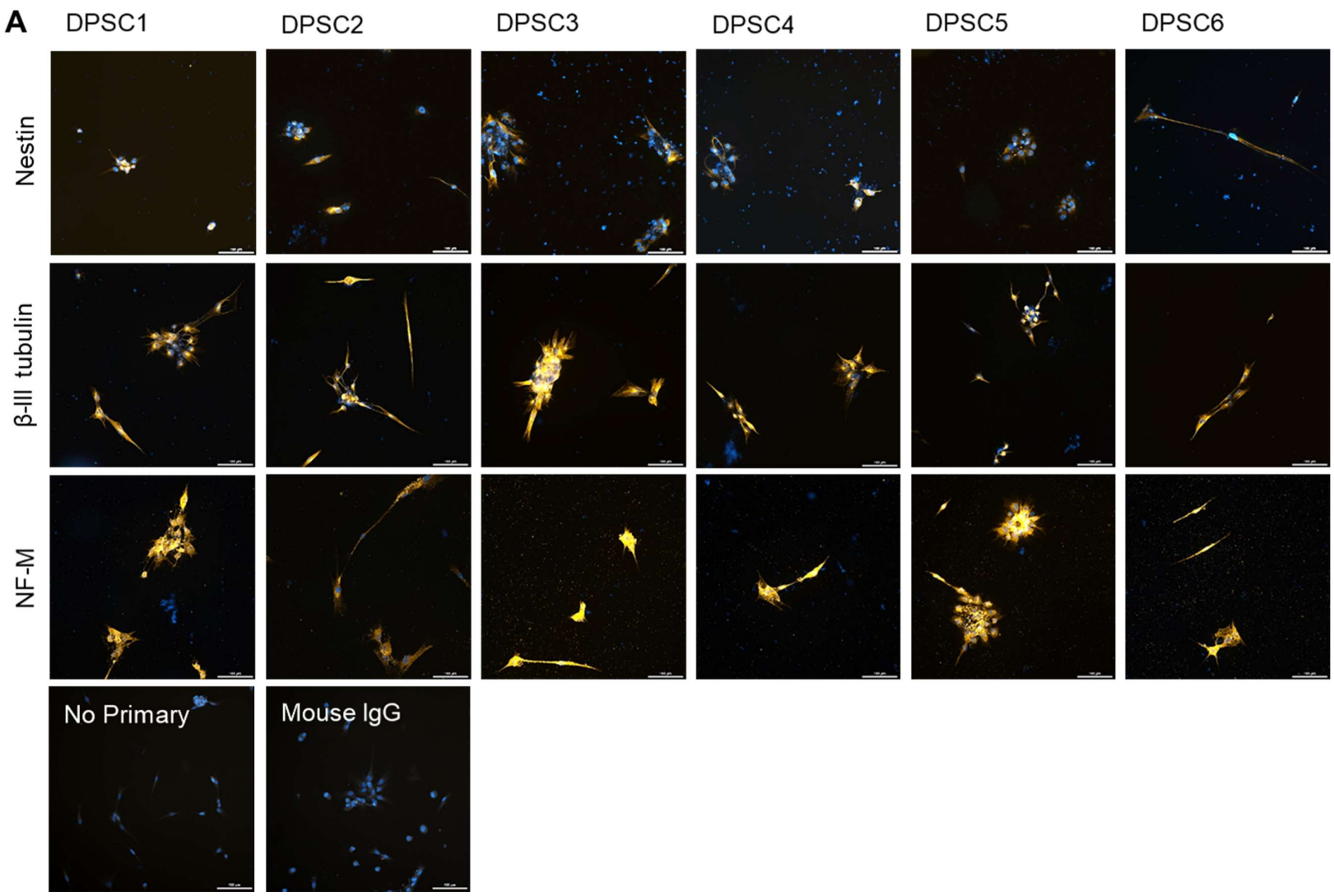
A
DPSC1
DPSC2
DPSC3
DPSC4
DPSC5
DPSC6
Nestin
β-III tubulin
NF-M
No Primary
Mouse IgG

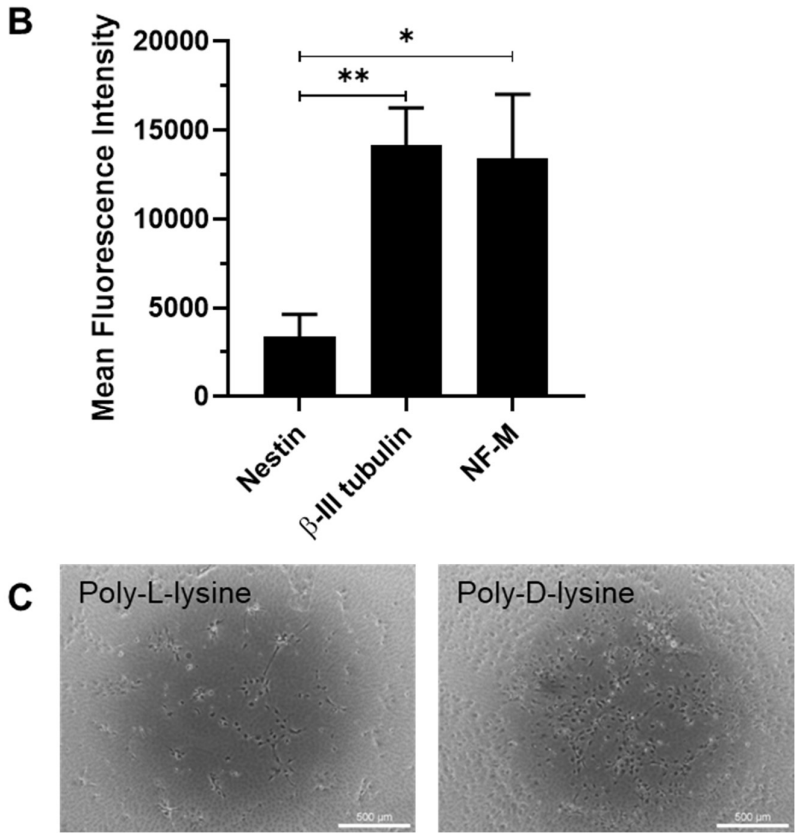

Figure 3.12 Neurogenic differentiation of human DPSC. **(A)** Human DPSC samples to be used for reprogramming experiments were differentiated (1 week monolayer neural induction and 4 weeks neuronal maturation) and immunostained for neuronal proteins: nestin, β-III tubulin and NF-M. Negative immunostaining controls shown. **(B)** Mean fluorescence intensity of proteins. **(C)** DPSC cultured on poly-L-lysine and poly-D-lysine -coated glass coverslips in standard DPSC culture medium. Data represents mean±SD, Kruskal-Wallis one-way ANOVA with Dunn's multiple comparisons test, n=6, scale bar=100µm (A) and 500µm (C), *$p<0.05$, **$p<0.01$.

3.4 | Discussion

Stem cells are able to self-renew and differentiate into multiple cell types. This chapter presents the results of several assays used to characterise human DPSC as a stem cell population. DPSC were isolated from human third molars using the enzymatic digestion method. These cells were characterised and stored for subsequent use in reprogramming experiments. The DPSC exhibited a spindle-shaped morphology, plastic adherence, and a high proliferation rate. They expressed common MSC surface antigens as determined by flow cytometry. They were also able to produce mineral indicating their potential to differentiate into osteoblasts and odontoblasts, expressed sGAGs for chondrogenic differentiation, stained for lipid droplets produced by adipocytes, and differentiated into neuronal-like cells *in vitro*.

In addition to the common MSC markers CD44, CD73, CD90 and CD105, the panel of surface antigens also included CD146, STRO-1 and NGFR. These three markers are co-expressed on all clonogenic MSC and are used to identify MSC (32-35). Staining for CD146 on cultured DPSC showed heterogeneous expression, while STRO-1 and NGFR were negative.

The endothelial biomarker CD146 is a cell adhesion molecule, and appears to be involved in cell mobility and adhesive interactions (44). It has been identified in MSC from different sources, indicating their association with the microvasculature (35). In MSC, expression of CD146 is linked with high proliferation and multipotency (45). The $CD146^+$ sub-population of DPSC has demonstrated greater regenerative capacity of the dentin-pulp complex than the negative sub-population (46), while a $CD146^-$ DPSC sub-population has led to positive outcomes in a stroke model (47). This suggests that these sub-populations differ in developmental potential. The heterogeneous staining of CD146 in DPSC presents the opportunity to study a sub-population of DPSC, as sufficient cell numbers can be obtained.

STRO-1 has been used to recognise and isolate MSC-like populations (33). The STRO-1 monoclonal antibody was produced using $CD34^+$ bone marrow cells as immunogen, and the antigen to which it binds was only recently identified (48). STRO-1 distinguishes a population of less than ten per cent of adult human bone marrow cells (33, 49). The $STRO\text{-}1^+$ cells display properties of multipotent stem cells, with high levels of STRO-1 antigen expression associated with an immature MSC phenotype, where loss of STRO-1 expression coincides with MSC maturation (33, 50-53). It is thus an early marker of MSC-like populations, and is seen to decrease early during *ex vivo* expansion in serum-supplemented media (33, 35). This may explain why STRO-1 was not detected in these DPSC. The DPSC used here were between

passages 3 and 6, as sufficient cell numbers were required for this and other assays. At that stage, the STRO-1 expression may have decreased. However, inter-donor variability appears to also be a factor to consider here, as expression closer to five per cent was observed in two samples which were of higher passage, while the rest of the samples of low and high passage remained negative for STRO-1 expression. Similar results with very low STRO-1 detection in DPSC have been reported by other research groups (31, 54).

Low-affinity NGFR has been relied upon as a surface marker for isolation of bone marrow-derived MSC that is co-expressed with STRO-1 (32, 34), and is recognised as a bona fide neural crest stem cell marker (55). NGFR is a receptor for neurotrophins, which are growth factors involved in neuronal survival and differentiation. In DPSC, positive expression is linked to higher levels of NSC markers (56), but expression is often quite low at less than ten per cent of the DPSC population, and decreases during *ex vivo* culture (31, 32, 54, 56-58). This down-regulation during *ex vivo* expansion corresponds to the maturation of MSC cultured in serum-supplemented media (32, 33). This sub-population may represent the neural crest-derived DPSC, and thus the low expression levels of NGFR may indicate the low percentage of neural crest-derived cells in the population (58). Another factor that may affect the expression levels detected is the antibody efficacy. With variation between DPSC samples and very low detection of NGFR, obtaining sufficient $NGFR^+$ DPSC for further study would prove to be difficult.

The DPSC demonstrated multi-lineage differentiation potential along all three lineages used to characterise MSC, as well as the neuronal lineage. They showed great potential to differentiate into osteoblasts or odontoblasts, with significant amounts of calcium deposition. They were also able to differentiate along the chondrogenic lineage, based on staining for sGAGs. On the other hand, the DPSC proved more difficult to direct along the adipogenic lineage. Three differentiation protocols were examined, with the Gimble (1998) method proving most effective for the DPSC (42). While the difference between the control and differentiated cells was significant and lipid droplets were visible in all samples, differences were observed between samples, with most showing a small increase in staining for differentiated cells. Prolonging the differentiation culture would lead to more adipogenic differentiation. DPSC in their natural environment are not prone to differentiate into fat cells as these cells are not a component of teeth and previous research has also shown the adipogenic potential of DPSC is not as great as odontogenic, osteogenic and chondrogenic (31, 59). This may be dependent on sub-optimal inductive conditions specific for DPSC.

Finally, the neurogenic potential of the DPSC was examined. Many neuronal differentiation methods have been investigated using DPSC (36), with varied success and efficacy.

The first method utilised was one of the earlier neuronal differentiation methods, developed by our research groups, and was first to examine the functionality of the cells following differentiation (1). This method involved three steps, one week in duration each, with the bFGF and EGF growth factors used for neuronal induction. In the experiments here, these cells did not resemble neurons and showed low staining for the intermediate β-III tubulin and mature NF-M neuronal markers with a lack of extensive processes. They stained for the early neuronal marker nestin, however this protein is detected in many cell types, including in undifferentiated DPSC, and alone cannot be used as a marker (58). The results varied from those that were previously published, which showed neuronal-like morphology and neuronal protein expression (1). The outcome may have been influenced by the differences in DPSC samples, which could be related to the heterogeneity and composition of the population as well as experimental aspects such as passage stage. Additionally, differentiation reagents may cause variation.

The second method was a two-week protocol, which in the original publication resulted in neuronal-like cells that exhibited voltage-dependent sodium and potassium ion currents (2). Instead of growth factors, this method used a demethylating agent to modify the epigenome and initiate neuronal induction, followed by the use of multiple neuronal promoting agents for the differentiation and maturation steps. The resulting cells here were more neuronal-like in morphology, though there was limited expression of neuronal markers.

The third method examined was more recently published and involved growing the DPSC in a three-dimensional structure (3). This two-week method was reported to produce neuronal-like cells with voltage-gated sodium and potassium ion channels and able to produce some action potentials. To initiate neuronal induction, the bFGF and EGF signalling molecules were incorporated, but the DPSC were allowed to grow in suspension in low-attachment plates and form spheres, rather than grow as monolayers. This better mimics the natural microenvironment and permits cell interactions, which is essential for neuronal commitment (3). Subsequent to this, the cells underwent neuronal maturation, similar to the previous method, with the incorporation of cyclic AMP, which has a role in differentiation of neuronal progenitors, and neurotrophin-3, which is essential for maturation (2). In the experiments here, a neuronal morphology was observed in most cells and nestin, β-III tubulin and NF-M were detected, with strong NF-M expression. Based on these results, this method was most successful and was

chosen to analyse all the DPSC to be used for future reprogramming experiments. All samples showed consistent neuronal-like morphology and expression of neuronal markers.

The MFI of the neuronal proteins was used to indicate the level of differentiation; more intense staining means greater protein expression, and greater expression of late markers means further progressed neuronal differentiation. The limitations of using MFI to compare different proteins are addressed by increasing the sample size. While percentages of the number of cells expressing the proteins of interest can be useful, they were not included here as the cell numbers varied and the distribution of cells was uneven due to the differentiation method, adherence to cover slips and loss during the staining procedure, and would lead to biased cell counts.

Both the suspension and monolayer cultures were tested in the initiation step but the monolayer culture was subsequently used. The drawback to the suspension culture was firstly monitoring size, as going over 250µm increases cell death in the centre of the sphere. The researchers that developed this method reported 40 to 50 per cent cell loss with higher diameters (3). These spheres needed to either be dissociated in preparation for the neuronal maturation step or the cells could be allowed to migrate out of the spheres. The dissociation was not effective, with cells lost in the process, while allowing the cells to grow out of the spheres did not allow for cell density to be controlled. Both ways resulted in lower cell numbers at the next stage, which provides an issue for downstream applications requiring sufficient cell numbers. A question that arises from this method using suspension cultures, is whether these spheres are a result of DPSC aggregation in solution or clonal expansion. The low numbers observed, and thus not proceeded with, suggested that the cells may be aggregating.

The cells using the Gervois *et al.* 2015 method (3) were cultured in neuronal maturation for four weeks; this may not be sufficient to detect many functional cells. Whilst not examined extensively, several DPSC differentiated using this method underwent patch-clamp analysis but no electrical activity was detected. The patch-clamping was kindly done by Dr. Grigori Rychkov. Pluripotent cells undergo differentiation into neurons in 30 to 60 days, using established protocols (60). These DPSC are multipotent, suggesting differentiation should be more efficient, however they are also heterogeneous and from a non-neural tissue. Thus, they may require longer periods to gain neuronal function, particularly since there is no established successful and efficient neuronal differentiation protocol.

There are several other practical considerations for neuronal differentiation methods, such as cell density and growth surfaces. Optimisation of cell density is required to prevent over-

confluency early in the method, while cells remain close to establish a network later in the method. This would eliminate the need to passage and lose cells that are undergoing differentiation and becoming post-mitotic. The surface the cells grow on (e.g. plastic or glass, substrate coating) can also affect survival and differentiation success. For neuronal differentiation, certain substrates are often required, most frequently poly-L-lysine and laminin (61). The concentration used and the method for coating (e.g. timing, washes) can affect how well the surface is coated and thus the cells adhere. It may be necessary to increase the concentration of laminin, as 10μg/mL is used for the neural differentiation of human ESC (62). Some substrates also perform better (63). The neuronal differentiation method by Gervois *et al.* 2015 reported poly-L-ornithine, performed well (3, 64), which was initially substituted with poly-L-lysine here, as this was more accessible and used in the other methods (1, 2). Once this method was chosen to continue with, poly-D-lysine was used instead, which has been shown to promote neural adhesion (65). When cells were cultured side-by-side on both, more cells were seen to adhere to the poly-D-lysine coated surface. This enantiomer is artificially produced unlike the natural poly-L-lysine, therefore it is believed to not be susceptible to enzymatic degradation and prolongs adherence.

These characterisation assays demonstrated the stem cell properties of the DPSC, but also highlighted the inter-donor variability. The DPSC used here were isolated from individual teeth and expanded in bulk (i.e. polyclonal population). Inter-donor variability can be attributed to factors such as age and health, both general health and dental health. The donors were all in the younger age group (18-40) and included both males and females. The molars were extracted due to impaction, suggesting otherwise healthy teeth, and no microbial contamination was detected. However, other lifestyle factors and medical conditions not relating to dental health may indirectly affect the dental cells. Whilst the ethics of this study did not permit obtaining specific information from donors due to privacy and identification, future studies could examine how other health factors may affect DPSC. It is also worth noting that our research group has not found any significant differences between DPSC from younger and older demographics, with regard to their stem cell properties (manuscript under review). Additionally, no differences were observed here regarding the donor sex. However, future research could examine greater numbers of samples from male and female donors of various ages. Furthermore, the physical force from the impaction may have an effect on cellular homeostasis. As previously mentioned, the cell passage can introduce variation (58, 66). Some of the differences between DPSC populations may also become more evident under certain conditions, such as differentiation down the neural lineage. There have also been studies that have found that commercial differentiation media give more consistency, and this is likely due to less variation in

components and composition (66). With these parameters in mind and the heterogeneous nature of DPSC populations, the efficiency of methods may be varied. This highlights the need to better understand the inter-donor variation, identify a homogeneous sub-population for study, and develop methods that are efficient and/or suitable for a varied population or specific to sub-populations.

This chapter demonstrated the stem cell properties of DPSC. The DPSC had multi-lineage differentiation capacity and possessed a stem cell marker profile as per the guidelines for classifying MSC. The DPSC displayed limited neuronal potential, with current methods providing low yields. The following chapters will utilise these characterised DPSC populations to investigate reprogramming into neural cells.

CHAPTER 4

CONSTRUCTION AND PREPARATION OF VIRAL VECTORS

4.1 | Introduction

Cellular reprogramming involves the introduction of transcription factors into cells to be modified. As outlined in Chapter 1, the transcription factors selected to be investigated in reprogramming human DPSC were OCT4, SOX2 and HES1. These transcription factors will be introduced into DPSC using viral vectors. This chapter focuses on the preparation of these viral vectors and functional validation in DPSC.

Viral vectors are tools that are widely used for gene transfer, and in the context of reprogramming, are used to introduce the transcription factors. Retroviruses have been central to the development of gene therapy and are widely used in molecular biology, as they can mediate stable genetic modifications (67). Their genome is a single-stranded positive-sense RNA molecule, which is reverse transcribed and then integrated into the target cell genome (68). Whilst this capability is undesired in terms of wild-type viral infection, in the context of gene therapy and molecular biology, these viral systems have been modified for safety while taking advantage of this integration feature (69).

Within the retroviridae family, two genera are commonly used in research; the simple γ-retrovirus (often referred to as retrovirus, and to be referred to as such here) and the complex lentivirus (67). Retroviral systems are based on the murine leukaemia viruses, while the lentiviral systems, which have a few extra genes, are based on the human immunodeficiency virus (HIV) (67).

The viral vector systems used for gene transfer have been developed to produce replication-incompetent viral particles by separating the viral elements over multiple plasmid constructs. The system components include the transfer plasmid, the envelope plasmid, and the packaging plasmid(s) (67). The transfer plasmid contains the gene of interest cDNA, while the necessary viral elements are delivered either in *cis* (sequences active as nucleic acid) or *trans* (protein-coding sequences) (70, 71). In the transfer plasmid containing the packaging signal, the transgene is flanked by the long terminal repeat (LTR) sequences, which facilitate integration into the target cell genome (70, 71). The packaging plasmids contain the open reading frames that encode for proteins essential for viral assembly; these are *gag*, *pol* and *env*. The gag poly-protein encodes for the structural proteins (matrix, capsid and nucleocapsid), the pol poly-protein encodes for the enzymes (protease, reverse transcriptase, and integrase), and *env* encodes for the envelope surface glycoprotein, which is placed on the envelope plasmid (67, 70). Lentiviruses encode for a few extra proteins, including tat and rev, which are involved in

regulation of gene expression (67). Tat enhances the efficiency of transcription while rev is required for nuclear export of micro RNAs to allow translation (72). All the plasmids are co-transfected into a cell line, typically human embryonic kidney 293T (HEK293T) cells, to produce replication-incompetent recombinant virus. The HEK293T cell line is a variant of the HEK293 cell line, containing the simian virus 40 (SV40) large T-antigen, which allows for amplification of transfected plasmids that carry the SV40 origin of replication (73). This increases the amount of recombinant virus produced.

The 5' LTR of retroviral and lentiviral vectors is a weak promoter, and in lentiviruses is tat-dependent (2nd generation lentiviral system) (67, 71). A hybrid promoter is more commonly used (3rd generation lentiviral system), which has a partially deleted 5' LTR fused to a heterologous enhancer/promoter (72). This makes the lentivirus tat-independent, and thus decreasing the viral genes used (72). With lentiviral systems, a 2nd generation transfer plasmid requires a 2nd generation packaging system (envelope plasmid, and packaging plasmid containing *gag*, *pol*, *rev* and *tat*), while a 3rd generation transfer plasmid can be used with 2nd or 3rd (envelope plasmid, packaging plasmid containing *gag* and *pol*, and packaging plasmid containing *rev*) generation packaging systems (69-71). Retroviral packaging systems are all the same (70).

A key consideration with these systems is the promoter in the transfer vector, which can affect the efficiency and stability of cDNA expression in target cells (74-76). Promoters for eukaryotic expression vectors include the viral cytomegalovirus (CMV) promoter and the human elongation factor-1α (EF-1α) promoter, amongst others. The CMV promoter is a strong promoter that constitutively expresses downstream genes and so is commonly used for general mammalian expression (75, 76). While it works well on most cells, it is possible that in some cells it is silenced by anti-viral mechanisms leading to poor expression (74). The EF-1α promoter is considered a 'housekeeping' gene and has been found to be a better promoter in some cells, such as haematopoietic cell lines (75).

Another important component is the envelope glycoprotein. The tropism of a virus is determined by the interaction of the surface glycoproteins on the viral envelope and the surface receptors on the target cell (71). In these viral systems, retroviruses and lentiviruses can be pseudotyped with different viral envelope proteins to broaden tropism (71). The vesicular stomatitis virus glycoprotein (VSV-G) is a commonly used envelope glycoprotein. It is stable, has broad tropism and leads to high infectivity (70, 77).

Both retroviral and lentiviral vectors integrate into the target cell genome and lead to stable genetic expression (67). They have a reasonable packaging capacity of approximately 8-9 kilobases, which is suitable to deliver most genes of interest (70). However, retroviruses infect only dividing cells while lentiviruses infect both dividing and non-dividing cells (70). Furthermore, retroviruses can lead to a moderate immune response while lentiviruses have low immune responses (70). Lentiviruses also result in greater periods of protein expression (70).

The disadvantages of using retroviral and lentiviral systems is that integration can occur in an arbitrary site in the target cell genome (68). Additionally, lentiviruses targeting dividing cells have a greater chance of integrating in areas of active transcription (69). Depending on where in the genome these integration events occur, they could lead to insertional mutagenesis (67, 68). For example; uncontrolled cell division can occur if the disrupted gene regulates cell division. This issue can potentially be addressed by directing the integration to specific loci (69). In tissues and organs, such as the brain, where most cells are terminally differentiated, there is a lower risk of inducing oncogenesis (69, 78). In stem cells that undergo proliferation, this risk would need to be considered. These integrating viral systems do however offer an efficient gene transfer method, which can be used for proof-of-concept. Subsequent optimisation of the delivery method can address safety issues.

The safety issues of using retroviral and lentiviral vectors are associated with oncogenesis and replication-competent viral particles. The risk of oncogenesis is based on the gene of interest cloned into the transfer vector and the integration site (67). The risk of producing replication-competent viral particles is addressed by the design of the viral vector system (71, 72).

Firstly, the genes required for viral assembly are provided on separate plasmids (67, 72). The transfer vector encodes the gene of interest and contains the packaging signal and the sequence that will incorporate into the target cell genome (LTRs and sequence between) (71). The packaging plasmids lack a packaging signal (71). Therefore, pseudoviral particles carry only a copy of the transfer construct, and replication-competent viral particles after the initial infection cannot be produced without the assembly components. Recombination would need to occur between at least three plasmids and the construct packaged into a viral particle for this to occur (67, 70). Additionally, the plasmids share no significant homology (70, 72). With lentiviral vector systems, 2nd and 3rd generation packaging systems exist. The 3rd generation uses a reduced number of HIV genes but also has an extra plasmid making recombination more difficult (72).

Secondly, the LTR can potentially activate transcription of cell genes after integration of the lentivirus, so many of the lentiviral transfer vectors are self-inactivating (67, 69-71). These vectors have a deletion in the 3' LTR (promoter region) of the viral genome that is transferred to the 5' LTR after one round of reverse transcription (72). This deletion stops transcription after integration into the genomic DNA of the target cell.

For the purposes of this thesis, the transcription factors OCT4, SOX2 and HES1 were introduced into human DPSC via replication-defective recombinant retroviral and lentiviral vectors, pseudotyped with VSV-G, with the transgenes under control of the LTR in the retroviral vector and the CMV promoter in the lentiviral vector. These systems are expected to be efficient in introducing transcription factor cDNA and creating stable expression in all cell types. Whilst all retroviruses integrate into the host cell genome, if a reprogramming method proves to be promising, the gene transfer method can then be modified for safety, such as using non-integrating vectors (67, 71). This chapter details the construction and preparation of the viral vectors and expression in DPSC.

4.2 | Materials and Methods

4.2.1 Cell Biology Techniques

4.2.1.1 Bacterial Culture

Vectors were maintained in *E. coli* strain DH5α. Bacteria were cultured in Luria broth (1% (w/v) tryptone, 0.5% (w/v) yeast extract, 1% (w/v) NaCl in ddH_20, pH 7) or grown on 1.5% (w/v) Luria broth agar, with 100µg/mL ampicillin, and incubated overnight at 37°C. Cultures were set up in 10mL tubes or conical flasks with aeration, and incubated with agitation at 1-3 x *g*. Petri dishes were sealed with parafilm and incubated upside-down. A sterile pipette tip was used to obtain bacterial cells from frozen glycerol stocks or bacterial agar stabs (Addgene, MA, USA) and streak onto a selective agar plate, and to pick colonies from selective agar plates and set up 10mL cultures. To set up 100mL cultures, 2mL of 10mL cultures was used. Glycerol stocks were made by mixing 500µL of 80% (v/v) glycerol with 500µL of bacterial culture, and freezing in a cryotube at -80°C.

4.2.1.2 Making Chemically-competent Bacteria

Using *E. coli* strain DH5α glycerol stock, 5mL culture with no antibiotics was set up and incubated overnight at 37°C with agitation at 1-3 x *g*. The next day, 2mL of the 5mL culture was used to set up a 200mL culture with 1mM glucose added to the broth. The culture was incubated at 37°C with agitation at 1-3 x *g*, until the optical density measured at 600nm was just over 0.3 but not 0.4. The 200mL culture was put into 50mL tubes, placed on ice for 10 minutes, and then centrifuged at 6000 x *g* for 15 minutes at 4°C. The supernatant was removed, the pellets were slowly resuspended in 20-25mL ice-cold 100mM $MgCl_2$, then placed on ice for 20 minutes, and centrifuged at 6000 x *g* for 15 minutes at 4°C. The supernatant was removed, the pellets were slowly resuspended in 20-25mL ice-cold 100mM $CaCl_2$, placed on ice for 1.5 hours, and then centrifuged at 6000 x *g* for 15 minutes at 4°C. The supernatant was removed and the pellets were resuspend in 10mL 100mM $CaCl_2$-glycerol (12.5% (v/v) glycerol) mix. 100µL aliquots in 1.5mL microcentrifuge tubes were snap frozen on dry ice, and stored at -80°C.

4.2.2 Molecular Biology Techniques

4.2.2.1 Molecular Cloning

Heat-shock Transformation of Competent Bacteria

E. coli DH5α chemically-competent cells were thawed on ice. For each transformation, 50µL of bacterial cells were used in a 1.5mL microcentrifuge tube, 1µL of plasmid DNA was added and gently mixed. After incubation on ice for 30 minutes, the bacterial cells were heat-shocked for 30 seconds at 42°C, and immediately placed on ice. 450µL of RT Luria broth was added and the culture was incubated at 37°C for 1 hour with agitation at 1-3 x *g*. 50µL of the culture was spread-plated on a pre-warmed selective agar plate and incubated overnight at 37°C.

Plasmid Purification

Plasmid purification was carried out using the GeneJet Plasmid Miniprep Kit (Thermo Scientific, MA, USA) for molecular biology-grade plasmid DNA, and QIAfilter Plasmid Midi Kit (Qiagen, Hilden, Germany) for transfection-grade plasmid DNA, per the manufacturer's instructions. For minipreps, 10mL cultures were set up and 3mL was used for purification. For use with the Midi kit, 100mL cultures were used. Plasmid DNA was eluted into Tris-EDTA buffer (10mM Tris-HCl pH 8, 1mM EDTA pH 8, in ddH_2O), and the quantity and quality was measured on the NanoDrop 8000 spectrophotometer (Thermo Scientific, MA, USA).

Restriction Enzyme Digests

Reactions were set up using an appropriate amount of plasmid DNA for subsequent application (500ng for diagnostic digests, 2.5µg for gel extraction), with the necessary restriction enzymes and appropriate enzyme buffer per the manufacturer's protocols (New England Biolabs, MA, USA). Total reaction volume was typically 20µL, with 0.5µL enzyme used for 1µg plasmid DNA. Volumes were scaled accordingly. The reactions were incubated for 1.5 hours at 37°C.

Agarose Gel Electrophoresis

Electrophoretic separation of DNA fragments was performed using a DNA gel electrophoresis system (Bio-Rad Laboratories Inc., CA, USA). Loading buffer (6x concentrate; 30% (v/v) glycerol, 0.25% (w/v) Bromophenol Blue dye, 0.25% (w/v) Orange O dye, 50mM EDTA, 10mM Tris-HCl pH 7.6, in ddH_20,) was added to the desired amount of DNA sample, to 1x concentration. Samples were loaded on a 0.8% or 1.5% (w/v) agarose gel (0.8% for vector purification, 1.5% for vector verification) in Tris-acetate-EDTA buffer (40mM Tris-base, 20mM acetate, 1mM EDTA, pH 8.6) containing 1µg/mL ethidium bromide or 1x GelRed

Nucleic Acid Gel Stain. 1kb DNA ladder was used. Gels were run at 85-100V until the dye front had migrated ¾ of the way through the gel. Images were taken using the Gel-Doc XR TM+ (Bio-Rad Laboratories Inc., CA, USA).

Gel Extraction

Desired DNA fragments were extracted and purified from agarose gels using the GeneJet Gel Extraction Kit (Thermo Scientific, MA, USA), according to the manufacturer's protocol.

Phosphatase Treatment

Vectors digested with a single enzyme leaving cohesive ends had terminal phosphates removed to prevent recircularisation of the vector. This was achieved using 1µL recombinant shrimp alkaline phosphatase in CutSmart buffer, incubated at 37°C for 30 minutes to 1 hour. The enzyme was inactivated at 65°C for 5 minutes.

Ligation

Ligation reactions were set up using a 3:1 insert to vector ratio (DNA molarity) with 50ng vector used. Total volume reaction was 20µL with 1µL T4 DNA ligase and 2µl 10x buffer. The reactions were incubated at RT for a minimum of 10 minutes to overnight. The ligase was inactivated at 65°C for 10 minutes. Negative controls included; no vector to control for contamination, no insert to control for recircularisation of the vector, and no ligase to indicate the presence of undigested vector.

Sanger Sequencing

Purified DNA of each transfer plasmid to be used for reprogramming was verified by Sanger sequencing (Australian Genome Research facility, VIC, Australia). Each reaction was prepared in a 1.5mL tube with 600-1500ng double-stranded plasmid DNA, 10pmol (1µL of 10µM stock) primer, and ddH_2O to a total volume of 12µL. For each construct, two sequencing reactions were prepared using two primers to capture either end of the cDNA inserts (Table 4.1). Sanger sequencing results were examined using SnapGene Viewer v 5.0.7 software (GSL Biotech LLC, CA, USA) and BLASTn (National Centre for Biotechnology Information, MD, USA).

Table 4.1 Sequencing primers.

Primer Name	**Primer Sequence**
RCF-1	TTG GGG GAC TCT GCT GAC CAC
IRES-reverse	ACA CCG GCC TTA TTC CAA G
EF1a-reverse	CCA GTA CAC GAC ATC ACT TTC CCA G
CMV-forward	CGC AAA TGG GCG GTA GGC GTG

4.2.2.2 Construction of Viral Vectors

Expression and Packaging Vectors

Table 4.2 lists the mammalian expression vectors used in this chapter, obtained from a plasmid repository (AddGene, MA, USA) or our research groups. These vectors were used to construct the transfer plasmids used for viral preparation. Table 4.3 lists the packaging and envelope plasmids using to assemble retroviral and lentiviral particles in HEK293T cells. Plasmid maps were viewed/constructed using SnapGene Viewer v 5.0.7 software (GSL Biotech LLC, CA, USA).

Table 4.2 Mammalian expression vectors.

Vector Type	Construct Name (size in base pairs)	Gene Insert (size in base pairs)	Selectable Markers	Bacterial Resistance	Source	Catalogue Number
Retroviral	pMXs-hOCT3/4 (5801)	Human *POU5F1* (1100)	N/A	Ampicillin	AddGene (Shinya Yamanaka)	17217
Retroviral	pMXs-hSOX2 (5796)	Human *SOX2* (960)	N/A	Ampicillin	AddGene (Shinya Yamanaka)	17218
Lentiviral (3rd gen.)	pEF-hHES1.Ubc.GFP (12 244)	Human *HES1* (850)	GFP	Ampicillin	AddGene (Linzhao Cheng)	17624
Retroviral	pRUF-iG2-Gateway (6071)	N/A	GFP	Ampicillin	Stan Gronthos	N/A
Lentiviral (3rd gen.)	pCDH-puro-cMyc (8715)	Human *MYC* (1323)	Puromycin	Ampicillin	AddGene (Jialiang Wang)	46970
Lentiviral (3rd gen.)	pLenti CMV Blast empty (w263-1) (7744)	N/A	Blasticidin	Ampicillin	AddGene (Eric Campeau, Paul Kaufman)	17486
Lentiviral (3rd gen.)	pLV-EF1a-IRES-Neo (8980)	N/A	Neomycin	Ampicillin	AddGene (Tobias Meyer)	85139

Notes: AddGene depositing laboratory names indicated in brackets.

Table 4.3 Packaging plasmids.

Vector Type	Vector	Components Encoded	Source	Catalogue Number
Retroviral	pEQ-PAM3	HIV-1 Gag/Pol poly-proteins and VSV-G	Stan Gronthos, Paul Moretti	N/A
2nd generation lentiviral (suitable for 2nd and 3rd generation transfer plasmids)	psPAX2	HIV-1 Gag/Pol poly-proteins, Rev and Tat	AddGene (Didier Trono)	12260
Retroviral and lentiviral	pCMV-VSV-G	VSV-G	AddGene (Bob Weinberg)	8454

Construction of Retroviral Vectors

Human OCT4, SOX2 and HES1 cDNAs were sub-cloned into the retroviral vector pRUF-iG2-Gateway, using restriction enzyme cloning techniques. This retroviral vector contains an internal ribosome entry site (IRES) and an enhanced GFP coding sequence downstream of the multiple cloning site (MCS). The vector with no gene insert was used as the empty vector control (referred to as pRUF-EV).

To construct pRUF-hOCT4, the OCT4 cDNA was sub-cloned from pMXs-hOCT3/4 (a gift from Shinya Yamanaka, Addgene plasmid # 17217 (79)) into pRUF-iG2-Gateway using *EcoRI* restriction sites. To construct pRUF-hSOX2, the SOX2 cDNA was sub-cloned from pMXs-hSOX2 (a gift from Shinya Yamanaka, Addgene plasmid # 17218 (79)) into pRUF-iG2-Gateway using the *BamHI* and *XhoI* restriction sites. To construct pRUF-HES1, the HES1 cDNA was firstly sub-cloned from pEF-hHES1.Ubc.GFP (a gift from Linzhao Cheng, Addgene plasmid # 17624 (80)) into pLenti CMV Blast empty (w263-1) (a gift from Eric Campeau & Paul Kaufman, Addgene plasmid # 17486 (81)) using *XbaI* restriction sites. From this intermediate construct, the HES1 cDNA was sub-cloned into the pRUF-iG2-Gateway vector using *EcoRI* restriction sites. Correct insertion and orientation was confirmed by restriction digests, before plasmids were purified for sequencing. Figure 4.1A shows the map of the retroviral transfer plasmid.

Construction of Lentiviral Vectors

Human OCT4, SOX2 and HES1 cDNAs were sub-cloned into a lentiviral vector (referred to as pCDH) under control of the human CMV promoter, using restriction enzyme cloning techniques. The final constructs all contained an enhanced GFP expression construct downstream of the inserted gene, separated by an IRES. Additionally, the OCT4 cDNA was cloned into another lentiviral vector (referred to as pLV) under control of the human EF-1α promoter.

To construct pCDH-OCT4, the OCT4 cDNA was firstly sub-cloned from pMXs-hOCT3/4 into pCDH-puro-cMyc (a gift from Jialiang Wang, Addgene plasmid # 46970 (82)) via *XbaI* and *NotI* restriction sites, to replace the MYC cDNA. This intermediate construct then had the OCT4 cDNA replaced with the OCT4-IRES-GFP segment from pRUF-OCT4 via the *BamHI* and *NotI* restriction sites. To construct pCDH-SOX2, the SOX2 cDNA was sub-cloned from pMXs-SOX2 into pCDH-OCT4 via the *BamHI* and *XhoI* restriction sites. To construct pCDH-HES1, the HES1 cDNA was sub-cloned from pRUF-HES1 into pCDH-SOX2 to replace the SOX2 cDNA, using *XbaI* and *XhoI* restriction sites. The OCT4 cDNA was removed from

pCDH-OCT4 using the *EcoRI* restriction sites, leaving behind the IRES-GFP segment. This vector with no gene insert was used as the empty vector control (referred to as pCDH-EV).

To construct pLV-OCT4, the OCT4-IRES-GFP segment was sub-cloned from pCDH-OCT4 into pLV-EF1a-IRES-Neo (a gift from Tobias Meyer, Addgene plasmid # 85139 (83)) using *BamHI* and *NotI* restriction sites. The OCT4 cDNA was removed using *EcoRI* restriction sites to form the empty vector control (referred to as pLV-EV).

Correct insertion and orientation was confirmed by restriction digests, before plasmids were purified for sequencing. Figure 4.1B shows the map of the pCDH lentiviral transfer plasmid.

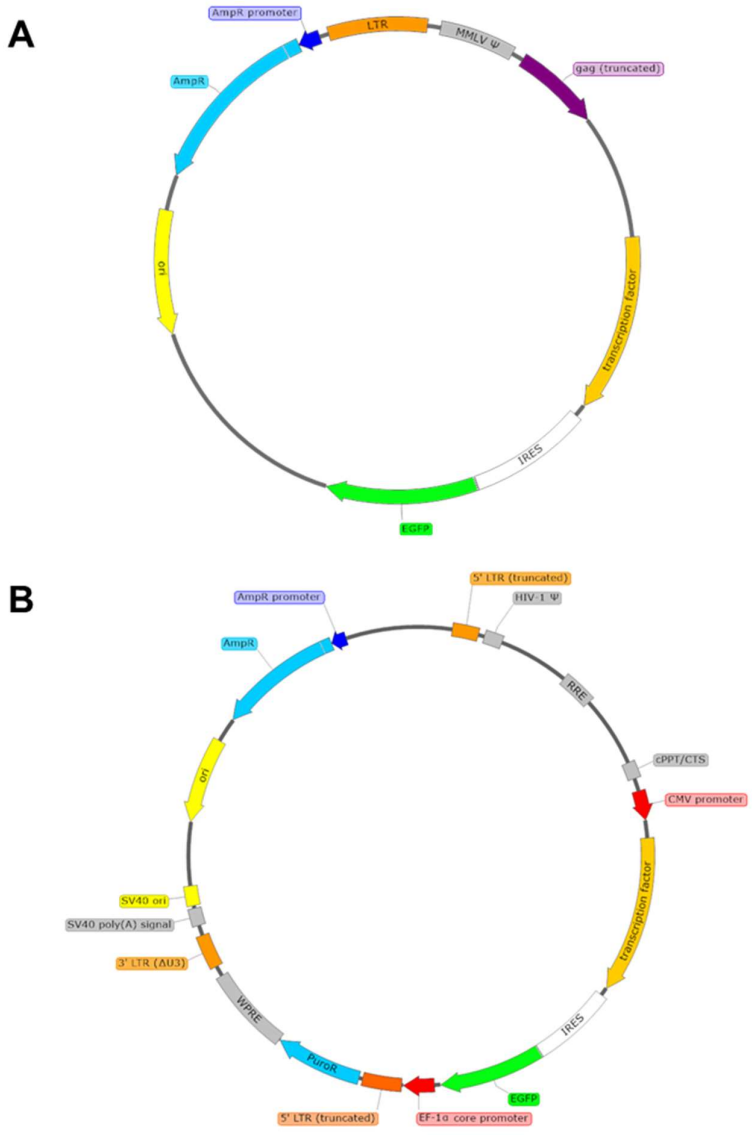

Figure 4.1 Transfer vectors. The cDNA sequences (approximately 1 kilobase) encoding for the transcription factors, either OCT4, SOX2 or HES1, were cloned into the MCS of the vectors. The transcription factor coding sequences are followed by the IRES and then the enhanced GFP (mammalian codon-optimised) coding sequence. **(A)** Retroviral transfer vectors (pRUF-EV, pRUF-OCT4, pRUF-SOX2, pRUF-HES1); Moloney murine leukaemia virus (MMLV)-derived, under control of the LTR. **(B)** Lentiviral transfer vectors (pCDH-EV, pCDH-OCT4, pCDH-SOX2, pCDH-HES1); 3rd generation, HIV-1-derived, under control of a hybrid promoter consisting of the truncated HIV-1 5' LTR fused to the constitutive human CMV immediate early promoter. The control empty vectors lack the transcription factor sequence between the promoters and the IRES. Other important viral elements include; MMLV and HIV-1 packaging signal psi (Ψ), MMLV *gag* gene lacking the start codon, HIV-1 rev response element (RRE) that allows for Rev-dependent micro RNA export from the nucleus to the cytoplasm, HIV-1 central polypurine tract and central termination sequence (cPPT/CTS) that is the recognition site for proviral DNA synthesis, woodchuck hepatitis virus post-transcriptional regulatory element (WPRE) that enhances translation, and HIV-1 3' LTR that is self-inactivating due to the deletion of the unique 3' region (ΔU3). Other components of the plasmids include; core promoter for human EF-1α with the truncated human T-cell leukemia virus type 1 5' LTR, *pac* gene from Streptomyces alboniger encoding for puromycin N-acetyltransferase that confers puromycin resistance (PuroR), SV40 polyadenylation (poly(A)) signal for transcription termination, SV40 origin of replication (ori) for stable propagation of the plasmid in mammalian cells, high-copy-number ColE1/pMB1/pBR322/pUC origin of replication (ori) for maintenance of the plasmid in *E. coli*, and the *bla* gene encoding for β-lactamase that confers resistance to ampicillin (AmpR) for plasmid selection in *E. coli*, and the corresponding promoter (AmpR).

4.2.2.3 Transfection

Viral Production

The transfer constructs (Table 4.4) were used to produce replication-incompetent, VSV-G-coated, recombinant retroviral and lentiviral particles, via transient transfection of HEK293T cells, along with the packaging plasmids (Table 4.3).

Table 4.4 Transfer constructs.

Vector Type		Vector	Gene Insert	Selectable Marker
Retroviral		pRUF-EV	N/A	GFP
		pRUF-OCT4	Human OCT4	
		pRUF-SOX2	Human SOX2	
		pRUF-HES1	Human HES1	
Lentiviral	CMV promoter	pCDH-EV	N/A	
		pCDH-OCT4	Human OCT4	
		pCDH-SOX2	Human SOX2	
	EF-1α promoter	pCDH-HES1	Human HES1	
		pLV-EV	N/A	
		pLV-OCT4	Human OCT4	

Retroviral Preparation

The HEK293T cells were plated at $7x10^5$ cells/6cm dish in 5mL standard medium. The next day, fresh 6mL medium was added. The retroviral transfer plasmid (5µg) and pEQ-Pam3 packaging plasmid (5µg) were transfected into the HEK293T cells using Lipofectamine 2000 reagent. The plasmid DNA was mixed with 500µL DMEM in a tube. In a separate tube, 20µL Lipofectamine 2000 reagent was added drop wise to 500µL DMEM, and incubated at RT for 5 minutes. The Lipofectamine 2000 mix was combined with the plasmid DNA mix, and incubated at RT for 20 minutes. The transfection mix was then added to the cells drop-wise, and cells were incubated for 48 hours. Successful transfection was assessed by examining the cells for green fluorescence. The supernatant containing the virus was collected and filtered through a low protein binding 0.45µm syringe filter (Pall Corporation, NY, USA), aliquoted, and stored at -80°C. Fresh 6mL medium was added to the cells and the viral supernatant was harvested after 24 hours.

Lentiviral Preparation

The HEK293T cells were seeded at $4x10^6$ cells/10cm dish in standard medium. The next day, 5mL fresh medium with no penicillin and streptomycin was added to the cells. Cells were transfected using the Lipofectamine 2000 reagent. In a 1.5mL tube, 52.4µL Lipofectamine 2000 reagent was added drop-wise to 1310µL Opti-MEM I reduced serum medium, and incubated at

RT for 5 minutes. In a separate 1.5mL tube, 13.1µg lentiviral transfer plasmid, 10.48µg psPAX2 and 10.48µg pCMV-VSV-G packaging plasmid, were added to 1310µL Opti-MEM I reduced serum medium. The Lipofectamine 2000 reagent mix was added drop-wise to the plasmid DNA mix, and incubated at RT for 20 minutes. The transfection mix was then added to the cells drop-wise. The cells were incubated for 8 hours, followed by a change of medium with fresh Opti-MEM I reduced serum medium, then 40 hour incubation. Successful transfection was assessed by examining the cells for green fluorescence. The viral supernatant was collected and filtered through a low protein binding 0.45µm syringe filter. The viral supernatant was concentrated using the Optima XPN Ultracentrifuge fitted with the SW40Ti rotor (Beckman Coulter, CA, USA), at 50,000 x *g* for 90 minutes at 4°C. The supernatant was removed and the pellet was resuspended in 50µL ice-cold PBS, aliquoted, and stored at -80°C. Fresh 7.5mL medium was added to the cells and the virus was harvested after 24 hours.

4.2.2.4 Transduction

When reached 80-90% confluency, cells were transduced with virus in standard culture medium without antibiotics, in half the normal volume (i.e. 1mL total volume for a well of a 6-well plate), supplemented with 8µg/mL polybrene. Medium was changed after approximately 4 hours to fresh culture medium with antibiotics. Cells were split the next day into a 25cm^2 flask.

4.2.2.5 Lentiviral Titration

Physical titres, the number of viral particles, were determined using a commercial kit; qPCR Lentivirus Titration Kit (Applied Biological Materials Inc., BC, Canada), following the manufacturer's protocol with half the recommended volumes. Functional titre, the number of transducing units, was measured by transducing HEK293T cells with 1 in 10 serial dilutions of virus and counting GFP$^+$ cells using flow cytometry (Chapter 2, section 2.2.1.5, pg.29). The number of GFP$^+$ cells as percentage of the total number were graphed.

4.2.2.6 Quantitative PCR

See Chapter 2, section 2.2.2.3, pg. 30 for qPCR protocol, using primers in Table 4.5.

Table 4.5 Primers for qPCR.

Gene	Protein	Source	Forward Primer Sequence	Reverse Primer Sequence
POU5F1	OCT4	Coding Sequence	ggaggaagctgacaacaatgaaa	ggcctgcacgagggttt
		Endogenous Gene	gggtttttgggattaagttcttca	gcccccacccttttgtgtt
		Transgene	ggctctcccatgcattcaaactg	aaacgcacaccggccttattcc
SOX2	SOX2	Coding Sequence	tgcgagcgctgcacat	tcatgagcgtcttggttttcc
		Endogenous Gene	caaaaatggccatgcaggtt	agttgggatcgaacaaaagctatt
		Transgene	agcagacttcacatgtcccagc	tgtacaagaaagctgggtcggc
HES1	HES1	Coding Sequence	accaaagacagcatctgagcacag	tgccgcgagctatctttcttcag
		Endogenous Gene	taaactccccaacccacctct	tctctcccagtattcaagttcct
		Transgene	ggaactgaggggctatcgaattc	aaacgcacaccggccttattcc
ACTB	β-actin	Endogenous Gene	agagctacgagctgcctgac	ttcgtggatgccacaggactc

4.2.2.7 Western Blot

See Chapter 2, section 2.2.2.5, pg. 32 for Western blot protocol, using antibodies in Table 4.6.

Table 4.6 Antibodies for Western blots.

Name	Dilution	Company	Catalogue Number
Primary Antibodies			
Goat anti-GFP	1:1000	Rockland Antibodies and Assays	600101215
Goat anti-OCT4	1:400	R&D Systems	AF1759
Mouse anti-β-actin	1:4000	Sigma-Aldrich	A2228
Secondary Antibodies			
Goat anti-mouse DyLight 800	1:20 000	Invitrogen	SA5-35521
Rabbit anti-sheep DyLight 680 *	1:20 000	Invitrogen	SA5-10058

* Kindly provided by the Cell Signalling and Gene Regulation research group (SAHMRI, SA, Australia).

4.3.1 Base-line expression levels of OCT4, SOX2 and HES1 transcription factors in human DPSC

The baseline expression levels of the three transcription factors selected for reprogramming were examined in DPSC (Figure 4.2). The gene expression levels of *POU5F1*, *SOX2* and *HES1* in DPSC, along with the endogenous control *ACTB* are shown in Figure 4.2A. The Ct values, the cycle at which the threshold was reached, are shown for each gene. Low to moderate expression of *POU5F1* is seen, while the expression of *SOX2* and *HES1* are much lower as they approach a Ct value of 40, which is the maximum cycle to reach threshold. Inter-donor variation was observed between samples, with some samples having low expression levels of *SOX2* and *HES1*, e.g. Ct value of 35, while other samples did not express these genes, e.g. Ct value of 40. The *POU5F1* expression levels were more consistent between donor samples, as seen by the smaller error bar. At the protein level, low expression levels of OCT4 were detected, very low levels of SOX2 and no expression of HES1 (Figure 4.2B).

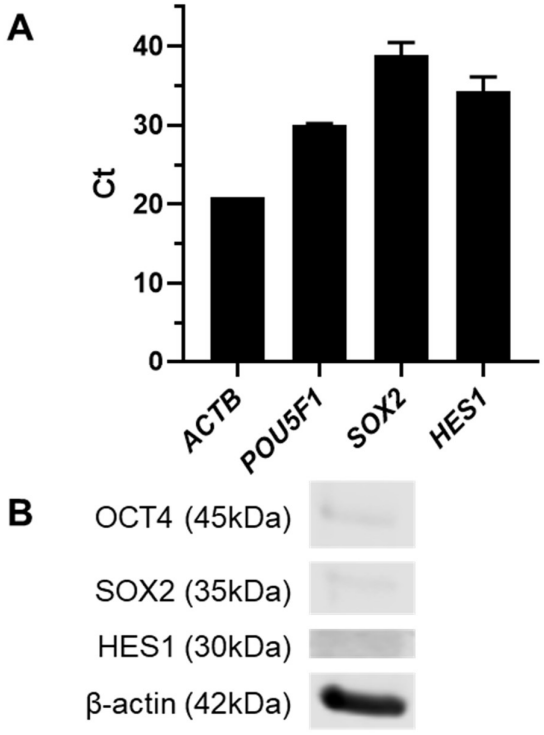

Figure 4.2 Expression levels of transcription factors selected for reprogramming, in human DPSC. **(A)** Gene expression levels of *POU5F1*, *SOX2* and *HES1*; the graph shows the Ct values for the endogenous control gene *ACTB* and the three transcription factors. **(B)** OCT4, SOX2 and HES1 protein expression; β-actin was the loading control. Representative blots (n=6), data represents mean±SD, n≥3 (A).

4.3.2 HEK293T cells produced virus using the lentiviral system

A retroviral vector was initially tested. The transcription factor cDNAs were cloned into the MCS, with the GFP construct downstream of the IRES. When this retroviral vector was transfected into HEK293T cells however, GFP expression was not observed (Figure 4.3A), suggesting that this vector system was unsuccessful in producing viral particles. The IRES-GFP segment was sub-cloned into a lentiviral vector, and the transcription factor cDNAs were inserted into the upstream MCS. When this lentiviral vector was transfected into HEK293T cells, GFP expression was observed indicating the successful production of viral particles (Figure 4.3A). This lentiviral vector (pCDH) was subsequently used. Expression of GFP was observed during the viral production using the control empty vector and the three vectors with the transcription factors cDNA inserts (Figure 4.3B).

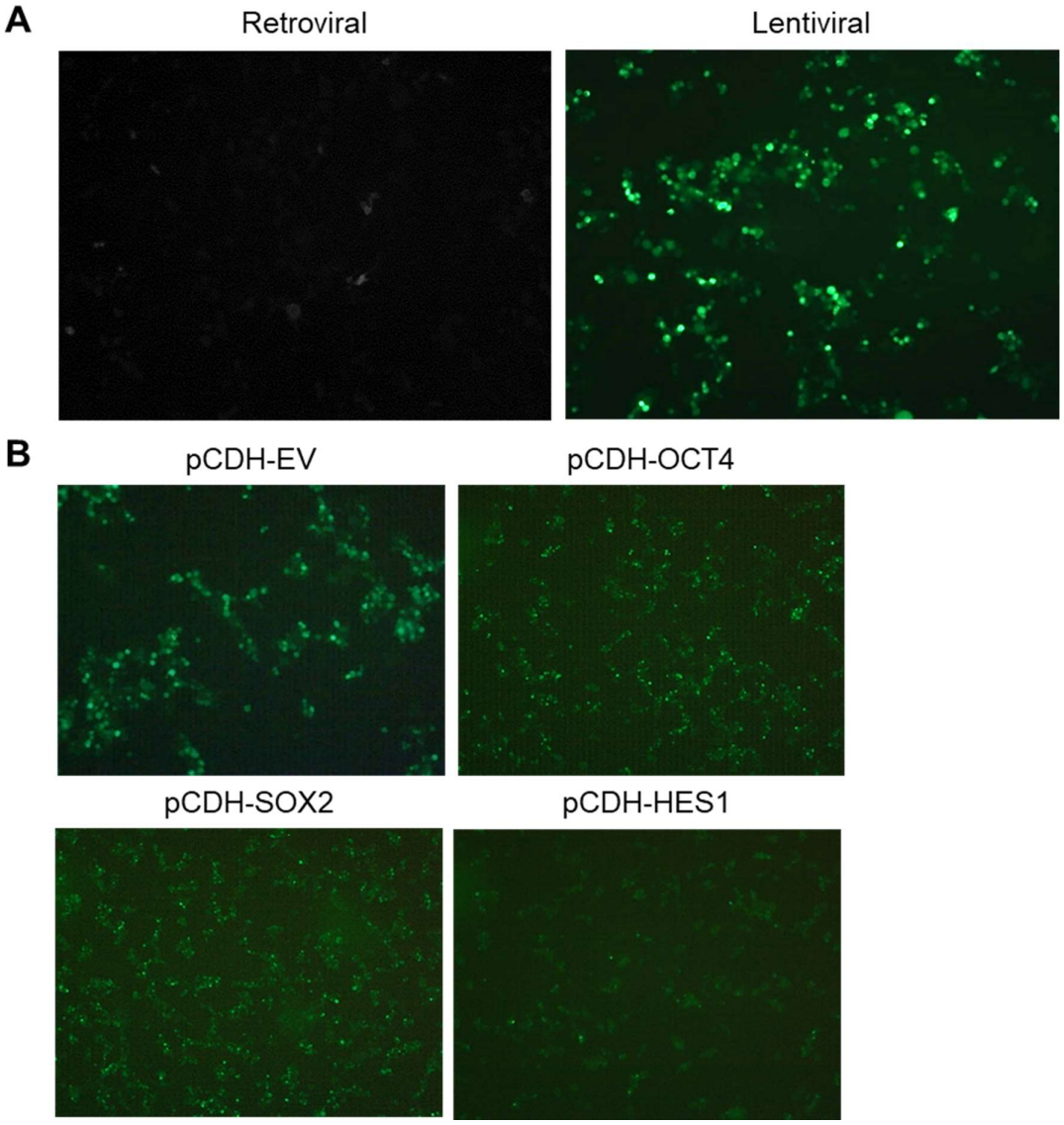

Figure 4.3 Virus production in HEK293T cells. **(A)** HEK293T cells were transfected using retroviral and lentiviral vector systems. **(B)** Lentiviral vector (pCDH) carrying the cDNA encoding for OCT4, SOX2 and HES1 transcription factors, along with the empty vector (EV) control, were used to produce lentivirus for DPSC transduction. Images taken at 100x magnification.

4.3.3 The CMV promoter lentiviral vector was not silenced in human DPSC

Since the lentiviral vector is driven by the CMV promoter, which may be silenced in some cell types by anti-viral mechanisms, another lentiviral vector under control of the EF-1α promoter was tested (Figure 4.4). Figure 4.4A shows DPSC transduced with both lentiviral vectors, each as the empty vector and with the OCT4 cDNA insert. The percentage of GFP^+ cells was lower with the EF-1α promoter, indicating lower transduction efficiency (Figure 4.4B). For both lentiviral vectors, the OCT4 cDNA insert resulted in fewer transduced cells. Western blot analysis was used to confirm protein expression of GFP and OCT4 (Figure 4.4C). Protein expression was detected using both promoters, indicating that the lentiviral vectors were not being silenced in the cells. The β-actin levels were consistent across samples. The OCT4 protein was expressed in the OCT4 vector-transduced cells, and GFP was detected in all samples, as it is the selectable marker for the transfer plasmid.

A

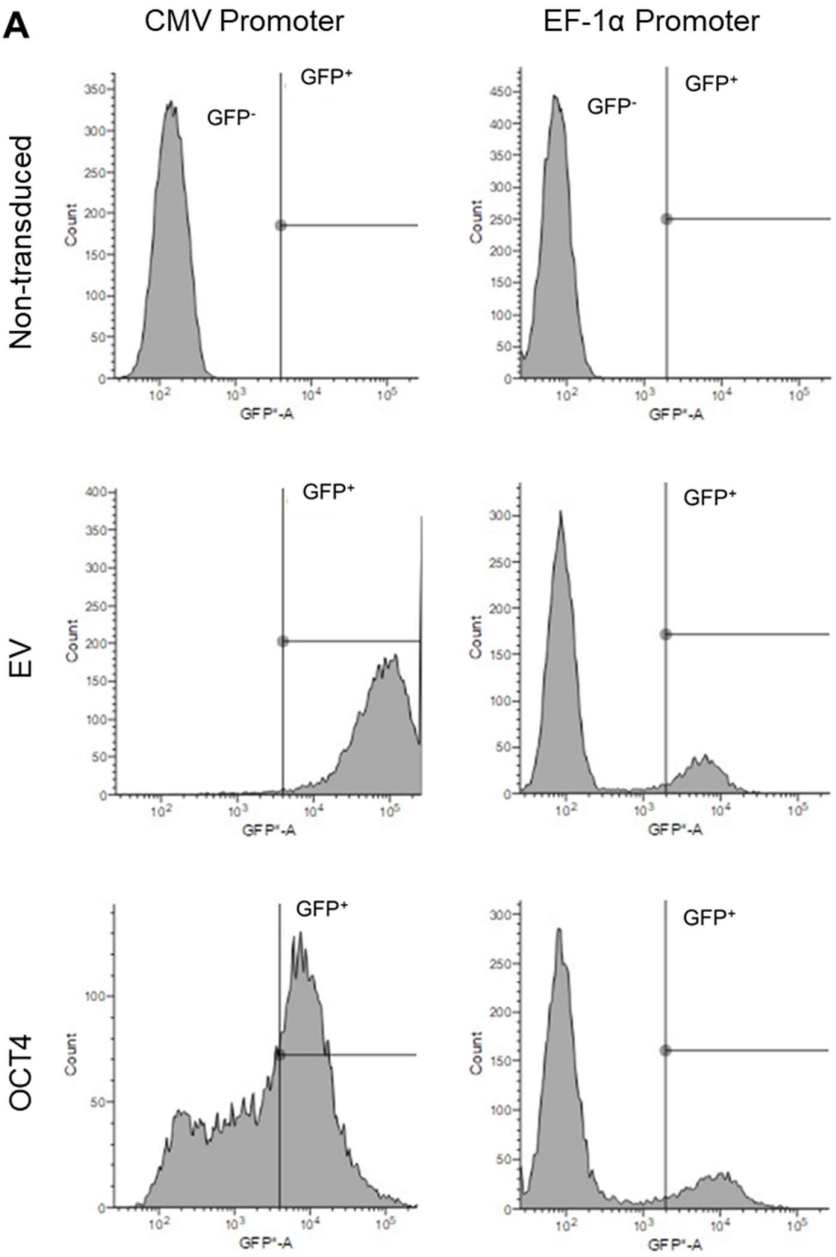

B

Promoter	Lentiviral Vector	GFP⁺ Cells (%)
CMV	pCDH-EV	87.3 ± 6.7
	pCDH-OCT4	42.7 ± 5.7
EF-1α	pLV-EV	18.0 ± 1.7
	pLV-OCT4	15.0 ± 3.5

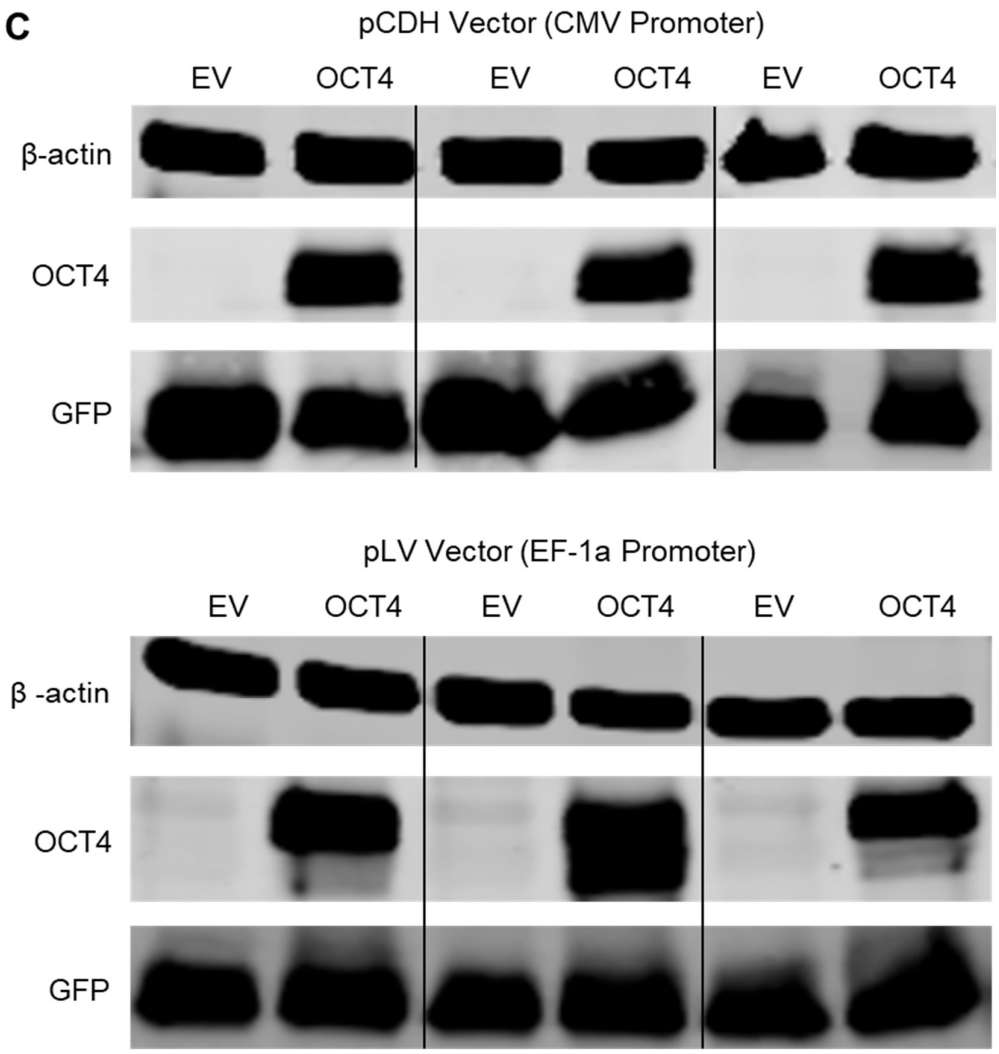

Figure 4.4 Human DPSC transduced by lentiviral vectors with different promoters. Cells were transduced with control empty vectors (EV) or vectors containing the OCT4 cDNA insert (OCT4), driven by either the CMV (pCDH vector) or EF-1α (pLV vector) promoters. **(A)** Cells were sorted based on GFP expression. **(B)** Percentage of GFP^+ cells obtained upon sorting. **(C)** Protein expression from both lentiviral vectors; β-actin was the loading control. Representative images of the gating for GFP^+ population are shown, data represents mean±SD, n=3.

4.3.4 Gene expression in HEK293T cells

Upon collecting the viral supernatants, the HEK293T cells were collected and qPCR performed, confirming the expression of the genes encoded by the transfer vectors. The expression levels were normalised to normal HEK293T cells. The expression of *POU5F1* was 14-fold higher (log2 scale), *SOX2* expression was 13-fold increased, and *HES1* expression levels showed close to a 9-fold increase (Figure 4.5A). Subsequently, a preliminary experiment was performed with serial dilutions of the viruses used to transduce HEK293T cells. It was observed that the transduction efficiency decreased from using the neat concentrated virus to a one in ten dilution by 50 per cent for pCDH-OCT4 and more than 50 per cent for the other three viruses (Figure 4.5B). This data was used to obtain an estimate of the functional viral titre, and compared to the physical titre determined using a commercial qPCR kit (Figure 4.5C). There was variation in the physical titre between different batches of the viruses, with the average physical titre being higher than the functional titre. The physical and functional titres using the same batch were similar.

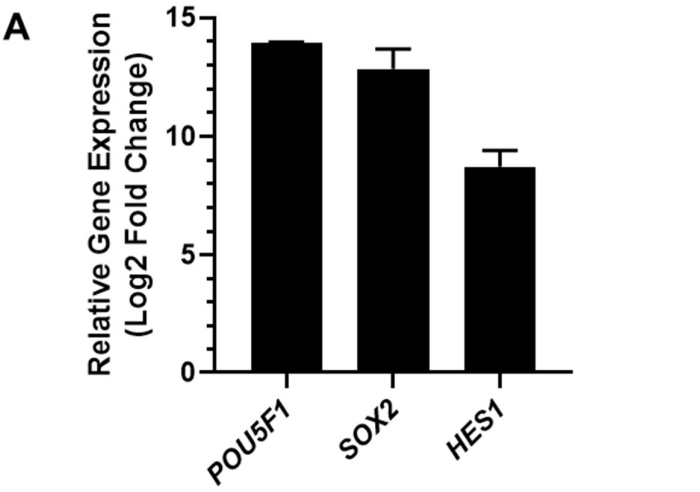

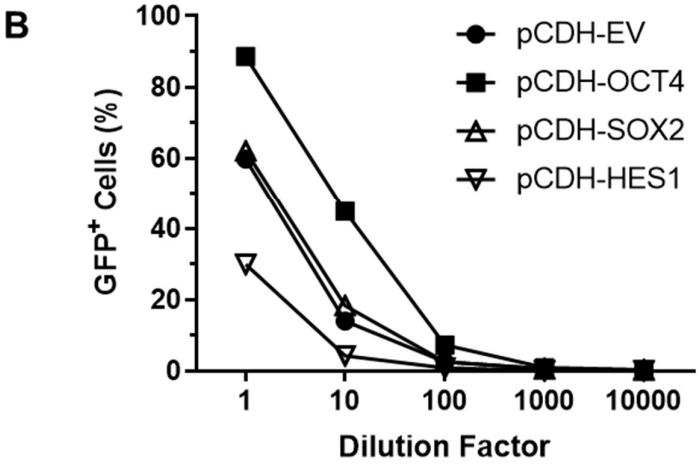

C

Lentivirus	Physical Titre (VP/mL)				Functional Titre (TU/mL) *
	1	2	3 *	Mean	
pCDH-EV	1.5×10^8	8.8×10^8	1.7×10^8	4.0×10^8	7.8×10^7
pCDH-OCT4	8.6×10^9	1.1×10^9	2.4×10^8	3.3×10^9	3.5×10^8
pCDH-SOX2	5.6×10^9	1.1×10^9	1.0×10^8	2.3×10^9	8.7×10^7
pCDH-HES1	5.6×10^7	6.5×10^8	2.7×10^7	2.4×10^8	2.7×10^7

Figure 4.5 Viral titration. **(A)** Gene expression of *POU5F1* for pCDH-OCT4, *SOX2* for pCDH-SOX2 and *HES1* for pCDH-HES1, in HEK293T cells upon completion of viral production, expressed relative to HEK293T cells. **(B)** HEK293T cells were transduced with 1 in 10 serial dilutions of each virus. The percentage of GFP^+ cells was measured by flow cytometry, and used to determine the functional viral concentrations (transducing units/mL; TU/mL). **(C)** Physical viral concentrations (viral particles/mL; VP/mL) were determined using a commercial qPCR lentiviral titration kit. * indicates the same batch of virus. Data represents mean±SD, n=1 (A, B) and 3 (C).

4.3.5 Gene expression in human DPSC

Human DPSC were transduced with each of the four lentiviruses, with volumes adjusted for consistent viral concentration. The control empty vector resulted in the greatest transduction efficiency, and decreased for the OCT4, SOX2 and HES1 vectors (Figure 4.6A). The qPCR data confirmed the expression of each gene. The expression levels were normalised to non-transduced DPSC. The primers used bind to the coding sequence and hence detected expression of the transgene and the endogenous gene. The expression of *POU5F1* showed a 13-fold increase (log2 scale), *SOX2* expression was 7-fold higher, and *HES1* expression levels showed a 3 to 4-fold increase (Figure 4.6B). In Figure 4.6C, two primer sets were used to distinguish between transgene and endogenous gene expression. This data showed that the main source of the gene expression was the transgene. Each of the transcription factors was expressed at the protein level, as confirmed by Western blot analysis (Figure 4.6D).

DPSC were also transduced with multiple lentiviral vectors, and the cells sorted for GFP. Figure 4.6E showed the percentage of GFP^+ cells. Analysis by qPCR performed on some combinations showed that despite using consistent viral concentrations, the expression levels changed in different combinations (data not shown). Unfortunately, due to mycoplasma contamination from external sources, these experiments as well as many of the single transcription factor experiments were lost, and unable to be repeated due to time constraints. The reprogramming experiments proceeded with investigating individual transcription factors.

A

Lentiviral Vector	GFP⁺ Cells (%)
pCDH-EV	87.3 ± 6.7
pCDH-OCT4	42.7 ± 5.7
pCDH-SOX2	40.5 ± 41.7
pCDH-HES1	3.5 ± 2.1

B

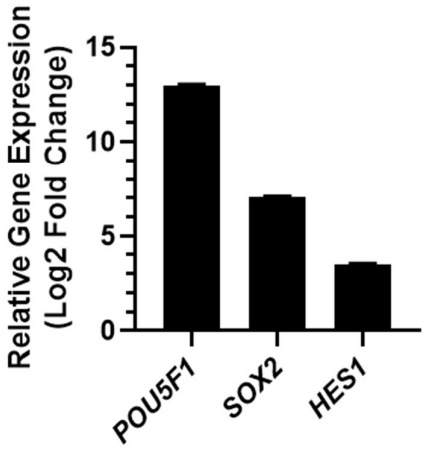

C

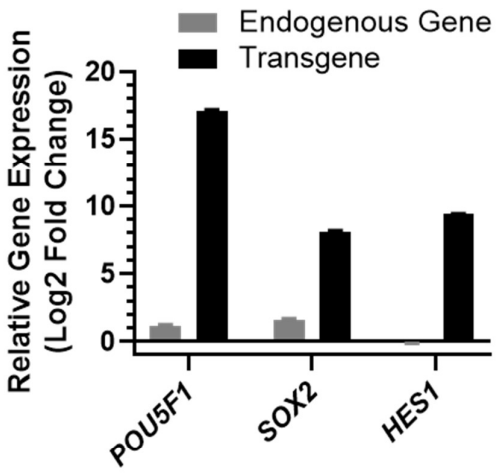

D

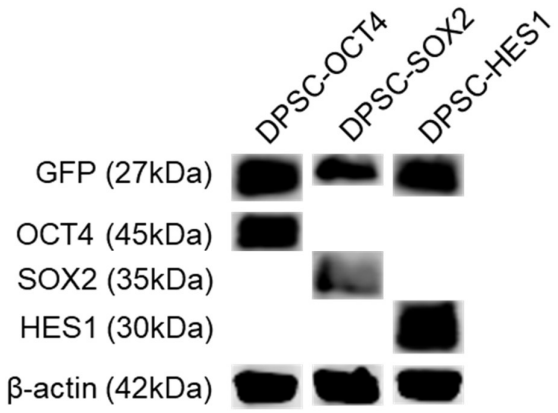

E

Transcription Factors	GFP⁺ Cells (%)
OCT4, SOX2, HES1	57.0 ± 38.2
OCT4, SOX2	53.0 ± 26.9
OCT4, HES1	23.0 ± 17.0
SOX2, HES1	9.0 ± 2.8

Figure 4.6 Transduction of human DPSC. **(A)** The percentage of GFP^+ cells. **(B)** Gene expression levels relative to non-transduced DPSC. Primers bind to the coding sequence of the transcription factor genes. **(C)** Gene expression levels relative to the control empty vector (pCDH-EV)-transduced DPSC. Two sets of primers recognise expression from the endogenous genes and the transgenes. **(D)** Protein expression levels in DPSC transduced with each vector construct; β-actin was the loading control. **(E)** Transduction with multiple lentiviral vectors. Representative blots, data represents mean±SD, n=3 (A; pCDH-EV and pCDH-OCT4), 2 (A; pCDH-SOX2 and pCDH-HES1, E), 1 (B, C).

4.4 | Discussion

In this chapter, the vectors for reprogramming were constructed and viral preparations were tested in DPSC. The transcription factor cDNAs were inserted into a 3rd generation lentiviral transfer vector driven by the CMV promoter (pCDH), with an enhanced GFP selectable marker downstream of an IRES. This transfer vector was packaged using a 2nd generation lentiviral packaging system. The transfer vector and packaging plasmids were transfected using Lipofectamine reagent into HEK293T cells. The resulting replication-incompetent, self-inactivating, VSV-G pseudotyped lentiviruses each encoded for the transcription factors and GFP. The empty vector with no insert upstream of the IRES was the control. The viruses successfully transduced DPSC, which were selected for GFP using FACS and pooled together. The transcription factors were expressed at the gene and protein levels.

The lentiviral vector was chosen over the retroviral vector due to successful production of viral particles based on GFP detection. Gene and protein expression from the lentivirus was subsequently confirmed. The retroviral preparation may have been unsuccessful due to a low titre as a result of lower virion stability (71). The lentiviral vector with the CMV promoter was used, since it resulted in better transduction efficiency than the EF-1α promoter, as seen in previous research with human cells (76). Protein expression under control of the CMV promoter was detected, thus the vector was not silenced.

After producing viral particles and concentrating, the titre was calculated. A physical titre can be determined by qPCR for a common viral gene (77). This method gave an indication of the number of viral particles, however not all viral particles will be functional. A functional titre can be determined by flow cytometry for a selectable marker, such as GFP (77). To do this, a permissive cell line, such as HEK293T cells, is transduced with viral serial dilutions. The functional titre may not translate to the target cell, however it is a good starting point (81). Here the viral titres were in the expected range; usually one million per millilitre using non-concentrated supernatant (71). Titre variation was seen between batches, and as expected the physical titre was greater than the functional titre. However, the two titration methods gave similar titres for the same batch. Variation between batches and within the same batch is usually observed (77, 84). This would result in variation in transduction efficiency, however transduced cells are subsequently selected for using selectable markers (e.g. fluorescent markers, antibiotic resistance).

The titres can be used to determine the amount of virus for transducing cells. The multiplicity of infection (MOI), which relates to the integrations and copy number per cell, can be considered as a guide for the amount of virus to use (71, 85). It was seen here that despite adjusting the viral concentrations for a consistent MOI, the transduction efficiency of each lentiviral vector in DPSC remained different. There could be multiple reasons for this variation in transduction efficiency. Each viral preparation would contain non-functional viral particles that would compete with the functional viral particles (85). Furthermore, not all integrations would be transcriptionally active (84). Due to variation between different vectors, the expression levels can be difficult to control (85). In many reprogramming studies, consistent protocols are used and cells are transduced with an equal volume of multiple viruses, while titres are disregarded (13, 79, 86, 87). Within a transduced population, cells with different copy numbers exist and expression levels can be examined by qPCR in a bulk population or in individual clones (77, 88, 89).

The viral production and transduction efficiency can also be affected by the vector inserts; the size, sequence and gene (81). Although the cDNA inserts used here were of similar size (OCT4; 1083 base pairs, SOX2; 954 base pairs, HES1; 843 base pairs), differences were seen between the titres and transduction efficiencies. All other vector components and virus protocols were consistent. This suggested that the genes themselves affected the efficiency of viral packaging and transduction. The OCT4 virus consistently had the highest titre and the HES1 virus had the lowest titre. This was observed with both titre methods.

Single vector transductions were investigated. Whilst multiple vector combinations were not investigated, having different selectable markers in the vectors would assist with investigating combinations in a timelier manner in future experiments. Using only GFP as a selectable marker means that sorted cells would need to be expanded from a single cell to allow for confirmation of two or more transcription factors via qPCR. If sorted and pooled, the population may consist of cells with single or multiple factors. Having different selectable markers would allow for simultaneous selection of each vector using different filters, for example green, blue and yellow fluorescent proteins (90). Alternatively, a single viral vector expressing multiple transcription factors can be generated. This can be achieved via multiple promoters or single promoters with multiple IRES or self-cleaving peptides (91).

Previous studies have suggested that DPSC, like other adult stem cell populations, have low expression levels of pluripotency factors, including OCT4 and SOX2 (16, 20, 92, 93). These levels were very low compared to those in pluripotent stem cells (94). In the current study,

using qPCR and Western blot analysis, low levels of OCT4 were detected while SOX2 expression was not present. OCT4 is expressed in ESC and is down-regulated during differentiation (10). It has been suggested that expression in adult stem cells is maintained and contributes to self-renewal (95). However, research using tissue-specific knock-outs showed that OCT4 is not functionally relevant for homeostasis and regeneration (96). Furthermore, using a reporter gene it was demonstrated that OCT4 is silenced in adult tissues, suggesting that the low levels are due to detection of OCT4 pseudogenes or other factors of the same family (96, 97). Thus, with the low levels detected in DPSC, it is likely a result from pseudogenes, related factors, or noise of the detection method, rather than functionally significant OCT4.

Following transduction, the three transcription factors were successfully expressed from the transgene. Gene and protein expression was evident in DPSC for each transcription factor. Thus, lentiviral particles for reprogramming were successfully produced and confirmed to be functional in DPSC. These lentiviral particles encoding for the three transcription factors were used in the subsequent chapter to reprogram human DPSC along the neural lineage.

CHAPTER 5

NEURAL REPROGRAMMING OF HUMAN DENTAL PULP STEM CELLS

5.1 | Introduction

This chapter examined the reprograming of human DPSC into NSC, following transduction with lentiviral constructs to over-express the selected transcription factors (OCT4, SOX2 or HES1). The reprogrammed DPSC were analysed for NSC properties following culture in neural inductive conditions. NSC are defined functionally by their ability to self-renew and differentiate into the main cells of the CNS.

The reprogrammed DPSC were analysed for expression of several neural markers throughout and at the completion of the two reprogramming methods investigated. There are a variety of markers associated with NSC, with variation observed between the type of NSC (e.g. foetal or adult, neuroepithelial cells, radial glial cells, progenitor cells, etc.) and the niche they occupy (e.g. the sub-ventricular zone and the sub-granular layer, and other minor neurogenic niches) (98). Some markers are common to all NSC, however there is no marker that is known to identify only NSC (99). The neural markers analysed here included transcription factor SOX1, transcription factor SOX2 and RNA-binding protein Musashi homolog 1 (Musashi-1), to identify NSC, the NSC and early neuronal marker nestin, the intermediate neuronal marker β-III tubulin and the mature neuronal marker NF-M. SOX1, encoded by *SOX1*, is involved in CNS development and NSC identity, while SOX2, encoded by *SOX2*, has a role in pluripotency and maintenance of ESC and NSC (15, 100). Musashi-1, encoded by *MSI1*, controls the balance between self-renewal and differentiation; it is highly expressed in neural progenitor cells (15). Nestin (*NES*) is an intermediate filament involved in axonal growth during the early stages of neuronal development, and is then replaced by cell type-specific intermediate filaments (98). The β-III tubulin (*TUBB3*) protein is a microtubule element in neurons, and the neurofilaments (NF-M analysed here) (*NEFM*) are intermediate filaments expressed in neurons (1). At the completion of neural reprogramming, the putative NSC were analysed for self-renewal and multi-lineage differentiation into the main cell types of the CNS; neurons, astrocytes and oligodendrocytes.

5.2 | Materials and Methods

5.2.1 Neural Reprogramming Methods

Human DPSC were transduced with lentiviruses, sorted for GFP by FACS, and cultured, using the following two neural induction protocols.

1) NSC Protocol (Figure 5.1A)

The day prior to lentiviral transduction, DPSC were seeded into 6-well tissue culture-treated plates at a density of $2x10^5$ cells/well/2mL standard DPSC culture medium. They were approximately 70-80% confluent on the day of transduction. The cells in each well were transduced with virus in 1mL DPSC medium (no antibiotics) supplemented with 8μg/mL polybrene. The cells were incubated for approximately 4 hours and then the medium was changed to fresh DPSC medium with antibiotics. The following day the cells were passaged, and cultured for up to 1 week to allow the cells to expand. They were sorted for GFP, and further cultured in DPSC medium for 5 days, allowing them to recover and expand. Subsequently, they were cultured in a 1:1 mix of DPSC/NSC medium for 3 days, and then in NSC medium for 1 or 2 weeks (Table 5.1). The medium was replaced every 2-3 days.

Table 5.1 NSC protocol.

NSC medium (1 week)
DMEM/F12 (1:1)
2% (v/v) B27
20ng/mL bFGF
20ng/mL EGF

2) Multi-step Neural Induction Protocol (Figure 5.1B)

The day prior to lentiviral transduction, DPSC were seeded into 6-well tissue culture-treated plates at a density of $1x10^5$ cells/well/2mL standard DPSC culture medium. They were approximately 70-80% confluent on the day of transduction. The cells in each well were transduced with virus in 1mL of 1:1 mix of DPSC medium (no antibiotics) and pre-inducing medium (Table 5.2), supplemented with 8µg/mL polybrene. The cells were incubated for approximately 4 hours and then the medium was changed to fresh 1:1 mix of DPSC medium with antibiotics and pre-inducing medium. The cells were cultured for 3 days. They were sorted for GFP, and cultured in gelatin-coated (0.2% (w/v) in PBS, 30 minute 37°C incubation, air dried at RT) 6-well plates in DPSC medium to recover. After 24 hours, the culture medium was changed to a 1:1 mix of DPSC medium and pre-inducing medium. After 24 hours, the culture medium was changed to pre-inducing medium (step 1 of the multi-step neural induction protocol). After eight days, the medium was changed to N2B27 medium (step 2) for seven days, and then NSC medium (step 3) for seven days (Table 5.2). The cells were passaged during step 1, as cell survival was low if passaged in medium supplemented with B27 (step 2 and 3 media), which requires initial cell attachment. Medium was replaced every 2-3 days.

Table 5.2 Multi-step neural induction protocol.

Step 1: Pre-inducing medium (8 days)	**Step 2: N2B27 medium (7 days)**	**Step 3: NSC medium (7 days)**
KnockOut DMEM/F12	DMEM/F12	DMEM/F12
1mM L-glutamine	1mM L-glutamine	1mM L-glutamine
20% (v/v) KnockOut serum replacement	2% (v/v) B27	2% (v/v) B27
1x non-essential amino acids	1% (v/v) N2	1% (v/v) N2
0.1mM BME	0.1mM BME	0.1mM BME
10ng/mL bFGF		20ng/mL bFGF
		20ng/mL EGF

Abbreviations: BME=β-mercaptoethanol.

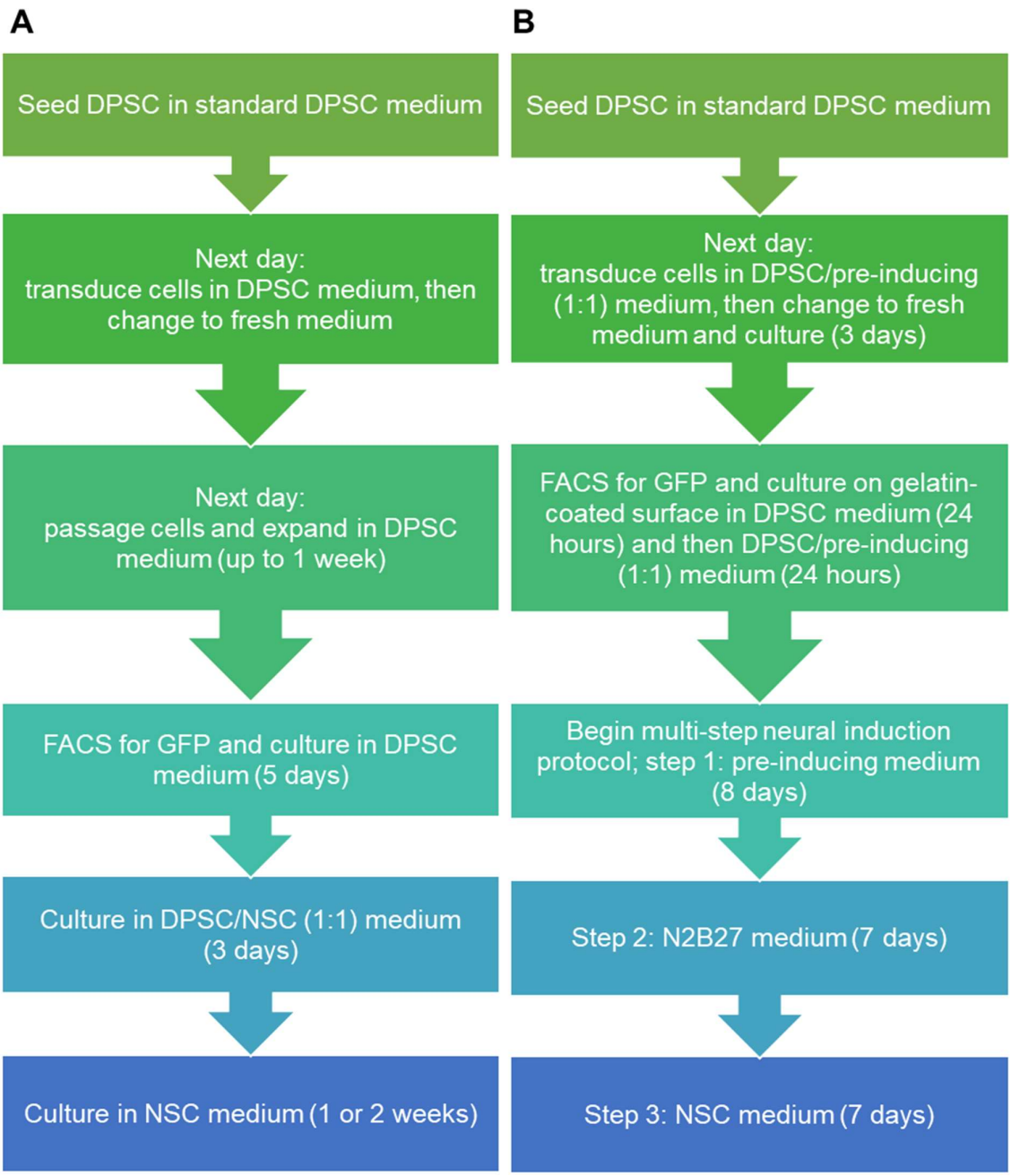

Figure 5.1 Neural reprogramming methods. **(A)** NSC protocol: culturing transduced DPSC in NSC medium. **(B)** Multi-step neural induction protocol: culturing transduced DPSC on gelatin-coated surfaces in three media (pre-inducing, N2B27 and NSC). In both methods, DPSC were seeded a day prior to transduction in 6-well plates. They were transduced with virus in 1mL media without antibiotics, supplemented with 8µg/mL polybrene. After approximately 4 hours, the viral media were removed and fresh media containing antibiotics were added. Transduced cells were sorted by FACS for GFP.

5.2.2 Neuronal Differentiation of Reprogrammed Human DPSC

For the generation of neurons, astrocytes and oligodendrocytes, DPSC that had been reprogrammed using the two protocols were seeded onto poly-D-lysine and laminin (neurons and oligodendrocytes) or gelatin (astrocytes) coated surfaces and differentiation media (Table 5.3) were added. The media were replaced every 3-4 days for the indicated time frames.

Table 5.3 Media for neuronal, astroglial and oligodendroglial differentiation.

Neuronal (4 weeks)*	**Astroglial (2 weeks)****	**Oligodendroglial (10 days)*****	
DMEM (5mM glucose)	DMEM	DMEM/F12	
2mM L-glutamine	1% (v/v) FBS	2mM L-glutamine	
2% (v/v) B27	2mM L-glutamine	2% (v/v) B27	
1% (v/v) N2	1% (v/v) N2	10ng/mL bFGF	first 5 days
1mM dbcAMP		10ng/mL platelet-derived growth factor	
30ng/mL neurotrophin-3		10nM forskolin	
		200nM L-ascorbate 2-phosphate	last 5 days
		30ng/mL triiodothyronine	

*Based on Gervois *et al.* 2015, with reduced glucose to mimic physiological levels and that have been shown to support NSC (3, 101, 102)

**ThermoFisher Scientific protocol; https://www.thermofisher.com/au/en/home/references/protocols/neurobiology/neurobiology-protocols/differentiating-neural-stem-cells-into-neurons-and-glial-cells.html

***Based on the method published by Lujan *et al.* 2012 (103)

5.2.3 Sphere Formation Assay

To allow the formation of spheres, cells were grown in suspension in ultra-low attachment 6-well plates (Corning Inc., NY, USA). For each sample, equal number of cells ($1x10^5$) were seeded into 3 wells. For the NSC protocol (Table 5.1), cells were cultured in low-attachment plates in NSC medium for 3 days, alongside the monolayer cultures. For the multi-step neural induction protocol (Table 5.2), following completion of the 3 steps, cells were further cultured in NSC medium for 1 week in low-attachment plates. The time point for counting spheres was based on the ability to detect spheres of the size-of-interest. For each well, micrographs of three fields of view at 100x magnification were taken. The fields of view were in the area of sphere growth (well centres). ImageJ software was used to measure the largest diameter of the spheres. Spheres ≥100µm in diameter, determined to be a suitable size to distinguish spheres and prevent cellular necrosis in oversized spheres, were counted. Well counts were averaged, then sample counts were averaged. Data was plotted as mean±SD and analysed using a Mann-Whitney test.

5.2.4 Surface marker staining and FACS for $CD146^{-/+}$ DPSC

Human DPSC were immunostained for the surface antigen CD146 as described in Chapter 3, section 3.2.2, pg. 38, and underwent FACS as described in Chapter 2, section 2.2.1.6, pg. 29, for negative and positive sub-populations.

5.2.5 Quantitative PCR

See Chapter 2, section 2.2.2.3, pg. 30 for protocol, using the primers in Table 5.4

Table 5.4 Primers for qPCR.

Gene		Protein	Forward Primer	Reverse Primer
POU5F1	Coding Sequence	OCT4	ggaggaagctgacaacaatgaaa	ggcctgcacgagggttt
	Endogenous		gggtttttgggattaagttcttca	gccccccacccttttgtgtt
	Transgene		ggctctcccatgcattcaaactg	aaacgcacaccggccttattcc
SOX1		SOX1	aaaagctgagttagtgcgcccg	ttcagctgactgtgcacgaagc
SOX2		SOX2	caaaaatggccatgcaggtt	agttgggatcgaacaaaagctatt
MSI1		Musashi-1	tgacaaaaccaccaaccggcac	acatcacctcctttggctgagc
HES1		HES1	accaaagacagcatctgagcacag	tgccgcgagctatctttcttcag
NES		Nestin	agacttccctcagctttcaggac	caggactgggagcaaagatccaag
TUBB3		β-III tubulin	ggcctcttctcacaagtacgtg	ttgtcaggcctgaagagatgtcc
NEFM		NF-M	tggaaaatgagcttcggggcac	gtacgcagcgatttctatatccagagc
ACTB		β-actin	agagctacgagctgcctgac	ttcgtggatgccacaggactc

5.2.6 Western Blot

See Chapter 2, section 2.2.2.5, pg. 32 for protocol, using the antibodies in Table 5.5.

Table 5.5 Antibodies for Western blots.

Name	Dilution	Company	Catalogue Number
Primary Antibodies			
Goat anti-GFP	1:1000	Rockland Antibodies and Assays	600101215
Goat anti-OCT4	1:400	R&D Systems	AF1759
Goat anti-SOX1	1:200	R&D Systems	AF3369
Rabbit anti-SOX2	1:1000	Cell Signaling Technology	3579
Rabbit anti-HES1	1:1000	Abcam	ab71559
Rabbit anti-NANOG	1:1000	Abcam	ab109250
Mouse anti-Nestin	1:1000	Abcam	ab22035
Mouse anti-β-III tubulin	1:1000	Merck Millipore	MAB1637
Mouse anti-NF-M	1:1000	Invitrogen	130700
Mouse anti-β-actin	1:4000	Sigma-Aldrich	A2228
Secondary Antibodies			
Rabbit anti-sheep DyLight 680 *	1:20 000	Invitrogen	SA5-10058
Goat anti-mouse DyLight 680 *	1:20 000	Invitrogen	35518
Goat anti-mouse DyLight 800	1:20 000	Invitrogen	SA5-35521
Goat anti-rabbit DyLight 680	1:20 000	Invitrogen	35568
Goat anti-rabbit DyLight 800 *	1:20 000	Invitrogen	SA5-35571

* Kindly provided by the Cell Signalling and Gene Regulation research group (SAHMRI, SA, Australia).

5.2.7 Immunofluorescence Staining

See Chapter 2, section 2.2.2.4, pg. 31 for protocol, using the antibodies in Table 5.6. ImageJ software was used to measure the MFI. For each image, measurements were made as triplicates. The background was averaged and subtracted from the signal. For each DPSC sample, the DPSC-OCT4 signals were normalised to the DPSC-EV signals, log (base 2) converted, and the triplicates averaged.

Table 5.6 Antibodies for immunofluorescence staining.

Name	Species	Stock Concentration	Dilution	Company	Catalogue Number
Primary Antibodies					
Anti-Nestin	Mouse	0.5mg/mL	1:250	Abcam	ab6320
Anti-β-III tubulin	Mouse	Not disclosed	1:250	Merck Millipore	MAB1637
Anti-NF-M	Mouse	0.5mg/mL	1:250	Invitrogen	130700
Anti-GFAP	Rabbit	2.9mg/mL	1:250	Dako	0334
Anti-PLP	Rabbit	Not disclosed	1:250	Abcam	ab28486
Anti-vimentin	Mouse	1mg/mL	1:250	Abcam	ab8978
Isotype Controls Antibodies					
Anti-mouse IgG	N/A	1mg/mL	1:250	*	
Anti-rabbit IgG	N/A	5mg/mL	1:250	*	
Secondary Antibodies					
Anti-mouse IgG Cyanin3	Donkey	1mg/mL	1:500	Merck Millipore	AP192C
Anti-rabbit IgG Cyanin3	Donkey	1.5mg/mL	1:500	Jackson Immunoresearch	711165152

* Kindly provided by Mesenchymal Stem Cell Laboratory research group (University of Adelaide and SAHMRI, SA, Australia).

5.2.8 Electrophysiology: Patch-clamping (Whole-cell Recording)

This analysis was carried out by Dr. Grigori Rychkov (University of Adelaide and SAHMRI, SA, Australia). Whole-cell patch clamping was performed at RT using a computer-based patch-clamp amplifier (EPC-9) and PULSE software (HEKA Electronics, Germany). The bath solution contained; 140mM NaCl, 4mM KCl, 2mM $CaCl_2$, 2mM $MgCl_2$, 10mM glucose and 10mM HEPES, adjusted to pH 7.4 with NaOH. The internal (pipette) solution contained; 80mM K gluconate, 40mM KCl, 10mM NaCl, 1mM $CaCl_2$, 5mM Egtazic acid and 10mM HEPES, adjusted to pH 7.3 with KOH. Patch pipettes were pulled from borosilicate glass and fire-polished; pipette resistance ranged between 2 and 4 MΩ. Series resistance did not exceed 10 MΩ and was compensated by 50-70%. Acquired currents were filtered at 2.7 kHz and sampled at 10 kHz. All voltages shown are nominal and have not been corrected for the liquid junction potential. The holding potential was -80mV throughout. Cell capacitance was compensated automatically by the EPC9 amplifier.

5.3 | Results

Two neural reprogramming methods were investigated and are addressed in two results sections; section 5.3.1 addresses the NSC protocol (Figure 5.1A and Table 5.1) and 5.3.2 addresses the multi-step neural induction protocol (Figure 5.1B and Table 5.2).

5.3.1 Transduced human DPSC cultured using the NSC protocol

This results section discusses the neural reprogramming of human DPSC using the NSC protocol (Figure 5.1A). This protocol was based on the neuronal differentiation method for DPSC published by Gervois *et al.* 2015, as it showed promising results for neuronal differentiation of non-modified DPSC (Chapter 3, section 3.3.7, pg. 56) (3). Since the aim was to convert the DPSC into NSC, the focus of this protocol was culturing the transduced DPSC in the NSC medium (Table 5.1), rather than the complete published method that aimed to differentiate the DPSC into neurons. Analysis was performed to determine if the DPSC could be converted to the 'intermediate' NSC stage instead of complete neuronal differentiation, and whether the transcription factors enhanced the conversion potential. Table 5.7 (pg. 128) summarises the outcomes of this reprogramming method.

5.3.1.1 OCT4, SOX2, HES1 over-expressing DPSC cultured in standard DPSC conditions

The DPSC were transduced with the pCDH lentiviral vectors encoding for either the OCT4, SOX2 or HES1 transcription factors (pCDH-OCT4, pCDH-SOX2, pCDH-HES1 respectively), or the empty vector as a control (pCDH-EV). The transduced cells were sorted based on GFP expression. The transduction efficiency varied based on the vector insert and between DPSC samples (Figure 5.2A). The control vector resulted in the highest transduction efficiency with 88.0±13.2 per cent GFP^+ DPSC, followed by pCDH-OCT4 (54.7±25.0), then pCDH-HES1 (40.0±9.6) and the lowest for pCDH-SOX2 (7.0±3.5), which was significantly lower than the control ($p<0.01$) (Figure 5.2A). The low transduction efficiency using pCDH-SOX2, combined with the stress from sorting, suggested that it may not be feasible to continue with these samples.

The GFP^+ DPSC were initially cultured in standard DPSC medium at the same seeding density in an appropriately-sized vessel based on recovered cell numbers after FACS. The response of the cells varied based on the vector insert. Figure 5.2B shows the cells cultured in standard DPSC medium. The control pCDH-EV-transduced DPSC (DPSC-EV) grew well and morphologically remained similar to non-transduced DPSC. The pCDH-OCT4-transduced DPSC (DPSC-OCT4) appeared to grow at a slower rate. They were similar in morphology to non-transduced DPSC but were less elongated. The pCDH-HES1-transduced DPSC (DPSC-

HES1) resembled DPSC-OCT4, however it was observed that they had slower proliferation, with low survival in DPSC2. The pCDH-SOX2-transduced DPSC (DPSC-SOX2) did not survive; this was seen with all three samples (dead cell aggregates seen in Figure 5.2B). Thus, reprogramming using the SOX2 transcription factor was excluded from subsequent analysis due to feasibility of obtaining sufficient viable cell samples for further analyses.

A proliferation assay was performed on the surviving samples, and compared with the proliferation rate of non-transduced DPSC cultured in standard DPSC medium (Figure 5.3). Over 24 hours, significant growth rates in the non-transduced DPSC ($p<0.01$) and the control DPSC-EV ($p<0.05$) were observed, with a non-significant increase for DPSC-OCT4 and a minor increase for DPSC-HES1 (Figure 5.3A). When reviewing the proliferation rates, the non-transduced DPSC had tripled over 24 hours (3.1±0.2), DPSC-EV (2.5±0.7) and DPSC-OCT4 (2.2±0.2) had doubled, while DPSC-HES1 (1.3±0.7) exhibited a modest increase (Figure 5.3B). Compared with the non-transduced DPSC, the proliferation rate was significantly lower in DPSC-HES1 ($p<0.05$). Figure 5.3C displays the proliferation rates of the individual DPSC samples, showing the inter-donor variation, particularly for DPSC-HES1. Whilst there was variation observed between samples with all vectors, DPSC-OCT4 grew better than DPSC-HES1. Based on these proliferation rates, DPSC-OCT4 were used for further analysis. Some analysis was also performed with DPSC-HES1 (DPSC1 and DPSC3) (Appendix C), however insufficient consistency with survival and proliferation rates across samples from different donors made it difficult to obtain sufficient cell samples to analyse.

A

Lentiviral Vector	GFP⁺ Cells (%)			
	DPSC1	DPSC2	DPSC3	Mean±SD
pCDH-EV	73	93	98	88.0±13.2
pCDH-OCT4	30	80	54	54.7±25.0
pCDH-SOX2	11	5	5	7.0±3.5
pCDH-HES1	47	29	44	40.0±9.6

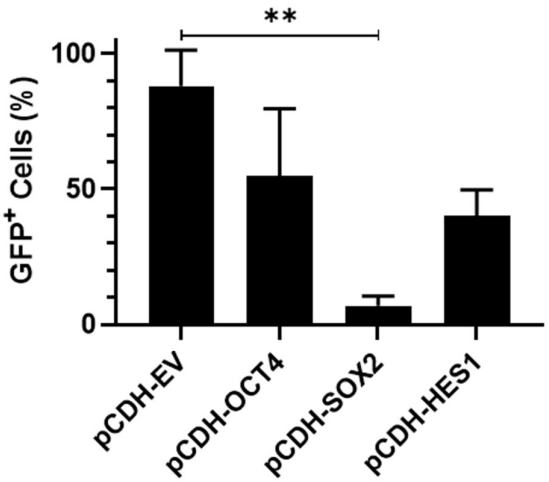

B

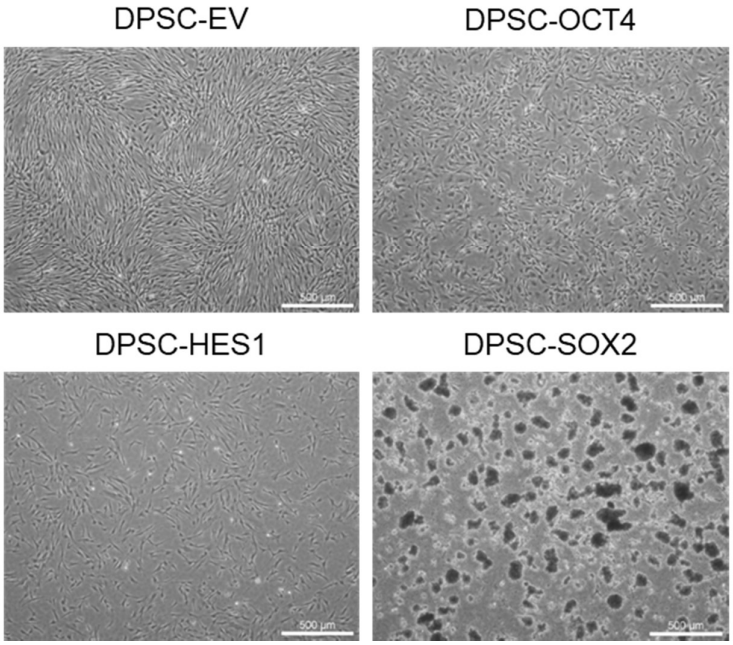

Figure 5.2 NSC protocol: single lentiviral transduction of DPSC. **(A)** Transduction efficiency for each vector demonstrated by the percentage of GFP⁺ cells. **(B)** After sorting, the transduced cells were cultured in standard DPSC medium to recover and expand. Representative images (n=2 for HES1), data represents mean±SD, Kruskal-Wallis test with Dunn's multiple comparisons test, n=3, scale bar=500µm, **p<0.01.

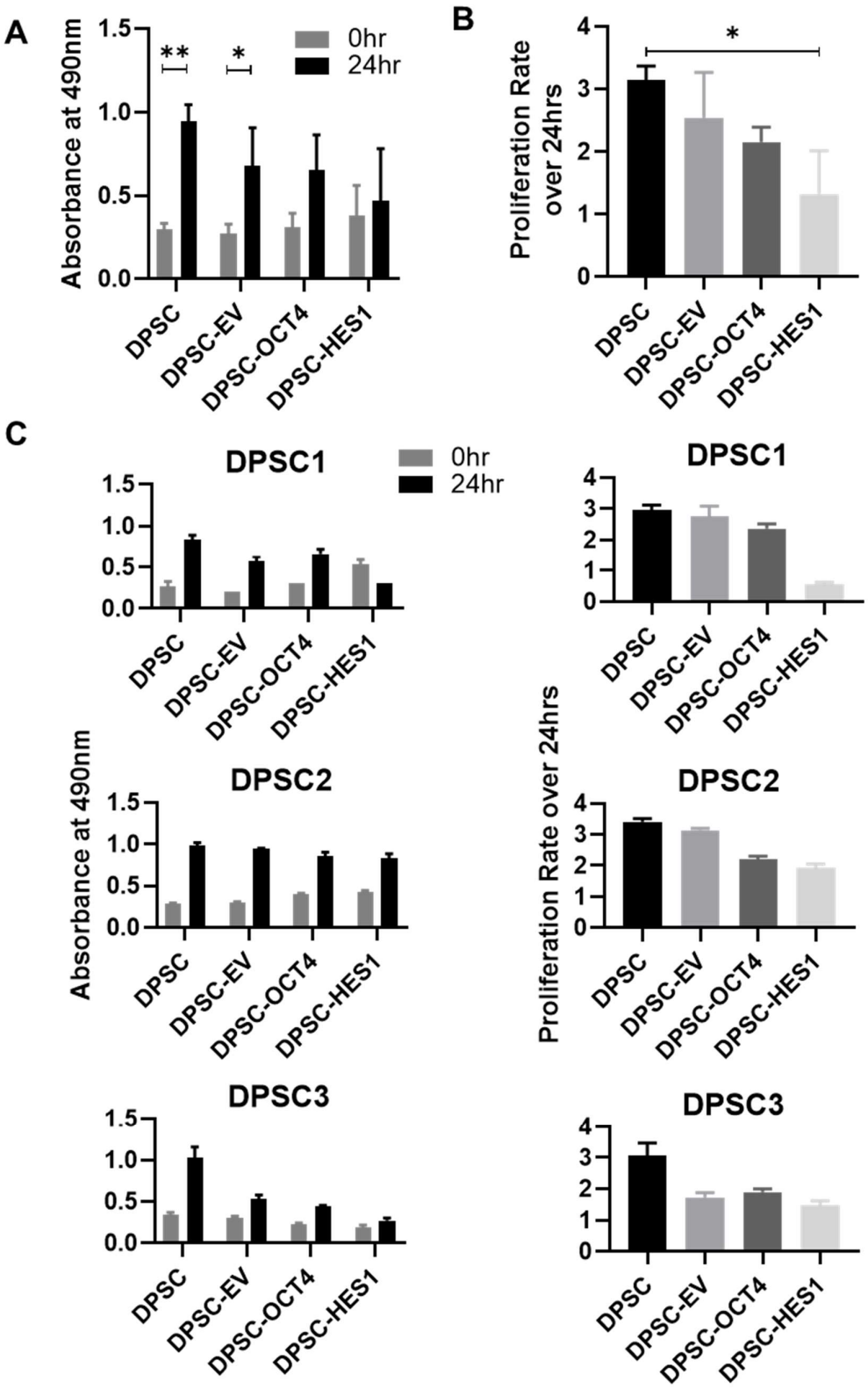

Figure 5.3 NSC protocol: proliferation rate of transduced DPSC. **(A)** Average absorbance values at 0 and 24 hours. **(B)** Average proliferation rate over 24 hours. **(C)** Individual absorbance values and proliferation rates. Data represent mean±SD, two-way ANOVA with Sidak's multiple comparisons test (A) and Kruskal-Wallis test with Dunn's multiple comparisons test (B), n=3, *p<0.05, **p<0.01.

5.3.1.2 OCT4 over-expressing DPSC cultured in NSC medium

To enhance survival after culturing the GFP^+ DPSC in standard DPSC medium, the medium was replaced with a 1:1 mix of DPSC medium and NSC medium, and subsequently replaced with NSC medium only. The cells were cultured in the NSC medium for one week, as per the Gervois *et al.* 2015 method (3), and for a further two weeks to determine any changes to cell viability.

When cultured in the NSC medium, both DPSC-EV and DPSC-OCT4 appeared to grow slower with variation observed between donors. Morphologically, DPSC-EV remained similar to non-transduced DPSC, appearing spindle-shaped, slightly elongated and not as flat. In contrast, DPSC-OCT4 exhibited a rounder, shorter and less flat morphology, compared to non-transduced DPSC. These morphological changes are shown in Figures 5.4A and in 5.4B, where cells were immunostained for Nestin, which is also detected in non-modified DPSC.

Due to the observed slower growth in NSC medium and difficulty in obtaining samples for analysis, cell counts were performed over two weeks (Figure 5.4C). For all three DPSC samples, DPSC-OCT4 had a greater number of cells at each time point than DPSC-EV. However, only DPSC1 showed an increase in the cell number from the original number of cells seeded. Due to sample availability, sufficient cell counts could not be performed, to obtain accurate cell counts. Nevertheless, it was consistently observed that the cells were growing slowly in the NSC medium, suggesting that this neural reprogramming method was not worth pursuing in terms of efficiency and cell availability for functional analyses.

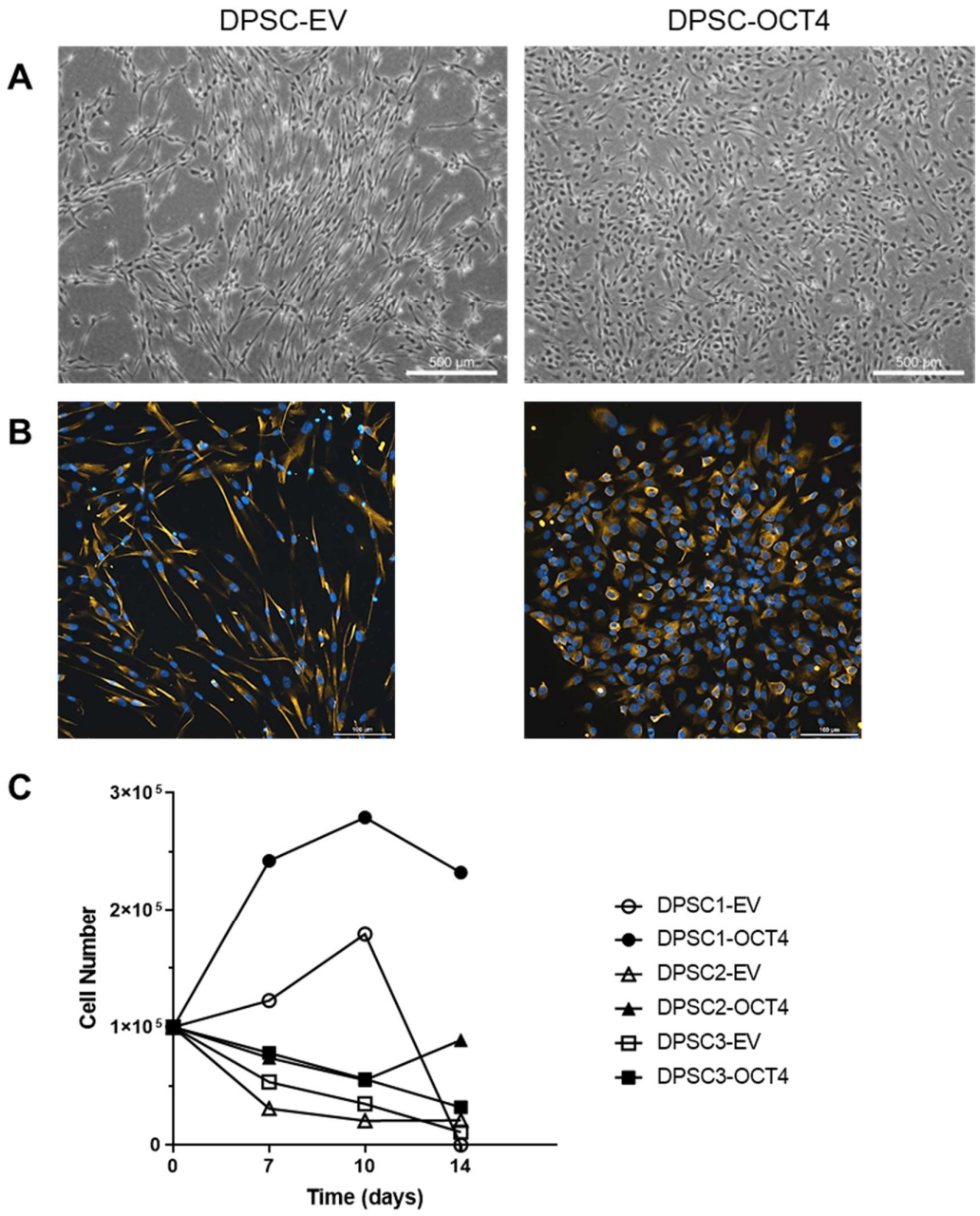

Figure 5.4 Transduced DPSC in NSC culture medium. Cells were cultured in NSC medium for 1 week. **(A)** Cell morphology. **(B)** Immunofluorescence staining highlighting the cell morphology (Nestin protein). **(C)** Cell counts from 1-2 weeks. Representative images, n=3, scale bar=500µm (A) and 100µm (B).

5.3.1.3 OCT4 over-expression in DPSC

The DPSC-EV and DPSC-OCT4 samples were cultured in NSC medium for one and two weeks, and samples were collected for gene expression analysis by qPCR and protein expression analysis by Western blot.

To confirm that the OCT4 gene, *POU5F1*, was over-expressed, DPSC-OCT4 were compared to DPSC-EV before culturing in NSC medium (0 week time point) and after one or two weeks in NSC medium. There was a significant increase in *POU5F1* expression at each time point, with a greater than 5-fold (log2 scale) change observed (Figure 5.5A, B shows individual DPSC samples). Western blot analysis confirmed protein over-expression (Figure 5.5C). Protein lysates were collected from DPSC1 only, as DPSC2 and DPSC3 protein lysates were too low to assess.

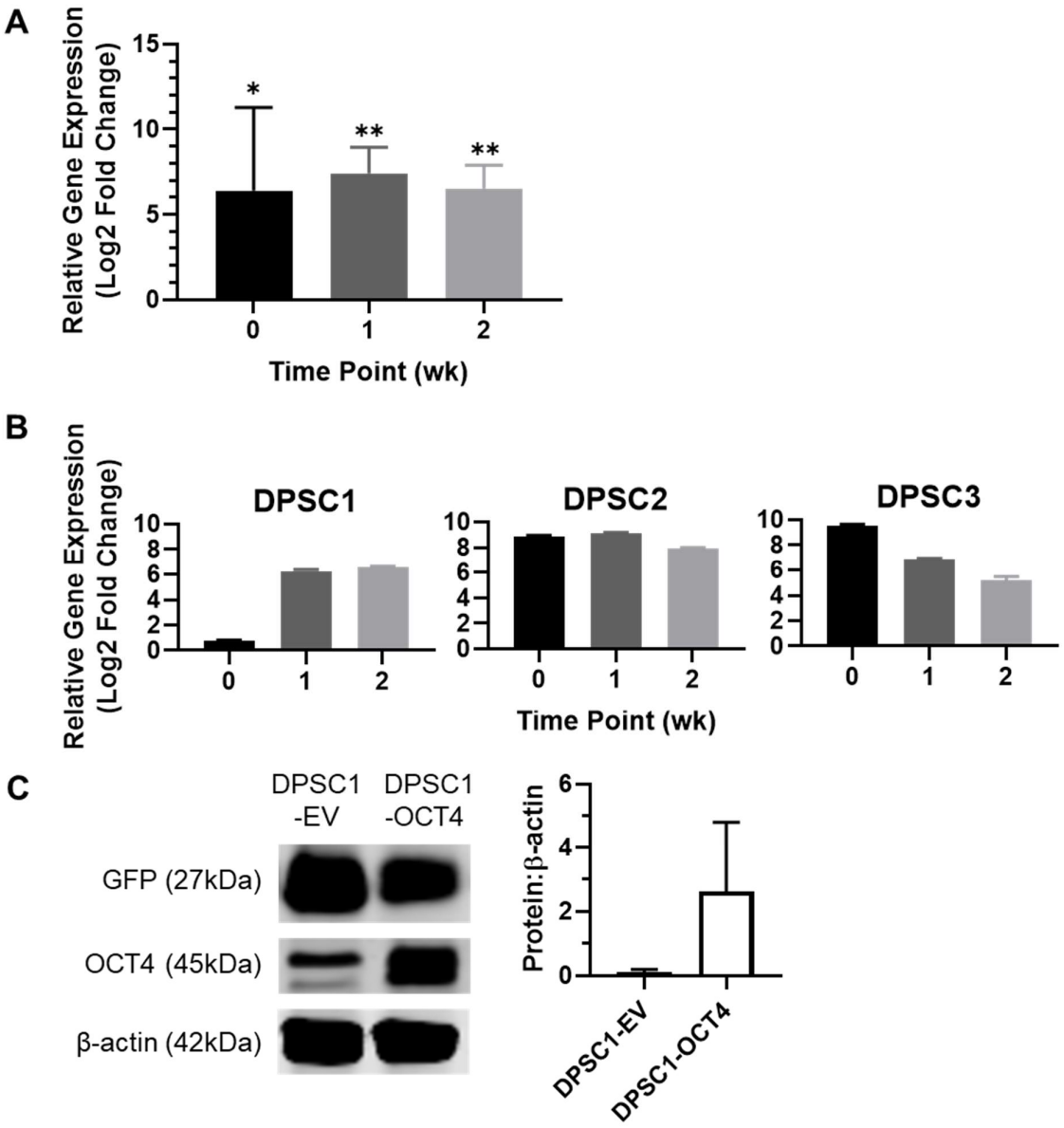

Figure 5.5 NSC protocol: OCT4 over-expression in DPSC-OCT4. DPSC-EV and DPSC-OCT4 were cultured in standard DPSC medium (time point 0) and in NSC medium for 1 and 2 weeks (time points 1 and 2). **(A)** *POU5F1* gene expression levels in DPSC-OCT4 relative to DPSC-EV. **(B)** Individual DPSC gene expression levels. **(C)** Protein expression of OCT4 and GFP. OCT4 levels quantified relative to the loading control β-actin. Representative blots of experimental triplicates of n=1, data represents mean±SD, two-way ANOVA with Sidak's multiple comparisons test (A), Mann-Whitney test (C), n=3, *$p<0.05$, **$p<0.01$.

5.3.1.4 Changes in neural gene expression: effect of NSC medium

To determine the effect of the NSC medium on the transduced DPSC, gene expression levels at one and two weeks in NSC medium were compared to the gene expression levels before culturing in NSC medium (Figure 5.6). The control DPSC-EV showed an increase in all of the neural genes at one and two weeks, with the greatest increase in *NEFM* (Figure 5.6A). The gene expression levels of the NSC genes *SOX1* and *SOX2* were significantly greater ($p<0.05$) at two weeks, however *SOX1* showed more variation between DPSC samples (Figure 5.6B). There was no significant increase in *MSI1*, *NES* and *TUBB3*, with levels between one and two weeks remaining similar. *NEFM* was significantly greater ($p<0.01$) at one and two weeks, with similar levels between the time points. For DPSC-OCT4, there was a decrease in *SOX1* ($p<0.05$), *SOX2* and *NEFM*, and minor increases in *MSI1* and *NES*, while *TUBB3* expression levels showed little change (Figure 5.6A). For each gene, there was a minor increase from one to two weeks in NSC medium but did not reach significance. Figure 5.6B shows the variation between the samples. There was little consistency in expression levels and trends between the three DPSC samples. In DPSC-EV, the neuronal genes showed more consistency, while *SOX1* and *SOX2* expression levels showed most consistency in DPSC-OCT4.

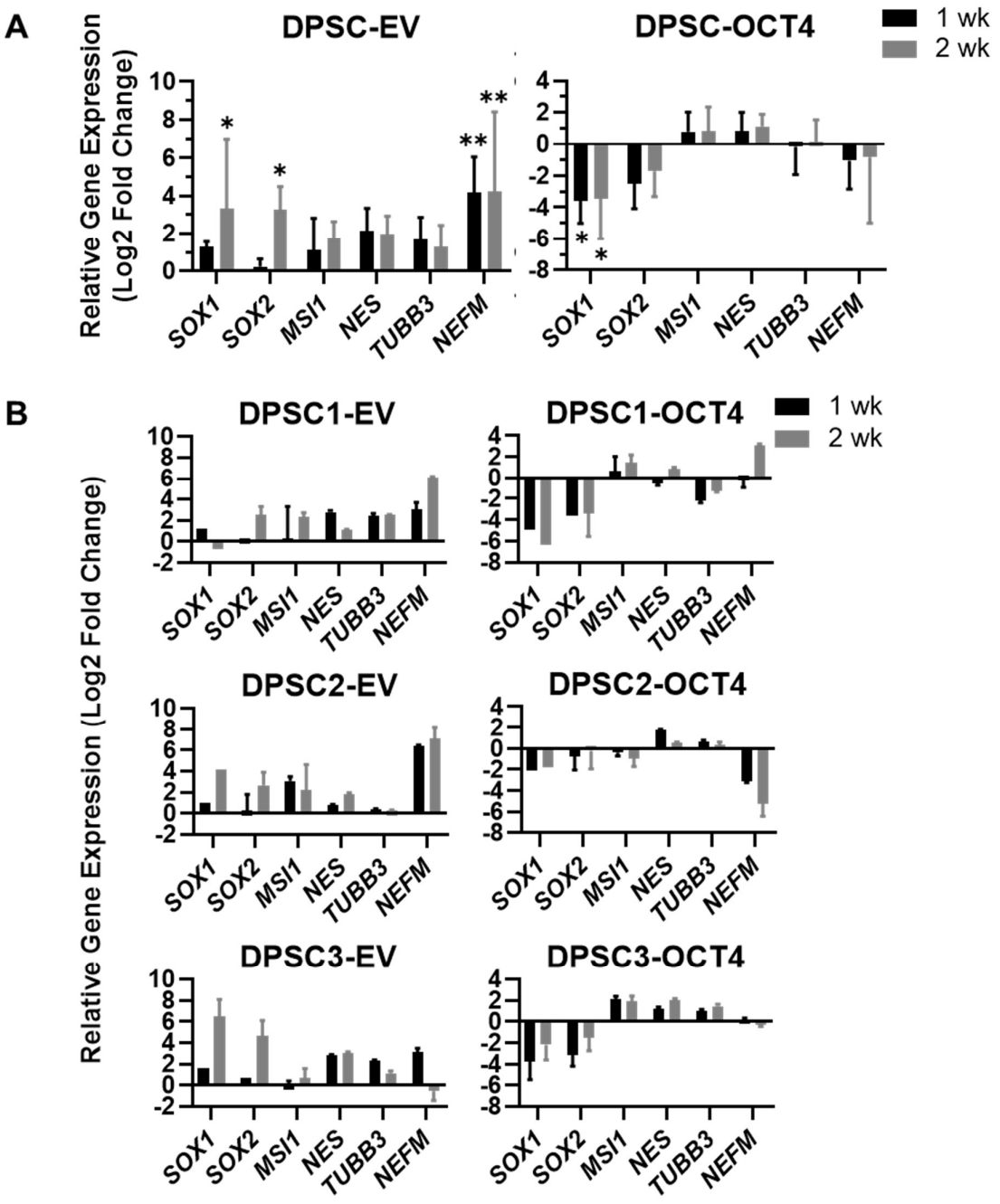

Figure 5.6 NSC protocol: effect of the NSC culture medium. **(A)** Gene expression levels in DPSC-EV and DPSC-OCT4 after 1 and 2 weeks in NSC medium relative to the corresponding transduced samples in standard DPSC culture medium. **(B)** Individual gene expression levels. Data represents mean±SD, two-way ANOVA with Tukey's multiple comparisons test, n=3, *p<0.05, **p<0.01.

5.3.1.5 Changes in neural gene expression: effect of OCT4 over-expression

To determine the effect of OCT4 over-expression, the gene expression in DPSC-OCT4 was compared to DPSC-EV when cultured in standard DPSC medium and NSC medium (Figure 5.7A). When cultured in DPSC medium, an increase was seen in *SOX1* ($p<0.01$), *SOX2* and *MSI*, minor changes were seen in *NES* and *TUBB3*, and the greatest increase was observed for *NEFM* ($p<0.0001$). Surprisingly, there was a decreasing trend over time when cultured in NSC medium, with only *MSI1* and *NEFM* showing elevated expression levels. Figure 5.7B shows the inter-donor variation, which on the whole shows lower expression levels in NSC medium than in DPSC medium.

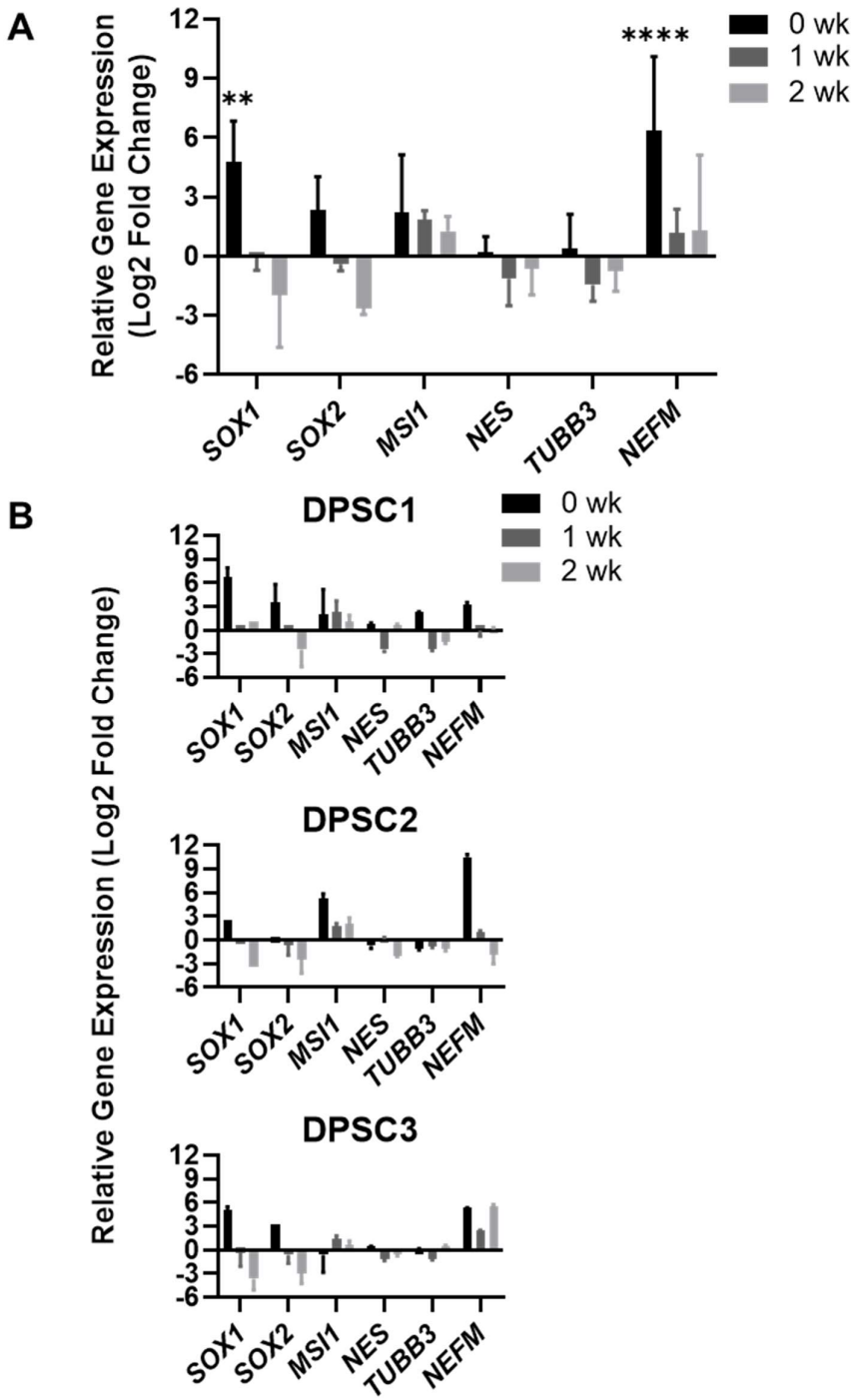

Figure 5.7 NSC protocol: effect of OCT4 over-expression. **(A)** Gene expression levels in DPSC-OCT4 before neural culture (0 wk) and after 1 and 2 weeks in NSC medium relative to DPSC-EV in the corresponding conditions. **(B)** Individual gene expression levels. Data represents mean±SD, two-way ANOVA with Dunnett's multiple comparisons test, n=3, **p<0.01, ****p<0.0001.

5.3.1.6 Protein expression supported gene expression

Protein expression analysis was performed by Western blot (Figure 5.8). The SOX1 and SOX2 protein levels were low (Figure 5.8A). An increase was observed in all the proteins when DPSC-EV were cultured in NSC medium. Protein levels appeared lower in DPSC-OCT4 than DPSC-EV when cultured in NSC medium. The Western blots were quantified (Figure 5.8B). This confirmed that there was some increase in protein expression in DPSC-EV in response to the NSC medium, which supported the gene expression analysis. There were minor differences between DPSC-EV and DPSC-OCT4 both cultured in NSC medium for one week, similar to the gene expression data in Figure 5.7A. Between DPSC-OCT4 cultured in NSC medium for one and two weeks, there were small decreases in expression levels at two weeks, corresponding to the gene expression data. The pluripotent marker NANOG was not detected. This protein expression data was from multiple samples of the same donor (DPSC1), due to insufficient cell numbers from the other two donors.

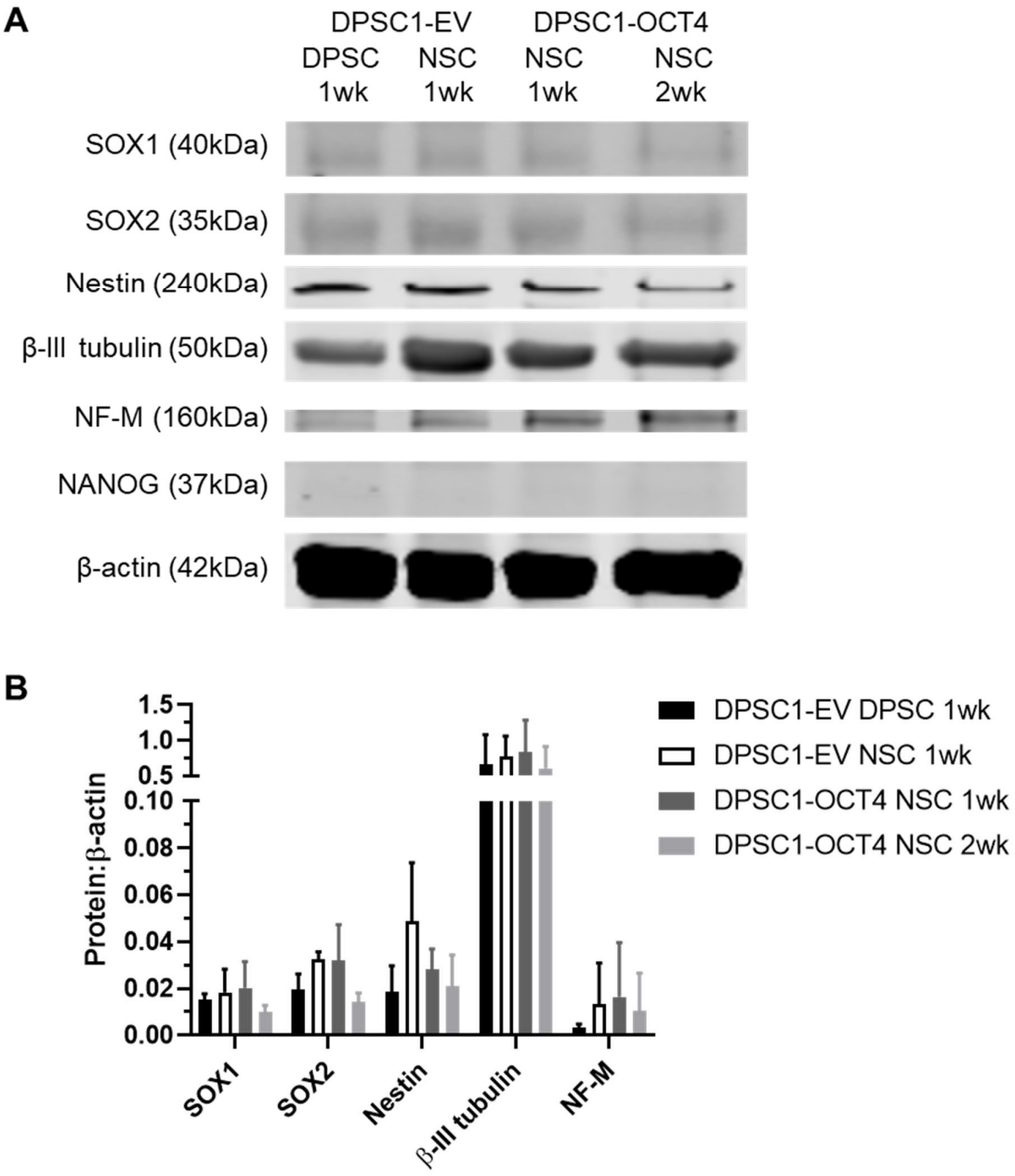

Figure 5.8 NSC protocol: protein expression. **(A)** Expression levels of proteins of interest in DPSC1-EV and DPSC1-OCT4 in standard DPSC culture medium and NSC medium. **(B)** Protein expression levels quantified and expressed relative to the loading control β-actin. Representative blots, data represents mean±SD, two-way ANOVA with Sidak's multiple comparisons test, representative of experimental triplicates of n=1.

5.3.1.7 DPSC-OCT4 consisted of a greater number of stem/progenitor cells

For this NSC protocol, the transduced DPSC were initially grown in NSC medium as monolayer cultures. In Chapter 3, Characterisation of Human DPSC, both monolayer and suspension cultures were tested, with monolayer cultures resulting in lower cell loss. Here, incorporation of suspension cultures similar to the Gervois *et al*. 2015 method, on which this NSC protocol is based, was investigated (3).

The transduced DPSC were cultured in NSC medium in suspension, alongside the monolayer cultures, to allow formation of spheres (Figure 5.9). Both DPSC-EV and DPSC-OCT4 formed spheres of varying sizes, as seen in Figure 5.9A. A greater number of spheres ≥100µm were formed by DPSC-OCT4, though the difference with DPSC-EV was not statistically significant (Figure 5.9B). The size range was greater in DPSC-OCT4, with some samples containing larger spheres. Further to this, the spheres were dissociated and reseeded for assessment of secondary sphere formation. However, secondary spheres ≥100µm were not detected in either group.

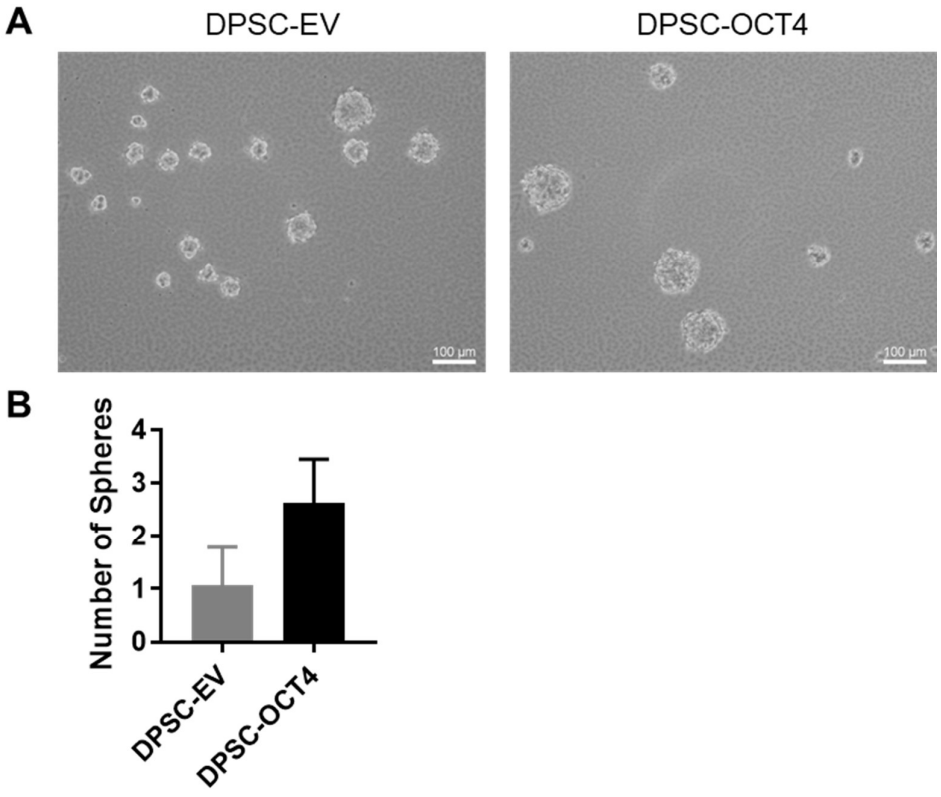

Figure 5.9 NSC protocol: sphere formation. **(A)** DPSC-EV and DPSC-OCT4 were cultured in NSC medium in suspension. **(B)** Spheres ≥100µm were counted. Data represents mean±SD, Mann-Whitney test, n=3, scale bar=100µm.

5.3.1.8 Gene expression in monolayer versus suspension cultures

Using the NSC protocol, gene expression comparisons were made between cells grown in monolayer and suspension cultures. Samples were collected after one week of culture in NSC medium in suspension. Three comparisons were made to analyse the difference between monolayer and suspension cultures.

In Figure 5.10, the gene expression levels in the transduced DPSC grown in NSC medium in suspension were compared to those grown as monolayers, to show the effect of the culture type. In both DPSC-EV and DPSC-OCT4, an increase was observed in *SOX1*, *SOX2* and *MSI1*, with higher levels in DPSC-EV. However, the individual DPSC samples showed that this varied between samples, where two of the three samples had an increase in *SOX1* in DPSC-OCT4 while one had a very high increase in *SOX1* in DPSC-EV. For *NES* and *TUBB3* there were minor changes in gene expression with an increase in DPSC-OCT4 and a decrease in DPSC-EV, whilst *NEFM* decreased in both. These results showed that suspension culture increased the expression of NSC genes and decreased expression of neuronal genes. The inter-donor variation was greater in DPSC-OCT4.

In Figure 5.11, the gene expression levels were assessed in DPSC-EV and DPSC-OCT4 grown in suspension or monolayer in NSC medium, and compared to DPSC-EV and DPSC-OCT4 maintained in standard DPSC culture medium as a monolayer, as in Figure 5.6A, to show the effect of the NSC medium in the two culture types. Whilst DPSC-EV showed increased expression levels of all genes in both the monolayer and suspension cultures, the suspension cultures had significant increases in the NSC genes while the monolayer culture had significant increase in *NEFM*. In DPSC-OCT4, there was a decrease in *SOX1* ($p<0.05$), *SOX2* and *NEFM* in the monolayer culture, while the suspension culture had greater levels than the monolayer cultures for all genes except *NEFM*.

The final comparison (Figure 5.12) was of DPSC-OCT4 relative to DPSC-EV, cultured in NSC medium as a monolayer or suspension, as in Figure 5.7A, to show the effect of OCT4 over-expression in the two culture types. Figure 5.12A shows that the effect of OCT4 over-expression was not significantly altered when the cells are cultured in suspension instead of a monolayer.

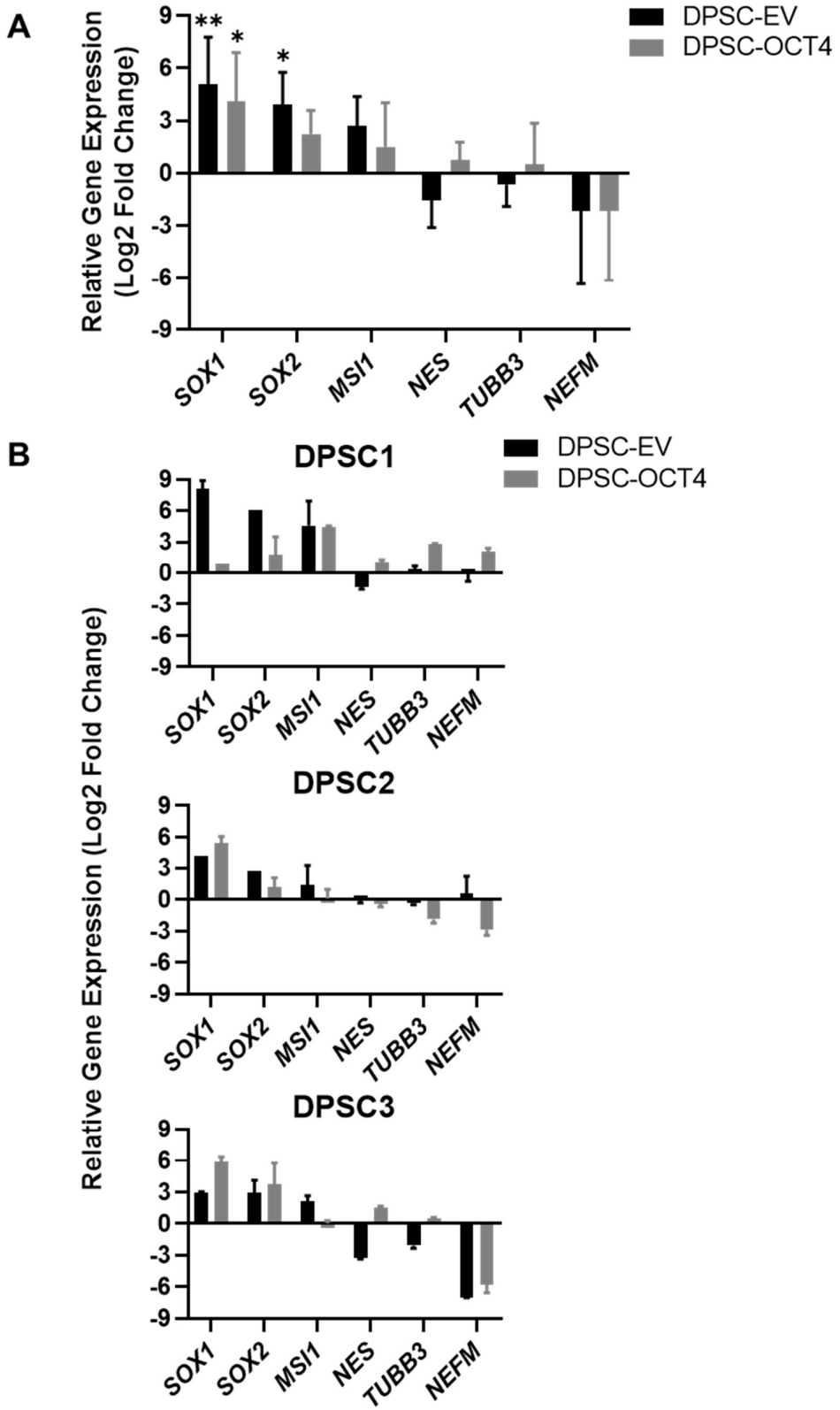

Figure 5.10 Comparison of monolayer and suspension cultures in NSC medium; effect of culture type. **(A)** Gene expression levels in DPSC-EV and DPSC-OCT4 cultured in suspension in NSC medium for 1 week relative to those cultured as a monolayer. **(B)** Individual gene expression levels. Data represents mean±SD, two-way ANOVA with Dunnett's multiple comparisons test, n=3, *p<0.05, **p<0.01.

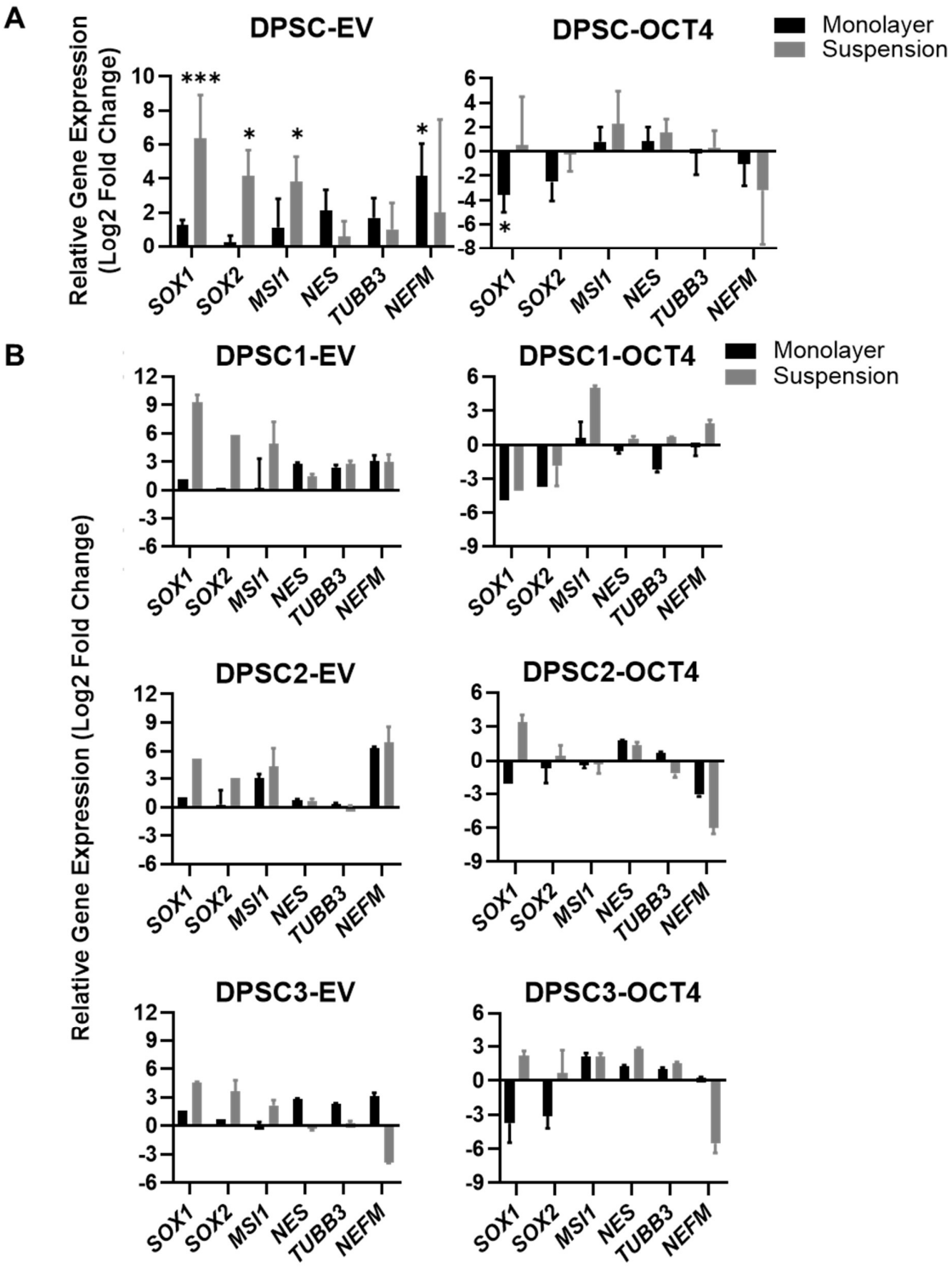

Figure 5.11 Comparison of monolayer and suspension cultures in NSC medium; effect of medium. **(A)** Gene expression levels in DPSC-EV and DPSC-OCT4 cultured in suspension or as a monolayer in NSC medium for 1 week relative to the samples cultured in DPSC medium as a monolayer. **(B)** Individual gene expression levels. Data represents mean±SD, two-way ANOVA with Dunnett's multiple comparisons test, n=3, *p<0.05, ***p<0.001.

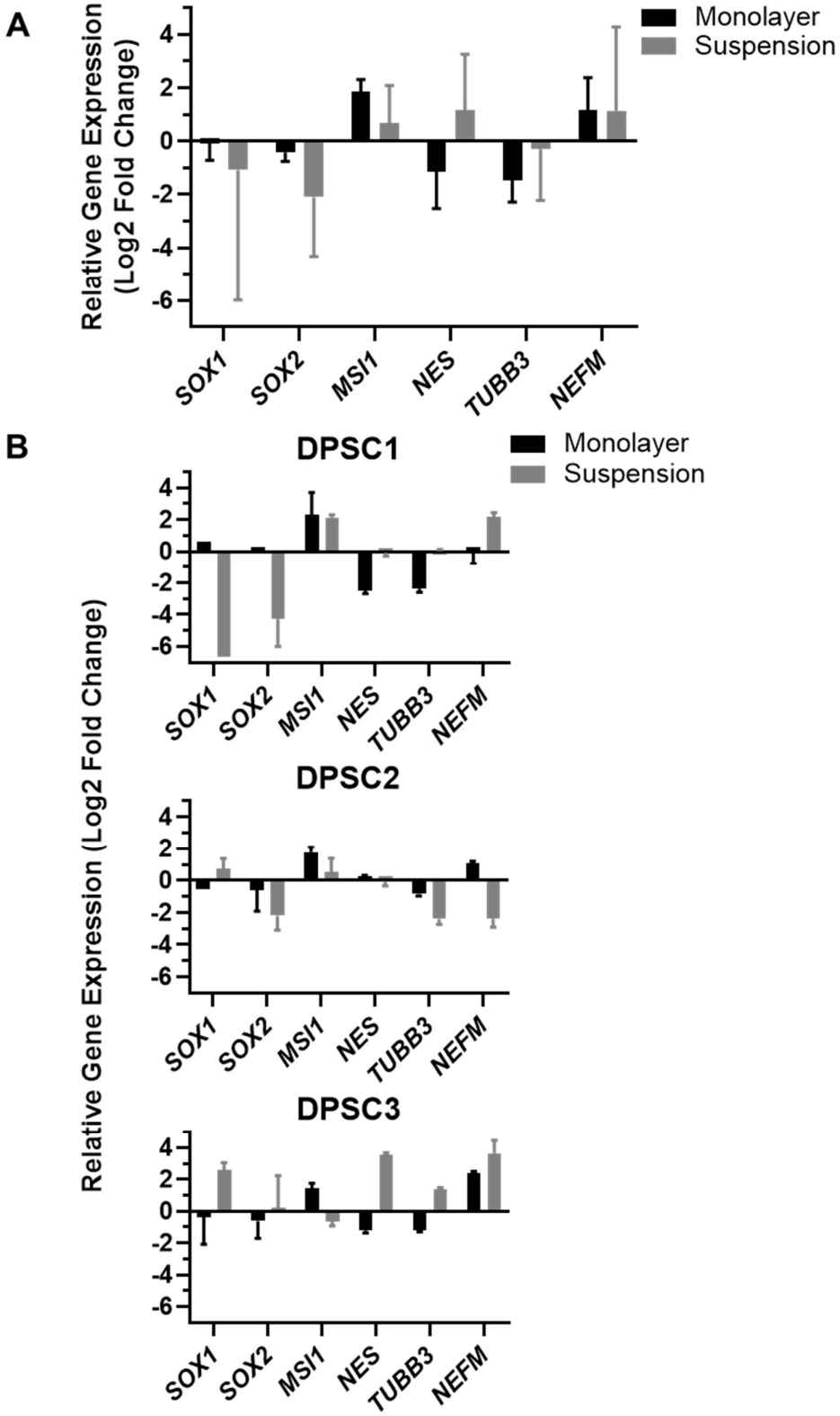

Figure 5.12 Comparison of monolayer and suspension cultures in NSC medium; effect of OCT4 over-expression. **(A)** Gene expression levels in DPSC-OCT4 cultured in suspension in NSC medium for 1 week relative to DPSC-EV cultured in the same conditions. **(B)** Individual gene expression levels. Data represents mean±SD, two-way ANOVA with Sidak's multiple comparisons test, n=3.

5.3.1.9 Neuronal differentiation following NSC protocol

After reprogramming DPSC using the NSC protocol, the cells were assessed for their neuronal differentiation capacity. The DPSC-EV and DPSC-OCT4 cultured in NSC medium for one week as a monolayer or in suspension, were then cultured for four weeks in neuronal differentiation medium (Table 5.3). This neuronal differentiation medium has been used as the final step in neuronal differentiation of DPSC in previous publications (2, 3). The differentiated DPSC were stained for the neuronal markers β-III tubulin and NF-M (Figure 5.13). A minor population of cells with neuronal-like morphology were detected in both DPSC-EV and DPSC-OCT4. Cells in both groups immunostained for β-III tubulin and NF-M, in both culture types. There was variation between the DPSC, the staining for each marker, and the monolayer and suspension cultures.

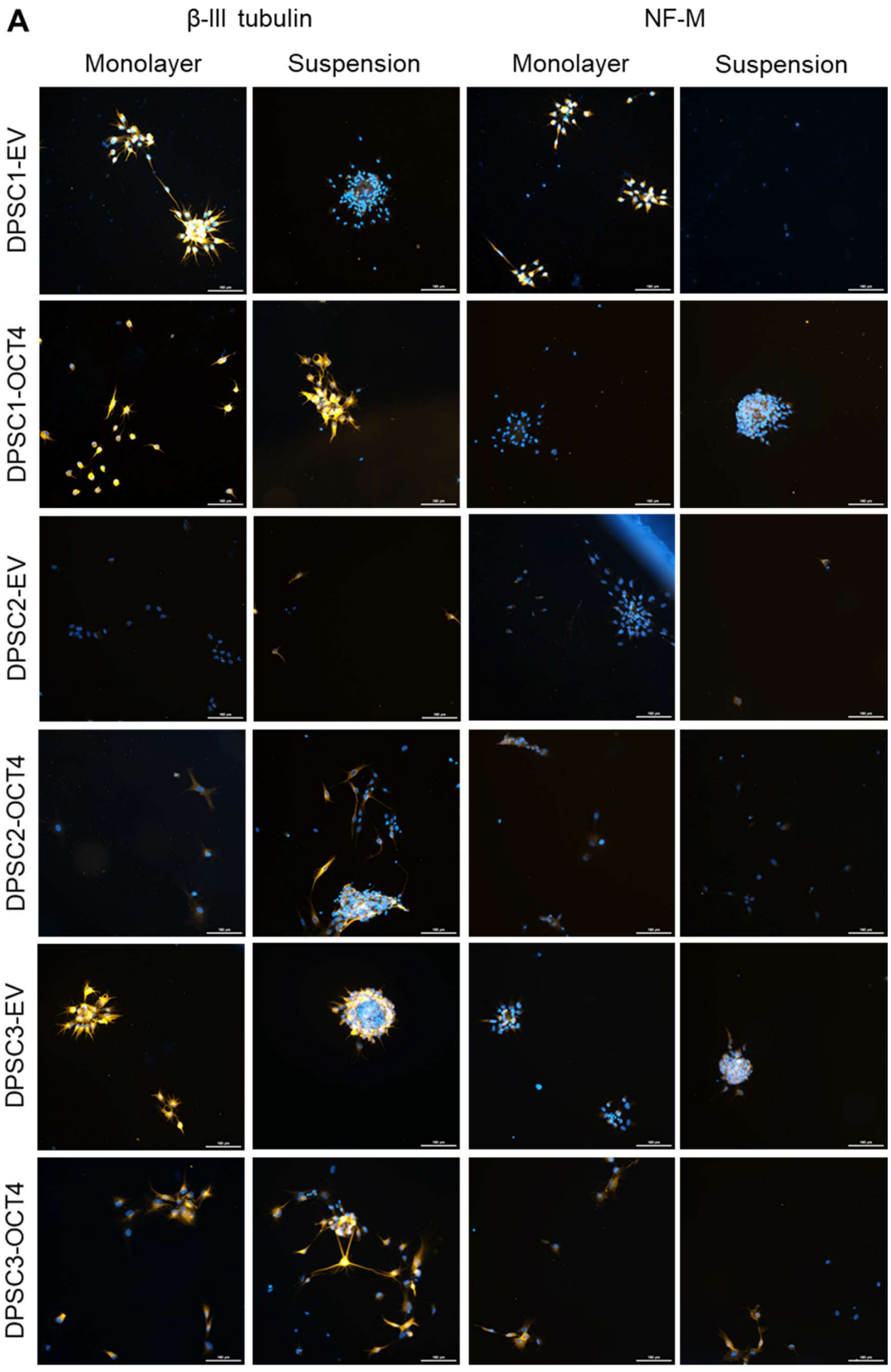
A
β-III tubulin
NF-M
Monolayer
Suspension
Monolayer
Suspension
DPSC1-EV
DPSC1-OCT4
DPSC2-EV
DPSC2-OCT4
DPSC3-EV
DPSC3-OCT4

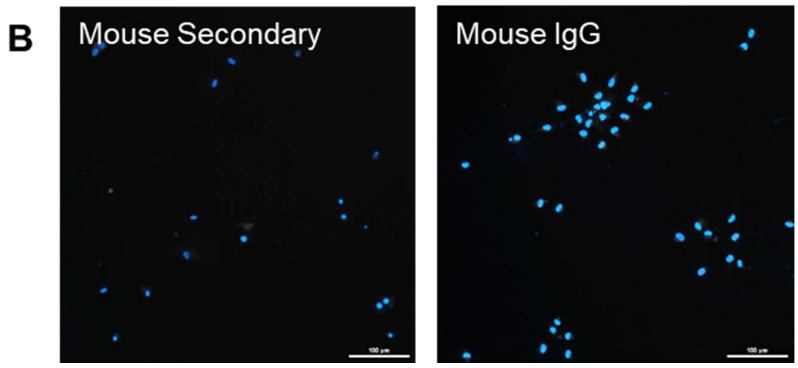

Figure 5.13. NSC protocol: neuronal protein expression following neuronal differentiation. Following 1 week culture in NSC medium as monolayer or suspension cultures, DPSC-EV and DPSC-OCT4 were further cultured in neuronal maturation medium for 4 weeks. **(A)** Immunofluorescence staining for β-III tubulin and NF-M. **(B)** Representative images of mouse secondary and IgG isotype antibody controls. Scale bar=100μm.

Table 5.7 Summary of NSC protocol results.

		DPSC-EV						DPSC-OCT4						DPSC-SOX2	DPSC-HES1
Transduction Efficiency		~90%						~55%						<10%	40%
Growth in DPSC Medium		✓						✓						Dead	Some survival
Proliferation Rate		>2						~2						N/A	~1
Morphological Change in NSC Medium		No						Yes						N/A	N/A
OCT4 Over-expression		N/A						Gene and protein						N/A	N/A
Change in Neural Marker Expression		***SOX1***	***SOX2***	***MSI1***	***NES***	***TUBB3***	***NEFM***	***SOX1***	***SOX2***	***MSI1***	***NES***	***TUBB3***	***NEFM***	N/A	
Effect of NSC Medium		+ (1wk), ++ (2wk)	+ (1wk), ++ (2wk)	+	+	+	+++	--	-	+	+	-(1wk), + (2wk)	-		
Effect of OCT4 Over-expression in DPSC Medium		N/A						+++	+	+	+	+	+++++		
Effect of OCT4 Over-expression in NSC Medium		N/A						-	-	+	-	-	+		
Monolayer vs. Suspension Cultures		+++	++	+	-	-	-	++	+	+	+	+	-		
Protein Expression		Supports gene expression						Supports gene expression						N/A	
NANOG Expression		-						-							
Sphere Formation		+						+						N/A	N/A
Neuronal Differentiation	**β-III tubulin**	+ (variation between samples)						+ (variation between samples)						N/A	N/A
	NF-M	+ (variation between samples)						+ (variation between samples)							

5.3.2 Transduced human DPSC cultured using the multi-step neural induction protocol

In an effort to identify suitable neural conditions, the neural reprogramming of human DPSC was examined using the multi-step neural induction protocol (Figure 5.1B), based on the method published by Feng *et al*. 2014 (104). The transduced DPSC were cultured in pre-inducing (step 1), N2B27 (step 2) and NSC (step 3) media (Table 5.2). In the first instance, non-modified human DPSC were cultured using the multi-step neural induction protocol, since this had not been investigated previously. The outcomes are summarised in Table 5.8 (pg. 137). Subsequently, transduced control DPSC-EV and experimental DPSC-OCT4 were examined under these neural inductive conditions. Table 5.9 (pg. 191) summarises the outcomes of this reprogramming method.

5.3.2.1 DPSC morphology remained spindle-shaped throughout the multi-step neural induction protocol

In standard DPSC culture medium, DPSC possess a spindle-shaped morphology (Figure 5.14). When cultured using the multi-step neural induction protocol, DPSC maintained their spindle-shaped morphology, with minor differences observed from standard conditions. A difference was observed following step 1, in which the cells appeared less flat and the cell body had a more pronounced boundary. The cells appeared flatter following step 2, but less so following step 3. These morphological changes were consistent between DPSC from all donors.

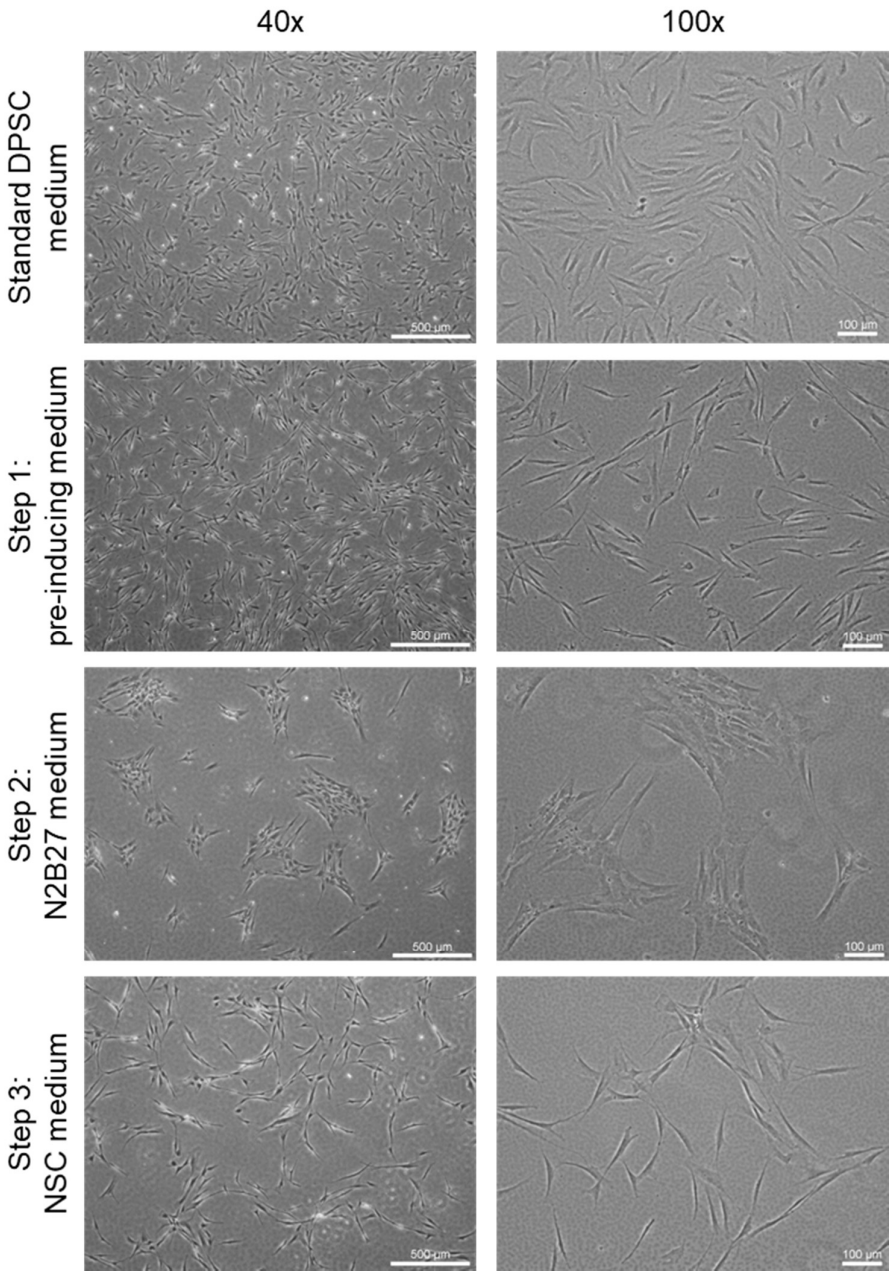

Figure 5.14 DPSC cultured using the multi-step neural induction protocol. Cells were cultured in standard DPSC medium, followed by culture in pre-inducing medium (step 1) for 8 days, N2B27 medium (step 2) for 7 days, and NSC medium (step 3) for 7 days. Images taken in normal conditions and at the end of each step of the protocol. Representative images, n=6, scale bar=500µm (40x) and 100µm (100x).

5.3.2.2 DPSC displayed increased gene and protein expression of neural markers

The expression levels of the neural genes were examined after each step of the multi-step neural induction protocol and compared to the expression levels in cells cultured in standard DPSC medium (Figure 5.15A).

An increasing trend was observed in the expression of the NSC genes *SOX1*, *SOX2* and *MSI1* throughout the method. Following step 1, *SOX1* and *SOX2* expression had decreased, but then increased following step 2 and further in step 3. At each step, *SOX2* had greater expression levels than *SOX1*. Unlike *SOX1* and *SOX2*, *MSI1* expression increased at each step of the protocol, with statistical significance detected at steps 2 and 3 ($p<0.01$ and $p<0.001$ respectively). Conversely, *NES* and *TUBB3* expression showed a decreasing trend with no significant difference. In contrast, an increasing trend in the expression of *NEFM* was observed, with significance at steps 1 ($p<0.05$) and 3 ($p<0.0001$). *NEFM* showed the greatest increase using this protocol.

Figure 5.15B shows the results of individual DPSC samples, highlighting the donor variability. An increasing trend in *SOX1* and *SOX2* expression was observed between donors, while *MSI1* expression was more varied, with increases and decreases observed but also similar levels between steps in some samples. The expression levels of *NES* and *TUBB3* were low with varied responses observed between steps. *NEFM* expression showed the most consistency between samples, showing an increase at each step of the protocol and reaching similar levels at the completion. Whilst the trends are similar between DPSC samples, the base levels and those at each step of the protocol varied for each gene. For example, while four samples showed a decrease in *SOX2* expression at step 1 and then an increase in step 2 and 3, one sample showed a decrease throughout all steps while another had an increase. Additionally, some genes were several fold greater in some samples, such as *MSI1* reaching almost a ten-fold (log2 scale) increase in DPSC4 but only 2.5-fold (log2 scale) increase in DPSC5, and in another maintaining a decreased expression level (DPSC1).

At the completion of the multi-step neural induction protocol, protein expression was examined and compared to levels in DPSC cultured in standard DPSC culture medium (Figure 5.16). DPSC cultured in standard DPSC medium had negligible levels of SOX1 and SOX2, but expressed NES, β-III tubulin and NF-M (Figure 5.16A). The levels detected were consistent between DPSC samples. Following the multi-step neural induction protocol, there was an increase in SOX2, which supports the gene expression data (Figure 5.16B). Quantification of the Western blots confirmed the increase in SOX2 expression ($p<0.0001$) (Figure 5.16C). There

was also an increase in NF-M ($p<0.05$), and decreases in NES and β-III tubulin ($p<0.05$), in accordance with the gene expression data. SOX1 expression was found to decrease following the protocol in contrast to the gene expression data, however the protein levels before and after neural induction were not significantly different.

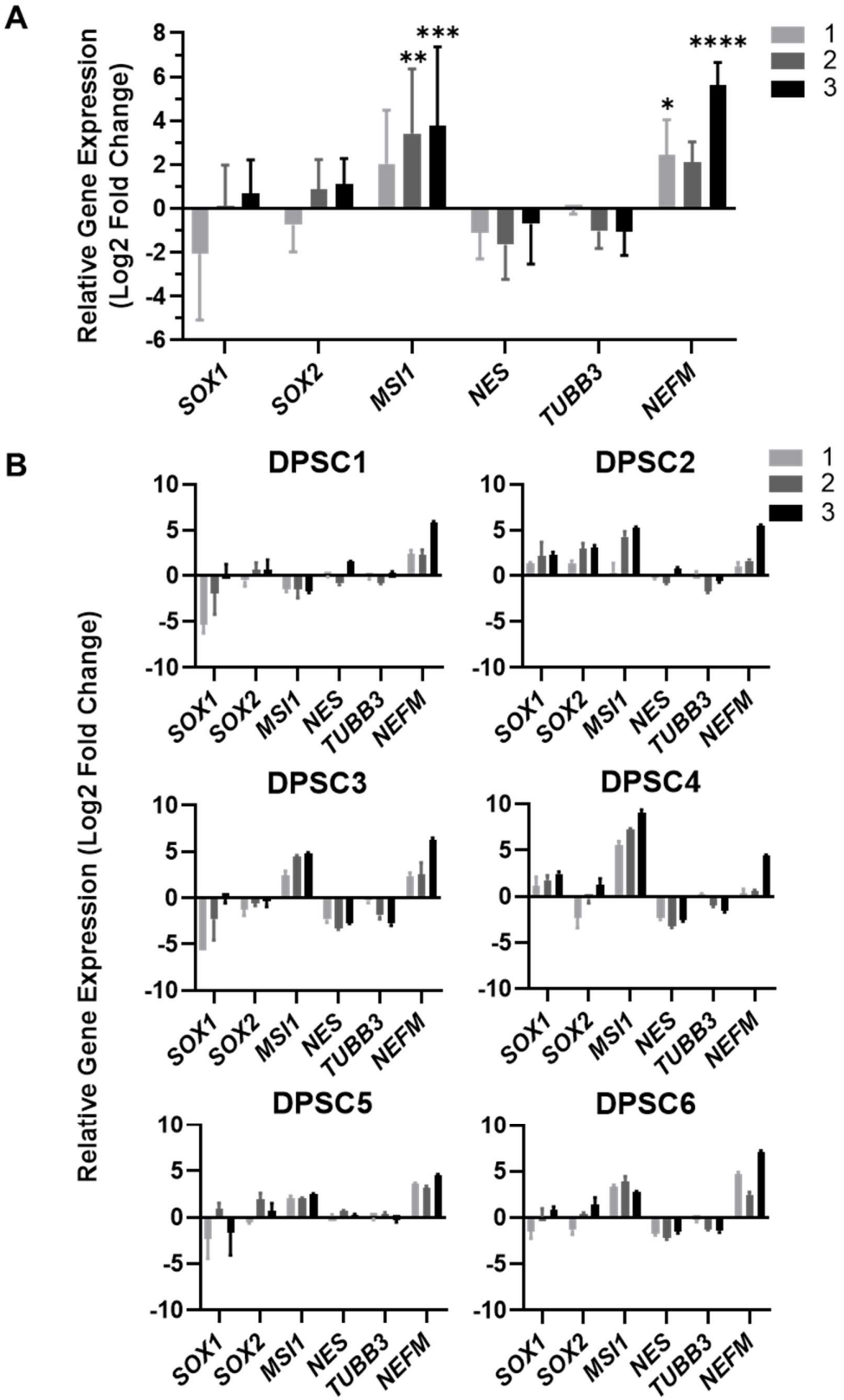

Figure 5.15 Gene expression in DPSC cultured using the multi-step neural induction protocol. Cells were collected at the completion of each step of the protocol (1, 2, 3). **(A)** Expression levels relative to DPSC cultured in standard DPSC medium. **(B)** Individual DPSC samples. Data represents mean±SD, two-way ANOVA with Tukey's multiple comparisons test, n=6, *p<0.05, **p<0.01, ***p<0.001, ****p<0.0001.

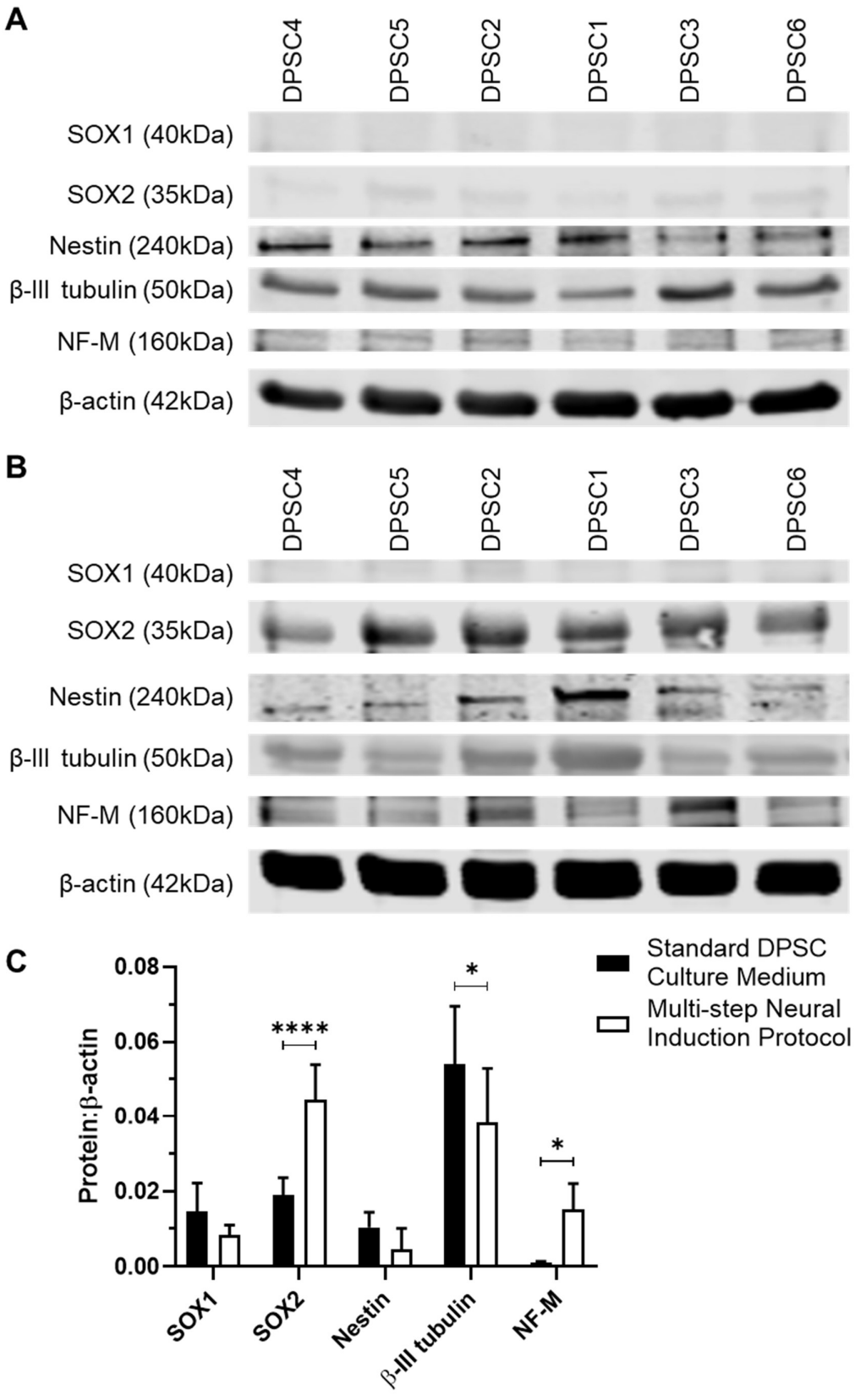

Figure 5.16 Protein expression in DPSC. **(A)** DPSC in standard DPSC culture medium. **(B)** DPSC cultured using the multi-step neural induction protocol and samples collected at the completion of the protocol. **(C)** Protein quantification. Data represents mean±SD, two-way ANOVA with Sidak's multiple comparisons test, n=6, *p<0.05, ****p<0.0001.

5.3.2.3 Neural-induced DPSC differentiated along the neuronal lineage

At the completion of the multi-step neural induction protocol, the DPSC were cultured in neuronal differentiation medium (2, 3). Immunofluorescence staining for β-III tubulin and NF-M showed the presence of these proteins but with variation between samples (Figure 5.17). DPSC1 stained for these proteins with greatest intensity, while some samples clustered more and showed less intense staining on cells extending out of the clusters.

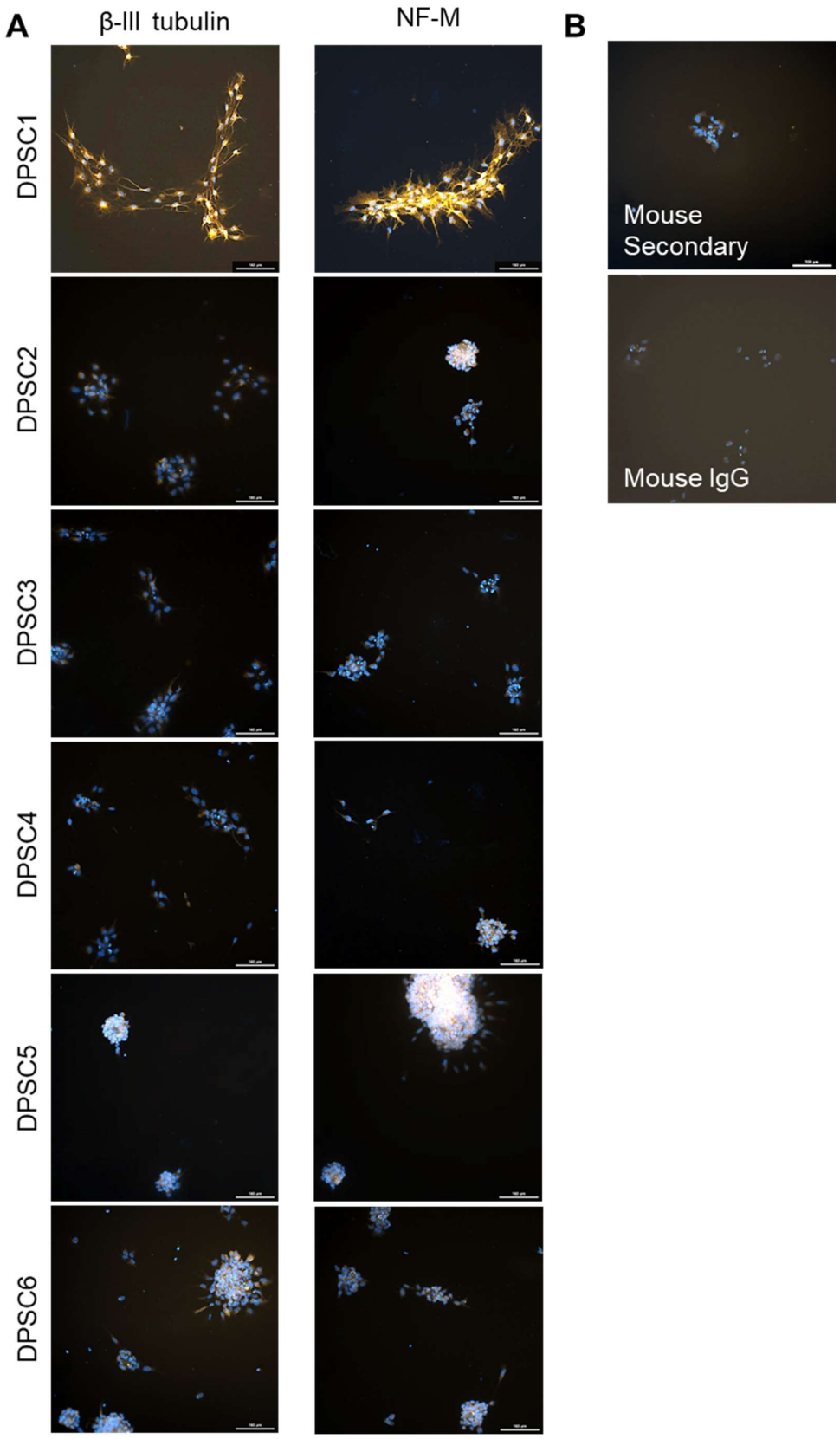

Figure 5.17 Neuronal differentiation of DPSC cultured using the multi-step neural induction protocol. After neural induction, cells were further cultured in neuronal maturation medium for 4 weeks. **(A)** Detection of β-III tubulin and NF-M. **(B)** Representative images of mouse secondary and IgG isotype antibody controls. Data from n=6, scale bar=100µm.

Table 5.8 Summary of multi-step neural induction protocol results for non-transduced DPSC.

		Step 1 (pre-inducing medium)	**Step 2 (N2B27 medium)**	**Step 3 (NSC medium)**	
Morphological Change		Less flat and cell body had a visible boundary	Flatter and clustered	Less flat	
Change in Neural Marker Expression (Note: step 3 protein levels in right sub-column)	***SOX1***	-	+	+	-
	SOX2	-	+	+	+++++
	MSI1	+	+++	++++	N/A
	NES	-	-	-	-
	TUBB3	-	-	-	--
	NEFM	++	+	+++++	++
Neuronal Differentiation	**β-III tubulin**	Intense expression in 1/6 DPSC			
	NF-M	Intense expression in 1/6 DPSC			

5.3.2.4 OCT4 over-expressing DPSC underwent a morphological change

Human DPSC were then transduced with the control empty vector pCDH-EV and the experimental vector pCDH-OCT4, as per Figure 5.1B. The aim was to determine whether the OCT4 over-expressing DPSC cultured using the multi-step neural induction protocol had more consistent outcomes compared with the non-modified DPSC, and whether this protocol was superior to the previous NSC protocol in terms of the cells displaying enhanced neural properties.

The transduced DPSC were sorted based on GFP expression. The transduction efficiency was over 90% for pCDH-EV (92.3±1.6) and over 50% for pCDH-OCT4 (63.1±8.8) (Figure 5.18A). The transduction efficiency for pCDH-OCT4 was significantly ($p<0.01$) lower than pCDH-EV. These vectors had a better transduction efficiency using this multi-step neural induction protocol compared to the NSC protocol, and showed more consistency between DPSC samples from different donors.

The control DPSC-EV and experimental DPSC-OCT4 cultured in standard DPSC medium had a similar morphology to the non-transduced DPSC (Figure 5.18B and 5.14). The transduced cells appeared less flat than the non-transduced, but no obvious difference was observed between DPSC-EV and DPSC-OCT4 (Figure 5.18B). Throughout the multi-step neural induction protocol, a change in morphology was observed between DPSC-EV and DPSC-OCT4, with DPSC-EV resembling the non-transduced DPSC (Figure 5.18B and 5.14). After culturing in the step 1 pre-inducing medium, both groups had a clear boundary of the cell body, similar to non-modified DPSC in this culture medium, however DPSC-OCT4 displayed bigger and rounder cell bodies while DPSC-EV were less flat. Following step 2, DPSC-OCT4 appeared to be shorter and rounder, and possibly ‘balled’ up, while DPSC-EV appeared to be flatter and elongated. Following step 3, there was no noticeable difference from step 2. Thus, an obvious morphological difference was observed between DPSC-EV and DPSC-OCT4, with DPSC-EV remaining similar to non-modified DPSC.

A

Lentiviral Vector	GFP⁺ Cells (%)						
	DPSC1	DPSC2	DPSC3	DPSC4	DPSC5	DPSC6	Mean±SD
pCDH-EV	93.2 ±3.3 (5)	92.5 ±0.7 (2)	89.7 ±6.0 (3)	93.0 ±2.6 (3)	91.3 ±3.5 (3)	94.0 ±2.8 (2)	92.3±1.6
pCDH-OCT4	53.0 ±13.2 (5)	78.5 ±3.5 (2)	62.7 ±9.8 (3)	66.3 ±11.9 (3)	58.0 ±16.0 (3)	60.0 ±9.9 (2)	63.1±8.8

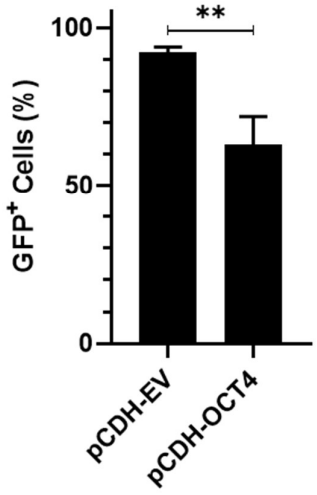

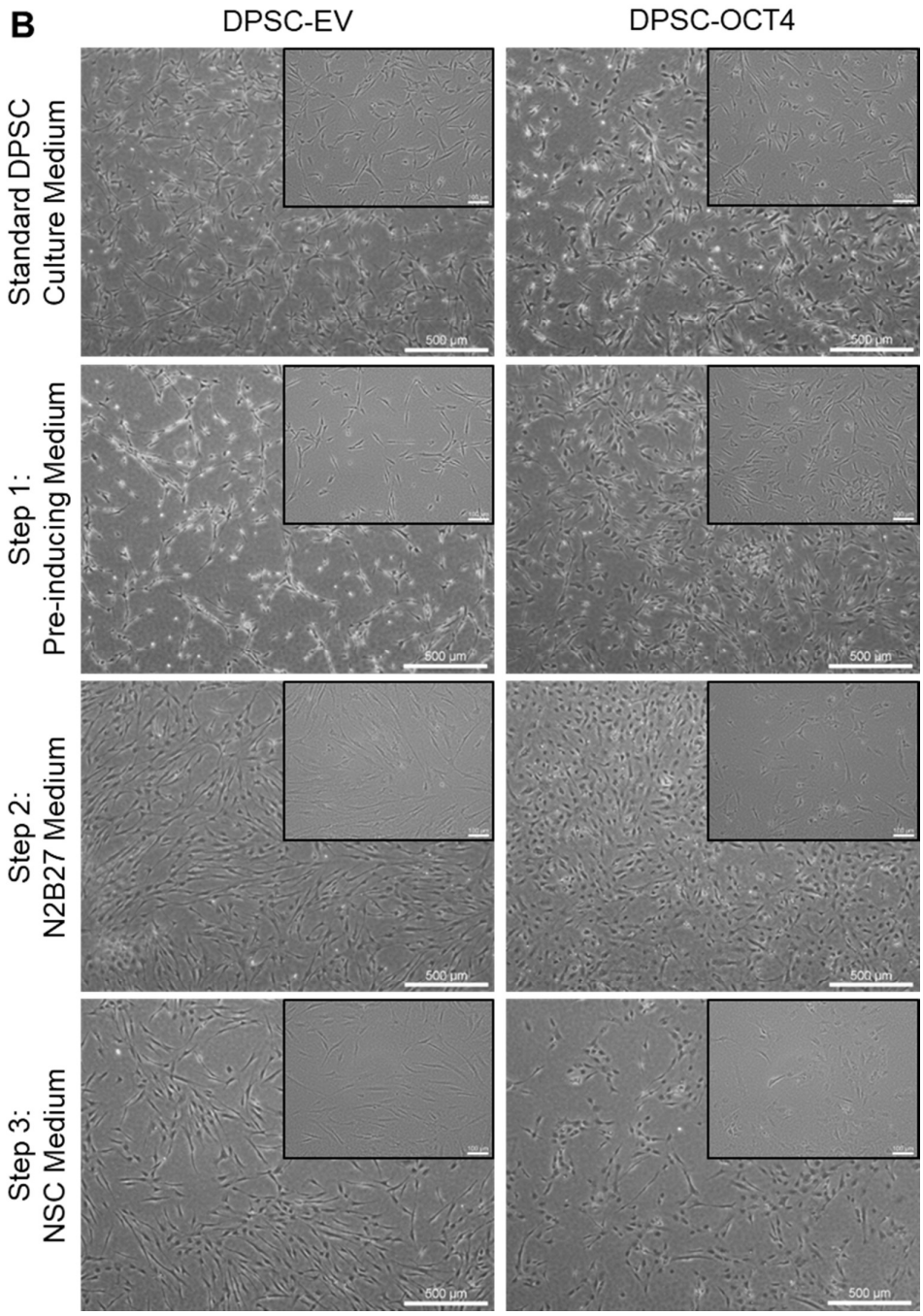

Figure 5.18 Multi-step neural induction protocol: single lentiviral transductions of DPSC. **(A)** Transduction efficiency for each vector demonstrated by the percentage of GFP^+ cells. **(B)** After sorting, the transduced cells were cultured in standard DPSC medium, followed by pre-inducing medium (step 1) for 8 days, N2B27 medium (step 2) for 7 days, and NSC medium (step 3) for 7 days. Images taken in normal conditions and at the completion of each step of the protocol. Representative images, data represents mean±SD, n=6 (technical replicates in brackets), Mann-Whitney test, scale bar=500µm and 100µm (inlet), **p<0.01.

5.3.2.5 Transduced DPSC maintained their proliferation rate

To confirm that the presence of the lentiviral vectors did not affect the proliferation rate of the DPSC, a WST-1 assay was used to compare non-transduced DPSC with DPSC-EV and DPSC-OCT4 all cultured in standard DPSC medium (Figure 5.19). There was a significant increase in absorbance over 24 hours for each group ($p<0.0001$) indicating that the cells had proliferated (Figure 5.19A). Over 24 hours, the cells had a proliferation rate of greater than two (DPSC, 3.17±0.55; DPSC-EV, 3.23±0.95; DPSC-OCT4, 2.39±0.49) indicating that they had doubled or tripled (Figure 5.19B). While the proliferation rate was lower for DPSC-OCT4, there was no statistically significant difference between the three groups. Between donors, the results were consistent.

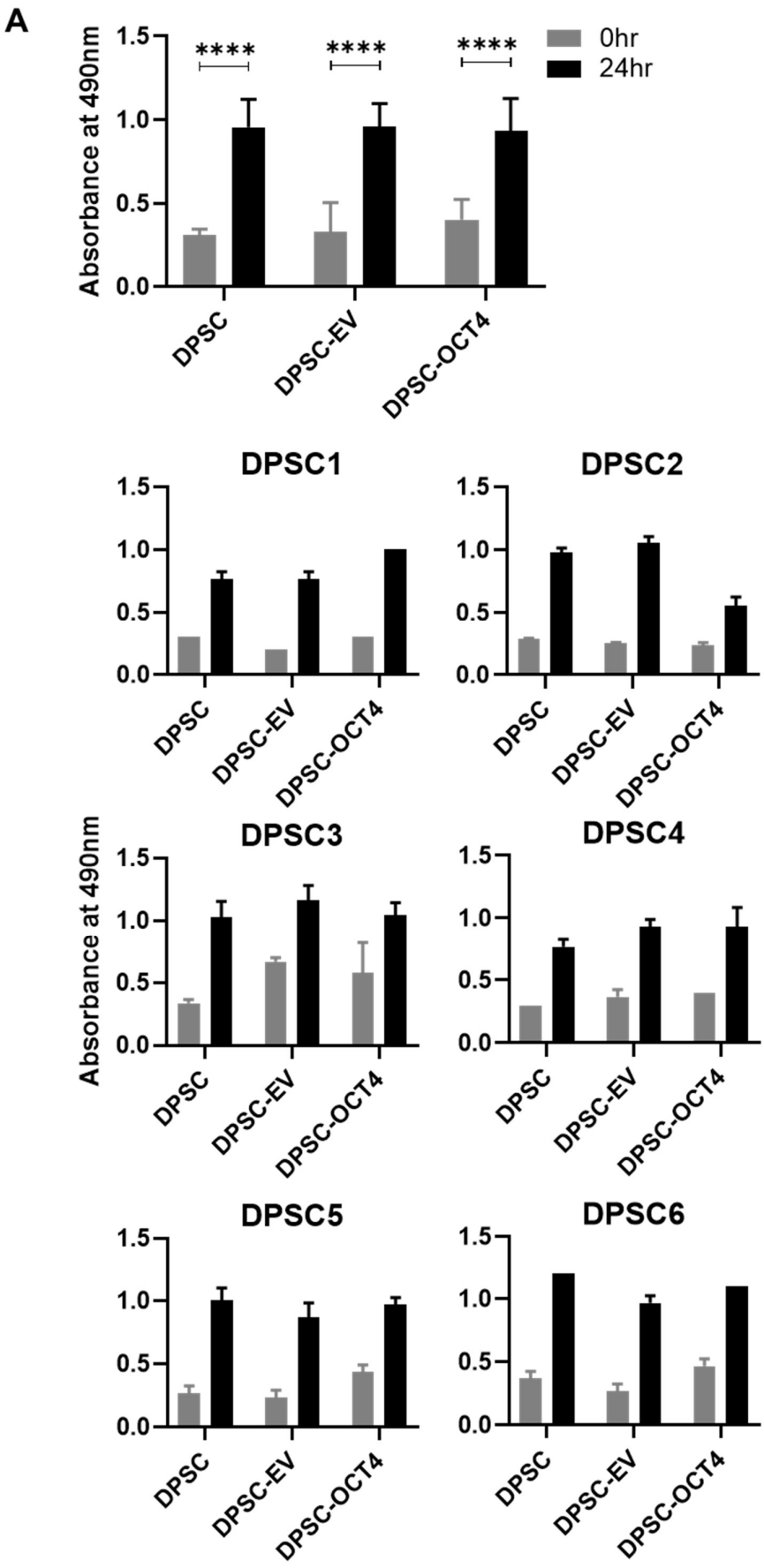
A
Absorbance at 490nm
0hr
24hr
****
****
****
DPSC
DPSC-EV
DPSC-OCT4
DPSC1
DPSC2
DPSC3
DPSC4
DPSC5
DPSC6
1.5
1.0
0.5
0.0

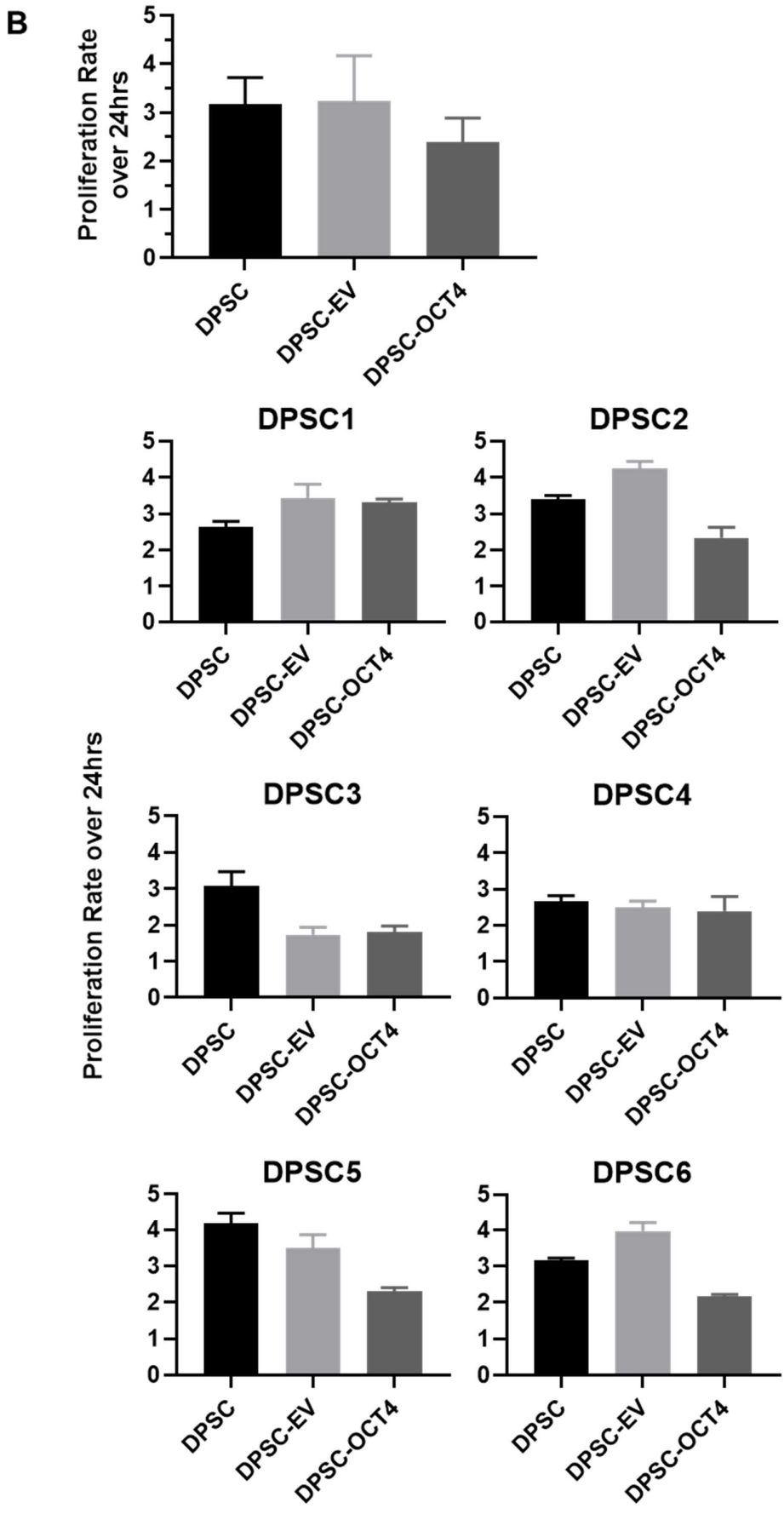
B
Proliferation Rate over 24hrs
0
1
2
3
4
5
DPSC
DPSC-EV
DPSC-OCT4
DPSC1
DPSC2
DPSC3
DPSC4
DPSC5
DPSC6

Figure 5.19 Multi-step neural induction protocol: proliferation rate of transduced DPSC. **(A)** Absorbance values at 0 and 24 hours. **(B)** Proliferation rate over 24 hours. Individual absorbance values and proliferation rates also shown. Data represents mean±SD, two-way ANOVA with Sidak's multiple comparisons test (A) and Kruskal-Wallis one-way ANOVA with Dunn's multiple comparisons test (B), n=6, ****$p<0.0001$.

5.3.2.6 OCT4 is over-expressed in DPSC throughout the multi-step neural induction protocol

Over-expression of OCT4 in transduced DPSC was confirmed by qPCR for the *POU5F1* gene and Western blot analysis for the OCT4 protein (Figure 5.20). Two sets of primers were used for qPCR; one set amplifying the endogenous gene and one set amplifying the transgene (Figure 5.20A). The primers for the endogenous source of *POU5F1* were located at the three prime end of the gene, in the final exon and not part of the coding sequence. The primers for the transgenic source of *POU5F1* amplified a region of the vector from the three prime end of the coding sequence to the five prime end of the IRES downstream of the coding sequence.

The gene expression levels in DPSC-OCT4 were compared to the levels in DPSC-EV in standard DPSC culture medium before initiation of neural induction protocol, and at the completion of steps 1, 2 and 3 (Figure 5.20B). A very low level of endogenous *POU5F1* was detected, while transgenic *POU5F1* was approximately 15-fold (log2 scale) greater ($p<0.0001$) than in DPSC-EV at each time point (0, 15.3±2.8; 1, 15.3±3.8; 2, 14.6±3.0; 3, 14.3±2.8). The difference between transgenic and endogenous *OCT4* was statistically significant ($p<0.0001$) at each time point. The levels for both endogenous and transgenic *OCT4* were similar throughout the protocol, showing no statistical difference between time points. The low endogenous levels and high transgenic levels were observed within all DPSC samples. Thus, OCT4 was successfully over-expressed at the gene expression level, and remained at a constant level throughout the protocol. The endogenous source was not activated.

The DPSC cultured in standard DPSC medium showed low expression levels of the OCT4 protein (Figure 5.20C). Following culture using the multi-step neural induction protocol, the OCT4 protein levels in non-transduced DPSC remained low (Figure 5.20D). The transduced DPSC cultured using the multi-step neural induction protocol showed low levels of OCT4 protein in DPSC-EV and high levels in DPSC-OCT4, confirming the successful translation of the increased levels of the message (Figure 5.20E). The OCT4 levels were significantly greater ($p<0.01$) in DPSC-OCT4 (Figure 5.20F). The GFP reporter, present in the vectors, was detected in all samples. It was more highly expressed in DPSC-EV than DPSC-OCT4, as it was present downstream of the cDNA following the IRES.

A OCT4 transcript variant 1 gene (1430 bp)

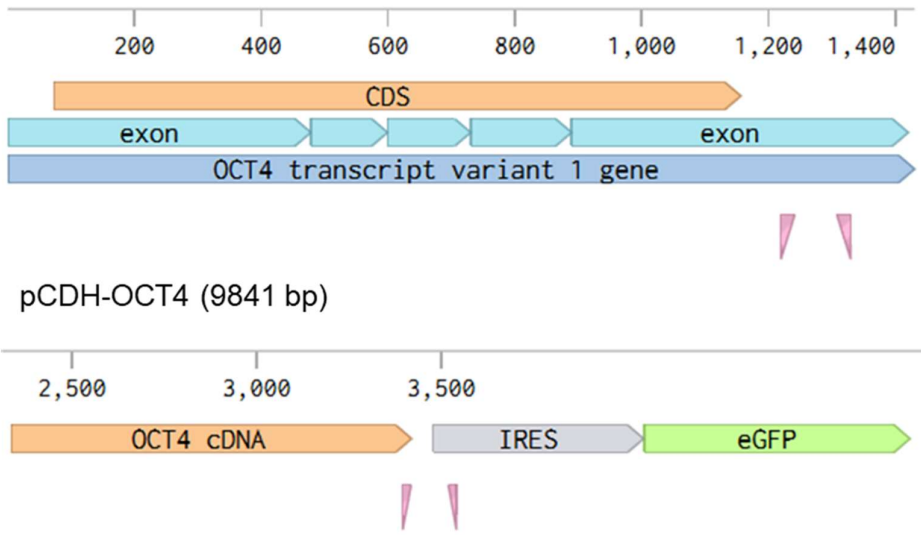

pCDH-OCT4 (9841 bp)

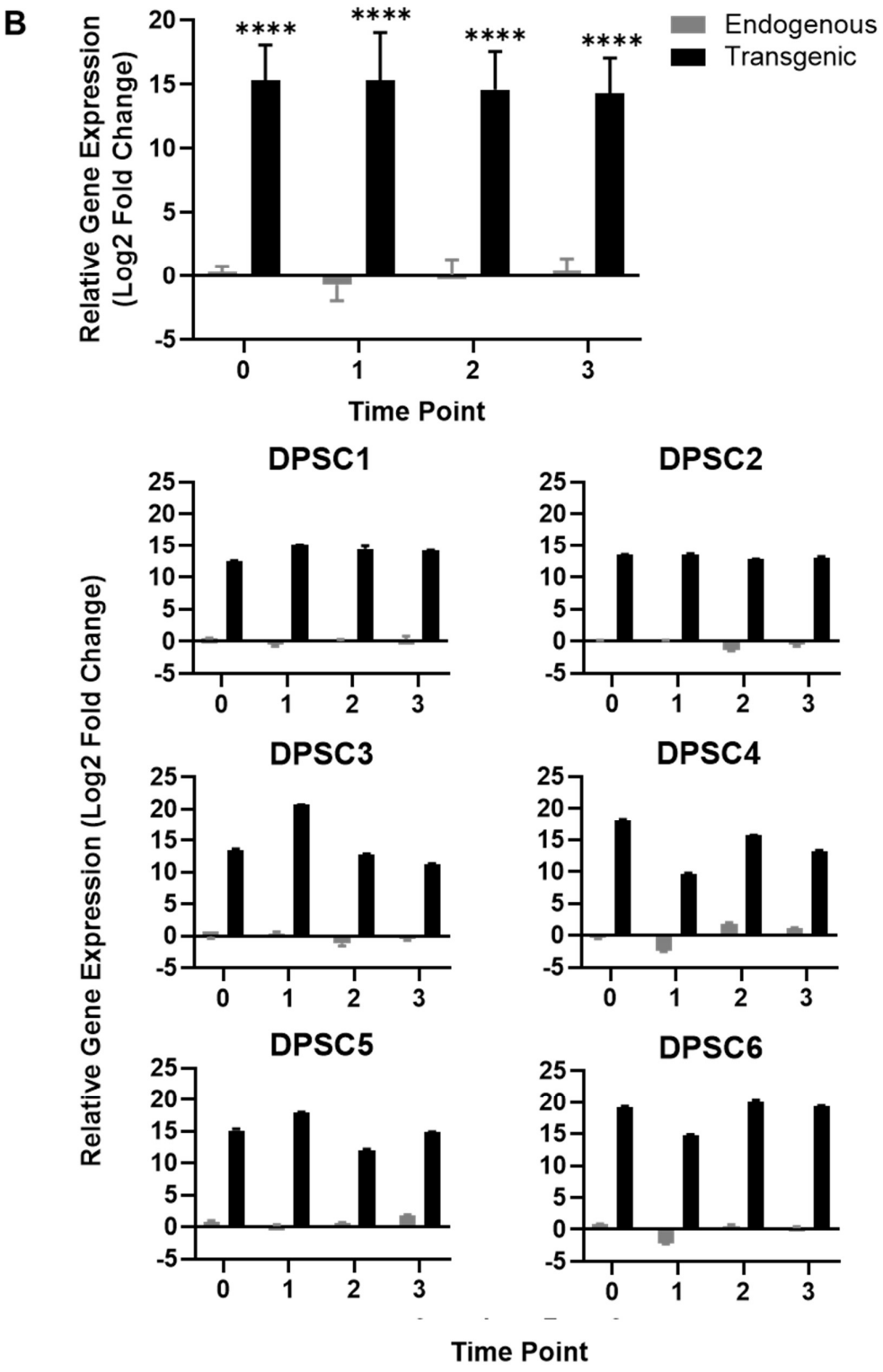
B
Endogenous
Transgenic
Relative Gene Expression (Log2 Fold Change)
****
****
****
****
Time Point
DPSC1
DPSC2
DPSC3
DPSC4
DPSC5
DPSC6
Relative Gene Expression (Log2 Fold Change)
Time Point

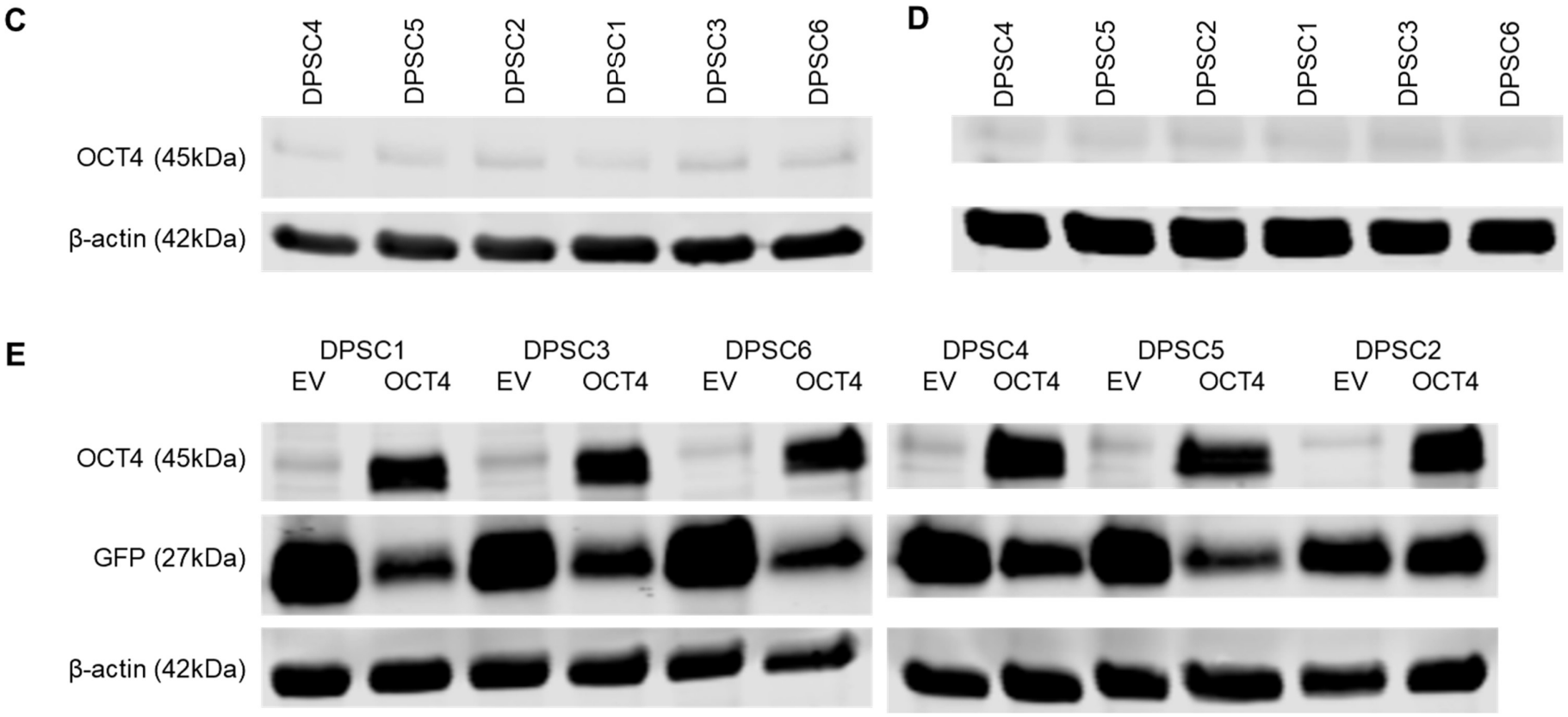
C
DPSC4
DPSC5
DPSC2
DPSC1
DPSC3
DPSC6
OCT4 (45kDa)
β-actin (42kDa)
D
DPSC4
DPSC5
DPSC2
DPSC1
DPSC3
DPSC6
E
DPSC1
DPSC3
DPSC6
DPSC4
DPSC5
DPSC2
EV
OCT4
OCT4 (45kDa)
GFP (27kDa)
β-actin (42kDa)

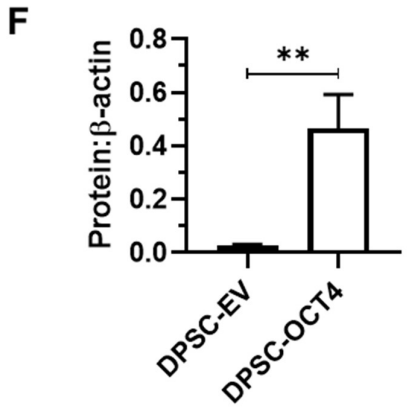

Figure 5.20 Multi-step neural induction protocol: OCT4 over-expression in DPSC-OCT4. **(A)** Two primer sets (shown in pink) were used to detect endogenous and transgenic sources of the OCT4 gene *POU5F1* by qPCR. Top diagram shows the human OCT4 transcript variant 1 gene (shortest OCT4 variant at 1430 base pairs), which produces isoform OCT4A (longest OCT4 isoform at 360 amino acids); there are five exons and the coding sequence (CDS) is 1083 base pairs. Bottom diagram shows a section of the pCDH-OCT4 lentiviral vector (9841 base pairs), with the human OCT4 cDNA (1083 base pairs), and the downstream IRES and enhanced GFP. **(B)** *POU5F1* expression levels from both sources (endogenous and transgene) in DPSC-OCT4 in standard DPSC culture medium (time point 0) and after each step of the multi-step neural inducing protocol (time points 1, 2, 3) relative to DPSC-EV. Individual DPSC samples also shown. OCT4 protein detection in **(C)** non-transduced DPSC cultured in standard DPSC medium, **(D)** non-transduced DPSC following the completion of the multi-step neural induction protocol, and **(E)** DPSC-EV and DPSC-OCT4 following the completion of the multi-step neural induction protocol. **(F)** Protein expression levels quantified and expressed relative to the loading control β-actin. Data represents mean±SD, two-way ANOVA with Sidak's multiple comparisons test (B) and Mann-Whitney test (F), n=6, **p<0.01, ****p>0.0001.

5.3.2.7 Overall effect of genetic modification and neural inductive conditions

The transduced control DPSC-EV and experimental DPSC-OCT4 were analysed throughout the multi-step neural induction protocol for expression of neural genes. Samples were collected before initiation of the protocol and after each of the three steps of the protocol. Firstly, to observe the overall change, DPSC-EV and DPSC-OCT4 at the completion of each step were compared to non-transduced DPSC cultured in standard DPSC medium (Figure 5.21).

In DPSC-EV, a non-significant decrease in the early neural genes *SOX1*, *SOX2*, *MSI1* and *NES* was observed prior to initiation of the multi-step neural induction protocol, while an increase was seen in *TUBB3* and *NEFM* expression (Figure 5.21A). For all genes, an increasing trend was observed throughout the protocol with positive expression observed at the completion of the protocol. An increase was observed in the first step for expression of *SOX1*, *SOX2* and less so of *MSI1*. The expression levels of *NES* and *TUBB3* decreased at step one, less so in step two, and increased in step three. *NEFM* was the only gene that showed increases at every step and had the greatest expression reaching more than 6-fold (log2 scale) at the completion of the protocol ($p<0.0001$).

Similar results were seen in DPSC-OCT4 with regard to the early neural genes (Figure 5.21B). Prior to initiation of the protocol, *SOX1*, *SOX2* and *NES* decreased, little change was observed for *MSI1* and *TUBB3*, while *NEFM* significantly increased ($p<0.0001$). An increase in *SOX1*, *SOX2*, *MSI1* and *NES* expression was seen at the completion of the protocol, with an increasing trend throughout the protocol. *TUBB3* and *NEFM* had decreasing trends, but *NEFM* expression remained significantly elevated.

Overall, the early neural genes increased throughout the protocol in both groups, but the late neural genes increased in DPSC-EV and decreased in DPSC-OCT4, suggesting that the neural conditions increased the neural markers and the OCT4 over-expression had a role in decreasing mature neural markers. The subsequent comparisons were made to better examine what effect the neural culture conditions and the OCT4 over-expression had on the DPSC.

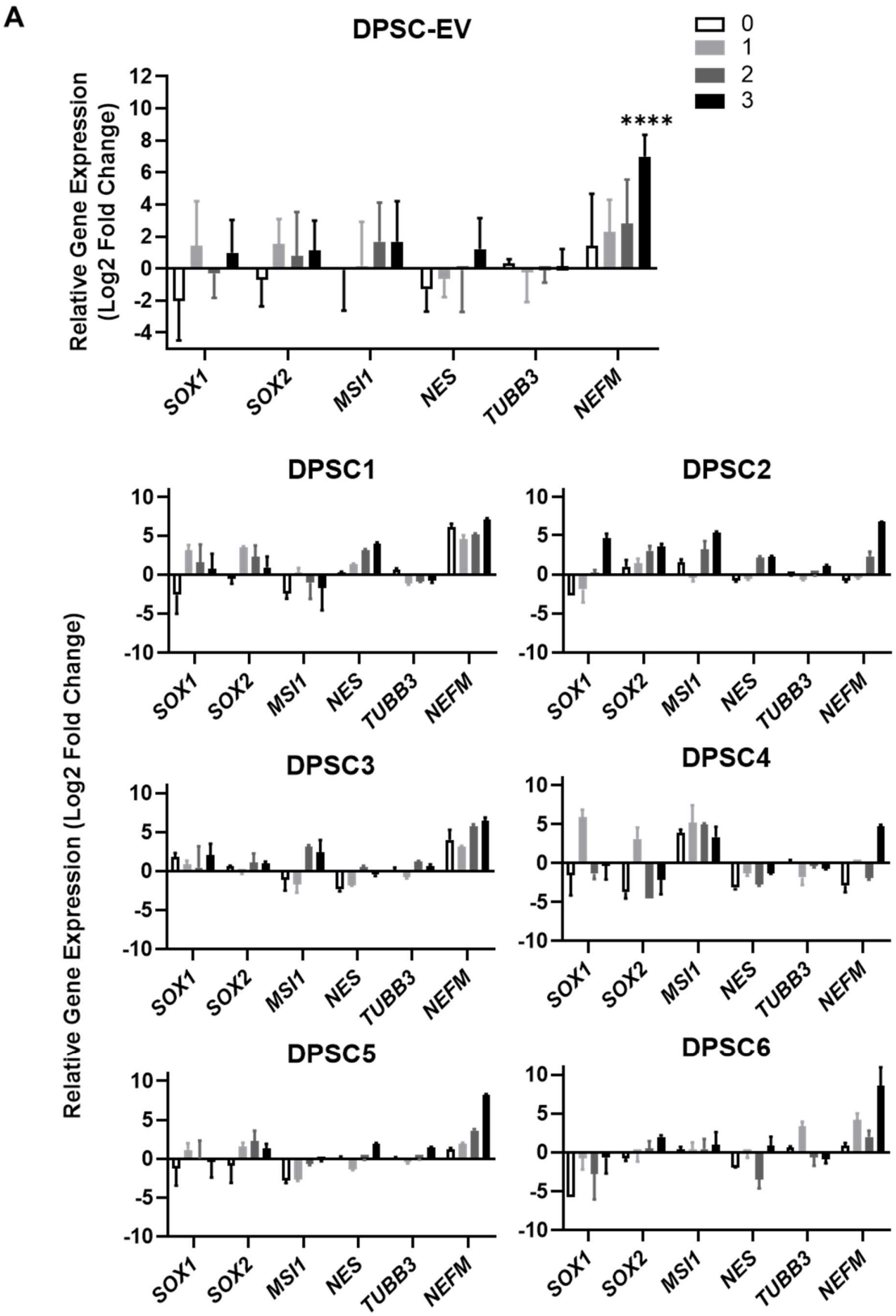
A
DPSC-EV
0
1
2
3
****
Relative Gene Expression (Log2 Fold Change)
SOX1
SOX2
MSI1
NES
TUBB3
NEFM
DPSC1
DPSC2
DPSC3
DPSC4
DPSC5
DPSC6
Relative Gene Expression (Log2 Fold Change)

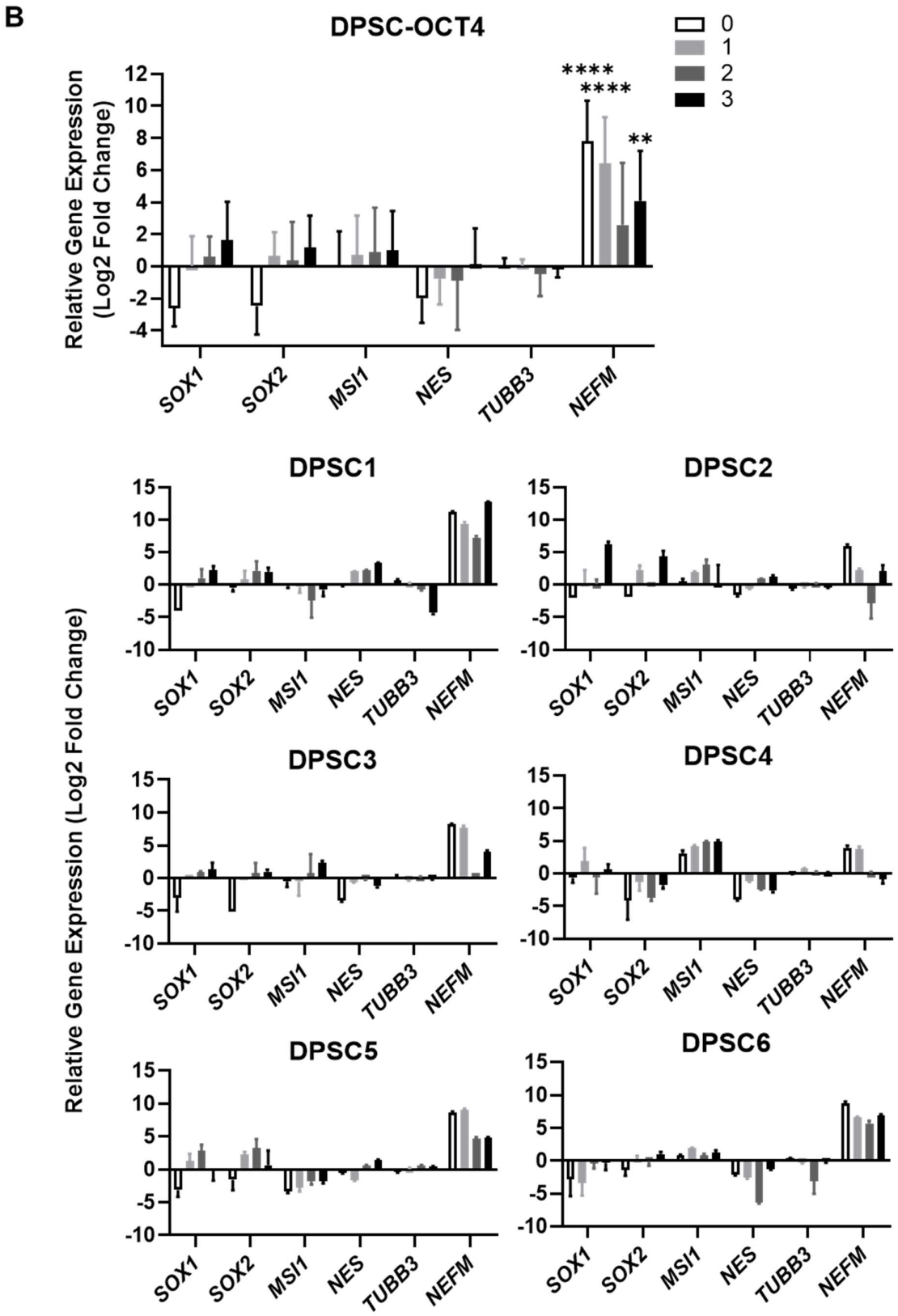
B
DPSC-OCT4
0
1
2
3
****
****
**
Relative Gene Expression (Log2 Fold Change)
SOX1
SOX2
MSI1
NES
TUBB3
NEFM
DPSC1
DPSC2
DPSC3
DPSC4
DPSC5
DPSC6
Relative Gene Expression (Log2 Fold Change)

Figure 5.21 Gene expression levels in DPSC-EV and DPSC-OCT4 cultured using the multi-step neural induction protocol. **(A)** DPSC-EV and **(B)** DPSC-OCT4 were collected at each time point (0, 1, 2, 3) and gene expression levels were analysed relative to non-transduced samples in standard DPSC culture medium. Gene expression levels in individual DPSC samples also shown. Data represents mean±SD, two-way ANOVA with Tukey's multiple comparisons test, n=6, **p<0.01, ****p<0.0001.

5.3.2.8 Effect of culture conditions: increased neural gene expression

To examine the effect of the multi-step neural induction protocol conditions, DPSC-EV and DPSC-OCT4 throughout the protocol were compared to DPSC-EV and DPSC-OCT4 before initiation of the protocol (Figure 5.22).

In DPSC-EV (Figure 5.22A), there was an increasing trend in gene expression throughout the protocol for all the genes analysed. After each step of the protocol, *SOX1*, *SOX2*, *MSI1*, *NES* and *NEFM* had increased expression levels. After step one, *SOX1* ($p<0.01$) and *SOX2* had the highest levels, after step two the levels of the genes were similar between 1- and 2-fold (log2 scale), and after step three *NEFM* had the highest expression at close to 6-fold (log2 scale) and was significantly greater ($p<0.0001$). The expression levels of *TUBB3* decreased at each step, but showed an overall increasing trend. These results were similar to non-transduced DPSC cultured using the multi-step neural induction protocol (Figure 5.15).

In DPSC-OCT4 (Figure 5.22B), there was an increasing trend in the early genes *SOX1*, *SOX2*, *MSI1*, and *NES*. The increases in *SOX1* and *SOX2* were significant at each step, with the levels at the end greater than the levels seen for DPSC-EV. There was little change in *TUBB3* expression. On the other hand, *NEFM* significantly decreased. These results were similar to DPSC-EV, with the exception of the change in *NEFM*.

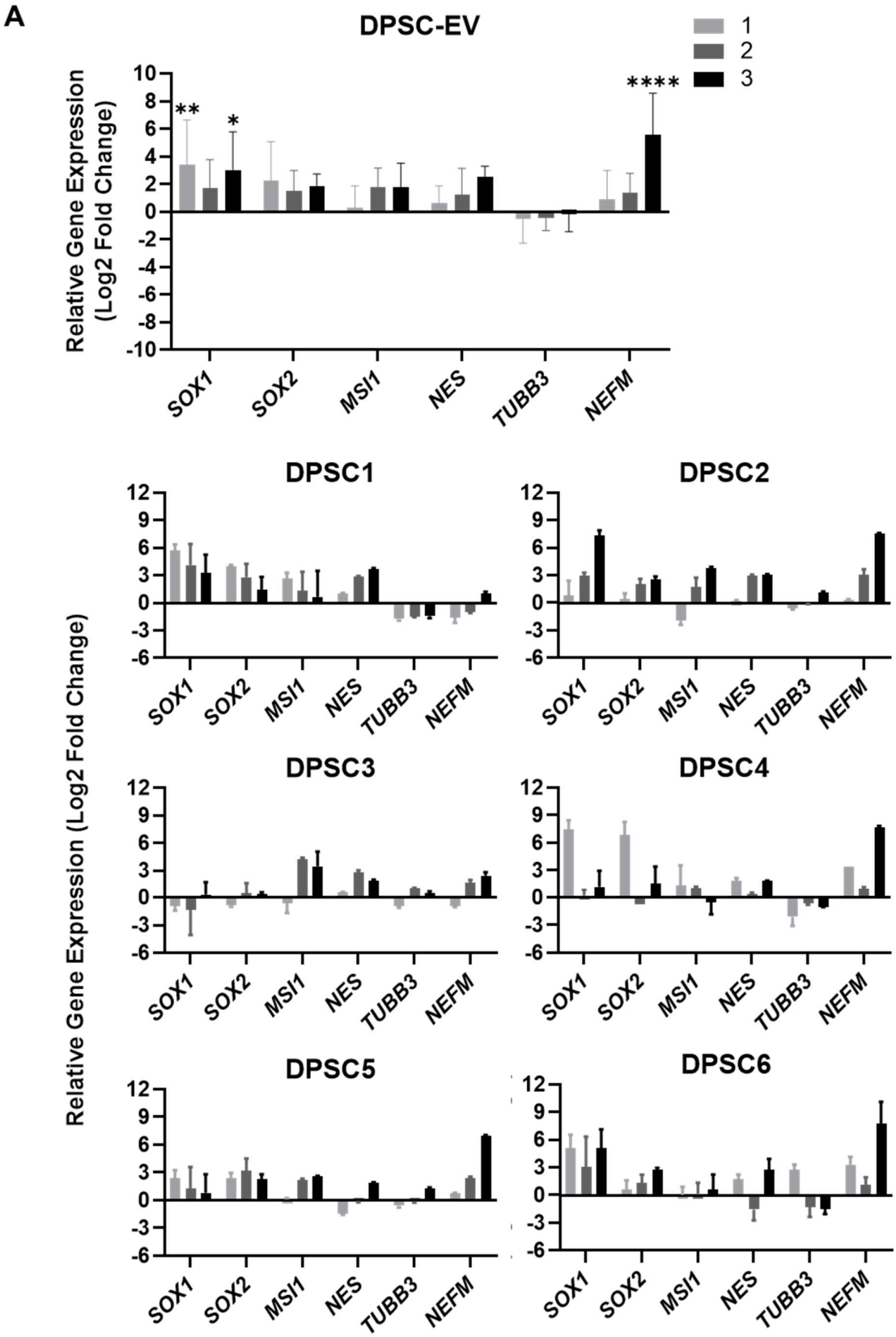
A
DPSC-EV
1
2
3
Relative Gene Expression (Log2 Fold Change)
**
*
****
SOX1
SOX2
MSI1
NES
TUBB3
NEFM
DPSC1
DPSC2
DPSC3
DPSC4
DPSC5
DPSC6
Relative Gene Expression (Log2 Fold Change)

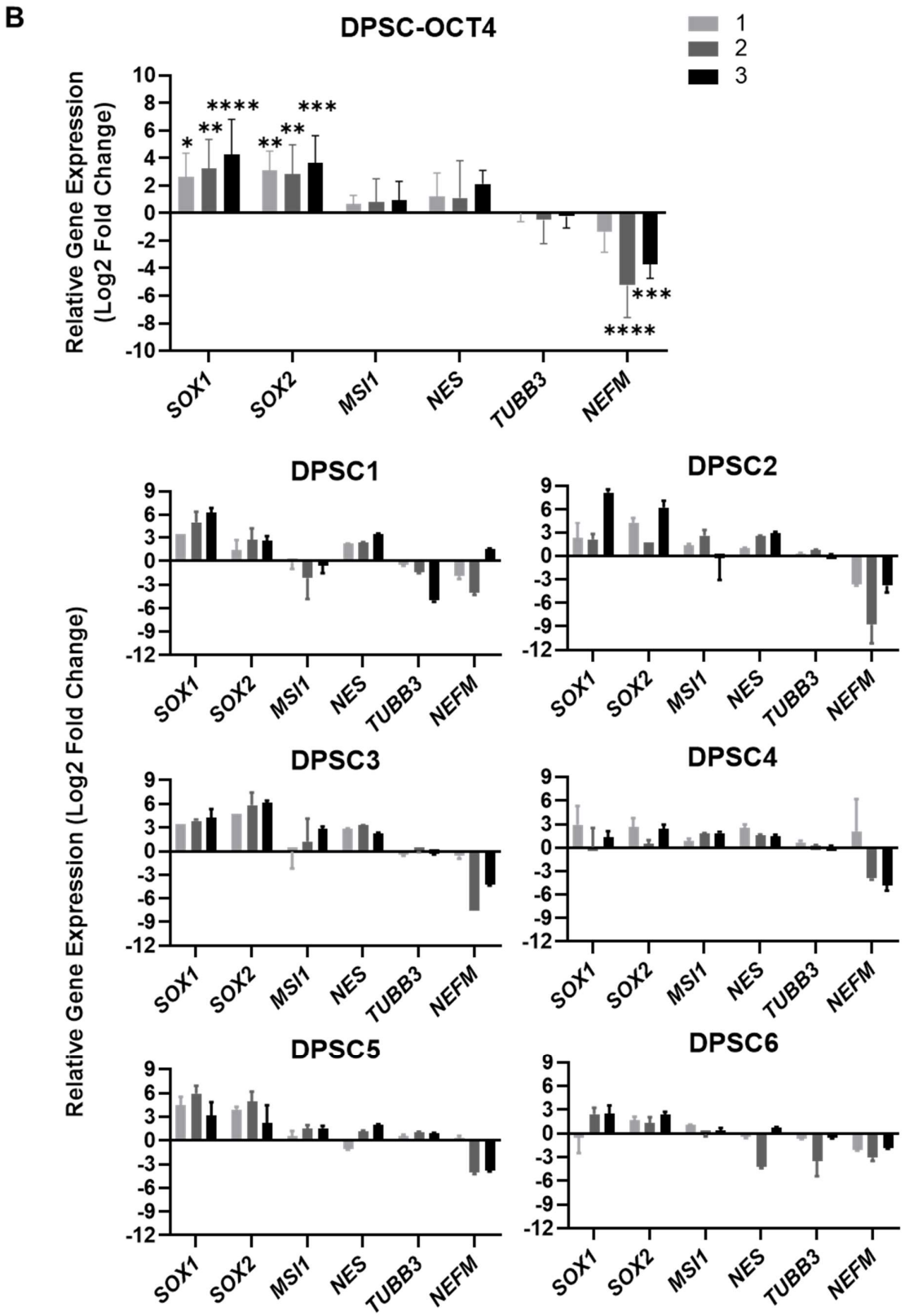
B
DPSC-OCT4
1
2
3
Relative Gene Expression (Log2 Fold Change)
SOX1
SOX2
MSI1
NES
TUBB3
NEFM
DPSC1
DPSC2
DPSC3
DPSC4
DPSC5
DPSC6

Figure 5.22 Multi-step neural induction protocol: effect of neural conditions. Gene expression levels in **(A)** DPSC-EV and **(B)** DPSC-OCT4 at each step of the protocol (1, 2, 3) relative to the base samples (standard DPSC culture medium). Gene expression levels in individual DPSC samples also shown. Data represents mean±SD, two-way ANOVA with Tukey's multiple comparisons test, n=6, *p<0.05, **p<0.01, ***p<0.001, ****p<0.0001.

5.3.2.9 Effect of lentiviral vector: increased *SOX1* and *SOX2* expression in neural conditions

To examine the effect of the lentiviral vector, DPSC-EV and DPSC-OCT4 at each step of the protocol were compared to non-transduced DPSC at the corresponding steps (Figure 5.23).

In DPSC-EV (Figure 5.23A), non-significant decreases were observed for *SOX1*, *SOX2* and *NES*, little change was seen for *MSI1*, and increases were observed for *TUBB3* and *NEFM*, in standard DPSC culture medium. An increase in *SOX1* ($p<0.05$), *SOX2* and *NES* expression was seen after step one, and decreases in *TUBB3* and *NEFM*. The expression of *MSI1* decreased and was reasonably constant between steps. Meanwhile, throughout the protocol there was an increasing trend in *NES*, *TUBB3*, and *NEFM*.

Similarly, DPSC-OCT4 (Figure 5.23B) cultured in standard DPSC growth medium, showed decreased expression levels for *SOX1*, *SOX2* and *NES*, significant increase in *NEFM* ($p<0.0001$), and little change in *MSI1* and *TUBB3*. *SOX1* and *SOX2* expression also increased after step one. Throughout the steps there was a decreasing trend in *MSI1* expression and an increasing trend in *NES* and *TUBB3* expression. The expression of *NEFM* showed the greatest change with a significant increase before the protocol and at step one, and showing a decreasing trend with decreased levels at step three.

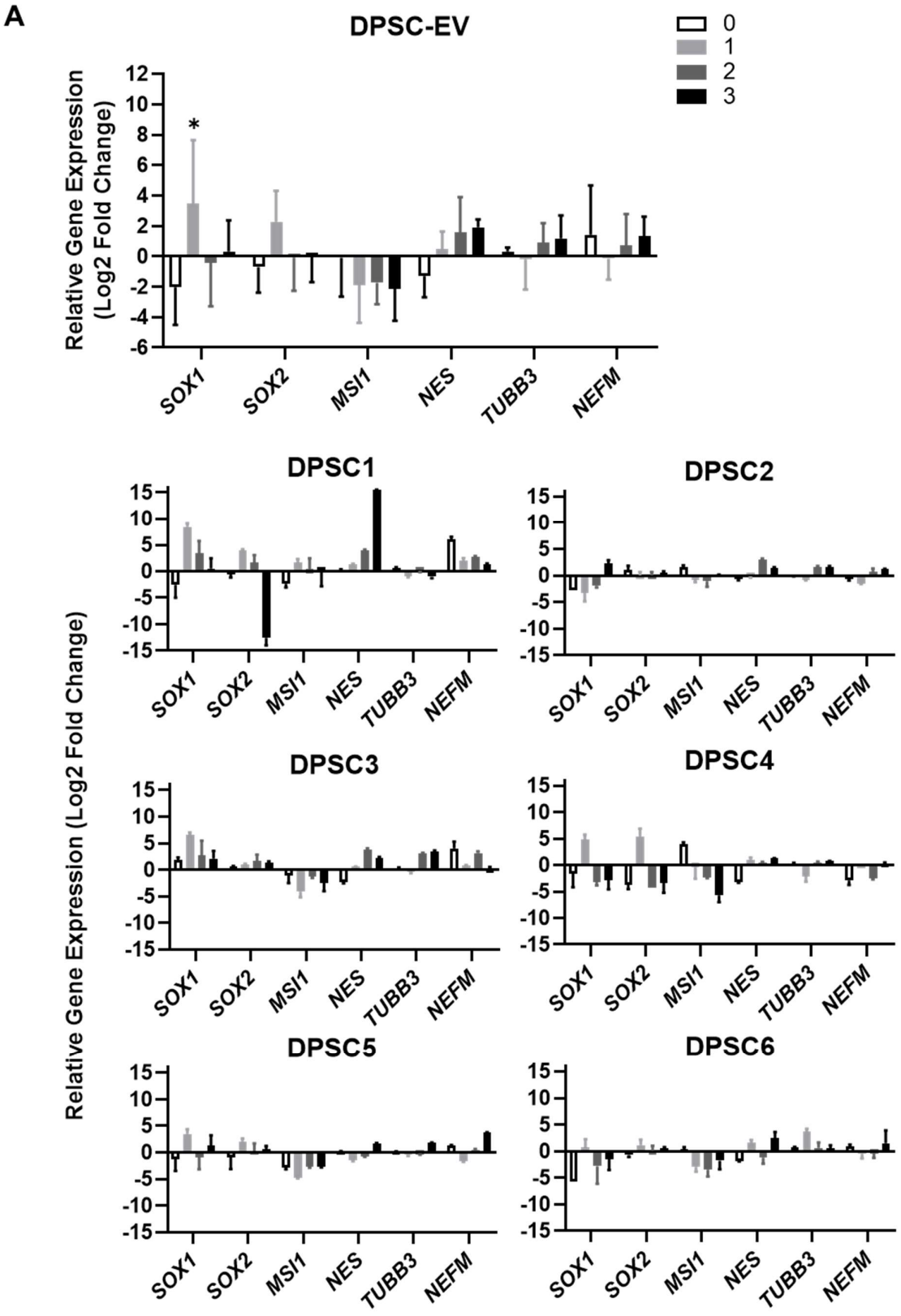
A
DPSC-EV
0
1
2
3
Relative Gene Expression (Log2 Fold Change)
*
SOX1
SOX2
MSI1
NES
TUBB3
NEFM
DPSC1
DPSC2
DPSC3
DPSC4
DPSC5
DPSC6

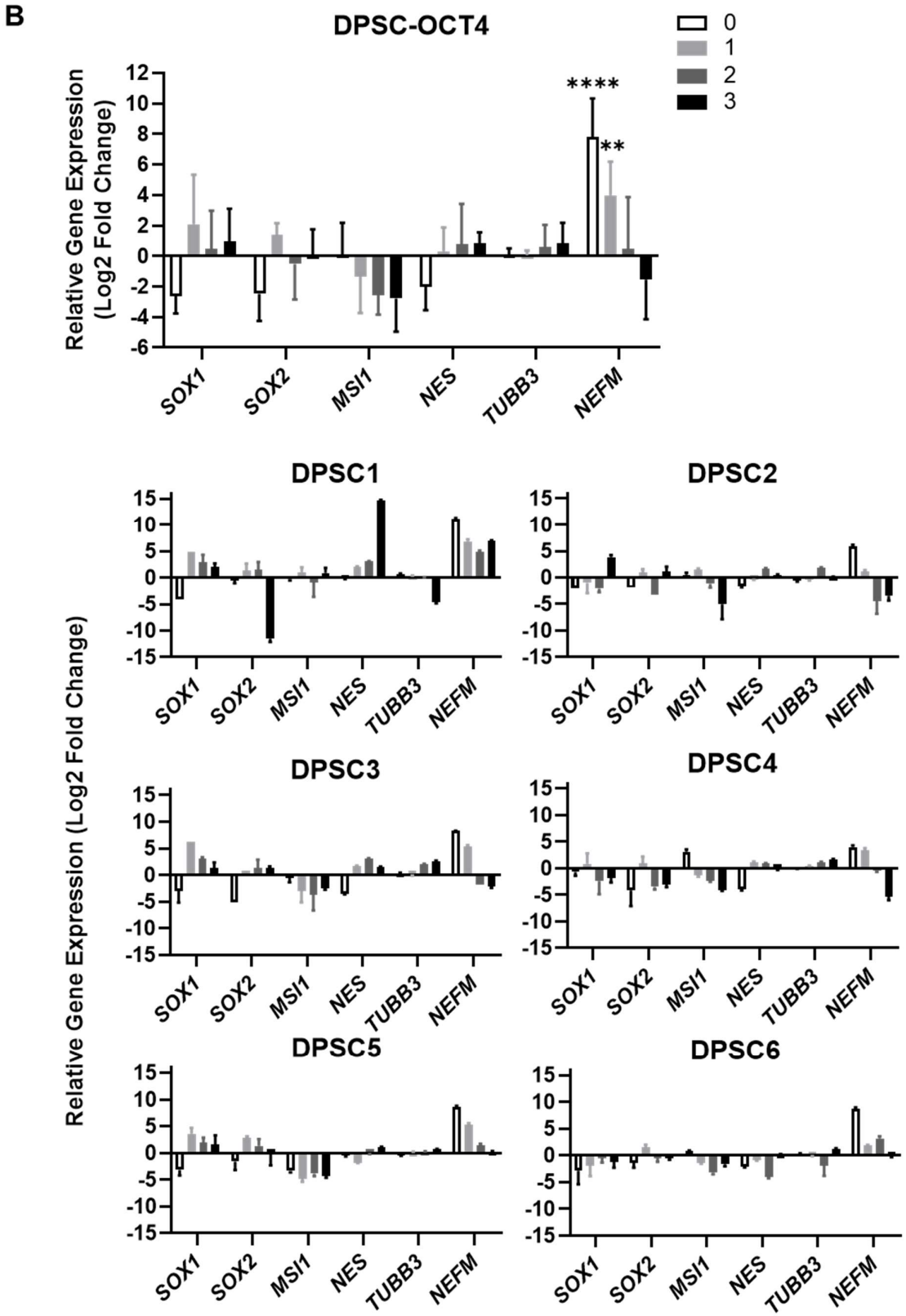
B
DPSC-OCT4
0
1
2
3
****
**
Relative Gene Expression (Log2 Fold Change)
SOX1
SOX2
MSI1
NES
TUBB3
NEFM
DPSC1
DPSC2
DPSC3
DPSC4
DPSC5
DPSC6

Figure 5.23 Multi-step neural induction protocol: effect of lentiviral vectors. Gene expression levels in **(A)** DPSC-EV and **(B)** DPSC-OCT4 before and at the completion of each step of the protocol (0, 1, 2, 3) relative to the non-transduced samples at the corresponding step. Gene expression levels in individual DPSC samples also shown. Data represents mean±SD, two-way ANOVA with Tukey's multiple comparisons test, n=6, *p<0.05, **p<0.01, ****p<0.0001.

5.3.2.10 Effect of OCT4: decreasing trend in *NEFM*

The gene expression levels in DPSC-OCT4 were compared to DPSC-EV at each step of the protocol, to examine the effect of OCT4 over-expression (Figure 5.24). In standard DPSC culture medium, there were non-significant decreases in *SOX1*, *SOX2*, *NES* and *TUBB3*, little change in *MSI1*, and significant increase in *NEFM* ($p<0.0001$). *SOX1* and *SOX2* increased while the rest of the genes decreased throughout the protocol. *NEFM* was significantly up-regulated at step one ($p<0.0001$) and down-regulated at step three ($p<0.05$).

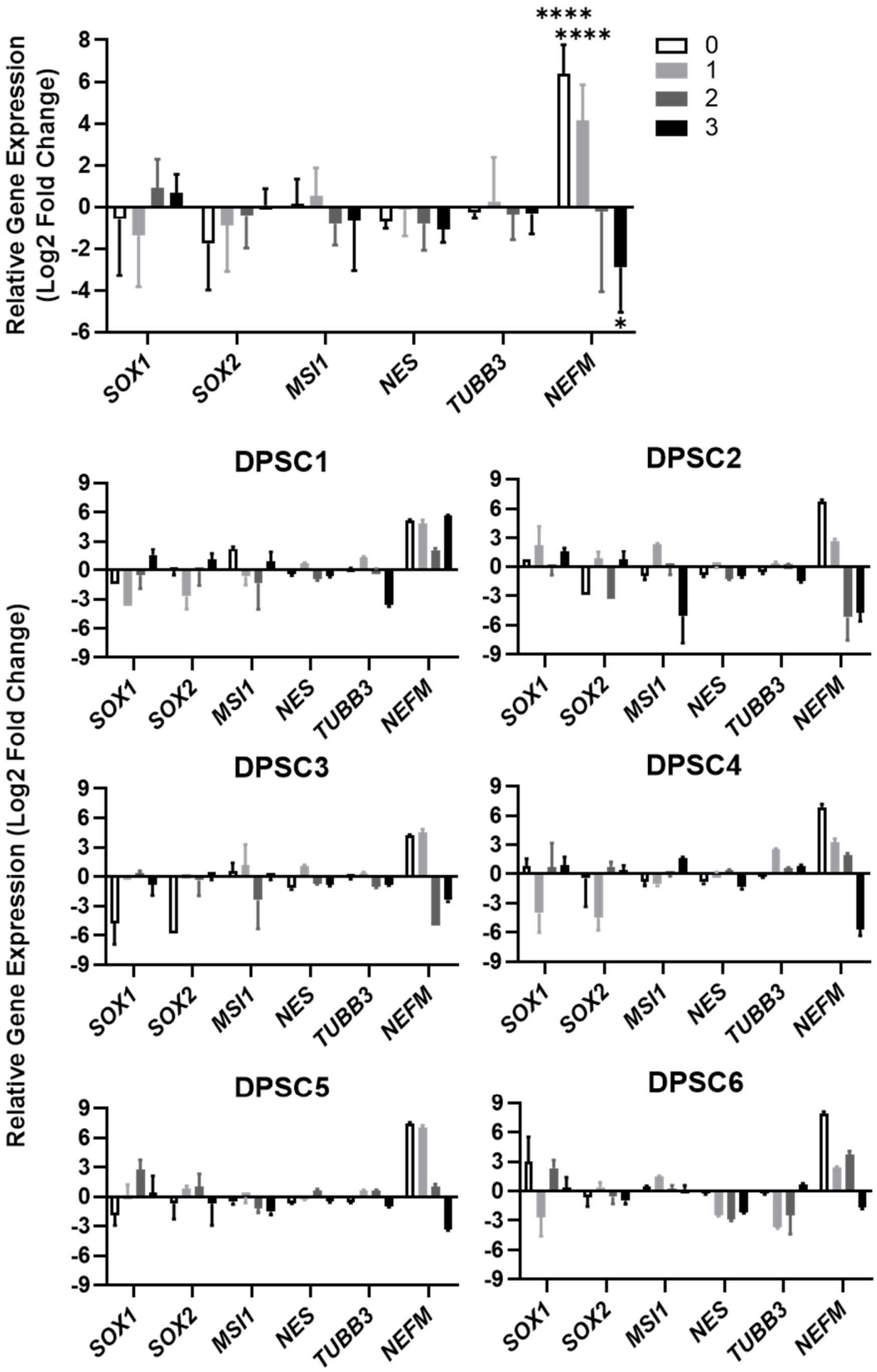

Figure 5.24 Multi-step neural induction protocol: effect of OCT4 over-expression. Gene expression levels in DPSC-OCT4 before and at the completion of each step of the protocol (0, 1, 2, 3) relative to the corresponding DPSC-EV. Gene expression levels in individual DPSC samples also shown. Data represents mean±SD, two-way ANOVA with Tukey's multiple comparisons test, n=6, ****p<0.0001.

5.3.2.11 Protein expression confirmed gene expression

At the completion of the multi-step neural induction protocol, protein expression was examined by Western blot (Figure 5.25). Across all six DPSC, protein levels for SOX1, SOX2, NES, β-III tubulin and NF-M were detected in DPSC-EV and DPSC-OCT4 (Figure 5.25A). The levels appeared higher in DPSC-EV than in DPSC-OCT4, however protein and gene expression levels may not always correlate as the message can be regulated in various ways. The protein expression levels were quantified and expressed relative to β-actin (Figure 5.25B). The early neural protein expression levels were similar between both groups, with slightly higher levels in DPSC-EV. The neuronal β-III tubulin ($p<0.0001$) and NF-M ($p<0.01$) proteins were significantly lower in DPSC-OCT4 than DPSC-EV, supporting the gene expression data.

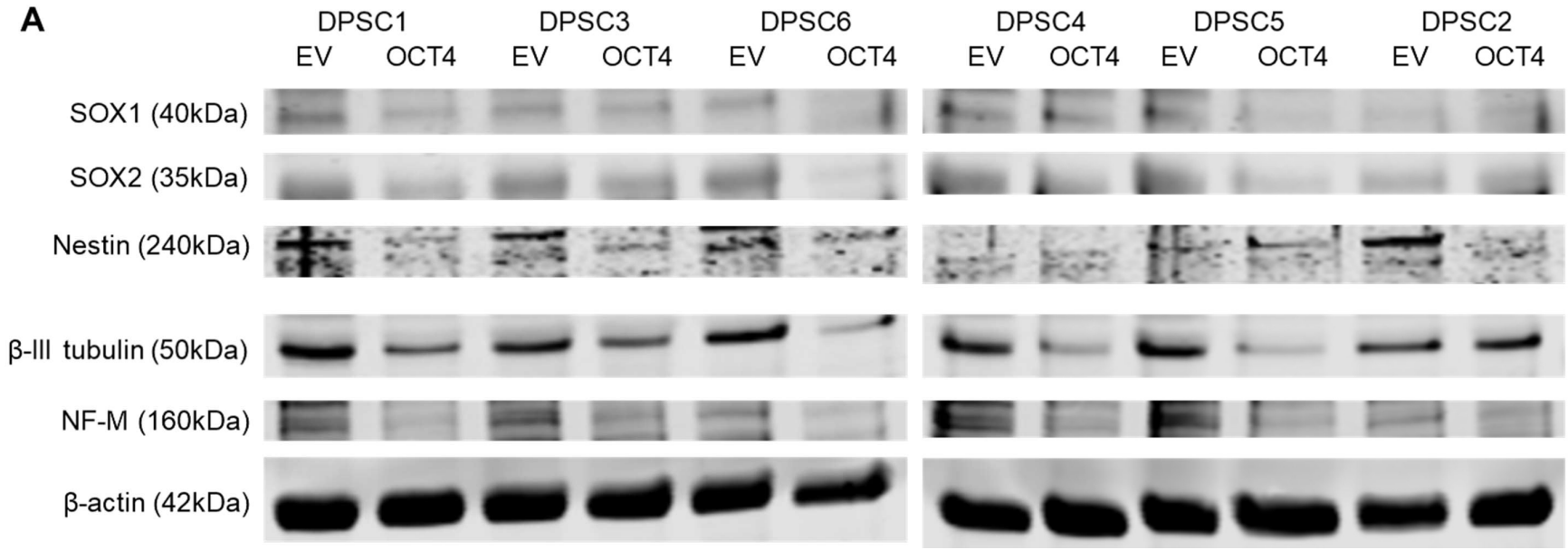
A
DPSC1
DPSC3
DPSC6
DPSC4
DPSC5
DPSC2
EV
OCT4
SOX1 (40kDa)
SOX2 (35kDa)
Nestin (240kDa)
β-III tubulin (50kDa)
NF-M (160kDa)
β-actin (42kDa)

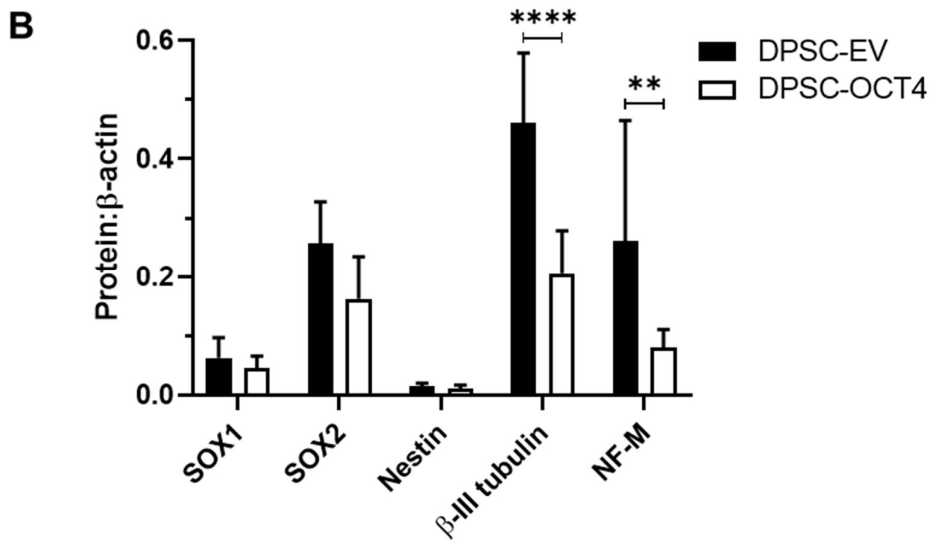

Figure 5.25 Multi-step neural induction protocol: protein expression. **(A)** DPSC-EV and DPSC-OCT4 were collected at the completion of the protocol for Western blot analysis. **(B)** Protein expression levels relative to the loading control β-actin. Data represents mean±SD, two-way ANOVA with Sidak's multiple comparisons test, n=6, **p<0.01, ****p<0.0001.

5.3.2.12 NANOG was not expressed under any conditions

The pluripotent marker, NANOG was also analysed by Western blot (Figure 5.26). NANOG is present in ESC and iPSC, and is lowly expressed or absent in somatic cells or during direct reprogramming. The Western blots showed that the NANOG protein was not expressed by DPSC cultured in standard growth medium (Figure 5.26A), nor was it present in non-transduced (Figure 5.26B) and transduced (Figure 5.26C) DPSC after culturing using the multi-step neural induction protocol. This was desired as direct reprogramming aims to bypass the pluripotent stage, where NANOG expression is one criteria used to confirm pluripotency.

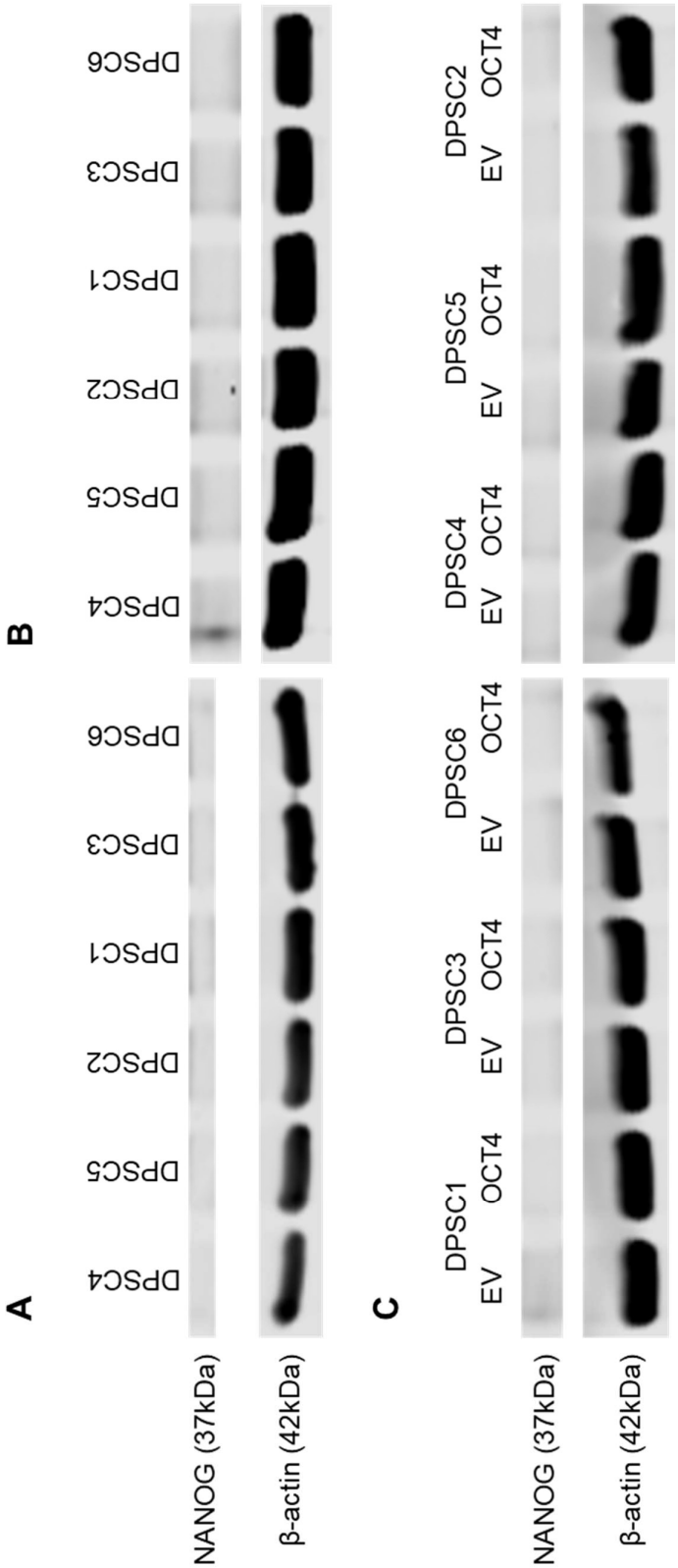

Figure 5.26 NANOG detection in DPSC. **(A)** DPSC in standard DPSC culture medium. **(B)** DPSC cultured using the multi-step neural induction protocol and samples collected at the completion of the protocol. **(C)** Transduced DPSC, DPSC-EV and DPSC-OCT4, cultured using the multi-step neural induction protocol and samples collected at the completion of the protocol. The loading control was β-actin, n=6.

5.3.2.13 DPSC-OCT4 formed more spheres than DPSC-EV

Following completion of the multi-step neural induction protocol, the cells were further cultured in the NSC medium as suspension cultures to examine their ability to form neurospheres (Figure 5.27A). After one week, spheres ≥100µm in diameter were counted. DPSC-OCT4 (3.5±2.6) formed a significantly greater number of spheres than DPSC-EV (0.9±1.3), at $p<0.05$ (Figure 5.27B). Figure 5.27C shows the spread of all the spheres of ≥100µm from both groups based on size, with significantly more spheres in DPSC-OCT4 (189 spheres) than DPSC-EV (47 spheres) from equal number of samples. There was no difference in the average sphere size between DPSC-OCT4 (131.6±30.3) and DPSC-EV (128.4±39.6). When broken down into 50µm ranges above 100µm, the majority of spheres were found in the range of 100 to 150µm, with significantly more spheres in DPSC-OCT4 ($p<0.001$) (Figure 5.27D). This suggested that DPSC-OCT4 contained a greater number of stem or progenitor cells, allowing the expansion of the spheres. However, as with the previous NSC protocol, when dissociated and reseeded, secondary spheres of ≥100µm did not form, indicating that a low percentage of proliferating precursors existed or that cells were differentiating.

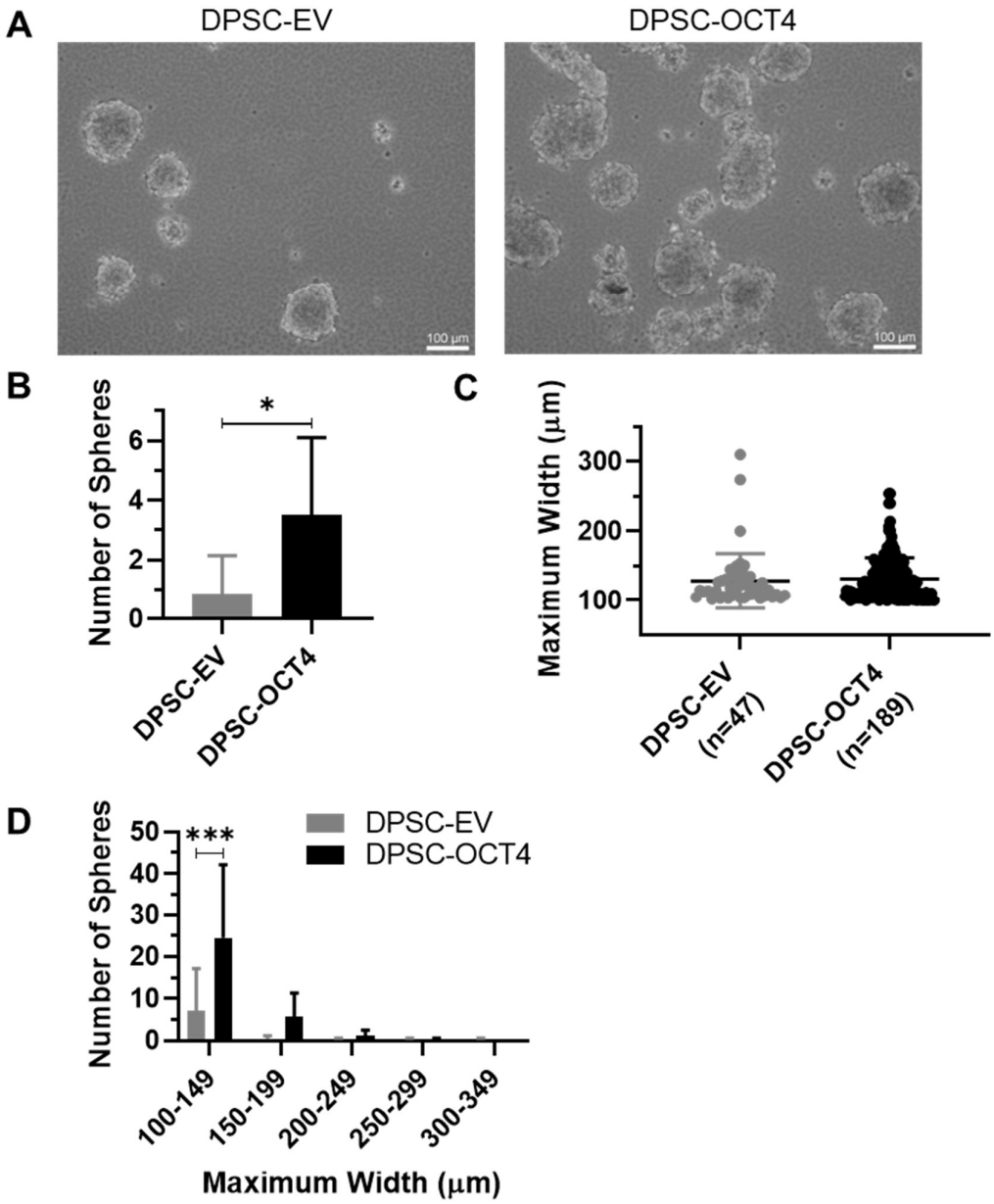

Figure 5.27 Multi-step neural induction protocol: sphere formation. **(A)** Following the completion of the multi-step neural induction protocol, DPSC-EV and DPSC-OCT4 were further cultured in NSC medium in suspension for one week. **(B)** Average number of spheres ≥100µm. **(C)** Spread of all spheres ≥100µm within each group. **(D)** Spheres grouped into 50µm ranges above 100µm. Representative images shown, data represents mean±SD, Mann-Whitney test (B, C), two-way ANOVA with Sidak's multiple comparisons test (D), n=6, scale bar=100µm, *p<0.05, ***p<0.001.

5.3.2.14 DPSC-OCT4 displayed enhanced neuronal differentiation capacity

Since it was hypothesised that OCT4 over-expressing DPSC cultured in neural conditions would be converted into NSC, the reprogrammed DPSC should be able to differentiate into the main neural cell types. Upon completion of the multi-step neural induction protocol, the control DPSC-EV and experimental DPSC-OCT4 underwent differentiation assays (Figure 5.28). The cells were subsequently analysed by immunofluorescence staining for β-III tubulin and NF-M markers for neuronal differentiation, glial fibrillary acidic protein (GFAP) for astroglial differentiation and proteolipid protein (PLP) for oligodendroglial differentiation (Figure 5.29).

For neuronal differentiation, cells were cultured for four weeks (Figure 5.28A). The density appeared to be greater in DPSC-EV than DPSC-OCT4. In both groups, the cells appeared to become less flat over time. At one week, DPSC-EV were more spindle-shaped while DPSC-OCT4 appeared smaller and with rounder cell bodies. After four weeks, more round cells with projections were seen and were more evident in DPSC-OCT4. After two weeks of astoglial differentiation, cells appeared larger and no obvious differences were observed between DPSC-EV and DPSC-OCT4 (Figure 5.28B). There were some signs of cell cytoplasmic processes spreading out in different directions and having more volume, which was more apparent in DPSC-OCT4. After ten days of oligodendroglial differentiation, far fewer cells were present in DPSC-OCT4 (Figure 5.28B). DPSC-EV appeared flat with varying morphologies. DPSC-OCT4 contained cells with big cell bodies and multiple projections.

After four weeks in neuronal maturation medium, all DPSC-OCT4 samples exhibited intense staining for β-III tubulin, whereas the staining in DPSC-EV was negligible (Figure 5.29A). Cells with long neuronal-like processes were detected. Furthermore, some cells were connecting or extending processes towards other cells. Similarly, DPSC-OCT4 stained for NF-M, and cells appeared to be in groups and making connections with other cells (Figure 5.29B). Both markers were expressed at significantly higher ($p<0.0001$) levels in DPSC-OCT4 than DPSC-EV (Figure 5.29E), showing that DPSC-OCT4 had better capacity for neuronal differentiation.

In astroglial differentiation conditions, after two weeks of culture, both DPSC-EV and DPSC-OCT4 stained positive for GFAP, which is an intermediate filament present in astrocytes (Figure 5.29C). These cells were larger than the neuronal differentiated cells, based on the DAPI staining. Morphological differences however were seen between DPSC-EV and DPSC-OCT4, as well as between DPSC samples. DPSC-EV were mostly spindle-shaped, while DPSC-OCT4 appeared smaller and rounder, with some samples displaying cells with

projections or fibrous cell-like morphology. No significant difference was observed between DPSC-EV and DPSC-OCT4 based on immunofluorescence staining of the astroglial marker (Figure 5.29E). After ten days of culture in oligodendroglial differentiation medium, there was no significant difference in expression of PLP, a major myelin protein, between DPSC-OCT4 and DPSC-EV (Figure 5.29D and E), and no clear morphological difference was observed.

Gene expression analysis of these markers was not possible due to the low levels of RNA obtained from the cultured cells. Since there was loss of cells during the differentiation process, large cell cultures are required to counteract the efficiency of the assays and obtain sufficient samples at the completion. These differentiation assays demonstrated that the OCT4 neural reprogrammed DPSC showed promising results for neuronal differentiation but not for glial differentiation.

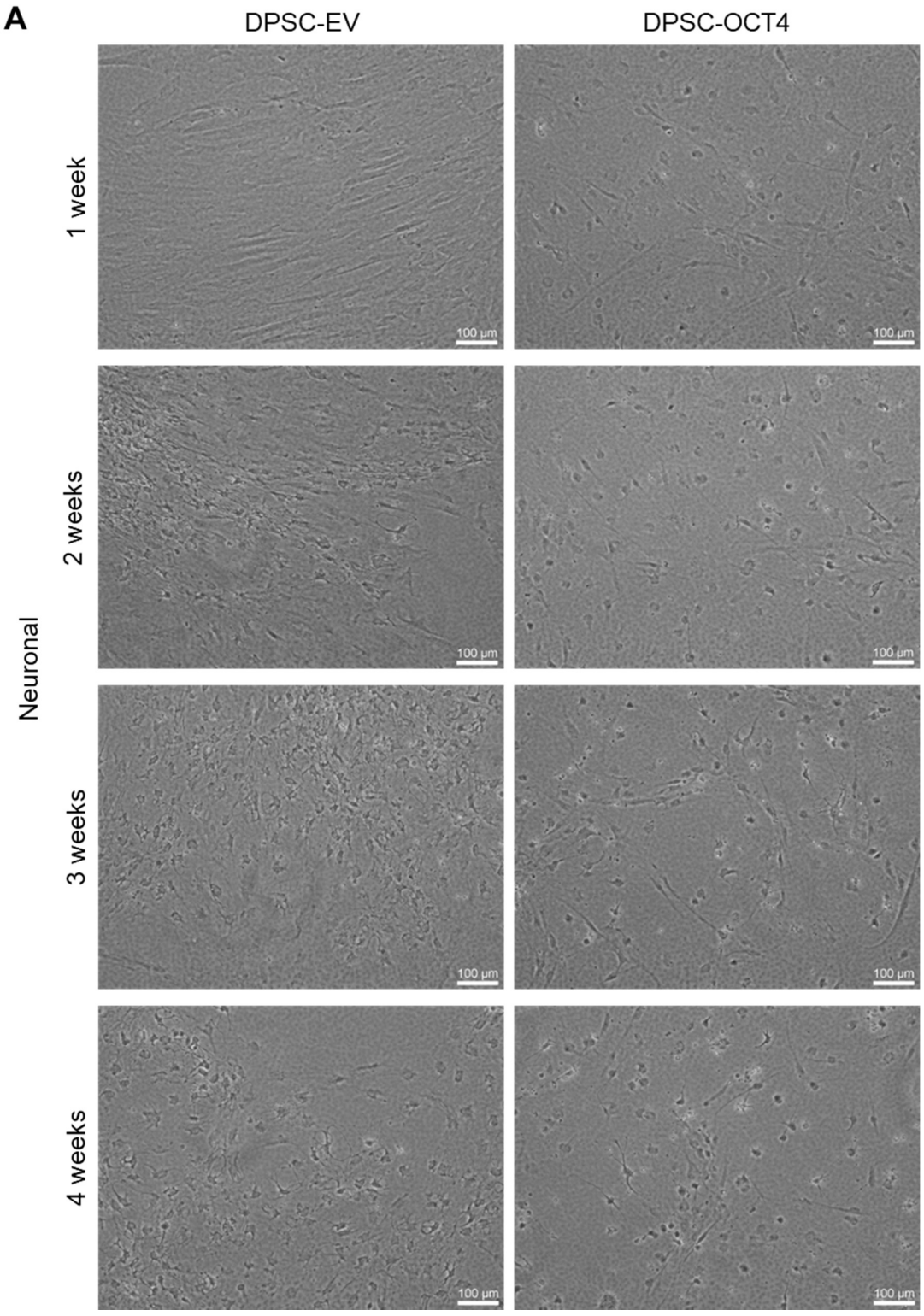
A
DPSC-EV
DPSC-OCT4
Neuronal
1 week
2 weeks
3 weeks
4 weeks
100 µm

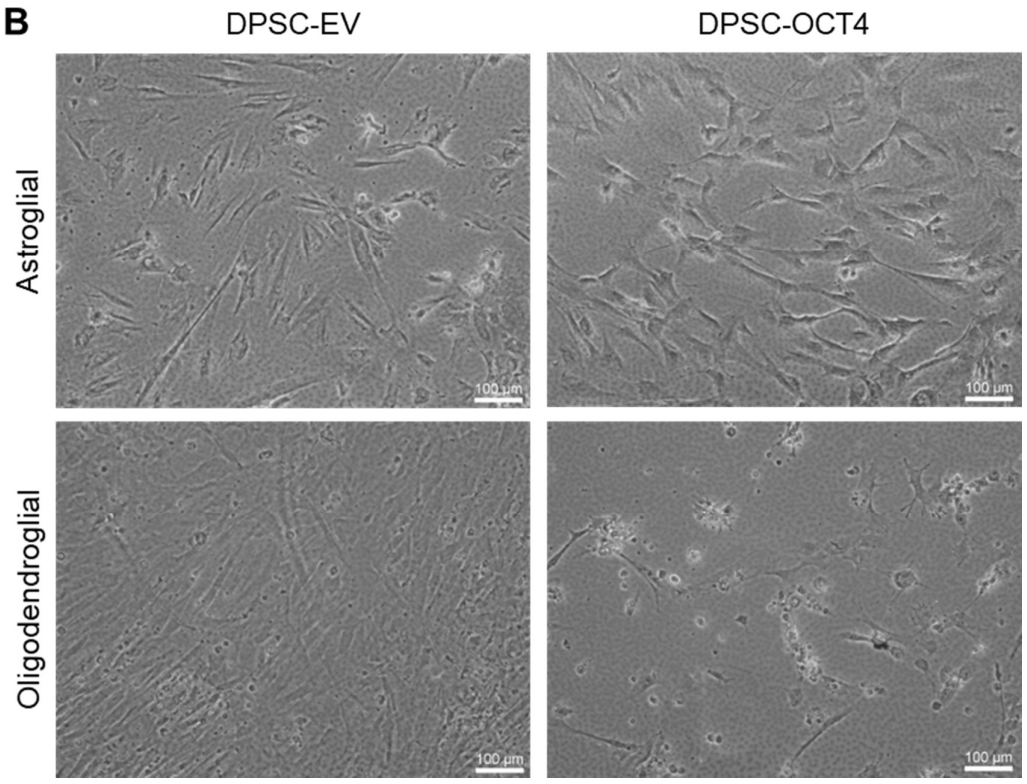

Figure 5.28 Multi-step neural induction protocol: terminal differentiation of reprogrammed DPSC. Upon completion of the multi-step neural induction protocol, DPSC-EV and DPSC-OCT4 were cultured in neuronal, astroglial and oligodendroglial differentiation media. **(A)** Neuronal differentiation was carried out for 4 weeks, with micrographs taken after each week. **(B)** Glial differentiation; astroglial differentiation was carried out for 2 weeks and oligodendroglial for 10 days, with micrographs taken at the completion. Representative images, n=6, scale bar=100µm.

A
DPSC-EV
DPSC-OCT4
DPSC1
DPSC2
DPSC3
DPSC4
DPSC5
DPSC6

B
DPSC1
DPSC2
DPSC3
DPSC4
DPSC5
DPSC6
DPSC-EV
DPSC-OCT4

C
DPSC1
DPSC2
DPSC3
DPSC4
DPSC5
DPSC6
DPSC-EV
DPSC-OCT4

DPSC1
DPSC2
DPSC3
DPSC4
DPSC5
DPSC6
DPSC-EV
DPSC-OCT4

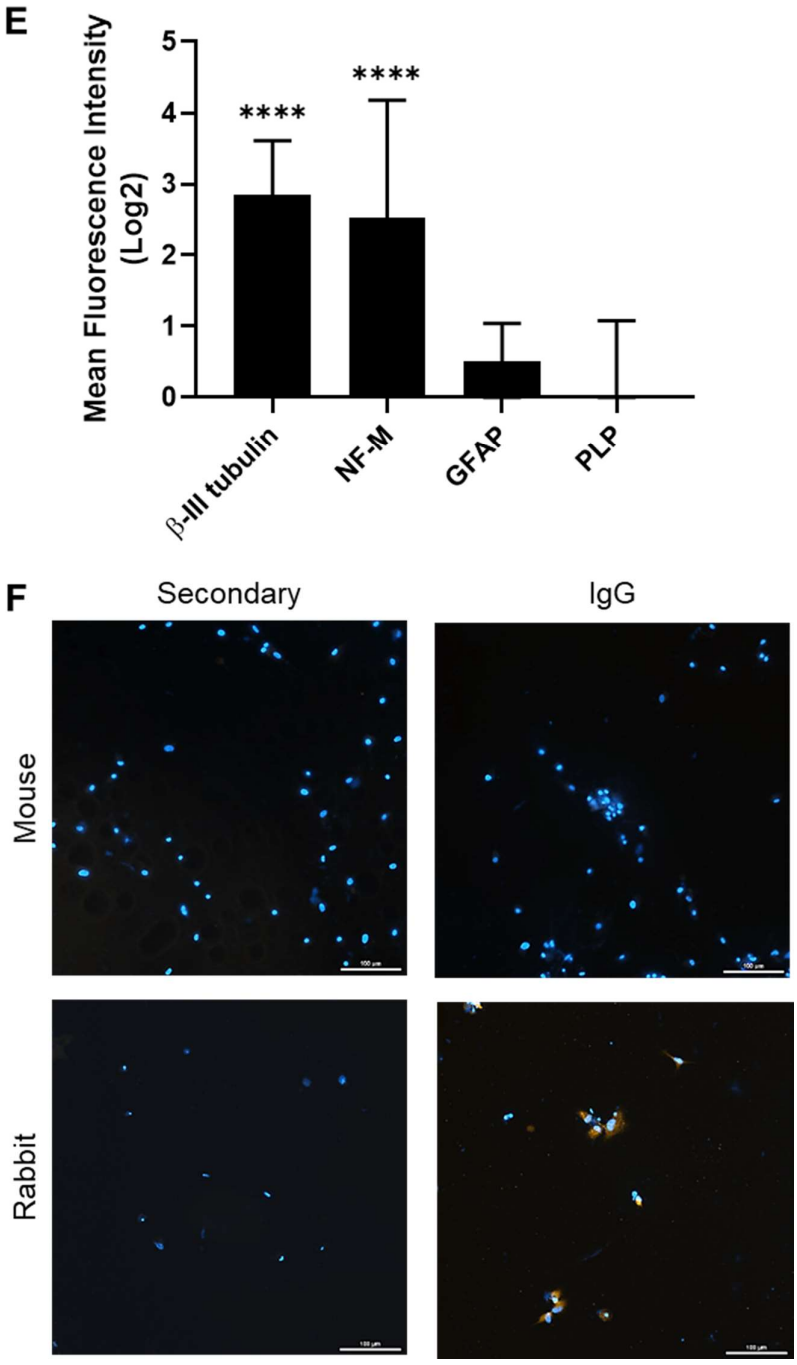

Figure 5.29 Multi-step neural induction protocol: protein expression following terminal differentiation. Immunofluorescence staining for the neuronal markers **(A)** β-III tubulin and **(B)** NF-M, **(C)** the astroglial marker GFAP and **(D)** the oligodendroglial marker PLP. **(E)** Mean fluorescence intensity in DPSC-OCT4 relative to DPSC-EV. **(F)** Representative images for control secondary and IgG isotype antibodies. Data represents mean±SD, two-way ANOVA with Sidak's multiple comparisons test, n=6, scale bar=100µm, ****p<0.0001.

5.3.2.15 Electrophysiology: preliminary patch-clamp analysis

To determine if the reprogrammed cells were capable of differentiating into functionally active neurons, patch-clamp analysis, kindly carried out by Dr. Grigori Rychkov, was performed. Patch-clamping is frequently used to study the electrophysiological properties of living, individual, excitable cells, such as neurons. It can be performed using the voltage-clamp technique where the membrane potential or voltage across the cell membrane is controlled and the resulting ionic currents passing through the membrane are recorded. The current-clamp technique is when the current passing across the membrane is controlled and the voltage changes are recorded, usually as action potentials. Here, the voltage-clamp technique was used. Many of the membrane ion channels in neurons are voltage-gated and open at specific membrane voltage ranges. Hence, we can determine what channels are expressed by the cells. In voltage clamp mode, positive charge moving into a cell (inward current) is shown as a downward deflection while a positive charge moving out of the cell (outward current) is shown as an upward deflection. Whole-cell patching was performed, allowing intracellular recording of currents through multiple channels of the cell.

Due to time constraints, patch-clamp analysis was performed on some DPSC1-OCT4 samples upon completion of the multi-step neural induction protocol and after a further three weeks of neuronal differentiation. Figure 5.30 shows the data for voltage-dependent sodium and potassium ion currents. Surprisingly, more activity was detected in DPSC1-OCT4 after the multi-step neural induction protocol rather than after the additional neuronal differentiation.

After the multi-step neural induction protocol, inward sodium ion currents (3/3 cells) due to activation of voltage-gated sodium ion channels and outward potassium ion currents (2/3 cells) due to activation of voltage-gated potassium ion delayed rectifier channels were detected in DPSC-OCT4 (Figure 5.30A, panel i). The voltage-gated sodium ion channels are responsible for depolarising a neuron during the initiation of an action potential while voltage-gated potassium ion delayed rectifier channels (outwardly rectifying) are responsible for repolarising a neuron at the completion of an action potential. The currents detected resembled those in neuronal cells in terms of size. The cells also resembled neuronal cells with regard to size and morphology. There were also inward voltage-dependent potassium ion currents present due to the activity of potassium ion inward rectifier channels (Figure 5.30A, panel ii). An inwardly rectifying potassium ion channel is one that passes the positive charge into the cell rather than out of the cell. This kind of current may play a role in regulating neuronal activity by stabilising the resting membrane potential of a cell. Cells that were further cultured in neuronal differentiation medium expressed the two types of potassium ion channels (delayed rectifiers

and inward rectifiers) but lacked voltage-dependent sodium ion currents (3/3 cells) (Figure 5.30B).

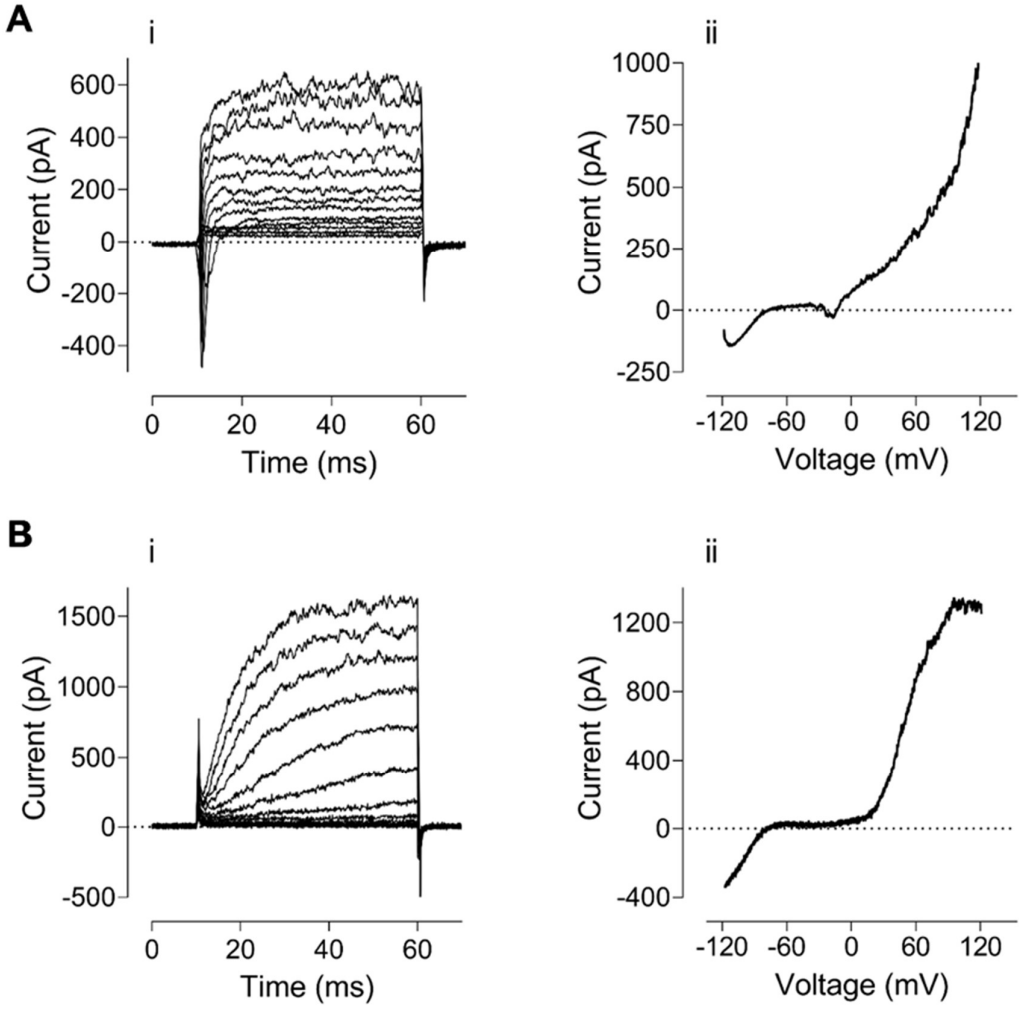

Figure 5.30 Membrane currents recorded in reprogrammed DPSC. **(A)** DPSC1-OCT4 at the completion of the multi-step neural induction protocol; **(i)** Membrane currents recorded in response to 50ms voltage steps ranging from -60mV to 60mV, applied in 10mV increments from a holding potential of -80mV. **(ii)** Instantaneous I-V plot recorded in response to 100ms voltage ramp ranging from -120mV to 120mV. Note the large inward Na^+ currents due to activation of voltage-gated Na^+ channels and outward K^+ currents due to activation of K^+ delayed rectifier (outward) channels (panel i). The inward K^+ currents due to the activity of K^+ inward rectifier channels were noticeable at membrane potentials between -120 and -70mV (panel ii). **(B)** DPSC1-OCT4 after the completion of the multi-step neural induction protocol and 3 weeks of neuronal differentiation. Membrane currents recorded in response to the same voltage protocols as in panel A. Note that these cells expressed two types of K^+ channels, delayed rectifiers and inward rectifiers, similarly to the cells in Panel A, but lacked voltage-gated Na^+ currents.

5.3.2.16 CD146 DPSC sub-populations

Human DPSC were separated using FACS into two sub-populations based on CD146 expression, a cell surface glycoprotein. CD146 is a cell adhesion molecule used as a marker for perivascular cells and is also used as a marker for MSC, where its expression may be linked to multipotency. This marker was used to characterise the DPSC (Chapter 3, section 3.3.3, pg. 47) and was expressed by 60 to 70 per cent of the DPSC (65.8±13.5, n=12), allowing investigation into the negative and positive sub-populations. These cells, non-transduced and transduced with pCDH-EV and pCDH-OCT4, were cultured using the multi-step neural induction protocol, in order to compare if there was a difference in neural induction between the $CD146^-$ and $CD146^+$ sub-populations, as well as whether there was more consistency.

Compared to the non-sorted DPSC, the $CD146^-$ and $CD146^+$ DPSC cultured in standard growth medium both displayed decreased *SOX1* and *SOX2* ($p<0.001$ for $CD146^-$ and $p<0.05$ for $CD146^+$) and increased *MSI1* ($p<0.05$ for $CD146^-$ and $p<0.01$ for $CD146^+$), with minor changes in the neuronal markers (Figure 5.31A). $CD146^+$ DPSC appeared to have slightly higher expression levels of the NSC markers while $CD146^-$ DPSC may have higher expression levels of the neuronal markers. Some variation was observed between the individual DPSC samples but mostly in the expression of the neuronal markers.

When the $CD146^-$ and $CD146^+$ DPSC underwent neural induction, all the genes except for *TUBB3* showed greater expression levels at each step of the protocol when compared to the DPSC cultured in standard growth medium (Figure 5.31B). The levels of *SOX1*, *SOX2* and *NEFM* were significantly elevated. There was an increasing trend throughout the protocol in the expression of all the markers in $CD146^-$ DPSC. However, in $CD146^+$ DPSC there was a decreasing trend throughout the protocol in *SOX1* and *SOX2* expression.

When the effect of the neural culture conditions was examined in the $CD146^-$ and $CD146^+$ DPSC-EV, there were mostly increasing trends in the expression levels of the neural genes as with the non-transduced cells, with significance in the early neural genes (Figure 5.31C). The main difference between the $CD146^-$ and $CD146^+$ DPSC-EV was in *TUBB3* expression, which was increased at the completion of the protocol in $CD146^-$ DPSC-EV but decreased in $CD146^+$ DPSC-EV ($p<0.01$). The $CD146^-$ and $CD146^+$ DPSC-OCT4 exhibited increasing trends and significantly high expression levels of the early neural genes and decreasing trend in *NEFM*, similar to what was seen previously in DPSC-OCT4 (Figure 5.31D). There was no significant difference between the $CD146^-$ and $CD146^+$ DPSC-OCT4 sub-populations.

The effect of the vectors throughout the protocol was then examined. There were no significant changes in the $CD146^-$ and $CD146^+$ DPSC-EV (Figure 5.31E). In the $CD146^-$ and $CD146^+$ DPSC-OCT4, there were significant increases in *NEFM* in standard growth medium but decreasing trends during the neural induction protocol, as previously shown in DPSC-OCT4 (Figure 5.31F). At the completion of the protocol, the $CD146^+$ DPSC-OCT4 had significantly greater ($p<0.01$) expression levels of *SOX1* and *SOX2*, as well as a significantly higher ($p<0.05$) expression level of *NES* compared to $CD146^-$ DPSC-OCT4.

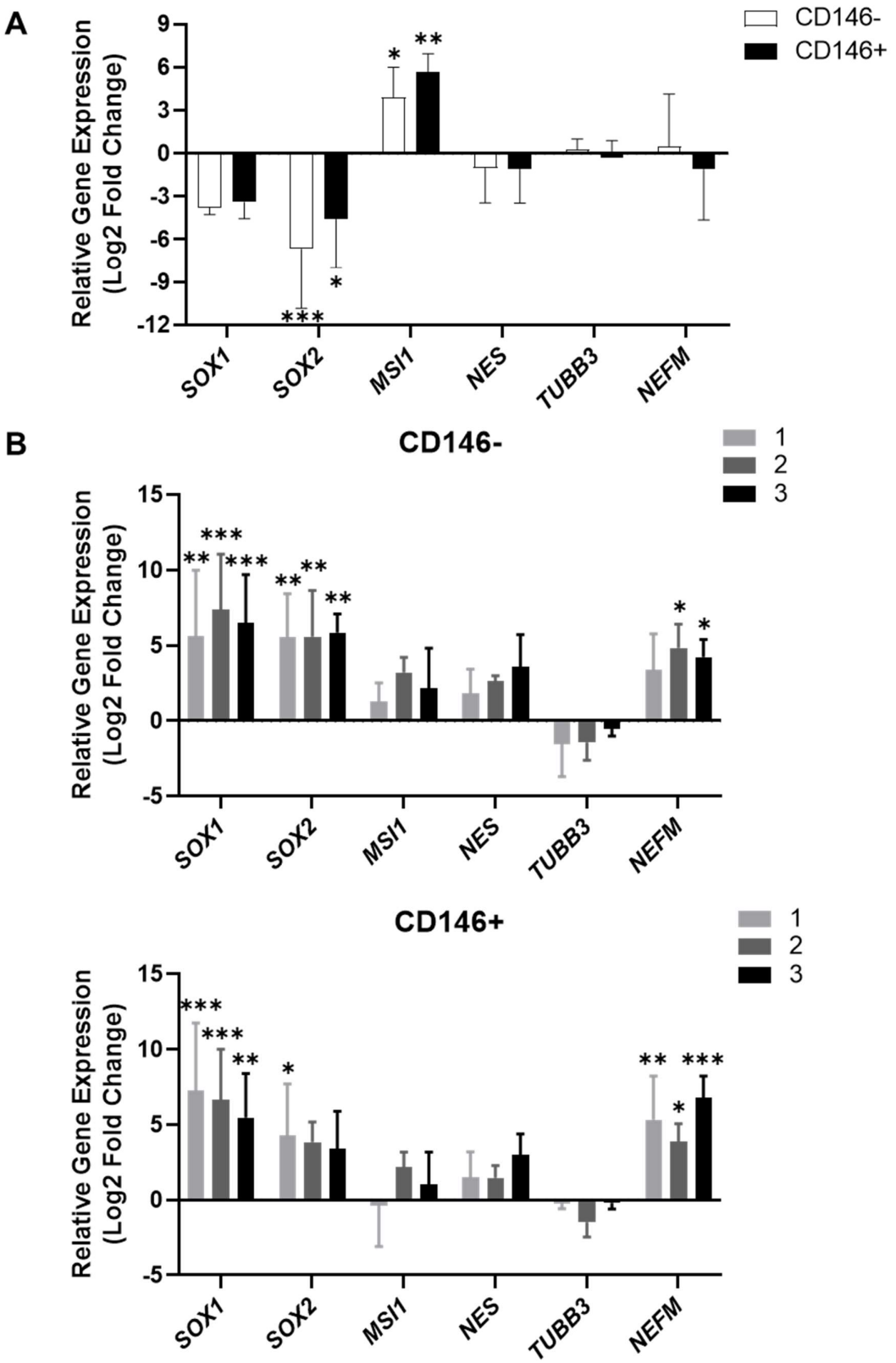
A
CD146-
CD146+
Relative Gene Expression (Log2 Fold Change)
9
6
3
0
-3
-6
-9
-12
SOX1
SOX2
MSI1
NES
TUBB3
NEFM
B
CD146-
1
2
3
Relative Gene Expression (Log2 Fold Change)
15
10
5
0
-5
SOX1
SOX2
MSI1
NES
TUBB3
NEFM
CD146+
1
2
3
Relative Gene Expression (Log2 Fold Change)
15
10
5
0
-5
SOX1
SOX2
MSI1
NES
TUBB3
NEFM

C

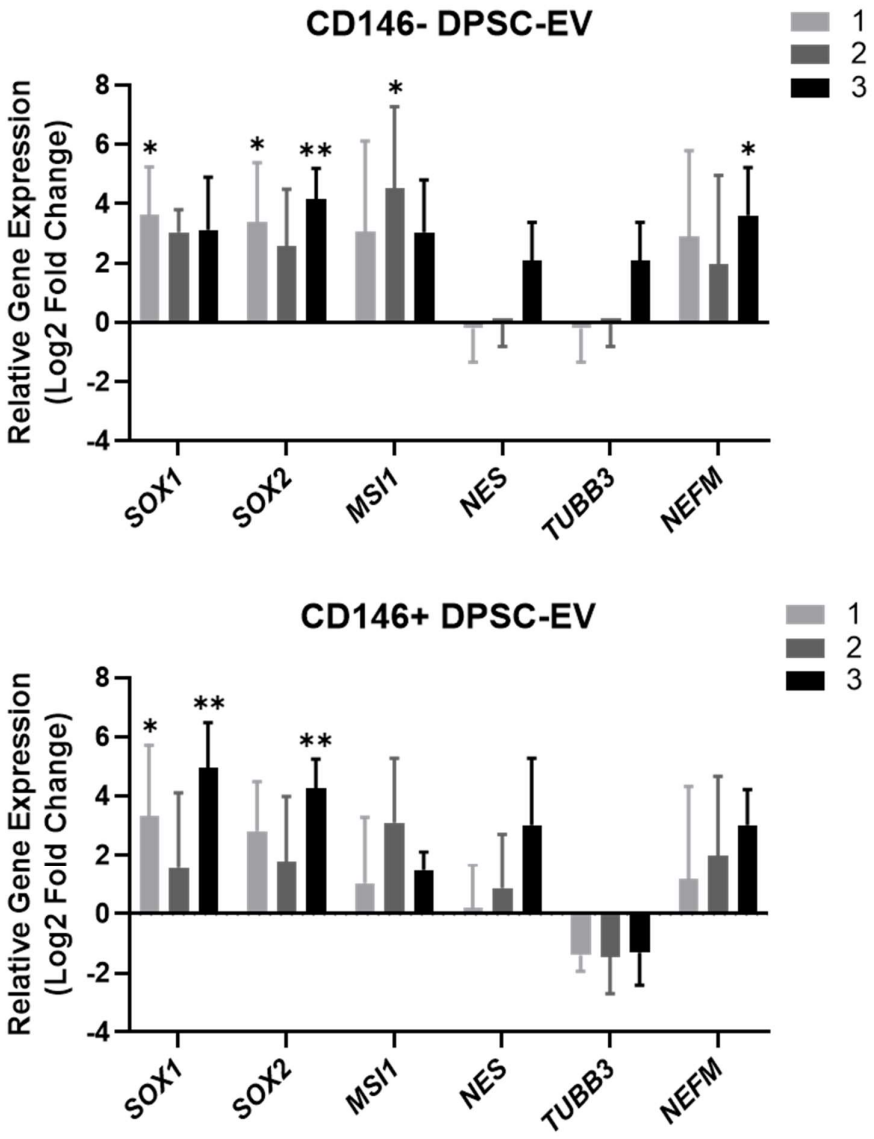
CD146- DPSC-EV
1
2
3
Relative Gene Expression
(Log2 Fold Change)
8
6
4
2
0
-2
-4
*
*
**
*
SOX1
SOX2
MSI1
NES
TUBB3
NEFM
CD146+ DPSC-EV
1
2
3
Relative Gene Expression
(Log2 Fold Change)
8
6
4
2
0
-2
-4
*
**
**
SOX1
SOX2
MSI1
NES
TUBB3
NEFM

D

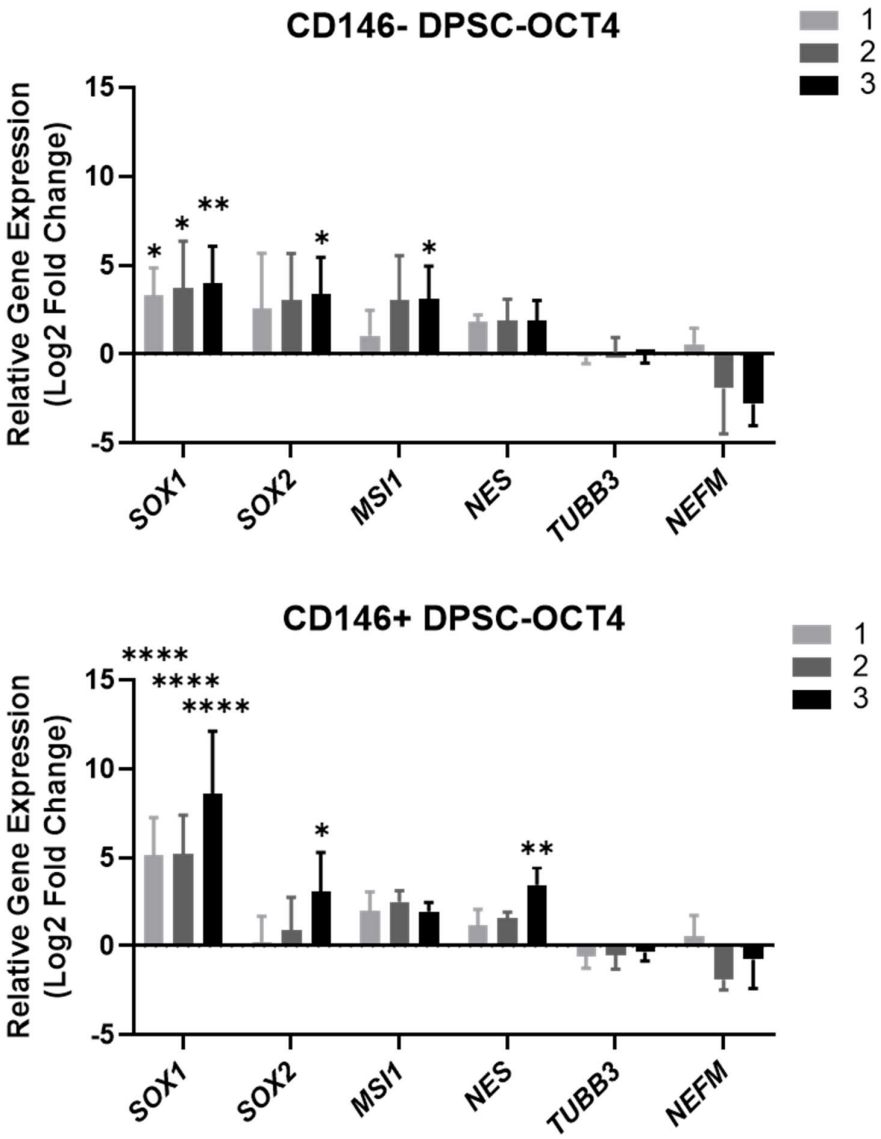
CD146- DPSC-OCT4
1
2
3
Relative Gene Expression (Log2 Fold Change)
15
10
5
0
-5
*
*
**
*
*
SOX1
SOX2
MSI1
NES
TUBB3
NEFM
CD146+ DPSC-OCT4
1
2
3
Relative Gene Expression (Log2 Fold Change)
15
10
5
0
-5
****
****
****
*
**
SOX1
SOX2
MSI1
NES
TUBB3
NEFM

E

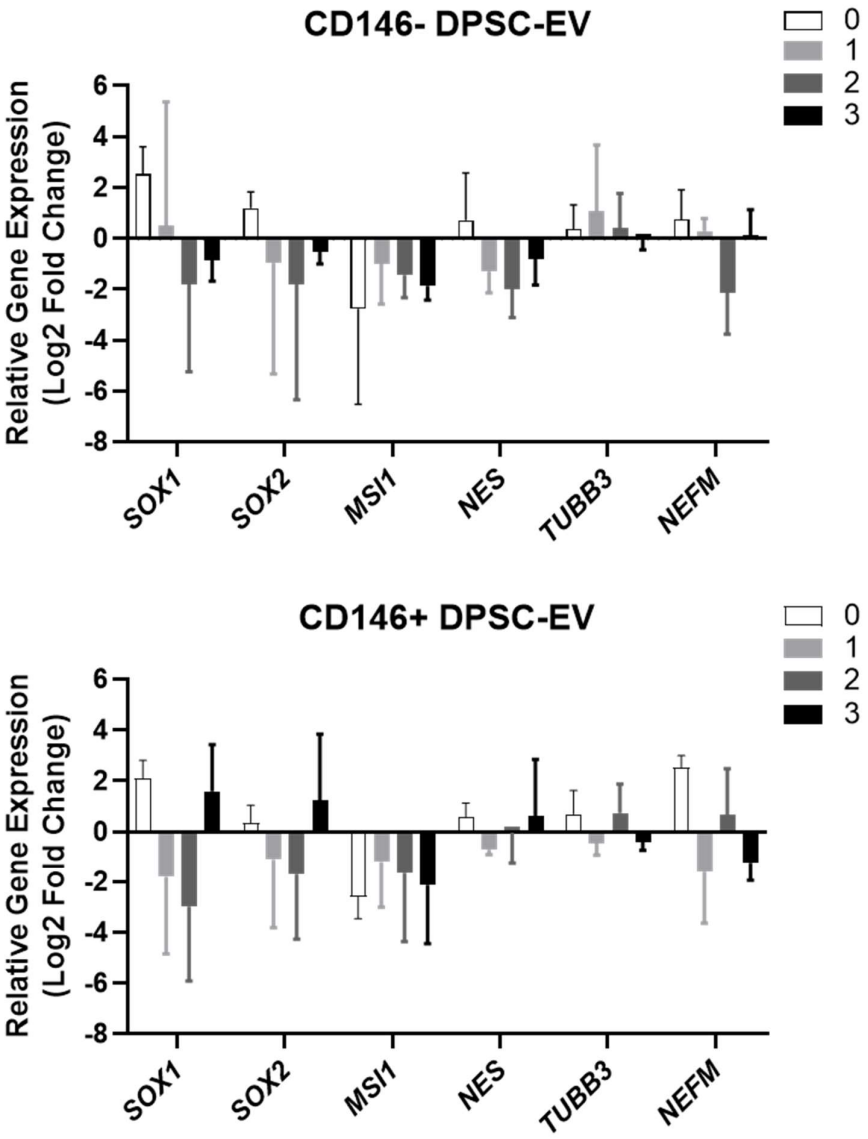
CD146- DPSC-EV
0
1
2
3
Relative Gene Expression
(Log2 Fold Change)
6
4
2
0
-2
-4
-6
-8
SOX1
SOX2
MSI1
NES
TUBB3
NEFM
CD146+ DPSC-EV
0
1
2
3
Relative Gene Expression
(Log2 Fold Change)
6
4
2
0
-2
-4
-6
-8
SOX1
SOX2
MSI1
NES
TUBB3
NEFM

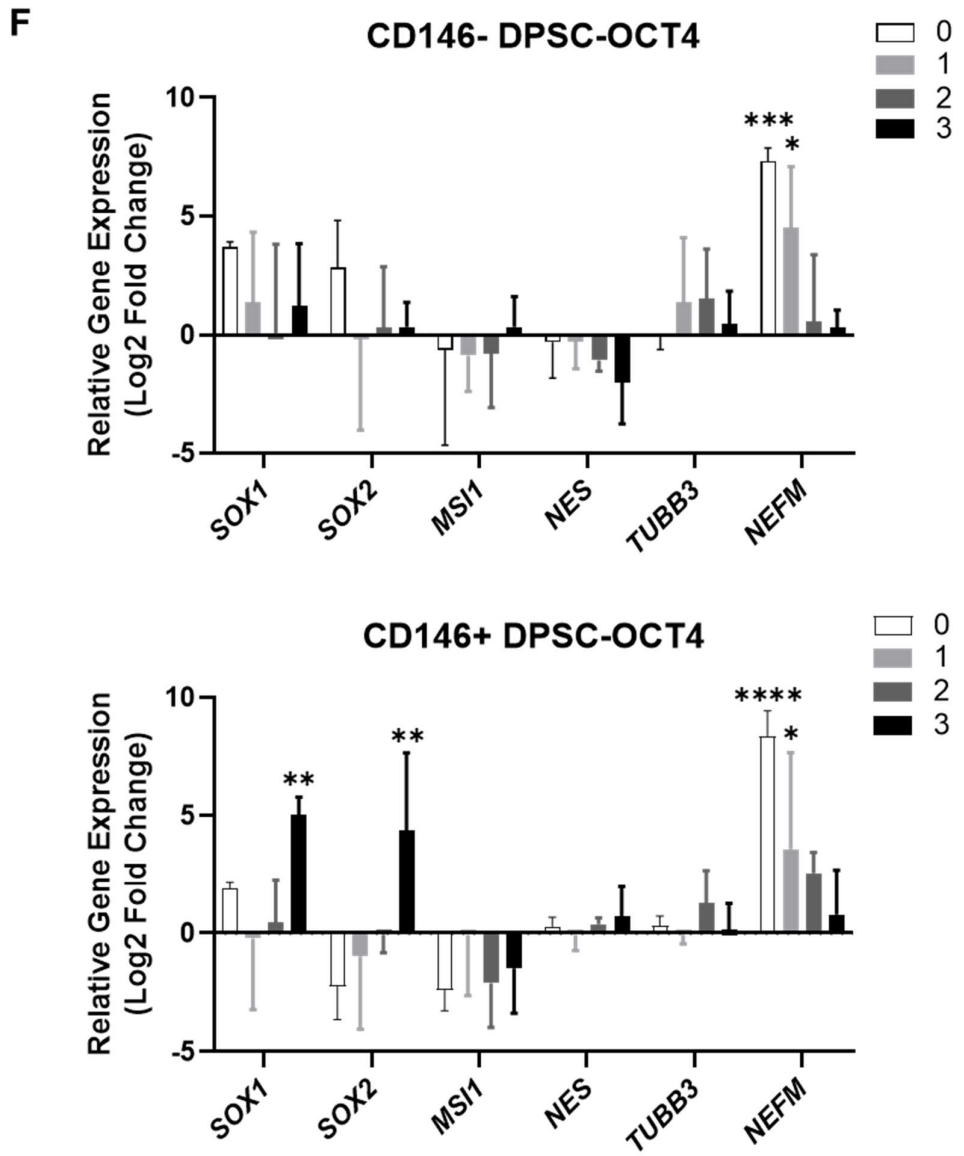

Figure 5.31 CD146$^{-/+}$ DPSC sub-populations. **(A)** Gene expression levels in CD146 sub-populations in standard DPSC culture medium relative to non-sorted DPSC in standard DPSC culture medium. **(B)** Gene expression levels in CD146 sub-populations cultured using the multi-step neural induction protocol relative to the samples before initiation of the protocol. The effect of the culture conditions on **(C)** DPSC-EV and **(D)** DPSC-OCT4; gene expression levels at each step of the protocol relative to levels before initiation of the protocol. The effect of the lentiviral vectors on **(E)** DPSC-EV and **(F)** DPSC-OCT4; gene expression levels at each step of the protocol relative to levels in the non-transduced cells at the corresponding step. Data represents mean±SD, two-way ANOVA with Dunnett's multiple comparisons tests (Sidak's multiple comparisons test between CD146$^{-/+}$), n=3, *p<0.05, **p<0.01, ***p<0.001, ****p<0.0001.

Table 5.9 Summary of multi-step neural induction protocol results for transduced DPSC.

		DPSC-EV						DPSC-OCT4					
Transduction Efficiency		>90%						>60%					
Growth in DPSC Medium		✓						✓					
Proliferation Rate		~3						~2.5					
Morphological Change	**Step 1 (pre-inducing medium)**	Less flat and cell body had a visible boundary						Clear boundary, and bigger and rounder cell body					
	Step 2 (N2B27 medium)	Flatter, elongated						Shorter and rounder					
	Step 3 (NSC medium)	Flat, elongated						Short and round					
OCT4 Over-expression		N/A						Gene (transgenic) and protein					
Change in Neural Marker Expression		***SOX1***	***SOX2***	***MSI1***	***NES***	***TUBB3***	***NEFM***	***SOX1***	***SOX2***	***MSI1***	***NES***	***TUBB3***	***NEFM***
Effect of Culture Conditions	**Step 1 (pre-inducing)**	+++	+	+	+	-	+	++	+++	+	+	-	-
	Step 2 (N2B27)	+	+	+	+	-	+	+++	+++	+	+	-	-----
	Step 3 (NSC)	++	+	+	+	-	+++++	+++++	++++	+	+	-	----
Effect of Lentiviral Vector	**Step 0 (DPSC)**	-	-	-	-	+	+	-	-	+	-	+	+++++
	Step 1 (pre-inducing)	++	+	-	+	-	-	+	+	-	+	+	+++
	Step 2 (N2B27)	-	-	-	+	+	+	+	-	-	+	+	+
	Step 3 (NSC)	+	-	-	+	+	+	+	+	-	+	+	-
Effect of OCT4 Transcription Factor	**Step 0 (DPSC)**	N/A						-	-	+	-	-	+++++
	Step 1 (pre-inducing)							-	-	+	-	+	+++++
	Step 2 (N2B27)							+	-	-	-	-	-
	Step 3 (NSC)							+	+	-	-	-	--
Protein Expression		Supports gene expression						Supports gene expression					
NANOG Expression		-						-					
Sphere Formation		+						++					
Differentiation	**Neuronal (β-III tubulin)**	-						+++++					
	Neuronal (NF-M)	-						+++++					
	Astroglial (GFAP)	+						+					
	Oligodendroglial (PLP)	+						+					

5.4 | Discussion

This chapter explored the reprogramming of human DPSC using specific transcription factors in neural inducing conditions. The aim was to convert the DPSC into NSC, and analyse the cells as functional NSC, with the ability to self-renew and multi-differentiate. The OCT4 transcription factor was selected as the most promising of the tested factors.

Overall, the NSC protocol was not very effective in enhancing the neural properties of the OCT4 over-expressing DPSC. The gene expression analysis showed that the NSC medium increased expression levels of the neural markers, particularly the neuronal markers. Meanwhile, OCT4 over-expression increased the expression of the NSC markers and *NEFM* in standard DPSC growth conditions, but these levels decreased when cultured in the NSC medium, in particular *SOX1*, *SOX2* and *NEFM*. Increased culture time in NSC medium showed minor neural enhancement. These results were unexpected with the hypothesis that OCT4 would enhance plasticity and the cells would respond to the NSC medium and increase expression of early neural markers.

The analysis between monolayer and suspension cultures showed that the suspension culture in NSC medium enhanced expression of early neural markers. Putative NSC can be cultured as neurospheres, a culture system that consists of a mixture of stem cells and differentiated cells, and is used to assess the renewal properties of stem cells. This involves growing cells in suspension on surfaces lacking adherent substrates and providing the necessary growth factors. Neurosphere formation has been reported to provide a better microenvironment for NSC maintenance. The neurosphere culture system has been incorporated in some DPSC neuronal differentiation methods, including the Gervois *et al.* 2015 protocol (3). Thus, it may be beneficial to use suspension culture, however this system would need to be improved for efficiency to make downstream applications feasible due to poor cell yield and viability. The sphere formation assay suggested that there were more stem or progenitor cells in DPSC-OCT4 than in DPSC-EV, but that these stem or progenitor cells were present at low frequency and/or underwent differentiation. This would explain why it was difficult to obtain sufficient cell numbers for analysis. The neuronal differentiation assay showed varied outcomes for TUBB3 and NF-M expression, and suggested that the NSC culture had a role with no enhancement from OCT4 over-expression.

Over-expression of OCT4 in combination with the multi-step neural induction culture protocol gave promising results, and this protocol is addressed in the remaining discussion. The culture

conditions enhanced the expression of neural genes in non-transduced and transduced DPSC. The panel of neural markers examined included some common markers for the different neural stages, including NSC, early neuronal and late neuronal stages. Since high levels of early markers are expected with low levels of later markers and vice versa, it is unclear by what mechanism the neural conditions stimulated the simultaneous increase in early and late neural markers. Meanwhile, the genetic modification had a conditional effect. In both DPSC-EV and DPSC-OCT4, there was an increase in *SOX1* and *SOX2* expression after step one, indicating the effect of the vectors. However, since there was a decrease in standard DPSC growth medium, the increase at step one was an effect of the vectors under these neural conditions. Similarly, under standard DPSC growth conditions, the OCT4 over-expressing DPSC had increased expression levels of NSC and neuronal markers, while in the neural inductive culture conditions the NSC markers increased and the neuronal markers decreased. The effect of OCT4 was most prominent on *NEFM* expression. Thus, it appears that some effects on the cells were a result of the combination of neural conditions and the OCT4 transcription factor, rather than just a single variable. Overall, these gene expression levels suggested that the OCT4 over-expressing DPSC that underwent neural induction were directed to an earlier neural state.

Throughout the multi-step neural induction protocol, the rate of cell expansion decreased suggesting that the cells were undergoing differentiation. Despite this, sphere formation was observed indicating the presence of potential stem or progenitor cells. With no subsequent secondary sphere formation capacity and limited self-renewal, it is presumed that the stem cells were few in number or had undergone differentiation. Additionally, neuronal differentiation but not glial differentiation, was enhanced in the OCT4 neural-induced DPSC, and voltage-dependent ion currents important for action potentials were detected. Combined, these observations the reprogrammed DPSC had been directed down the neural lineage and may be similar to neuronal progenitor cells rather than NSC.

The *OCT4* transcription factor is expressed at low levels in DPSC (16, 58, 93). Here, we saw a conditional effect of OCT4 over-expression in DPSC. It therefore influences the response of the cells, as previous research has suggested via OCT4-induced plasticity (12). While this transcription factor gave promising results and allows for further research using the multi-step neural induction protocol, many transcription factors are often investigated when aiming to develop a reprogramming method. Two other transcription factors, *SOX2* and *HES1*, were also briefly examined but with less potential were not investigated further due to time constraints. The *SOX2*-expressing DPSC did not survive under the neural inductive culture conditions investigated, indicating the need for alternative conditions. The *HES1*-expressing DPSC

demonstrated some potential but with inconsistent response to the standard DPSC culture conditions. This transcription factor was not expected to be successful in reprogramming cells individually, but rather in combination with other factors. Future research could investigate this transcription factor, which is important for maintenance of NSC, in combination with other promising transcription factors.

The research by Feng *et al.* 2014 on which the multi-step neural inductive culture conditions were based, showed that the step one pre-inducing medium was required for *SOX1* expression, and *SOX1* expression was important to obtain NSC, in their case from adipose-derived MSC (104). Furthermore, *SOX1* underwent nuclear translocation allowing it to act as a transcription factor. This highlighted the importance of *SOX1* in neural induction. Here, we saw that *SOX1* expression levels increased in step one, and then further increased throughout the multi-step neural induction protocol. This was coupled with an increase in nestin expression that was greatest at the completion of the neural induction, similar to the paper (104). The OCT4 over-expressing DPSC demonstrated more consistent increasing trends throughout the multi-step neural induction than the control empty vector DPSC. This was also the case with the other NSC genes (*SOX2*, *MSI1*) (104).

The most striking difference observed in the gene expression analysis was the significant decrease in the mature neuronal marker, *NEFM* in the OCT4 over-expressing DPSC following neural induction compared to the empty vector control DPSC. *NEFM* expression increased in DPSC-EV and decreased in DPSC-OCT4 throughout the multi-step neural induction protocol, suggesting that the effect is neither a result of the neural conditions nor the vectors. By comparing DPSC-OCT4 to DPSC-EV, it was confirmed that the OCT4 over-expression is driving the decrease in *NEFM*. However, this decrease was only occurring under neural induction, with elevated expression levels observed in standard DPSC culture conditions. Hence, it was evident that the response to the genetic modification was conditional. This highlights the importance of the environmental conditions, and the ability to modify the conditions to obtain different outcomes.

The media in both the NSC protocol and the multi-step neural induction protocol were based on DMEM/F12, a commonly used basal medium for neural cultures. In the multi-step neural induction protocol, the step one pre-inducing medium was serum-free, supplemented with KnockOut serum replacement and non-essential amino acids. This medium composition may be more suitable for our aims than commonly used neural media, on which the NSC method was based (3). Neural cultures typically exclude FBS due to factors that lead to differentiation.

However, other necessary growth factors and small molecules that would otherwise be present in FBS may not be sufficiently supplemented from other sources in the commonly used neural media. In this medium, the KnockOut serum replacement and non-essential amino acids may act as better substitutes and provide the factors that the cells need for proliferation and survival without encouraging differentiation. Additionally, it was supplemented with a low concentration of bFGF, a mitogen essential for NSC cultures and sometimes combined with EGF (105).

The cells were initially seeded onto a gelatin-coated surface. Gelatin, a mix of peptides and proteins formed by collagen hydrolysis, is one of the coating materials used for monolayer cultures of stem cells and neural cells (61). Methods for neuronal cultures typically use poly-L-lysine and laminin to encourage neuronal differentiation (61). These coatings have also been used in NSC cultures (106), however a coating that does not encourage differentiation is required for NSC and this one could be more suitable.

The subsequent medium in step two contained B27 and N2 supplements. These supplements are serum-free and are used to support the growth of neuronal cells (102). The N2 supplement may be used at the initial stages for neuronal commitment and differentiation, while the B27 supplement is used for long term survival of neurons. Combined, they may help to achieve a more potent neuronal phenotype. It is thus a surprise that many NSC culture media in publications include these supplements, typically with bFGF and EGF, as with the NSC method used here (106). The response of NSC in media containing these supplements may differ to the response of cells undergoing reprogramming. There may be more suitable supplements for NSC cultures to help maintain proliferation and prevent differentiation (e.g. StemPro Neural Supplement), and these may be worth substituting to determine if a more immature neural phenotype is achieved. Exact formulations of such commercial supplements are not often disclosed, however many studies find more consistent results when using commercial products (66).

In the third step, bFGF and EGF were introduced. These growth factors are effective mitogens that regulate NSC development and are routinely included in NSC cultures (105). They stimulate cell proliferation at lower concentrations (4-20ng/mL) and together have an additive effect, though they may enhance differentiation at higher concentrations (100ng/mL) (105, 107). Here, they were supplemented at a concentration of 20ng/mL. Whilst this is in the lower range, it is higher than the 4ng/mL of bFGF used in step one, and it may be worth comparing the same concentration at step three. There is some evidence that these growth factors favour

the neural lineage, in terms of stem cell potential (105, 107). We observed enhanced neuronal potential in the OCT4 over-expressing DPSC, therefore in these conditions a lower concentration may be better.

All three media were also supplemented with BME. The role of BME, a reducing agent, in cell culture is to reduce toxic levels of oxygen radicals. It is commonly used in stem and progenitor cell assays (108). Stem cells typically reside in areas of tissues with low oxygen levels, so under standard cell culture conditions, production of reactive oxygen species is amplified and cells may suffer oxidative stress. Whilst cells have mechanisms to deal with this stress to some extent, reducing agents can assist, or alternatively, using low oxygen culture systems. BME may also have a role in stabilising the cell culture media by stabilising the oxidation of unstable compounds such as glutamine. BME is rather unstable itself and needs to be supplemented often. Its use in this protocol may be similar to other protocols that use Insulin-Transferrin-Sodium Selenite supplement for neural cultures, where the transferrin and selenite components are anti-oxidants in media (106). BME is commonly used in neural reprogramming and while the mechanism by which it helps is not clear, it can increase the proliferation rate and expression of neural markers (109).

Serum-free and defined culture media are important if research is to be considered for downstream clinical applications. Efficacy in reprogramming and maintaining cells is also important for feasibility. Whilst this multi-step neural induction protocol has several components that may make it better than the standard NSC culture media, with regard to DPSC, there are some modifications that can be examined as well as further analysis of cells throughout the protocol.

The results showed that the OCT4 over-expressing DPSC were guided along the neural lineage and had better outcomes than the empty vector control DPSC with regard to stem cell and neuronal properties. At the completion of the multi-step neural induction protocol they may be more similar to neuronal progenitors or immature differentiating neurons. It is possible that they are more immature at other points throughout the protocol, for example at step one since some components in the media at steps two and three may be encouraging neuronal differentiation. Further work could examine the sphere formation and differentiation capacity following step one and two, to see if spheres can be propagated and cells stain for neural markers (NSC, neuronal and glial). Preliminary patch-clamp analysis further suggested that the cells upon completion of the protocol are more neuronal-like, and additional neuronal differentiation may not be necessary. Thus, it is possible that the protocol selected for the

neuronal lineage with the later steps initiating neuronal differentiation. Further analysis is required after step three for neuronal and glial markers. Additionally, alternative methods for glial differentiation should be examined for better outcomes.

Since there was a reduction in the gene expression of *NEFM* in DPSC-OCT4, it was somewhat surprising that voltage-dependent ion currents were detected at the completion of the multi-step neural induction protocol, suggesting that the cells were more mature. Unexpectedly, upon further neuronal differentiation, the functional properties did not appear to be enhanced, and in fact were not as promising. It is yet to be determined if the control cells have ion currents. Additionally, a greater sample size needs to be included in the patch-clamp analysis. This would inform us of the contribution of the neural conditions and the genetic modification. However, the enhanced neuronal differentiation suggests that the currents in the controls may not be at the level of those in the OCT4 over-expressing DPSC. If similar results are seen in the functionality of control empty vector DPSC upon completion of the multi-step neural induction protocol, OCT4 over-expression will be thought unnecessary with the potential lying in the neural induction protocol.

Further work should examine the levels of the markers in neurons (at varying levels of maturity), to determine how the levels of *NEFM* for example in the empty vector control and OCT4 over-expressing DPSC compare. It would also be interesting to examine whether prolonging the third step produces more mature neurons. Thus, this culture system may be promising for neuronal priming, while some modifications may be necessary to be more suited for NSC. If that is the case, further studies can examine if they can be maintained at that stage without inducing differentiation until desired.

While the NSC protocol was not as promising as the multi-step neural induction protocol with regard to neural gene expression, it did provide insight into the use of suspension cultures and how they compare to monolayer cultures. Suspension culture increased the NSC markers while the monolayer cultures increased neuronal markers. This has also been reported by other studies, where the expression levels of NSC and neural crest markers increased in DPSC after four days in suspension culture (58). Suspension cultures could be used to select for stem cells in order to obtain more homogenous populations and this in turn may decrease the variation observed. However, the efficiency is a major limitation making it difficult to work with spheres. Future research should examine how to decrease cell loss from suspension cultures and how to effectively separate the stem cells from the heterogeneous spheres.

As with previous neuronal differentiation assays for DPSC, inter-donor variation was prominent. Cellular heterogeneity is an intrinsic property of stem cell populations, as cells have different developmental origins (66). There are no clear parameters for isolating and distinguishing DPSC and NSC populations. As seen, heterogeneity can reduce the efficacy. A better understanding of the DPSC population and the response of various sub-populations is required. Whilst the samples here showed no major differences in the characterisation assays, differences became apparent in the neural assays. There are some studies that have found commercial media to produce more homogenous results (66), likely due to less variation in the formulations. Here, some analysis was performed on the CD146 sub-populations, however similar outcomes were observed to using the whole DPSC population. Previous research has suggested differences in lineage preference, between mesenchymal or neural lineages (46, 47). Here, the differences between the CD146 sub-populations were not major, with $CD146^{+}$ DPSC possibly having greater expression levels of NSC genes in DPSC-OCT4 under neural conditions. There are other markers, for example NGFR and STRO-1, and combinations of markers that can be further investigated. Standardising culture conditions, media and all environmental factors, may produce more homogenous cell populations.

In summary, OCT4 over-expression in DPSC cultured using the multi-step neural induction protocol resulted in cells with improved neural properties. Expression of early neural genes was detected, more spheres were formed, and neuronal differentiation was enhanced. The results suggested that the reprogrammed DPSC were neuronal progenitor-like cells.

CHAPTER 6

TRANSCRIPTOMIC ANALYSIS OF OCT4 OVER-EXPRESSING, NEURAL-INDUCED HUMAN DENTAL PULP STEM CELLS

6.1 | Introduction

The aim of this chapter was to examine the transcriptome-wide changes in OCT4 over-expressing, neural-induced human DPSC in comparison to control cells. To do this, RNA sequencing was performed. The controls were non-modified human DPSC cultured in standard DPSC conditions, and empty vector-transduced, neural-induced human DPSC. The neural reprogramming was performed using the multi-step neural induction protocol. Together, these comparisons gave insight into the transcriptomic changes that occurred in human DPSC under neural induction and the effect of OCT4 over-expression.

6.2 | Materials and Methods

6.2.1 Cells

Human DPSC from one donor, randomly selected, were used. There were three groups: non-modified DPSC cultured in standard DPSC medium (Chapter 2, section 2.2.1.1, pg. 27), control empty vector-transduced DPSC following neural induction, and experimental OCT4 over-expressing DPSC following neural induction. The modified human DPSC were transduced with pCDH-EV and pCDH-OCT4 and cultured using the multi-step neural induction protocol outlined in Chapter 5, section 5.2.1, pg. 101 (Figure 5.1B, pg. 102). Each group had four biological replicates. StemPro cortical foetal brain-derived NSC were cultured as per manufacturer's protocol (Gibco, MD, USA). Cortical neurospheres derived from iPSC (007 line) and ESC (H9 line) were a gift from Mirella Dottori (University of Wollongong, NSW, Australia) (62, 110).

6.2.2 RNA Extraction and Assessment

Total RNA was extracted from cells using the PureLink RNA Mini Kit according to the manufacturer's protocol (Invitrogen, CA, USA), with an on-column DNase I treatment step. The RNA concentration was quantified using the NanoDrop 8000 spectrophotometer (Thermo Scientific, MA, USA), and the quality and integrity were assessed on an Agilent Bioanalyser RNA Picochip using the Agilent 2100 Bioanalyzer (Agilent Technologies Inc., CA, USA). RNA for qPCR validation was extracted using TriReagent (Chapter 2, section 2.2.2.1, pg.29).

6.2.3 RNA-sequencing

Library preparation and RNA-sequencing were performed at SAHMRI Genomics (SAHMRI, SA, Australia). Up to 400ng of total RNA was used to generate barcoded cDNA libraries from poly(A)-enriched mRNA, using Universal Plus mRNA-Seq Library Preparation Kit according

to the manufacturer's recommendations (NuGEN Technologies Inc., CA, USA). Sequencing was performed on the NextSeq 500 with a high output v2 (75 cycle) kit (Illumina, CA, USA), to generate on average 30 million single-end reads of 75 base pairs length per sample.

6.2.4 Bioinformatics Analysis of RNA-sequencing Dataset

Analysis was performed by the SAHMRI Bioinformatics Facility (SAHMRI, SA, Australia). Initial raw read processing was performed using an in-house pipeline developed at SAHMRI. Quality of raw 75 base pair single-end sequence reads was assessed using FastQC (111) and results summarised using the R/Bioconductor package *ngsReports* (112). The raw FASTQ sequence reads were trimmed for sequence adaptors using *AdapterRemoval* (113) and aligned to the GRCh37 version of the human genome using the transcriptome algorithm *STAR* (114). Mapped sequence reads were summarised to the mm10 gene intervals using the tool *featureCounts* (115). Gene annotation was obtained from Ensembl (116). Data was filtered for low gene expression counts according to the number of counts per million mapped reads. The filtered data was normalised using the trimmed mean of M-values algorithm (117). Differential gene expression analysis was performed using *limma-voom* (118, 119). Clustered heat maps were generated using the *pheatmap* function in R (120), which were further filtered for specific gene sets. See Appendix D for the analysis code.

6.2.5 Functional Enrichment Analysis using GO and KEGG Pathway Databases

To categorise the differentially expressed genes (DEGs) functionally, they were analysed using the web-based gene ontology (GO) and Kyoto Encyclopedia of Genes and Genomes (KEGG) search tool ShinyGO v0.60 (121), for enrichment of GO terms and KEGG pathways. GO analysis categorises the gene products into biological processes, molecular functions, and cellular components, providing biological meaning to the DEGs. KEGG is a knowledge base for the systematic analysis of gene function. Genes often have multiple roles that can differ in cell types, thus many genes are annotated to multiple KEGG pathways. This restricts analysis to well-annotated genes. Gene sets of interest were obtained from the Gene Set Enrichment Analysis Molecular Signatures Database v7.1 (122, 123), which is a collection of annotated gene sets. These gene sets were obtained from several of the database collections, which were: hallmark gene sets that summarise well-defined biological states and processes; curated gene sets that contain canonical pathways derived from the KEGG pathway database; and GO gene sets that are annotated by biological processes, cellular components and molecular functions terms. These were used to filter the DEGs and generate defined heat maps. $P<0.05$ was considered statistically significant.

6.2.6 Quantitative PCR Validation

See Chapter 2, section 2.2.2.3, pg. 30 for qPCR method, using the primers in Table 6.1.

Table 6.1 Primers for qPCR.

Gene	Forward Primer	Reverse Primer
ALOX15	atcactgaaatcgggctgcaagg	acaaagtggcaaacctggtcc
SLC8A2	tgctgttgtcttcgttgccctg	aaggaacacgttcaccgcgttg
SLC5A5	atctgcaccttctacacggctg	agccacttagcatcaccacgac
PTPRN	aagcagagccaaacacctgtgc	tggcgttgatgtaatcgctccg
HES1	taaactccccaacccacctct	tctctcccagtattcaagttcct
NRCAM	tccaaccatcacccaacagtctc	aatgagtcccattacgggtccag
KCNB1	tttggacaaggctgtgctgagc	acacccgcctcaaagttgaacg
*SOX11**	aaaatgcatggcaaagtttc	cacaagccactgatattctc
MAP2	aagcgctcttctctcccaagac	tgctctgcgaattggctctgac
ACTB	agagctacgagctgcctgac	ttcgtggatgccacaggactc

*Pre-designed primers (Sigma-Aldrich, FH1 and RH1).

6.3 | Results

6.3.1 Quantity and quality of RNA

DPSC1 was used for RNA sequencing, with four biological replicates per group: control non-modified DPSC cultured in standard DPSC conditions (referred to as DPSC), control empty vector-transduced DPSC following neural induction (referred to as DPSC-EV), and experimental OCT4 over-expressing DPSC following neural induction (referred to as DPSC-OCT4). The RNA was extracted using a column-based method. The RNA concentration for each group was 314.5±17.2ng/μL (DPSC), 210.4±93.9ng/μL (DPSC-EV), and 43.5±15.0ng/μL (DPSC-OCT4). RNA samples used for RNA-sequencing all had RNA integrity number scores of >8. For each sample, 400ng of RNA was used for RNA-sequencing.

6.3.2 RNA-sequencing

To investigate the transcriptome-wide effects of OCT4 over-expression in DPSC cultured in neural inductive conditions, RNA-sequencing was performed on DPSC, DPSC-EV and DPSC-OCT4. Over 29 million single-end reads were generated per sample after removal of low quality reads and adapter sequences (Table 6.2). Approximately 40 per cent (38.1±1.0 DPSC, 38.7±0.9 DPSC-EV, 41.8±0.7 DPSC-OCT4) were unique reads. The average read length was 75 base pairs. Samples displayed high quality metrics with a Phred quality score of more than 30 (99.9% base call accuracy) (124).

Table 6.2 Raw reads for each sample.

Sample	Total Sequences	Unique Reads				Duplicate Reads			
		Number	%	Mean	SD	Number	%	Mean	SD
DPSC (1)	31 308 402	12 342 304	39.4	38.1	1.0	18 966 098	60.6	61.9	1.0
DPSC (2)	29 163 743	11 043 297	37.9			18 120 446	62.1		
DPSC (3)	32 202 304	11 949 329	37.1			20 252 975	62.9		
DPSC (4)	32 497 669	12 355 056	38.0			20 142 613	62.0		
DPSC-EV (1)	29 767 258	11 563 322	38.8	38.7	0.9	18 203 936	61.2	61.3	0.9
DPSC-EV (2)	30 337 625	11 616 359	38.3			18 721 266	61.7		
DPSC-EV (3)	31 481 877	12 563 273	39.9			18 918 604	60.1		
DPSC-EV (4)	29 826 836	11 241 277	37.7			18 585 559	62.3		
DPSC-OCT4 (1)	29 644 874	12 668 889	42.7	41.8	0.7	16 975 985	57.3	58.2	0.7
DPSC-OCT4 (2)	31 466 748	13 030 525	41.4			18 436 223	58.6		
DPSC-OCT4 (3)	29 718 926	12 234 030	41.2			17 484 896	58.8		
DPSC-OCT4 (4)	30 744 262	12 889 944	41.9			17 854 318	58.1		

6.3.3 Alignment of sequencing reads

RNA-sequencing reads were mapped to the GRCh37 version of the human genome, with over 30 million alignments per sample (Table 6.3). Approximately 80 per cent (78.9±0.9 DPSC, 78.9±0.5 DPSC-EV, 80.1±0.4 DPSC-OCT4) of the total alignments were successfully assigned to features. The percentage mapped, an indicator of overall sequencing accuracy, was expected to fall in the range of 70 to 90 per cent (125). The percentage of mapped reads was similar between the three groups; an indication of minimal bias in the sequencing data between groups. Of the total alignments, just under 40 per cent (35.2±0.4 DPSC, 36.3±0.5 DPSC-EV, 38.2±0.6 DPSC-OCT4) were unique alignments, and more than 60 per cent (62.1±1.5 DPSC, 62.6±1.0 DPSC-EV, 65.2±0.3 DPSC-OCT4) of these unique alignments were mapped to reference genes.

Table 6.3 Mapped reads for each sample.

Sample	Mapped to Reference Genome					Unique Gene Mapping				
	Total Alignments	Assigned to Features	%	Mean	SD	Total Alignments	Assigned to Features	%	Mean	SD
DPSC (1)	33 763 460	27 017 196	80.0	78.9	0.9	12 055 939	7 705 469	63.9	62.1	1.5
DPSC (2)	31 464 093	24 915 864	79.2			11 090 046	6 972 310	62.9		
DPSC (3)	35 074 560	27 390 772	78.1			12 152 391	7 359 534	60.6		
DPSC (4)	35 366 991	27 659 811	78.2			12 518 227	7 660 615	61.2		
DPSC-EV (1)	31 648 866	24 895 115	78.7	78.9	0.5	11 516 923	7 243 673	62.9	62.6	1.0
DPSC-EV (2)	31 953 348	25 378 587	79.4			11 523 479	7 273 309	63.1		
DPSC-EV (3)	33 097 365	26 193 758	79.1			12 216 591	7 737 531	63.3		
DPSC-EV (4)	31 687 292	24 778 693	78.2			11 340 910	6 936 173	61.2		
DPSC-OCT4 (1)	31 432 518	25 176 025	80.1	80.1	0.4	12 292 335	8 071 223	65.7	65.2	0.3
DPSC-OCT4 (2)	33 456 615	26 639 526	79.6			12 669 268	8 214 117	64.8		
DPSC-OCT4 (3)	31 668 467	25 409 407	80.2			12 033 546	7 845 081	65.2		
DPSC-OCT4 (4)	32 542 468	26 181 634	80.5			12 370 630	8 078 994	65.3		

6.3.4 Sample groups displayed distinct transcriptional profiles

A multi-dimensional scaling plot evaluated library similarities and clustering. The less that groups clustered, the more different their gene expression values were expected to be. This visualisation clearly distinguished the transcriptional profiles of all three groups, which were clustered away from the other groups, with separation along both dimensions (Figure 6.1). Along dimension one, DPSC and DPSC-EV were closer, and along dimension two, DPSC and DPSC-OCT4 were closer. Within each group, the replicates were clustered well together, indicating their similarity. This analysis indicated the likelihood of detecting DEGs with significant changes between the groups.

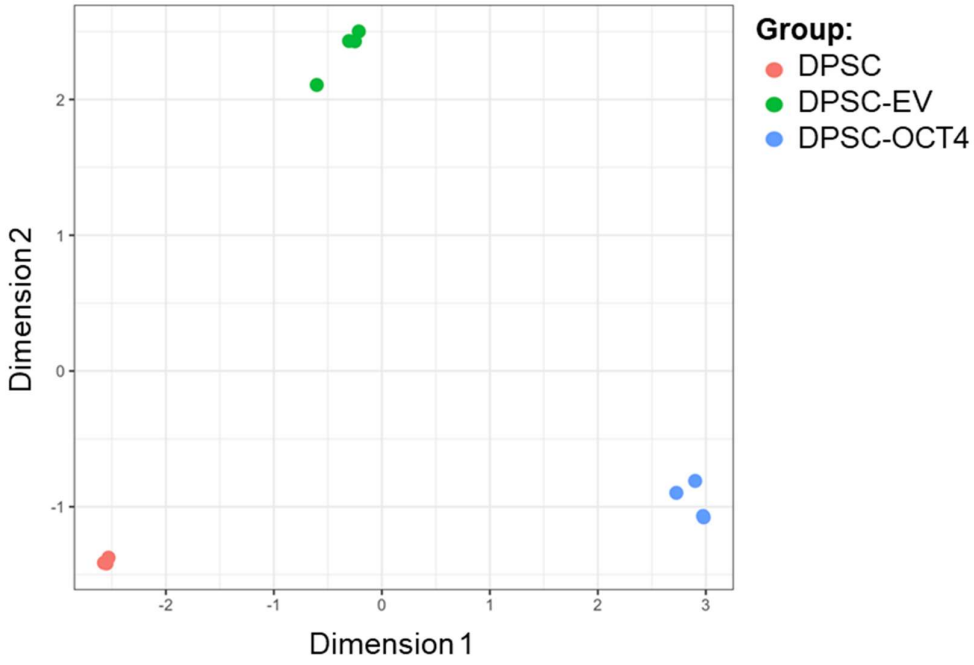

Figure 6.1 Sample similarity. Multi-dimensional scaling plot showing group similarity and difference along two dimensions. Data set consists of three groups (DPSC, DPSC-EV and DPSC-OCT4) with four replicates in each. Each group is different from the other groups, and all samples within a group are similar.

6.3.5 Differentially expressed genes

RNA-sequencing analysis uses gene expression profiles between groups to identify significant DEGs, based on specific cut-off parameters. Genes with expression of less than 1 count per million in more than 4 samples, the size of the smallest group, were filtered out from downstream analysis. Significance was set at a false discovery rate (FDR) of <0.05 and DEGs were selected using a log (base 2) fold change (logFC) cut-off of 2, which is a linear fold change of 4, meaning 4-fold or greater changes in mean expression were included. This provided a list of genes in the range of several hundred. Three comparisons for DEGs were made: DPSC-EV compared to DPSC, DPSC-OCT4 compared to DPSC, and DPSC-OCT4 compared to DPSC-EV. There were 580 significant DEGs between DPSC-EV and DPSC, 1037 between DPSC-OCT4 and DPSC, and 480 between DPSC-OCT4 and DPSC-EV (Table 6.4).

Table 6.4 DEGs between the three groups.

	DPSC-EV vs. DPSC	**DPSC-OCT4 vs. DPSC**	**DPSC-OCT4 vs. DPSC-EV**
Up-regulated	245	624	337
Non-significant	13 377	12 920	13 477
Down-regulated	335	413	143

The hierarchical clustering heat map visualised all the DEGs across the three groups (Figure 6.2). The sample dendrogram showed that the biological replicates had the highest degree of correlation represented by the short vertical distances on each branch. Both control groups were more similar to each other than to DPSC-OCT4, as seen by the greater vertical distance of the branch. The colour-scale gave an overview of the level of similarity and difference between the groups. For example, DPSC-OCT4 and DPSC-EV were similar to each other with genes in the lower half of the heat map, and this was different to DPSC. However, in the top half of the heat map, DPSC and DPSC-EV have more similarity than with DPSC-OCT4. Later on in this chapter, specific comparisons are examined with heat maps generated using filtered gene lists, to obtain a better visualisation of the changes between groups.

The DEGs were also visualised using volcano plots based on significance (negative log (base 2) of the FDR) and fold change (logFC) (Figure 6.3). The labelled genes were selected for qPCR validation in the next section.

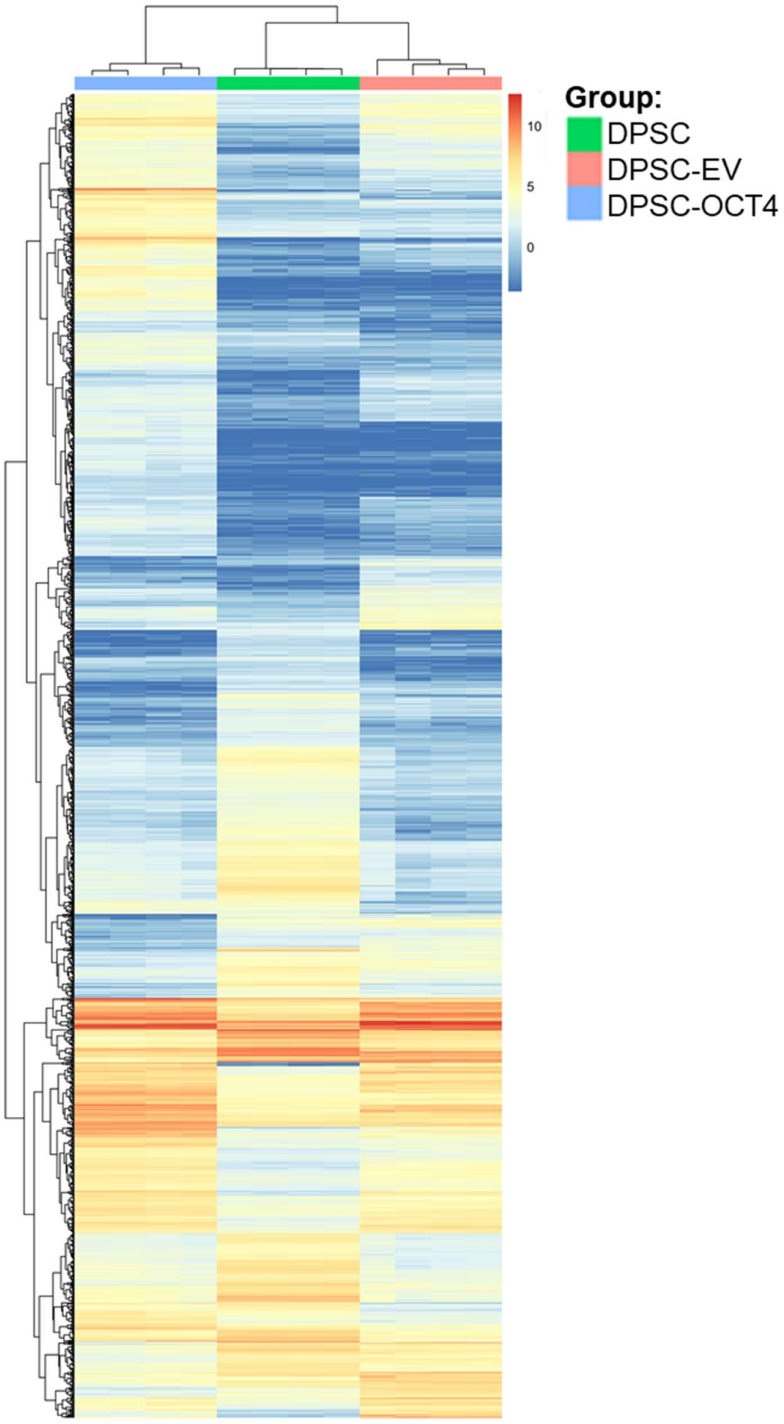

Figure 6.2 Hierarchical clustering heat map of all DEGs between samples and groups. The top dendrogram shows the sample clustering. The vertical distances on each branch represent the degree of similarity between the gene expression profiles of the samples. The dendrogram to the left shows the gene clustering. The colour-scale indicates which genes are up-regulated (warmer colours) and down-regulated (colder colours). Data set consists of three groups (DPSC, DPSC-EV and DPSC-OCT4) with four replicates in each.

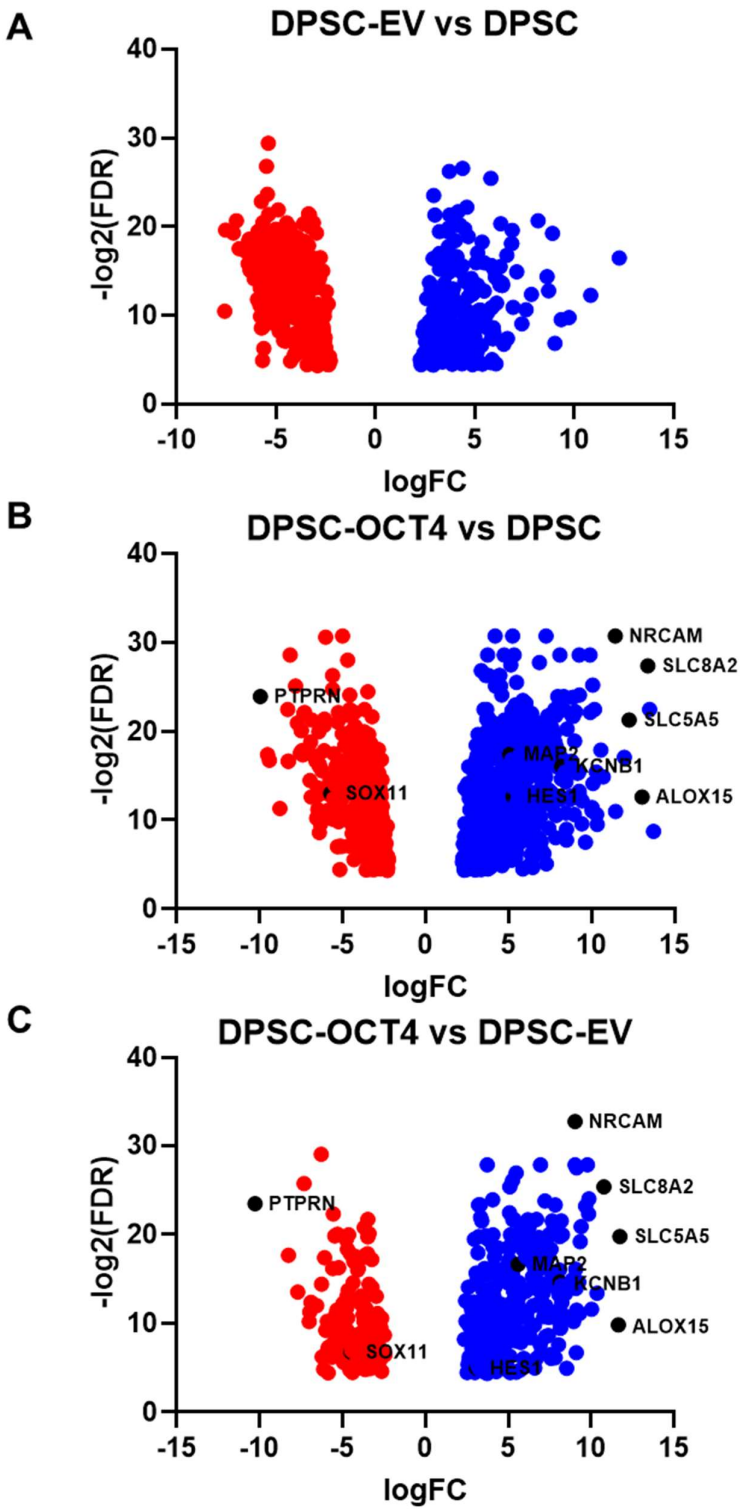

Figure 6.3 Volcano plots of significant DEGs. Significance was set at FDR<0.05. The greater the *y* value, the greater the significance. Fold change is indicated by the *x* values. Positive (blue) values are up-regulated and negative (red) values are down-regulated. **(A)** DPSC vs. DPSC-EV, **(B)** DPSC-OCT4 vs. DPSC, and **(C)** DPSC-OCT4 vs. DPSC-EV. The values in black are the genes selected for qPCR validation; two down-regulated and seven up-regulated genes in DPSC-OCT4 vs. both DPSC and DPSC-EV but not between the two controls DPSC vs. DPSC-EV.

6.3.6 Quantitative PCR validation of RNA-sequencing data

To confirm that the biological conclusions formulated based on the RNA-sequencing data would be a result of the reprogramming, a selection of genes were validated by qPCR. The six DPSC samples analysed in Chapter 5, section 5.3.2, pg. 129 were used (DPSC, DPSC-EV and DPSC-OCT4 for each), which included the sample used for RNA-sequencing (DPSC1) and five other biological samples.

Firstly, genes were selected based on the following criteria: (a) gene expression changes in DPSC-OCT4 relative to DPSC and DPSC-EV but not between DPSC and DPSC-EV, and (b) present in the top ten up-regulated and top ten down-regulated genes with regard to fold change. Using this criteria, four genes were identified; *ALOX15*, *SLC8A2* and *SLC5A5* were up-regulated and *PTPRN* was down-regulated in DPSC-OCT4. To increase the number of genes for qPCR validation, additional genes were selected based on: (a) gene expression changes in DPSC-OCT4 relative to DPSC and DPSC-EV but not between DPSC and DPSC-EV, and (c) relevance to question (i.e. do they have a neural/neuronal role). With this criteria, *HES1* (up-regulated), *NRCAM* (up-regulated), *KCNB1* (up-regulated), *SOX11* (down-regulated) and *MAP2* (up-regulated) were added to the list of genes for qPCR validation. This selection criteria gave a list of nine genes, which included genes with highest and lowest fold change, high significance, and relevance to the question. Table 6.5 lists the genes and indicates the function of the gene product, the fold change observed from the RNA-sequencing and the presence or absence in brain tissue (126).

Table 6.5 Genes selected for qPCR validation.

Gene	Function	RNA-seq logFC		Presence in Brain Tissue
		DPSC-OCT4 vs. DPSC	DPSC-OCT4 vs. DPSC-EV	
ALOX15	Lipoxygenase: regulates inflammation and immunity, role in membrane remodelling.	13.1	11.7	low
SLC8A2	Solute carrier: sodium-calcium exchange, calcium ion homeostasis in excitable cells, modulates synaptic plasticity.	13.4	10.8	moderate to high
SLC5A5	Solute carrier: sodium-iodide transporter in the thyroid gland.	12.3	11.8	high in pons and medulla
PTPRN	Protein tyrosine phosphatase: vesicle-mediated secretory processes, required for accumulation of some neurotransmitters.	-10.0	-10.3	moderate to high
HES1	Transcriptional repressor: represses genes that require a bHLH activator, maintains the NSC pool and inhibits neuronal differentiation.	5.3	3.1	low to moderate
NRCAM	Neuronal cell adhesion molecule: adhesion in CNS and PNS, directional signalling during axonal cone growth, neurite outgrowth.	11.4	9.0	moderate to high
KCNB1	Voltage-gated potassium channel: delayed rectifier in excitable cells, regulates repolarisation.	8.2	8.1	moderate
SOX11	Transcriptional activator: role in developing CNS and neurogenesis.	-5.7	-4.5	low to moderate
MAP2	Microtubule-associated protein; microtubule assembly and stabilisation in neurogenesis.	5.1	5.6	moderate to high

The fold change in gene expression levels calculated from the qPCR correlated with that from the RNA-sequencing (Figure 6.4). The expression levels of *ALOX15*, *SLC8A2*, *SLC5A5* and *NRCAM* in DPSC-OCT4 relative to both DPSC and DPSC-EV were highest at a log (base 2) fold change of approximately 10. These were significantly greater than DPSC-EV relative to DPSC ($p<0.001$). *KCNB1* and *MAP2* were also up-regulated in DPSC-OCT4 with similar levels to the RNA-sequencing, and significantly higher than the controls ($p<0.0001$ and $p<0.05$ respectively). As expected from the RNA-sequencing, *PTPRN* and *SOX11* were down-regulated in DPSC-OCT4 relative to both DPSC and DPSC-EV, with *PTPRN* significantly lower than the controls ($p<0.0001$). The levels of *SOX11* displayed small changes. *HES1* showed an up-regulation in all three comparisons with no significant differences. The levels were similar between DPSC-EV and DPSC-OCT4 both relative to DPSC, and lower in DPSC-OCT4 relative to DPSC-EV. The gene expression levels between the different DPSC samples were similar, with more variation observed in genes that had a lower fold change, such as *SOX11* and *HES1*.

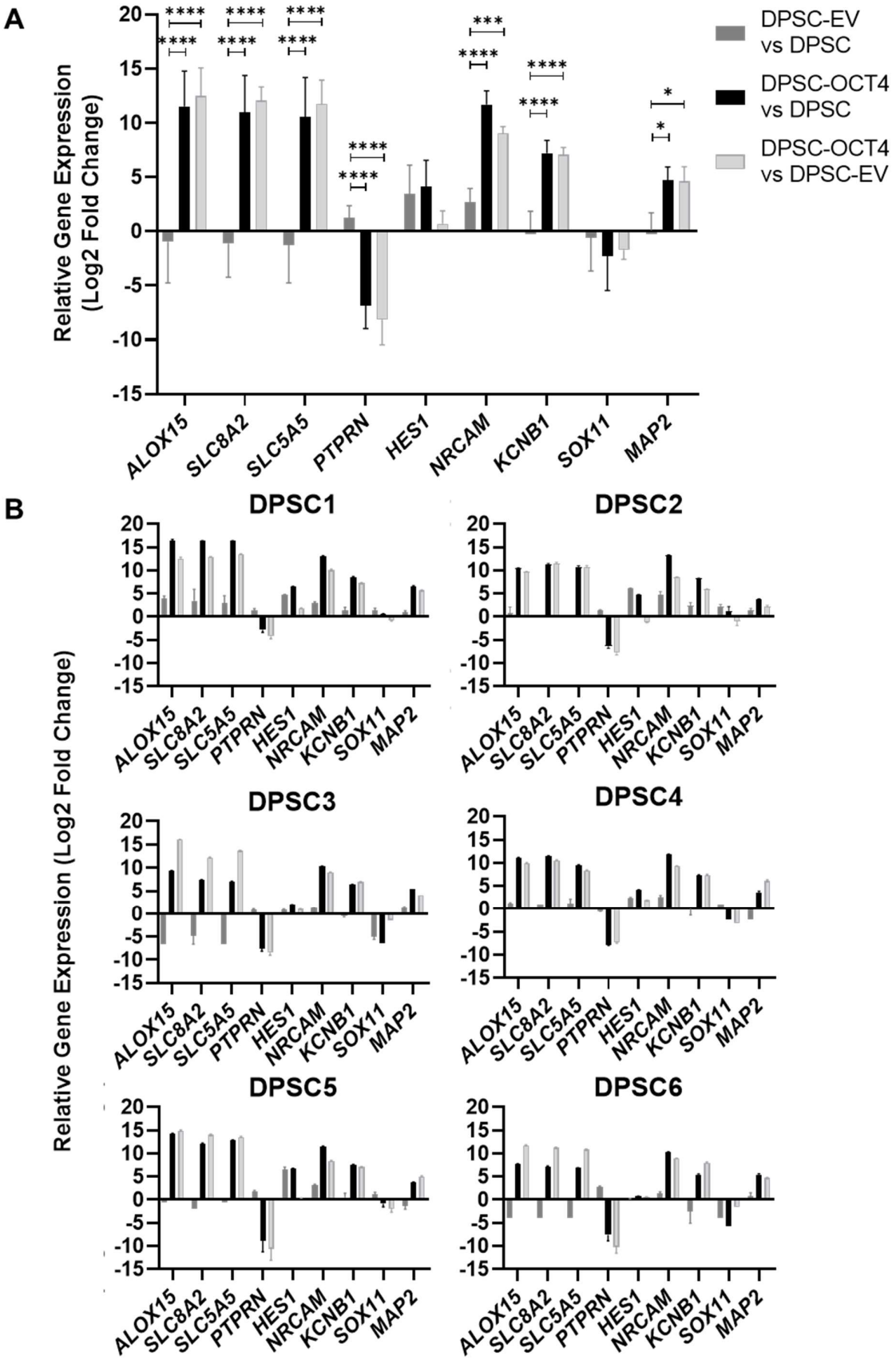
A
Relative Gene Expression (Log2 Fold Change)
DPSC-EV vs DPSC
DPSC-OCT4 vs DPSC
DPSC-OCT4 vs DPSC-EV
ALOX15
SLC8A2
SLC5A5
PTPRN
HES1
NRCAM
KCNB1
SOX11
MAP2
B
Relative Gene Expression (Log2 Fold Change)
DPSC1
DPSC2
DPSC3
DPSC4
DPSC5
DPSC6

Figure 6.4 Validation of selected genes. Gene expression levels in DPSC (standard DPSC culture conditions), and DPSC-EV and DPSC-OCT4 (neural inductive conditions). Three comparisons were made: DPSC-EV relative to DPSC, DPSC-OCT4 relative to DPSC, and DPSC-OCT4 relative to DPSC-EV. **(A)** Average of biological replicates and **(B)** individual samples. Data represents mean±SD, two-way ANOVA with Sidak's multiple comparisons test, n=6, $p<0.05$, *$p<0.05$, ***$p<0.001$, ****$p<0.0001$.

6.3.7 Similarity with NSC

Since the project aim was to reprogram the DPSC into NSC, the expression of the selected validation genes was compared to the expression levels in NSC. Three NSC populations were examined: foetal brain (cortical)-derived NSC, ESC-derived NSC, and iPSC-derived NSC. These would provide an overview of how the reprogrammed DPSC compare with NSC from early and late stages of development (ESC-derived NSC and foetal brain (cortical)-derived NSC), and with cells that have undergone successful indirect reprogramming (iPSC-derived NSC).

The three NSC populations showed great similarity with one another in the expression levels of the selected genes (Figure 6.5). All of the genes were up-regulated, with the exception of *PTPRN*, which showed smaller fold changes. The expression levels of *ALOX15*, *SLC8A2* and *SLC5A5* were up-regulated in the NSC relative to the control DPSC, with higher expression levels than DPSC-EV but lower than DPSC-OCT4. However, in DPSC1, which was sequenced, DPSC1-EV displayed similar expression levels to the NSC, while DPSC1-OCT4 displayed elevated expression levels. The *PTPRN* levels were decreased in DPSC-OCT4 while the levels in DPSC-EV were similar to the NSC samples, in particular with the ESC- and foetal-derived NSC, with little change observed but in the same direction. Whereas the *PTPRN* levels in the reprogrammed cells (iPSC-derived NSC and DPSC-OCT4) showed a decrease. *HES1* showed the most similar levels between the NSC and DPSC-EV and DPSC-OCT4. On the other hand, *SOX11* levels were completely different. This gene displayed high levels in the NSC, while DPSC-EV and DPSC-OCT4 had low levels, as with the RNA-sequencing data. *NRCAM* and *KCNB1* levels were similar in DPSC-OCT4 and NSC, whereas DPSC-EV was lower by more than half. Similarly, *MAP2* levels were high in NSC, with DPSC-OCT4 expression levels closer than DPSC-EV.

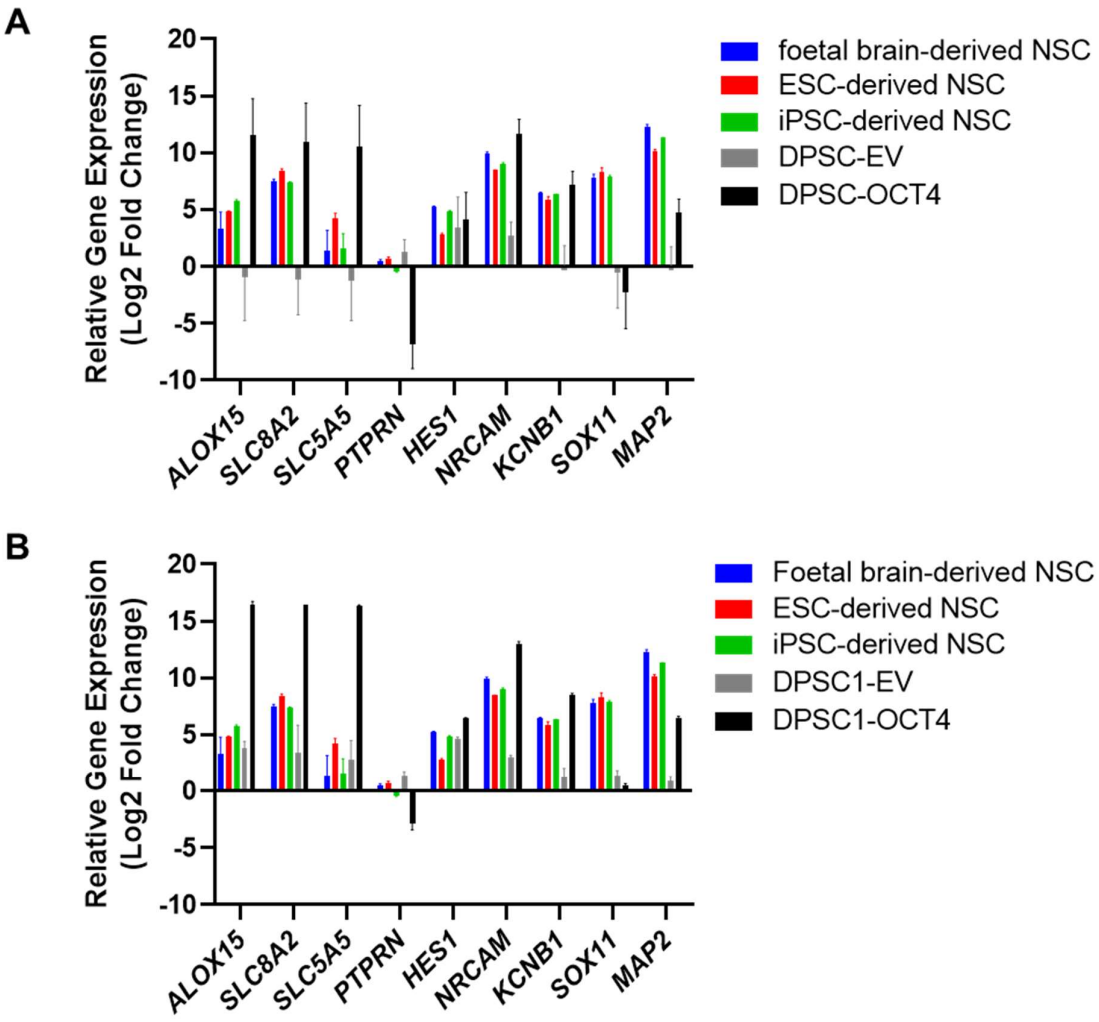

Figure 6.5 Gene expression levels in DPSC and NSC. NSC populations include cortical foetal brain-derived NSC, ESC-derived NSC and iPSC-derived NSC. Gene expression levels were expressed relative to the DPSC control. **(A)** All biological replicates of DPSC. **(B)** Only DPSC1, which was used for RNA-sequencing. Data represents mean±SD, n=6.

6.3.8 Functional enrichment analysis of the DEGs

The DEGs were applied in post hoc functional enrichment analyses, in order to understand the biological relevance. This was done by searching the DEG lists for each comparison against the GO and KEGG pathway databases, to test for an over-representation of particular terms.

Enrichment analysis using the GO and KEGG pathway databases demonstrated that the DEGs in DPSC-OCT4 relative to DPSC and DPSC-EV were enriched for processes, functions, components and pathways related to the nervous system. For the control comparison of DPSC-EV relative to DPSC, the up-regulated DEGs were related to adhesion, migration and motility, while the down-regulated DEGs were associated with the cell cycle (Table 6.6). The top ten enriched GO biological process terms for the up-regulated DEGs of the DPSC-OCT4 versus DPSC comparison included nervous system development, neurogenesis and generation of neurons (Table 6.7). These DEGs were also associated with neuronal cellular component terms, such as neuron part and synapse, and molecular functions including membrane transporters and ion channel activity (sodium, potassium, calcium). Similar to the DPSC-EV versus DPSC comparison, the down-regulated DEGs were associated with the cell cycle (Table 6.7). The DPSC-OCT4 versus DPSC-EV comparison also showed that the up-regulated DEGs were related to neural function and components (Table 6.8).

Table 6.6 GO annotations of DEGs in DPSC-EV relative to DPSC. The top ten up-regulated and down-regulated terms in the biological processes category are listed.

GO Biological Process	Number of Genes	Total Genes	Enrichment FDR
Up-regulated			
Regulation of multicellular organismal process	76	3382	4.60E-09
Cell adhesion	47	1541	4.80E-09
Biological adhesion	47	1548	4.80E-09
Anatomical structure morphogenesis	66	2785	6.00E-09
Cell migration	45	1506	1.30E-08
Locomotion	52	1921	1.30E-08
Cell motility	46	1670	8.20E-08
Localisation of cell	46	1670	8.20E-08
Movement of cell or subcellular component	53	2139	1.10E-07
Extracellular matrix organisation	21	392	1.20E-07
Down-regulated			
Cell cycle	153	1957	1.10E-74
Mitotic cell cycle	117	1068	3.30E-70
Mitotic cell cycle process	108	920	2.50E-67
Cell cycle process	126	1468	4.70E-64
Cell division	82	633	5.10E-53
Chromosome segregation	62	334	6.30E-49
Nuclear division	68	454	1.40E-47
Organelle fission	69	498	4.60E-46
Mitotic nuclear division	57	298	1.20E-45
Chromosome organisation	97	1293	2.40E-42

Table 6.7 GO annotations of DEGs in DPSC-OCT4 relative to DPSC. The top ten up-regulated and down-regulated terms in the biological processes category are listed.

GO Biological Process	Number of Genes	Total Genes	Enrichment FDR
Up-regulated			
Regulation of multicellular organismal process	195	3382	6.30E-28
Anatomical structure morphogenesis	162	2785	1.40E-22
Nervous system development	149	2474	5.40E-22
Regulation of multicellular organismal development	136	2138	5.50E-22
Regulation of developmental process	158	2763	1.80E-21
Cell development	137	2230	6.40E-21
Generation of neurons	107	1575	7.70E-19
Neurogenesis	111	1683	1.00E-18
Regulation of signalling	189	3952	8.10E-18
Regulation of nervous system development	78	953	8.10E-18
Down-regulated			
Cell cycle	140	1957	2.80E-49
Mitotic cell cycle	104	1068	4.40E-47
Mitotic cell cycle process	97	920	9.50E-47
Cell cycle process	114	1468	1.60E-42
Nuclear division	65	454	2.50E-38
Organelle fission	66	498	5.70E-37
Cell division	73	633	5.70E-37
Chromosome segregation	56	334	1.20E-36
Mitotic nuclear division	52	298	8.10E-35
Regulation of cell cycle	91	1298	1.00E-29

Table 6.8 GO annotations of DEGs in DPSC-OCT4 relative to DPSC-EV. The top ten up-regulated and down-regulated terms in the biological processes category are listed.

GO Biological Process	Number of Genes	Total Genes	Enrichment FDR
Up-regulated			
Regulation of multicellular organismal process	101	3382	9.10E-12
Nervous system development	77	2474	3.80E-09
Regulation of multicellular organismal development	69	2138	7.00E-09
Cell development	71	2230	7.00E-09
Ion transport	61	1775	9.20E-09
Anatomical structure morphogenesis	81	2785	9.30E-09
Generation of neurons	56	1575	1.40E-08
Neurogenesis	58	1683	1.80E-08
Regulation of localisation	82	2905	1.80E-08
Multicellular organismal signalling	19	205	1.80E-08
Down-regulated			
Regulation of cell proliferation	33	1756	9.90E-07
Cell proliferation	36	2165	1.70E-06
Positive regulation of cell proliferation	24	1022	1.70E-06
Movement of cell or subcellular component	34	2139	6.10E-06
Cell migration	28	1506	6.10E-06
Locomotion	32	1921	6.10E-06
Regulation of localisation	40	2905	8.90E-06
Cell motility	29	1670	8.90E-06
Localisation of cell	29	1670	8.90E-06
Leukocyte migration	15	491	2.30E-05

The KEGG pathway analysis revealed that the up-regulated DEGs in DPSC-OCT4 were annotated to multiple signalling pathways, including Wnt, PI3K-Akt, cAMP, cGMP-PkG, Ras, calcium and neurotrophin (Figure 6.6). Some of these (Wnt, PI3K-Akt) were enriched in DPSC-EV but were further enriched in DPSC-OCT4.

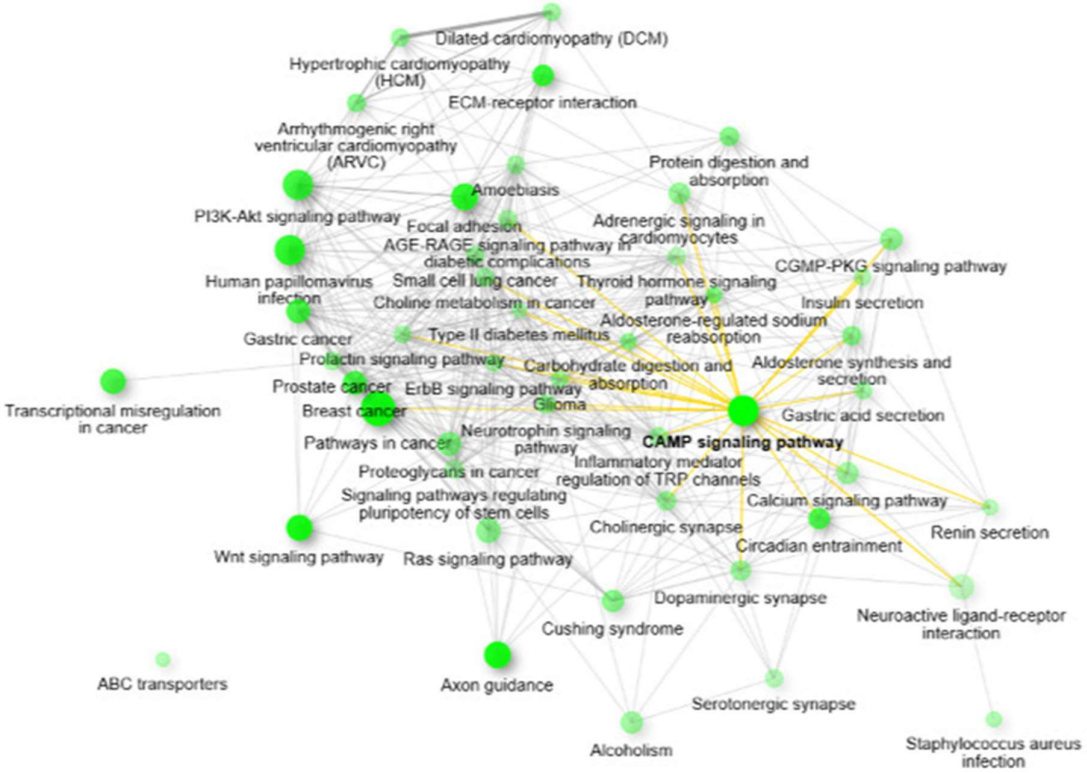

Figure 6.6 Network diagram of enriched KEGG pathways by up-regulated DEGs in DPSC-OCT4 relative to DPSC. The top 50 terms are shown. Two pathways (green circles) are connected if they share at least 20 per cent of genes. Bigger circles represent larger gene sets, and darker circles are more significantly enriched than lighter circles. Thicker connecting lines represent more overlapped genes. The top five pathways are: cAMP signalling pathway (highlighted), Wnt signalling pathway, axon guidance, pathways in cancer, and focal adhesion.

Notably, enrichment for neurotrophin signalling was present in DPSC-OCT4 relative to both DPSC and DPSC-EV (Figure 6.6). The DEG lists were filtered for genes involved in neurotrophin signalling. The heat map in Figure 6.7 displays the levels in the three groups. Compared to the control groups, DPSC-OCT4 displayed up-regulated expression levels, as seen by the warmer colours. The genes detected that are involved in the pathway encode for neurotrophin receptors (NTRK2, NTRK3 and NGFR), neurotrophins (NGF), and components of connecting signalling pathways (e.g. MAPK and PI3K signalling pathways). The notch signalling pathway is another important pathway in the neural system that was examined (Figure 6.8). The DEGs were filtered for a list of genes involved in the notch signalling pathway, with an overall up-regulation observed in DPSC-OCT4, and similarity between the controls. The gene products included ligands, co-activators, regulators, and targets, including HES1 and components of the Wnt signalling pathway, which often act synergistically. Genes annotated to the calcium signalling pathway, important for neurotransmission, were also detected (Figure 6.6).

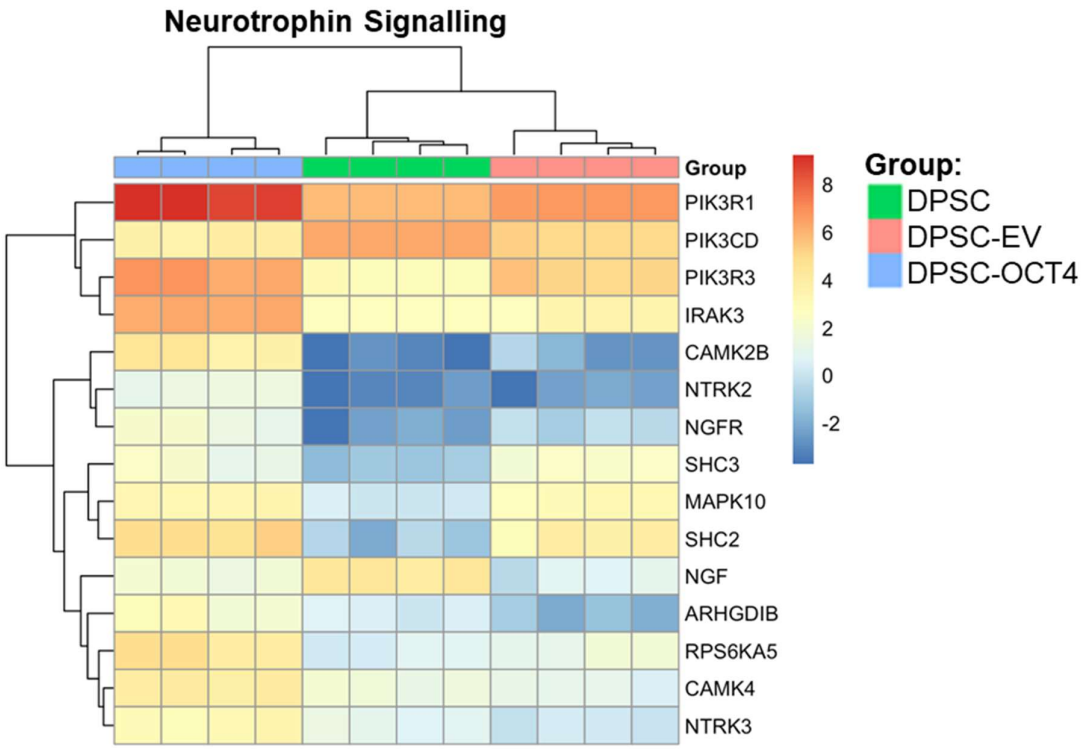

Figure 6.7 Genes involved in the neurotrophin signalling pathway. The control groups DPSC and DPSC-EV were more similar to each other than with DPSC-OCT4.

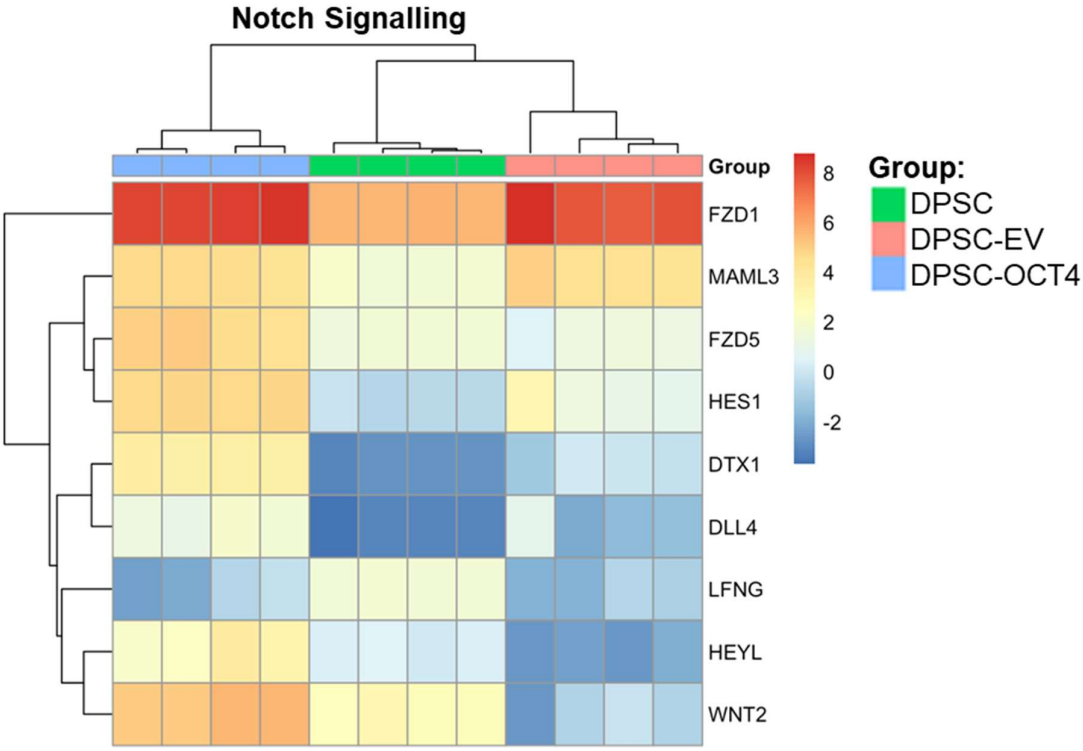

Figure 6.8 Genes involved in the notch signalling pathway. The control groups DPSC and DPSC-EV were more similar to each other than with DPSC-OCT4.

Additionally, axon guidance, an important stage in neuronal network formation, was enriched for in DPSC-EV and further enhanced in DPSC-OCT4 (Figure 6.6 and 6.9). Furthermore, DPSC-OCT4 was enriched for genes associated with dopaminergic, cholinergic, serotonergic and GABAergic synapses (Figure 6.6). The DEGs were also filtered for genes involved in gated channel activity (Figure 6.10). The controls were more similar, with DPSC-OCT4 displaying more up-regulated genes involved in transmembrane transport via channels that respond to specific stimuli, including voltage-gated ion channels and neurotransmitter channels.

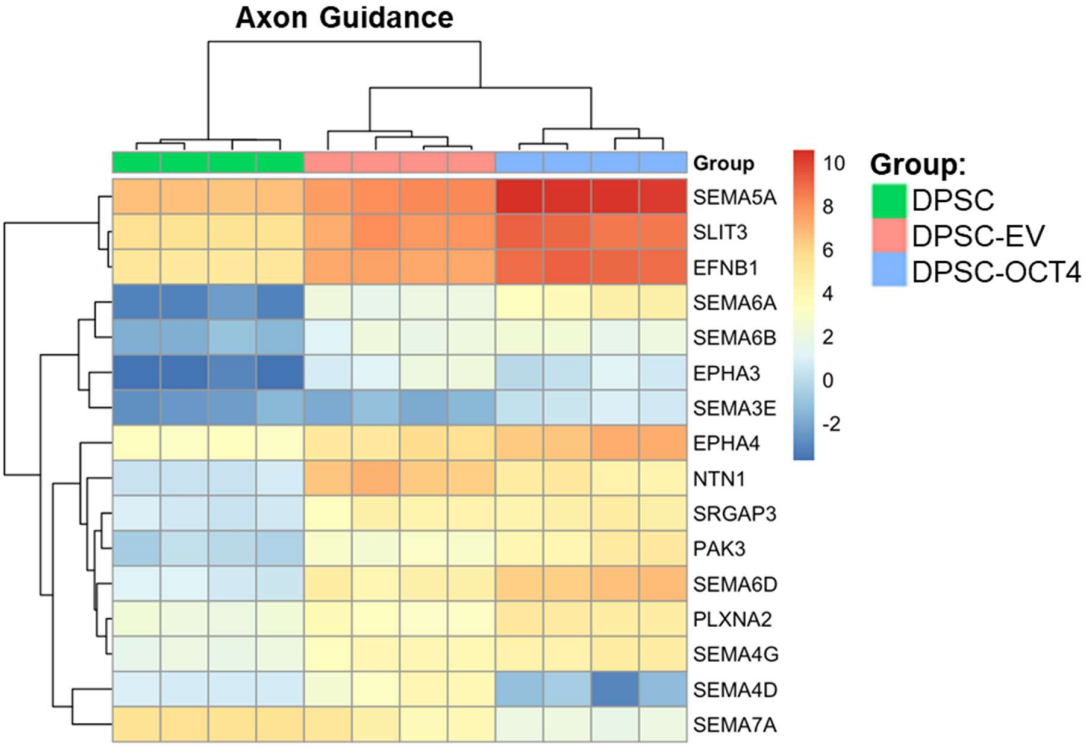

Figure 6.9 Genes involved in axon guidance. The DPSC-EV and DPSC-OCT4 groups showed more similarity.

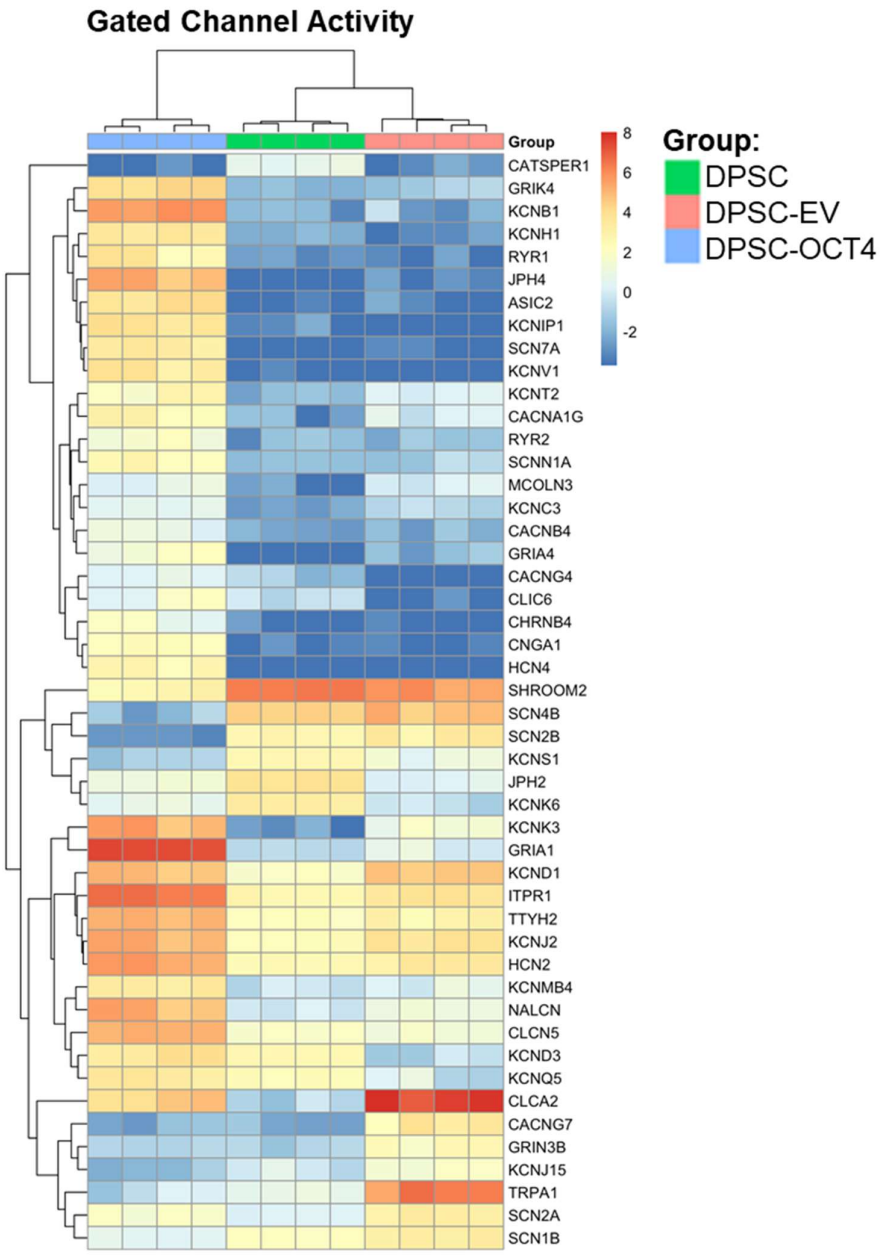

Figure 6.10 Genes involved in gated channel activity. The control groups DPSC and DPSC-EV were more similar to each other than with DPSC-OCT4.

6.4 | Discussion

By performing transcriptomic analysis we were able to examine the changes in the DPSC in response to OCT4 over-expression in neural inductive conditions.

The RNA-sequencing data demonstrated that the sample groups had distinct transcriptional profiles. The neural inductive conditions altered the transcriptome of the DPSC, with some DEGs annotated to several neural-related terms. However, the OCT4 over-expression under these neural inductive conditions further altered the transcriptional profile of the DPSC, enhancing their neural association. This was evidenced by the functional enrichment of many terms and pathways associated with the CNS, neurogenesis and neuronal cells. The two control groups, DPSC and DPSC-EV, were in many ways similar to one another, whilst DPSC-OCT4 was different to both controls. DPSC-OCT4 also showed some similarity with NSC.

The panel of genes selected for qPCR validation included genes whose expression levels in brain tissue range from low to high, with some restricted to specific regions. The genes included encode for transporter proteins, transcriptional factors involved in neurogenesis, and proteins relevant to neuronal cell processes. The RNA-sequencing and qPCR data were reasonably consistent with regard to direction of gene expression and fold change ranges. Most of these genes showed a change in response to the OCT4 over-expression. The data suggested that the up-regulation of *ALOX15*, *SLC8A2*, *SLC5A5*, *NRCAM*, *KCNB1* and *MAP2* and down-regulation of *PTPRN* was a result of the OCT4 over-expression in DPSC. There were small changes in the expression level of *SOX11*.

Variation was also observed in *HES1* expression. The qPCR data indicated that *HES1* is mostly up-regulated in response to the neural inductive conditions, with only a small increase in response to OCT4 over-expression. The RNA-sequencing data suggested that the levels were increased in response to the neural inductive conditions, though not detected between DPSC-EV and DPSC using the cut-off parameters, and then further increased in DPSC-OCT4, as seen by the up-regulation in fold change relative to DPSC (logFC=5.3) and DPSC-EV (logFC=3.1). Combined, the data suggested that both the neural inductive conditions and OCT4 over-expression had a role in increasing *HES1* expression levels, but that OCT4 was not the main contributing factor. This gene showed more variation between the biological samples and the expression changes. Three of the samples (DPSC1, DPSC3 and DPSC4) showed an increase in response to the neural inductive conditions and OCT4 over-expression, two of the samples

(DPSC2 and DPSC5) showed an increase in response to the neural inductive conditions, and one sample (DPSC6) showed a small increase in response to OCT4 over-expression.

The genes that were most up-regulated and down-regulated based on the RNA-sequencing were most consistent in the qPCR analysis. The five different biological replicates correlated indicating that subsequent biological conclusions based on the RNA-sequencing data could be made with confidence. The inclusion of DPSC1 in the qPCR analysis provided validation for the technology.

The validation genes were all detected and up-regulated in the three types of NSC, with the exception of *PTPRN*, which showed minor changes in gene expression. The expression levels of *HES1* in DPSC-EV and DPSC-OCT4 were similar with that of the NSC. *HES1* is a transcription factor that has a role in NSC and neurogenesis, and is a marker of NSC (23). It was thus a promising result that the expression levels were similar in the DPSC groups. However, *HES1* expression appeared to be a result of the neural inductive conditions, while the effect of OCT4 over-expression was minor. *SOX11* is another transcription factor with a role in neurogenesis and as such it was detected in the NSC (127). It was surprising that the RNA-sequencing showed that both DPSC-EV and DPSC-OCT4 had down-regulated expression levels of *SOX11*. This was validated with the qPCR. These similarities and differences to NSC suggested that the DPSC were directed along the neural lineage but there remain differences in comparison to NSC gene expression indicating variation in specific NSC genotyping still exists.

It was also interesting to see that genes with a greater role in neuronal cells, such as *NRCAM*, *MAP2* and *KCNB1*, were also detected in the NSC, and at higher fold changes than *HES1*, which is well known for its role in maintenance of the NSC pool (23). These genes would be expected in more mature cells restricted to the neuronal lineage (98). This highlights the difficulty in classifying NSC and establishing a panel of genes that can distinguish neural cells at different stages of development and maturity (22, 98). Overall, the DPSC-OCT4 samples showed similar levels to the NSC in the expression of *HES1* and the more mature, neuronal genes.

The functional enrichment analysis demonstrated that the neural inductive conditions lead to a down-regulation in genes associated with cell proliferation. This was observed in both DPSC-EV and DPSC-OCT4. This would be expected in cells becoming more restricted to a specific lineage and thus differentiating from a stem cell state (99). The OCT4 over-expression under these neural inductive conditions lead to an increase in genes associated with the nervous

system and neurons. Some neural terms were observed in DPSC-EV, however these were fewer and less enriched. This suggested that the neural conditions had some effect and OCT4 over-expression significantly enhanced this effect. The DEGs were enriched for genes involved in many of the signalling pathways, most of which have wide-spread roles in cell growth, cell differentiation, gene transcription and protein translation. As such, many signalling pathways are interconnected. It was therefore no surprise that many genes were also annotated to cancer related pathways.

Importantly, the neurotrophin signalling pathway was enriched in DPSC-OCT4 relative to both controls. Neurotrophin signalling is important for neuronal development, survival and function (98, 128). The neurotrophin family consists of nerve growth factor, brain-derived neurotrophic factor, neurotrophin-3 and neurotrophin-4. They bind to tyrosine kinase receptors and nerve growth factor receptor. Several of these were present in the DEG lists. Notch signalling is also important in the development of the CNS and is also present in the adult brain (129, 130). It is crucial for neural stem and progenitor cell maintenance, and inhibition of notch signalling leads to neural differentiation. Growth factors, such as bFGF and EGF, promote notch signalling, hence why they are supplemented in culture medium for NSC.

Enrichment was also observed for the calcium signalling pathway, axon guidance and gated channel activity. The calcium signalling pathway is important for neurotransmission (99). Axon guidance is important for neuronal development (128). Axons are guided by a variety of factors, including ephrins, netrins, slits and semaphorins. These factors are sensed by the growth cone receptors leading to signal transduction and cytoskeletal changes. These were enriched for in DPSC-EV and further enriched in DPSC-OCT4. Gated channel activity is another enriched group of importance, which includes many voltage-gated and ligand-gated channels that are involved in signal transduction in neurons (99).

These observations supported the hypothesis that OCT4 plays a role in plasticity. The environmental conditions had some effect on the DPSC, but the effect was significantly different when OCT4 was over-expressed. This was similar to previous research that demonstrated OCT4-induced plasticity allowed fibroblasts to respond to changes in the extracellular environment (12). A similar response had been anticipated in the DPSC, since both have hallmarks of the neural lineage. The OCT4 over-expressing, neural-induced DPSC had increased expression of genes associated with many neural and neuronal processes. Rather importantly, there were genes more relevant to neuronal processes. This aligns with the results

in Chapter 5, suggesting the cells are not as immature as NSC but more likely restricted to the neuronal lineage and may be neuronal progenitor-like or immature neuronal-like.

Whilst the RNA-sequencing was performed using DPSC samples from one donor, we ensured that the experiment was set up such that reliable results were obtained. The DPSC1 sample was used to obtain DPSC, DPSC-EV and DPSC-OCT4, and each of the three groups had four biological replicates with good quality RNA input. With the need for at least three replicates per group, this increased the likelihood of a successful output. As was seen, all four replicates clustered well, with no need to exclude samples from downstream analysis. With regard to primary cells such as these, there are biological differences between samples from different donors that would be evident upon RNA-sequencing and lead to difficulty in detecting significant DEGs. It is thus necessary to analyse biological samples separately in order to detect differences. Here, significant DEGs were detected and a selection of genes for qPCR validation showed that the trends and fold changes were similar in DPSC from multiple other donors. Other experimental groups that would be informative include DPSC-EV and DPSC-OCT4 in standard DPSC culture conditions, to better observe the effect of the vectors. DPSC-EV in standard conditions would be expected to be similar to non-modified DPSC in standard conditions (included here). Additionally, DPSC following neural induction would show the effect of the neural inductive conditions with no genetic manipulation, and would be expected to be similar to DPSC-EV following neural induction (included here). Further analysis could also include a neuronal population for comparison.

RNA-sequencing of these samples provided information on how the neural inductive conditions and OCT4 over-expression altered the transcriptome of human DPSC. The DPSC cultured in neural inductive conditions were different to DPSC in standard conditions. However, the OCT4 over-expressing, neural-induced DPSC were significantly different to both controls and showed up-regulation of many neural-related genes and enrichment for neural terms and pathways. Combined with the results of Chapter 5, this transcriptomic analysis provides support for the neural conversion of the DPSC and the resemblance to neuronally-restricted cells.

CHAPTER 7

RESPONSE OF OCT4 OVER-EXPRESSING, NEURAL-INDUCED HUMAN DENTAL PULP STEM CELLS IN A DEVELOPMENTAL AVIAN MODEL

7.1 | Introduction

The chicken (*Gallus gallus*) embryo is a classical animal model for studying normal vertebrate embryogenesis, and has a history of being used as a model for xenotransplantation to study the behaviour of mammalian cells *in vivo*. The chicken embryo has been studied extensively at the anatomical, cell biological and molecular levels. The developmental stages have been well characterised, allowing for experimental standardisation (131).

There are multiple advantages of using the chicken embryo as a model for xenotransplantation (132). The cost is low and fertilised eggs are highly accessible. The handling of embryos is easy with visualisation and manipulation of the embryo occurring through a 'window' in the egg shell, and the injections are made under visual rather than stereotaxic control. The embryos are able to continue development *in ovo*, and with a 21-day incubation period, there is the potential to generate large amounts of data in a timely manner. The lack of a fully developed immune system allows investigation of human cells with no rejection. There is also a low level of ethical concern due to minimum welfare cost to the animal; there is no need to kill the mother in order to harvest the embryos and experiments can be performed before or up to day 10 which is when pain perception develops. This is a good 'first port-of-call' system to determine if the cells of interest are promising, before venturing into costly and timely mouse studies, with a greater impact on animal welfare.

The disadvantages of using chicken embryos relate to their small size and differences to mammals (132). In terms of size, they are poor models for human organs. In terms of physiology and anatomy, their similarity to humans is organ specific. They have features not found in mammals. However, the basic organisation of many organs is similar, particularly the brain (133). Additionally, it has been suggested that they have similarity to humans with regard to bipedal locomotion, compared to quadrupedal rodent models.

The chicken embryo has been used to study stem cells (1, 134-136). Xenotransplantation of stem cells into chicken embryos can provide information about survival, proliferation, migration, differentiation, integration, response to microenvironment, and tumorigenic potential. This model has been used to examine the neurogenic potential of stem cells following transplantation into neural anlage. For example, human ESC-derived neural crest stem cells and neurons have been transplanted, resulting in integration and differentiation into appropriate phenotypes (137-139). This model has also highlighted the neuroplasticity of somatic stem cells, including DPSC (140). Thus, the chicken embryo provides a convenient platform for the

in vivo characterisation of human stem cells. This model can be used as a step towards transplantation experiments in other animal models, to identify neural cells for replacement therapy of a variety of neurological diseases.

Previous research examined the response of human DPSC in the chicken embryo (1, 140). DPSC injected at developmental stages 10 to 12 acquired a neuronal morphology and localised to regions similar to endogenous cranial neural crest stem cells (1). At 48 hours post-injection, the DPSC co-localised with neuronal markers, β-III tubulin and NF-M (1). The DPSC were also shown to induce neuroplasticity (140). DPSC are known to secrete neurotrophic factors, including nerve growth factor, brain-derived neurotrophic factor, and glial-derived neurotrophic factor (141, 142). Neurotrophic factors are involved in neuronal growth and survival. In the chicken embryo, chemo-attraction of trigeminal ganglion axonal outgrowth was mediated in part via the CXCL12 chemokine, also known as stromal cell-derived factor-1, secreted by the DPSC and the cognate receptor CXCR4 expressed on the axons (140). This interaction has been shown to be involved in axonal guidance in the nervous system (143, 144).

The aim of this chapter was to analyse the capacity of the OCT4 over-expressing, neural-induced DPSC to survive and neuronally differentiate *in vivo* during development of the nervous system. They were compared to; empty vector-transduced DPSC, expected to be most similar to non-modified DPSC; empty vector-transduced DPSC post neural induction, to show the effect of the culture conditions; and OCT4 vector-transduced DPSC, to show the effect of OCT4 over-expression. If the injection conditions are favourable, with cells being injected into the right area at the right time, cells can be incorporated into derivatives of endogenous cells, such as neural crest-derived peripheral ganglia. As with the previous research, the DPSC were injected in the peripheral tissue directly adjacent to the developing hindbrain, more specifically the anterior region of the hindbrain, of the chicken embryo between developmental stages 10 to 12 (1, 131, 140). The location and timing coincide with endogenous cranial neural crest stem cell activity (145).

During vertebrate embryogenesis, the ectodermal germ layer develops into the surface and neural ectoderm, with the latter forming the neural tube and the neural crest. The neural crest is a multipotent, transient embryonic neural-derived cell population that arises at the dorsal margins of the neural tube. The neural tube forms the CNS while the neural crest stem cells migrate and contribute to the peripheral nervous system and peripheral tissues according to environmental signals and their position on the anterior-posterior axis (cranial, trunk, vagal and

sacral, and cardiac). The cranial neural crest arises in the anterior and contributes to craniofacial tissues, sensory nerve ganglia, Schwann cells and melanocytes (146).

In the developing hindbrain, the cranial neural crest stem cells reside in rhombomeres, which are transient segments of the neural tube. The cranial neural crest stem cells in rhombomeres 1 to 3 migrate from the hindbrain into the surrounding tissue to contribute to the formation of the trigeminal ganglion (located near rhombomere 2), the first branchial arch (corresponds to first pharyngeal arch) and the surrounding facial structures (133, 146). The trigeminal ganglion contains the trigeminal nerve (fifth cranial nerve). It is bilateral and bilobed, with the first lobe forming the ophthalmic nerve (sensory) and the second lobe bifurcating and forming the maxillary (sensory) and mandibular (sensory and motor) nerves (133). The trigeminal ganglion and its three branches provide sensation in the face and motor functions involved in eating. In the chicken embryo, the trigeminal ganglion begins to develop at stage 12, with the migration and condensation of the cranial neural crest stem cells and cells of placodal origin (area of ectodermal thickening in the cranial region) (147). Therefore, by injecting cells into this area by stage 12, the cells can be incorporated into the pathways followed by the endogenous cranial neural crest stem cells and their response examined amongst the well-structured trigeminal ganglion and its branches (1, 131, 133, 140, 145, 146). The embryos are staged by examining external features such as the number of somites, the clarity of the brain vesicles, and the turning of the head (131).

7.2 | Materials and Methods

7.2.1 DPSC Preparation

The DPSC transduced with the empty vector or the OCT4 vector were either maintained in standard DPSC culture conditions or cultured using the multi-step neural induction protocol as detailed in Chapter 5, section 5.2.1, pg. 101 (Figure 5.1B, pg. 102). The cells were all GFP^+. Following staging and preparation of the embryos (see below), the GFP^+ DPSC were prepared for injection in an efficient manner. The cells were harvested and counted per standard protocol. The concentration was adjusted to $5x10^3$ cells/µL in culture medium, and fast green FCF dye (0.1% (w/v) in water, 0.22µm filtered) was added to the cells to help visualise them during the injection procedure. The cells were drawn up in a 1mL syringe attached to a needle (22G or smaller, in order to fit into the glass needle) (Terumo, Tokyo, Japan) and expelled into a glass needle. The glass needles were pulled from thin wall borosilicate glass with filament capillaries (SDR Scientific Pty Ltd, NSW, Australia) using a conventional electrode micropipette puller (Sutter Instrument Co, CA, USA). The puller settings used were: P=500, heat=850, pull=empty, vel=100, time=200. From one micropipette, two needles were obtained with approximately 1-1.5cm tips. Once in the glass needle, the cell solution remained near the top and needed to be guided to the bottom of the needle. The method to do this can be varied; here the needle was briefly centrifuged (200 x *g*, 5-10 seconds) to direct the cells to the tip of the needle but not force them to aggregate. During the injection procedure, the cell solution was kept on ice.

7.2.2 Chicken Embryo Staging and Preparation

Ethical approval (SAM126) was obtained from the South Australian Health and Medical Research Institute, SA, Australia. Freshly fertilised White Leghorn chicken eggs (HiChick Breeding Company Pty Ltd, SA, Australia) were placed long-ways (for easier manipulation) in egg trays and incubated in a 37°C (37-39°C is suitable) humidified (approximately 60% relative humidity) incubator (Hybaid Hybridisation Oven, Thermo Scientific, MA, USA) for approximately 40 hours to reach embryonic stages 10-12 (131). Eggs that were not required immediately (on the same day as fertilisation) were placed in a modified-temperature fridge of approximately 15°C (15-18°C is suitable) to pause development up to a maximum of one week. If stored for longer or at lower temperatures, the rate of subsequent development and survival decreases. When resuming development, eggs were pre-warmed to RT prior to being placed in the incubator.

Following incubation, eggs were wiped over with 70% ethanol. Before opening the egg, an air pocket was created above the embryo to separate it from the inner surface of the egg shell (148).

Using an 18G needle attached to a 10mL syringe, the egg shell was pierced at the blunt end of the egg, gently to avoid cracking the egg shell and not too deeply to avoid disrupting the yolk. About 3mL of albumin was drawn into the syringe and extracted from the egg. The hole was then sealed with tape (3M Scotch Magic tape). If an insufficient volume of albumin is extracted, the yolk may remain stuck to the egg shell, and will be disrupted once the egg is opened.

Tape was placed on top of the egg to add support to the egg shell and prevent fragments from falling onto the embryo when creating an opening (148). A round window was cut into the top of the egg (Figure 7.1A). Some eggs can be rather fragile, so care must be taken when applying pressure during the cutting of the opening. The embryo lies on the surface of the yolk. If the embryo was not sitting at the top when opened, the yolk was gently rotated to avoid disrupting it while locating the embryo and positioning it at the top. Any air bubbles from the air pocket were popped using a pipette tip. Unfertilised eggs were discarded.

Embryos were visualised by injecting non-toxic black Indian ink (10% (v/v) in freshly prepared Ringer's solution (7.2g NaCl, 0.17g $CaCl_2$, 0.37g KCl, 0.115g Na_2HPO_4, 5mM HEPES in 1L ddH2O, pH 7.4, 0.22µm filtered and autoclaved)) underneath the embryo to contrast. To do this, the ink was drawn using a 26G needle attached to a 1mL syringe. Air bubbles in the needle and syringe were removed. The needle was angled at 45° and inserted at any point outside the embryonic plate, which is seen as a ring of blood vessels (148). The needle was guided close beneath the embryo and the ink was ejected until the desired contrast was achieved. Piercing within the embryonic plate increases mortality. The embryo could be seen clearly against the dark background, and the stage of development was determined by observation under a dissecting microscope (Wild M3C, Heerbrugg, Switzerland) (Figure 7.1A). A few drops of Ringer's solution were placed on top of the embryo to maintain moisture, and then the embryo was incubated while cells were prepared for injection. Abnormal (undeveloped, delayed development, deformed) embryos were discarded.

7.2.3 Needle Preparation

The glass needle containing the GFP^+ DPSC was secured into the needle holder, which was placed on the micromanipulator (Narishige, Tokyo, Japan). The needle holder was attached to a MPPI-2 pressure injector (Applied Scientific Instrumentation, OR, USA), which was attached to a medical oxygen tank (BOC, NSW, Australia) fitted with a Series-O regulator oxygen yoke and Ezi-Flow Oxygen Flowmeter (BOC, NSW, Australia). The pressure injector settings were: mode of operation=pulse, output pressure=50 PSI, pulse duration=300 ms; and the gas flow rate was set at 1.5 L/minute. While viewing under the dissecting microscope, the tip of the glass

needle was guided into a dish with sterile PBS. The tip of the needle was removed using forceps and adjusted to allow cells to flow through with each pulse of air without clogging the needle (opening too small) or letting them freely flow through with no pressure provided (opening too big). The needle tip needed to be as even as possible around the perimeter of the glass in order to be sharp. The needle had to be adjusted efficiently to prevent cell aggregation, and further adjustments between embryos were usually necessary. The needles were typically discarded after several embryos and a new needle was prepared.

7.2.4 DPSC Injections into Chicken Embryos

The egg was placed under the dissecting microscope. The vitelline membrane was gently removed from around the head of the embryo only, using a sharp clean instrument, e.g. a 25G needle. Embryos that were too young (<stage 10) or too old (>stage 12) at the time of injection were not used and acted as controls. The micromanipulator was used to direct the needle into the embryo in the region adjacent to the developing hindbrain (Figure 7.1B) (1). The needle was carefully positioned above the area of interest. The embryo was then pierced. This motion needed to be rapid in order to reduce the resistance from the embryonic tissue, which caused the embryo to move down and the needle tip would otherwise only dimple the surface rather than pierce through. Care was taken to avoid going too far through to the other side of the embryo, as injected cells would be able to flow out and embryo viability would be affected. To avoid this, at the moment the needle penetrated, it was pulled back as the embryo gave in to the pressure. In some embryos, the needle tip once inside could be clearly seen.

Cells were then injected into the embryo using a foot pump/pulse button attached to the pressure injector. In some embryos, a white clump of cells could be clearly seen. The gas and pressure injector settings had to be checked frequently, as incorrect pressure increased the difficulty of injecting cells. The glass needle was removed and a few drops of Ringer's solution were placed on top of the embryo to prevent it from drying. The egg was sealed with tape and placed back in the incubator for 48 hours (1). The egg needed to be taped and positioned well to avoid leakage. In some cases, leakage occurred through the tape, so the egg shell needed to be wiped dry and the tape replaced. It was best to prepare the embryos and inject the cells in a timely manner; this minimised the time outside the incubator, which is important for both cell and embryo viability.

7.2.5 Removing the Tissue of Interest

Following the incubation period (Figure 7.1C), embryos were humanely killed by cutting out of the egg and placing in ice-cold PBS, followed by removal of the aortic sac. Embryos were

then dissected; the head removed and then cut as an open book (from the cranium towards the hindbrain down the length of the head, along the ventral side). To ensure a clean cut down the middle, the embryos needed to be held in place carefully due to being mobile. Tissues were placed in 1.5mL tubes and fixed in 1mL of 4% (w/v) paraformaldehyde (pH 7.4) for either 2 hours at RT or overnight at 4°C, and then washed twice with PBS and stored in PBS prior to immunofluorescence staining (1).

7.2.6 Whole-mount Chicken Embryo Immunofluorescence Staining

Tissue samples were immunostained for GFP, to enhance detection of the selectable marker in the transfer vector, and neuronal markers, to detect neuronally differentiating cells. Following fixation in 4% (w/v) paraformaldehyde (see section 7.2.5), tissue samples were washed 5 times, 5 minutes per wash, with PBS and 0.3% Triton X-100 (PBS-TX). Embryos were then incubated with constant movement in blocking solution (10% normal horse serum in PBS containing 1% Triton X-100) for 5 hours at RT. The solution was then replaced with goat anti-GFP antibody and mouse anti-β-III tubulin clone TUJ1 or anti-NF-M antibodies (Table 7.1) in PBS containing 10% normal horse serum and 0.1% Triton X-100; samples were incubated with constant movement for 24 hours at RT. Embryos were washed with PBS-TX and incubated with donkey anti-goat Alexa Fluor 488-conjugated and donkey anti-mouse Cyanin3-conjugated secondary antibodies (Table 7.1) in PBS containing 10% normal horse serum and 0.1% Triton X-100, overnight at 4°C in the dark with constant movement. Samples were washed with PBS-TX, then stained with DAPI for 10 minutes in the dark at RT, and washed. Samples were then transferred to 80% glycerol; once equilibrated in glycerol (sink to the bottom), the embryos were placed as open books on a microscope slide and cover slipped with Prolong Gold Antifade Mountant with DAPI. Double-sided tape was used to raise the coverslip.

Table 7.1 Antibodies for whole-mount immunofluorescence staining.

Antibody	Species	Stock Concentration	Dilution	Manufacturer	Catalogue Number
Primary Antibodies					
Anti-GFP	Goat	1mg/mL	1:250	Rockland Immunochemicals	600101215
Anti-β-III tubulin TUJ1 clone	Mouse	1mg/mL	1:250	BioLegend	801201
Anti-NF-M	Mouse	0.5mg/mL	1:250	Thermo Scientific	130700
Secondary Antibodies					
Anti-mouse IgG Cyanin3	Donkey	1mg/mL	1:500	Jackson ImmunoResearch	AP192C
Anti-goat IgG Alexa Fluor 488	Donkey	1mg/mL	1:200	Jackson ImmunoResearch	705485147

7.2.7 Cell Imaging

Immunostained whole-mount chicken embryos were imaged using the Nikon Eclipse NI fluorescent microscope using NIS Elements BR4.40 software (Nikon, Tokyo, Japan), to determine which samples contained GFP^+ DPSC and where the cells were located. The samples with cells were then imaged using the Olympus FV3000 confocal microscope and FV31S-SW software (Olympus, Tokyo, Japan) at Adelaide Microscopy (University of Adelaide, SA, Australia). The confocal microscope was used to obtain serial optical slices (z-stack series) at 200x magnification for the blue, green and red channels, captured simultaneously, for each sample. The step size for the z-stacks was set to 5µm, with the average size of the cells being 12µm.

7.2.8 Image Analysis

Confocal image series (z-stacks) were analysed using the Imaris software version 6.3.1 (Bitplane, Zürich, Switzerland). Image series were converted into an Imaris format using the Imaris batch converter. After generating 3D reconstructions from the imaging datasets, analysis using the software's built-in tools and automated options was performed. The spot detection algorithm (Imaris Spots tool application) simplified the counting procedure by assigning spots to the GFP+ DPSC (green channel), i.e. each spot represents a GFP^+ cell. The 'minimum diameter' option was selected for the GFP channel in the algorithm step of the application. Using the measurement point application, the cell width was measured. In most samples, 8µm diameter spots were determined suitable for identifying individual cells and provided the best discrimination between GFP^+ cells and non-specific background labelling or particulate debris. Manipulation of the 3D reconstructed z-stack was essential to ensure the threshold level was correct and to best match the spots to the GFP fluorescence. Each spot was assessed for the mean intensity of β-III tubulin expression (red channel). The threshold for β-III $tubulin^+$ staining was set at a mean channel intensity of 200, i.e. above 200 is β-III $tubulin^+$ and below 200 is β-III $tubulin^-$. This threshold was chosen based on the background intensity and the intensity of GFP^+ cells that appeared β-III $tubulin^-$ across several datasets. During the experiment, samples were identified by numbers, which aided blinding. After analysis, samples were re-identified and sorted into the four groups.

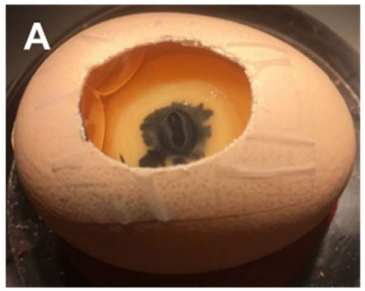

Incubate fertilised eggs to embryonic stage 10-12 (~40 hours), prepare embryos and inject cells.

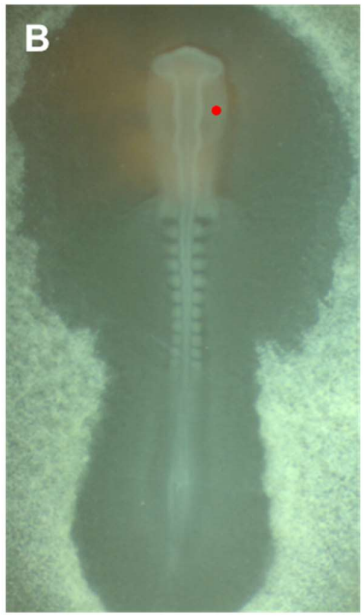

48hr incubation

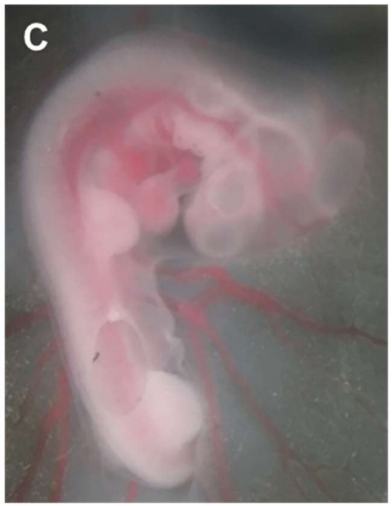

Collect (approx. embryonic stage 23).

Immuno-fluorescence

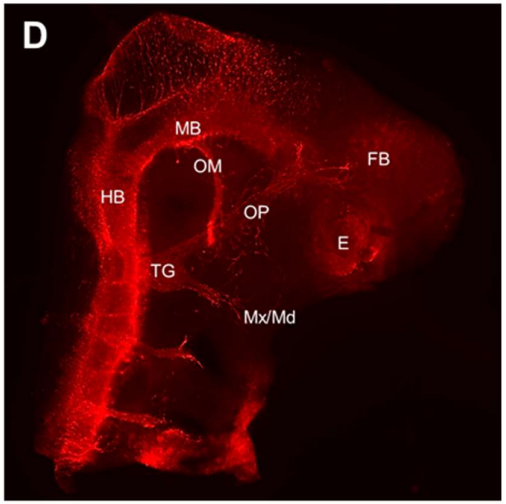

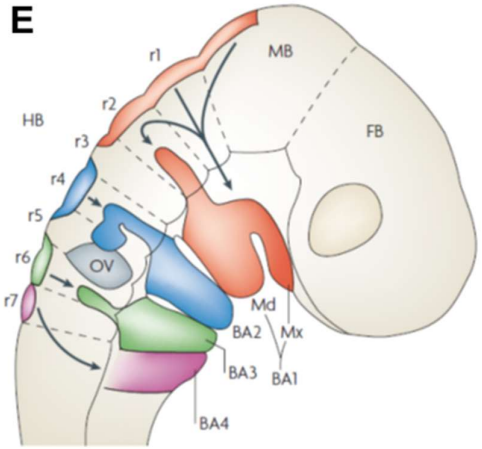

Figure 7.1 Chicken embryo assay workflow. Fertilised White Leghorn chicken eggs were incubated in a 37°C humidified incubator to reach developmental stages 10-12, which takes approximately 40 hours. The embryos and the GFP^+ DPSC were prepared for injection. **(A)** A 'window' was cut out in the egg shell and the embryo was visualised by contrasting with injected ink. **(B)** An embryo at approximately stage 11; the red dot indicates the approximate injection area. **(C)** After two days of incubation, at approximately stage 23, the embryo was collected. **(D)** Whole tissues were immunostained for GFP and a neuronal marker (β-III tubulin or NF-M). Image shows β-III tubulin staining highlighting the structures. The trigeminal ganglion (TG) is located to the left and right of the hindbrain (HB). It is comprised of two lobes that migrate as three separate nerves. The first lobe produces the ophthalmic nerve (OP), which extends above the eye (E). The second lobe splits into two and produces the maxillary nerve (Mx), extending below the eye, and the mandibular nerve (Md), extending into the first branchial arch (BA). The oculomotor nerve (OM) originates from nuclei in the midbrain (MB). FB=forebrain. **(E)** The pattern of neural crest migration in the chicken embryo at day 2 of development (133). The hindbrain consists of rhombomeres (r).

7.3 | Results

7.3.1 Assay efficiency

Freshly fertilised chicken eggs were ordered in dozens, with a total of 17 orders used for the purposes of this thesis. Batches of eggs ranged from a minimum of 3 dozen eggs to a maximum of 15 dozen eggs. Each batch of eggs was used within one week. The average percentage per batch (n=17) of unfertilised eggs was 20±16 and fertilised eggs was 80±16. The eggs were initially used to set up the assay, learn the techniques and optimise the methods.

The data from injected embryos presented in this thesis was obtained from 6 batches of eggs, ranging from 6.5 to 10 dozen eggs per batch, and were used within three days. The subsequent assay efficiency data is based on these 6 batches of eggs from which the experimental data was obtained. There were a total of 592 eggs, with 15±11% unfertilised (n=90) and 85±11% fertilised (n=502) (Figure 7.2A). Of the 502 fertilised eggs, 14±6% (n=71) were abnormal (undeveloped, delayed development, deformed), 5±3% (n=28) were discarded due to human error (e.g. cracked egg shell), 20±7% (n=100) were controls (too young or too old for cell injections by a few hours), and 60±9% (n=303) were experimental (injected with cells) (Figure 7.2B).

Within the 6 batches, there were 17±6 control embryos/batch. Of the controls (n=100), 51±30% survived (n=52 ranging from 2-19/batch) and 49±30% died (n=48 ranging from 3-16/batch) after the 48 hour incubation (Figure 7.2C). Within the 6 batches, there were 51±14 injected embryos/batch. Of the injected embryos (n=303), 35±10% survived (n=107 ranging from 10-30/batch) and 65±10% died (n=196 ranging from 23-49/batch) following the injecting procedure and 48 hour incubation (Figure 7.2D). Some of the injected embryos that survived (n=107) were used to optimise the antibodies (n=17). The remaining embryos (n=90) were double stained for GFP to detect the injected DPSC and β-III tubulin to detect neuronal differentiation. From these samples, 76±15% (n=67) contained GFP^+ cells and 24±15% (n=23) did not contain GFP^+ cells (Figure 7.2E). In total, the final data was obtained from 11% of the initial number of eggs, and 22% of the injected embryos.

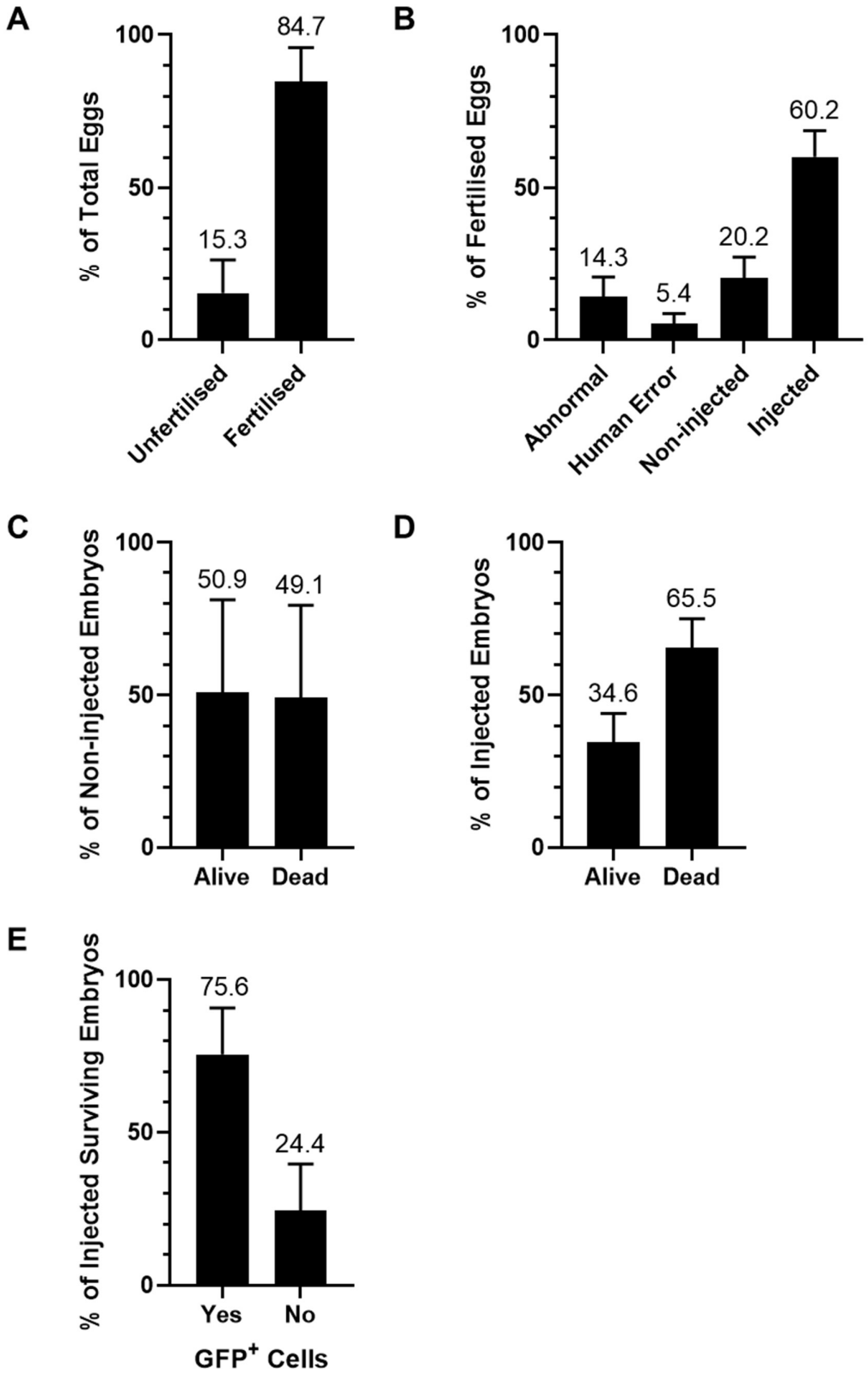
A
% of Total Eggs
100
50
0
15.3
84.7
Unfertilised
Fertilised
B
% of Fertilised Eggs
100
50
0
14.3
5.4
20.2
60.2
Abnormal
Human Error
Non-injected
Injected
C
% of Non-injected Embryos
100
50
0
50.9
49.1
Alive
Dead
D
% of Injected Embryos
100
50
0
34.6
65.5
Alive
Dead
E
% of Injected Surviving Embryos
100
50
0
75.6
24.4
Yes
No
GFP+ Cells

Figure 7.2 Chicken embryo assay efficiency. White-leghorn chicken eggs were used. **(A)** The number of unfertilised and fertilised eggs as a percentage of the total eggs. **(B)** The number of abnormal embryos (undeveloped, delayed development, deformed), embryos discarded due to human error, non-injected embryos (controls), and injected embryos, as a percentage of the fertilised eggs, at approximately stage 10-12. **(C)** Percentage of non-injected embryos (controls) that are alive and dead after a further 48-hour incubation. **(D)** Percentage of injected embryos (experimental) that are alive and dead after a 48-hour incubation post-injection. **(E)** The percentage of alive injected embryos that contained and did not contain GFP^+ DPSC. Data represents mean±SD (mean annotated above bars), n=6 (batches of eggs, ranging from 6.5-10 dozen eggs/batch).

7.3.2 Optimisation of immunofluorescence staining

This chicken embryo assay had previously been established in our research group. The current setup was similar to that which was previously published (1). Whole-mount tissue staining allowed for visualisation of injected cells in three dimensions. Tissue samples were stained for GFP to detect the injected DPSC, and a neuronal marker to detect cells undergoing neuronal differentiation (Figure 7.3). The GFP expression levels were too low to be detected directly, so an antibody against GFP was used to enhance the signal. Staining for the intermediate neuronal marker β-III tubulin and the mature neuronal marker NF-M were both tested with antibodies previously used in this assay. Both antibodies worked, however the β-III tubulin clone TUJ1 antibody stained the structures better across more samples. Thus, the tissue samples were stained for β-III tubulin. The cell nuclei were stained using DAPI, though this staining was not useful for quantitating cell numbers due to cell density.

The anti-GFP primary antibody was detected by a secondary antibody conjugated to Alexa Fluor 488 fluorophore (excitation 488, emission 510) and the anti-β-III tubulin primary antibody was detected by a Cyanin3-conjugated secondary antibody (excitation 550, emission 570). While these two fluorophores are used in combination, there is a small amount of spectral overlap. Generally, the peak excitation and emission wavelengths of the two fluorophores should be separated by at least 50-60nm. This difference was observed here but if possible a fluorophore with greater separation could be used. Cyanin5 and Alexa Fluor 647 conjugated secondary antibodies were tested. However, these antibodies in combination with the primary antibody did not stain the tissue well. Whole tissue samples and tissue sections were tested. Initially, no staining was detected. After optimisation of the blocking buffer, these antibodies highlighted the head structures but not individual axonal processes as seen with the Cyanin3-conjugated secondary antibody (data not shown). The blocking buffer may have affected the staining with the primary antibody, which was optimised using a different blocking buffer. It was determined best to proceed with the anti-β-III tubulin primary antibody and Cyanin3-conjugated secondary antibody combination, which was optimised and previously used and published.

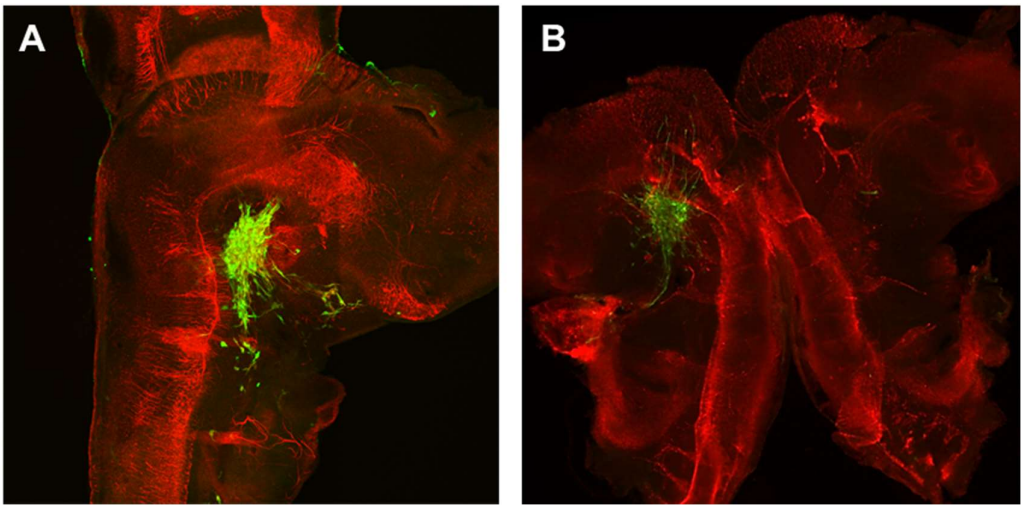

Figure 7.3 Whole-mount chicken embryo tissues stained for GFP and neuronal markers. GFP detects the injected DPSC. **(A)** Embryo stained for GFP (green) and β-III tubulin (red). **(B)** Embryo stained for GFP (green) and NF-M (red).

7.3.3 Injected DPSC exhibited neuronal-like morphology and localised in the vicinity of established endogenous axonal processes

The DPSC were injected adjacent to the developing hindbrain. Between stages 10 and 12, this area was easily accessible and large enough to act as the receptacle for the cells. Stage 11 was most ideal, as the boundaries were better established than at stage 10, whilst later in stage 12 the embryo tissue became less amenable to injection. Transduced DPSC from one donor were used (DPSC1). There were four groups of cells: DPSC with the empty vector before neural induction, i.e. time-point 0 (DPSC-EV t0, control for non-modified DPSC); DPSC with the empty vector after the multi-step (three) neural induction protocol, i.e. time-point 3 (DPSC-EV t3, control for the culture conditions); DPSC with the OCT4 vector before neural induction, i.e. time-point 0 (DPSC-OCT4 t0, control for OCT4 over-expression); and DPSC with the OCT4 vector after neural induction, i.e. time-point 3 (DPSC-OCT4 t3, experimental reprogramming group).

The injected cells were detected in the vicinity of the trigeminal ganglion and the established axonal processes. At 48 hours post-injection, the GFP^+ cells in all four groups exhibited neuronal-like morphologies (Figure 7.4). Bipolar cells consistent with morphology of trigeminal ganglion sensory neurons were present, as well as some multipolar cells seen in Figure 7.4 C and D (white arrows). Cells extended processes towards other cells and in some samples wrapped around established axonal processes, such as the oculomotor nerve (third cranial nerve) in Figure 7.4B.

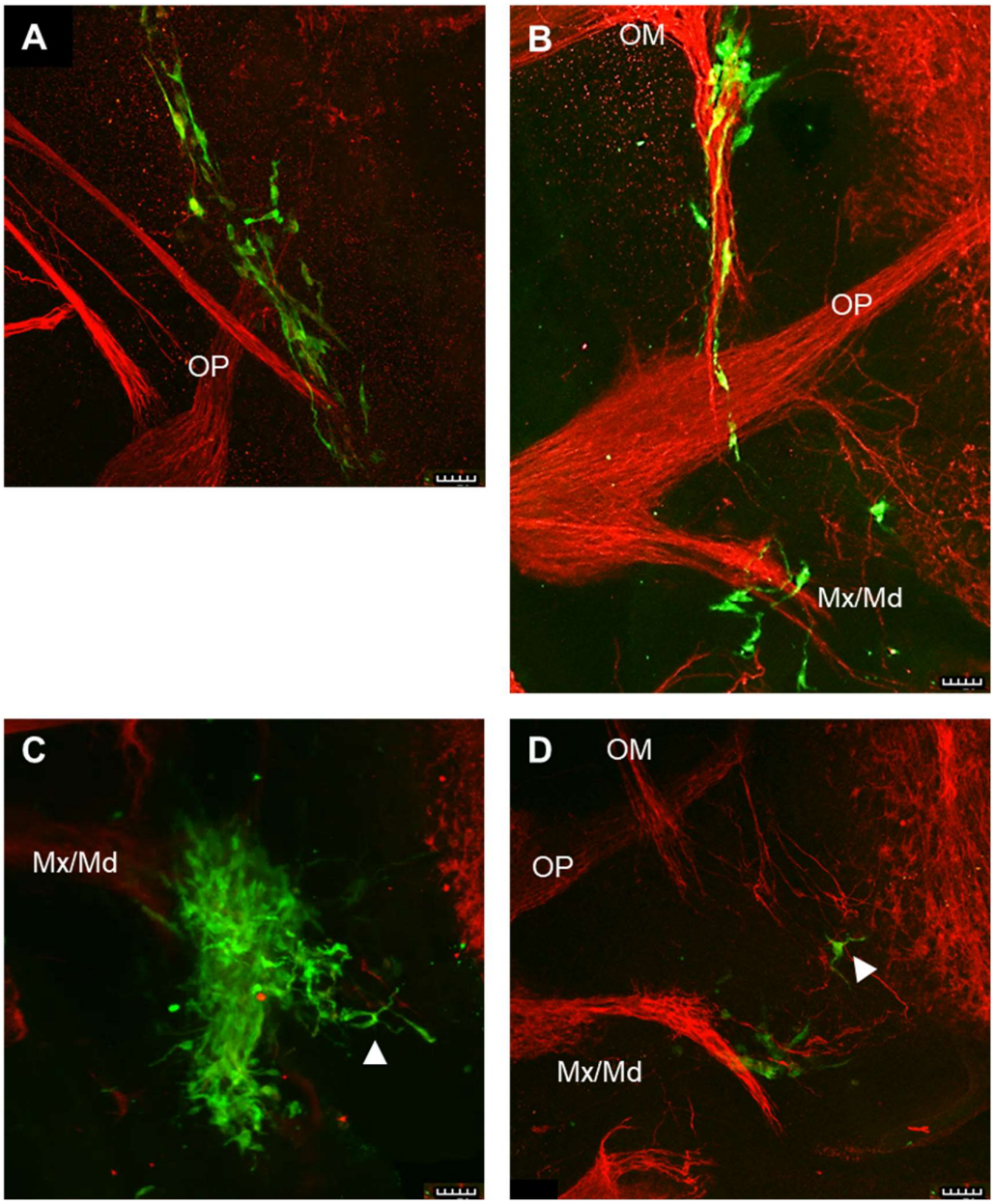

Figure 7.4 DPSC transplanted into the chicken embryo localised with established axonal processes and displayed neuronal-like morphologies. Tissues were immunostained to detect GFP (green) and β-III tubulin (red). There were four groups of cells; **(A)** control for normal DPSC (DPSC-EV t0), **(B)** control for culture conditions (DPSC-EV t3), **(C)** control for OCT4 over-expression (DPSC-OCT4 t0), and **(D)** experimental OCT4 over-expressing, neural-induced DPSC (DPSC-OCT4 t3). OP=ophthalmic nerve, OM=oculomotor nerve, Mx/Md=maxillary/mandibular nerves. Representative images, scale bar=50µm.

7.3.4 DPSC induced neuroplasticity

Human DPSC have previously been shown to induce neuroplasticity (1, 140). Cells in all four groups demonstrated the ability to influence the endogenous neuronal axon guidance (Figure 7.5). Depending on the location of the DPSC aggregates, different patterns of aberrant host axonal branching were observed. The DPSC caused established branches to deviate from their normal developmental path by attracting axonal processes, reshaping and redirecting, and causing branches to bifurcate. Figure 7.5 highlights some of the changes observed around DPSC with some measurements of these changes indicated. In Figure 7.5A, outgrowth from the ophthalmic branch of the trigeminal nerve was observed towards a superior DPSC aggregate. While in Figure 7.5C, distal projections from the maxillary and mandibular branches of the trigeminal nerve extended towards the DPSC aggregate near the ophthalmic branch, with the DPSC extending processes towards the maxillary and mandibular branches. Figure 7.5B displays the bifurcation of the oculomotor nerve, while the maxillary/mandibular branches curved around the DPSC aggregate towards inferior distal DPSC. Similarly in Figure 7.5D, the oculomotor nerve bifurcated towards two clusters of DPSC.

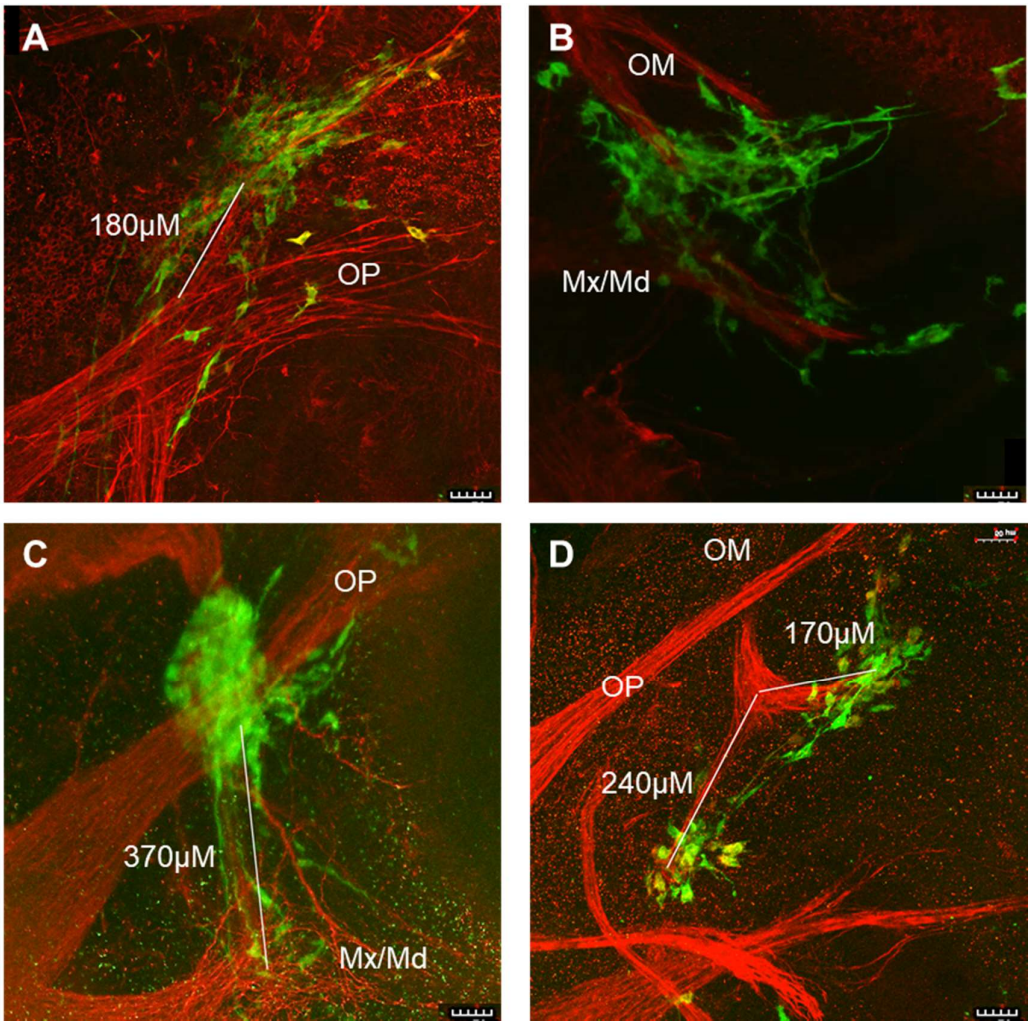

Figure 7.5 DPSC transplanted into the chicken embryo induced neuroplasticity. Tissues were immunostained to detect GFP (green) and β-III tubulin (red). GFP^+ DPSC caused endogenous axonal processes to deviate from their normal path towards the transplanted cells. There were four groups of cells; **(A)** control for normal DPSC (DPSC-EV t0), **(B)** control for culture conditions (DPSC-EV t3), **(C)** control for OCT4 over-expression (DPSC-OCT4 t0), and **(D)** experimental OCT4 over-expressing, neural-induced DPSC (DPSC-OCT4 t3). OP=ophthalmic nerve, OM=oculomotor nerve, Mx/Md=maxillary/mandibular nerves. Representative images, scale bar=50μm.

7.3.5 Survival of DPSC in chicken embryos

In Figure 7.6, the number of GFP^+ cells per embryo within each of the four groups is shown. Within each group, each symbol represents an embryo, and its location on the *y*-axis indicates the number of GFP^+ cells in that embryo. In the EV groups, the average number of GFP^+ cells per embryo before neural induction (n=19) was 94.1±49.6 while after neural induction (n=15) was 122.8±61.2. For the OCT4 groups, the average number of GFP^+ cells per embryo before neural induction (n=20) was 94.4±52.6 and after neural induction (n=12) was 75.6±57.7. There was no significant difference between the four groups, indicating that the groups may be compared for differentiation without the number of surviving cells confounding the analysis.

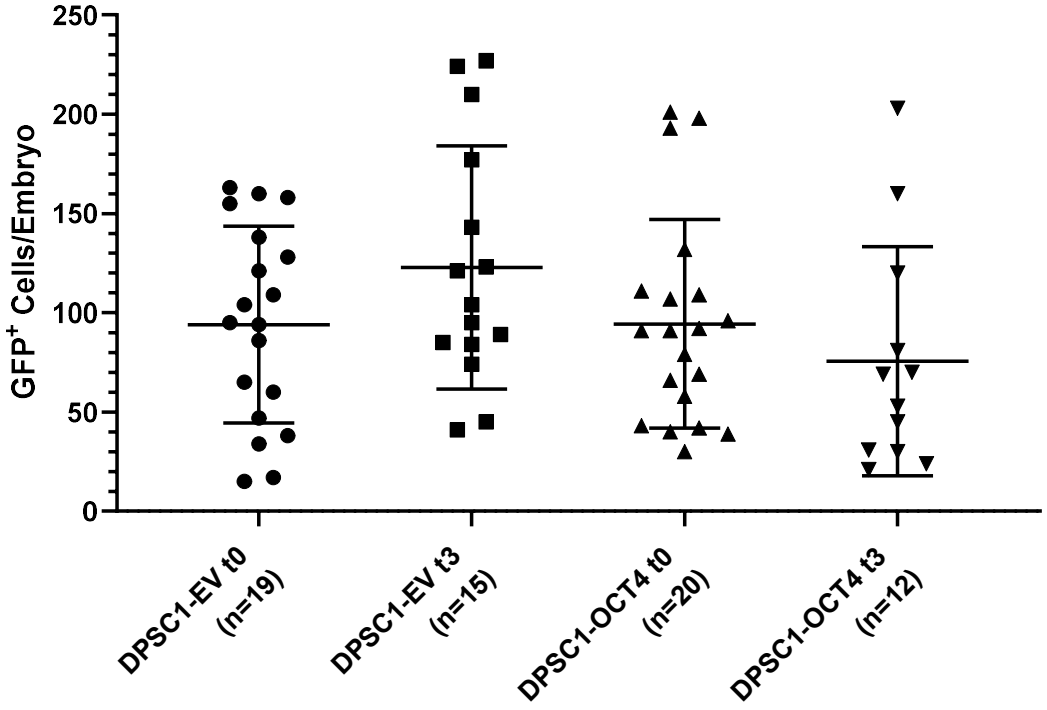

Figure 7.6 DPSC survival in chicken embryos. Transduced DPSC from one donor were used (DPSC1). There were four groups of cells: empty vector (EV) before neural induction (time point 0) for normal DPSC control (DPSC-EV t0), EV after neural induction (time point 3) for culture conditions control (DPSC-EV t3), OCT4 vector before neural induction (time point 0) for OCT4 over-expression control (DPSC-OCT4 t0), and OCT4 vector after neural induction (time point 3) as experimental samples (DPSC-OCT4 t3). Tissue samples were immunostained for GFP expression. Imaris software was used to assign spots to GFP, i.e. each spot represented a GFP^+ DPSC. Scatter plot displays the number of GFP^+ DPSC per embryo within each of the four groups. Data represents mean±SD, Brown-Forsythe and Welch ANOVA tests with Holm-Sidak's multiple comparisons test, n=12-20 (number of embryos).

7.3.6 OCT4 over-expressing, neural-induced DPSC had greater expression of the neuronal marker β-III tubulin

Within each of the four groups, the number of GFP^+ cells that were β-III $tubulin^+$ were counted in every embryo and expressed as a percentage (Figure 7.7). There was a greater number of double-stained cells per embryo in the OCT4 over-expressing, neural-induced DPSC (44.8±22.9) than in the three control groups. There was no statistical significance with the control group DPSC1-EV t0 (30.1±30.4), which displayed greater variation. The difference with the neural induction control group DPSC1-EV t3 (17.0±17.2) and the OCT4 over-expression control group DPSC1-OCT4 t0 (17.3±19.3) was significant at $p \leq 0.05$. There was no significant difference between the three control groups; the neural induction and OCT4 over-expression control groups showed greater similarity.

In Figure 7.8**,** the mean intensity of the red channel (β-III tubulin expression) for every GFP^+ cell in the embryos of each group is shown. The horizontal line marks the threshold for β-III $tubulin^+$ staining (mean channel intensity of 200). In this figure, the sample size indicated is the number of GFP^+ cells combined from all the embryos in each group. There was statistical difference in the spread of all groups ($p<0.0001$) except between the neural induction and OCT4 over-expression control groups. The control and experimental groups had a higher minimum and maximum mean intensity than the other two control groups. A greater percentage of GFP^+ cells were plotted above the threshold for the experimental group (51%) compared to the control groups (32% for normal DPSC control, 18% for neural induction control, 19% for OCT4 over-expression control). These results were observed despite the experimental group, which had fewer embryos, having half the sample size (number of GFP^+ cells) than the three control groups.

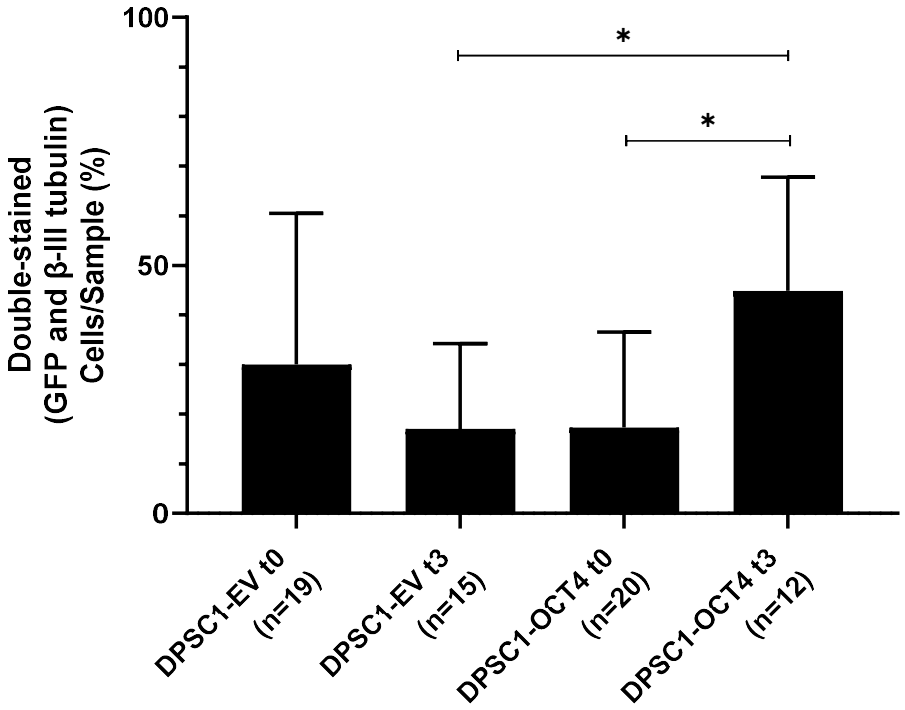

Figure 7.7 Double-stained DPSC in chicken embryos. Tissue samples were immunostained for GFP and β-III tubulin expression and analysed. Imaris software was used to assign spots to GFP, i.e. each spot represented a GFP^+ DPSC. These spots were analysed for expression of β-III tubulin. The threshold for β-III $tubulin^+$ staining was set at the mean channel intensity of 200. The percentage of β-III $tubulin^+$ cells from total GFP^+ cells was calculated per embryo within each group. Data represents mean±SD, Kruskal-Wallis ANOVA test with Dunn's multiple comparison test, n=12-20 (number of embryos), *$p \leq 0.05$.

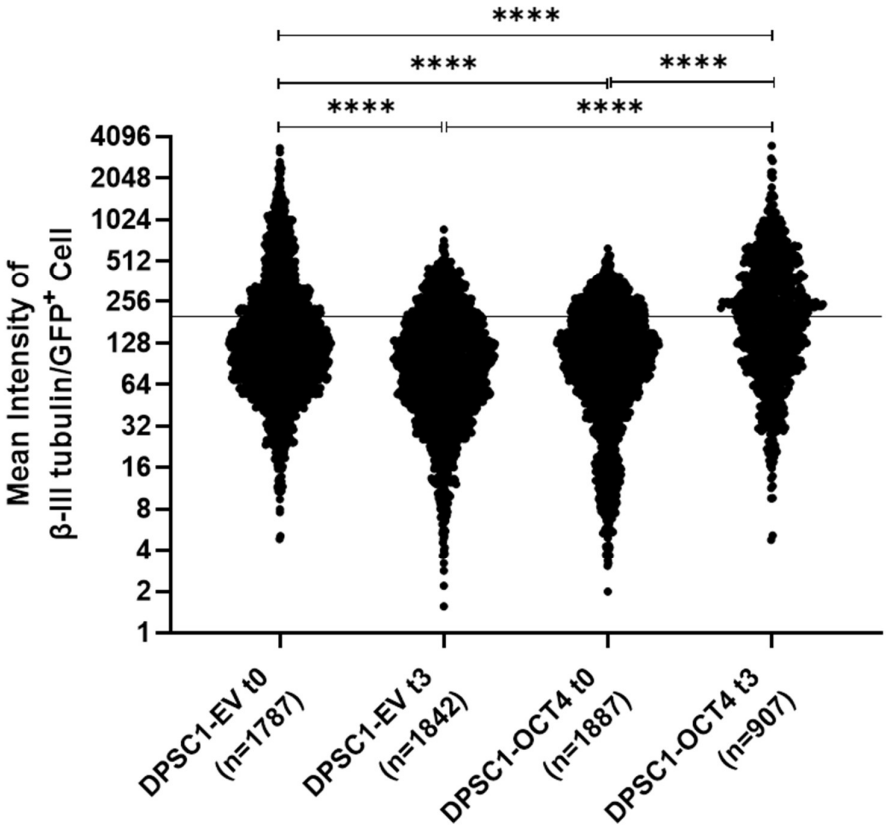

Figure 7.8 Mean intensity of β-III tubulin staining. Tissue samples were immunostained for GFP and β-III tubulin expression. Imaris software was used to assign spots to GFP, i.e. each spot represented a GFP^+ DPSC. These spots were analysed for expression of β-III tubulin. Scatter plot displays every GFP^+ cell within each embryo in every group, based on the mean intensity of the β-III tubulin channel (line at 200 represents the threshold for β-III $tubulin^+$ staining). Data points represent each GFP^+ cell (sample size indicated), Kruskal-Wallis ANOVA test with Dunn's multiple comparison test, ****$p<0.0001$.

7.4 | Discussion

In this chapter, the *in vivo* neuronal differentiation potential of modified human DPSC was examined using the chicken embryo model. The DPSC were injected between stages 10 to 12 of embryonic development, and the embryos were allowed to continue development for 48 hours post-injection, reaching approximately stage 23 (131). The injected DPSC were detected via GFP staining. The OCT4 vector-transduced DPSC cultured using the multi-step neural induction protocol were the experimental group. As with previous research, the cells were able to survive, integrate and differentiate in the developing chicken embryo (1). These results demonstrated their capacity to respond to endogenous signals within a short developmental time-frame.

The DPSC in all four groups were in the vicinity of the trigeminal ganglion and localised to regions similar to the endogenous migrating cranial neural crest stem cells. The DPSC were detected in close proximity to the ophthalmic, maxillary and mandibular branches of the trigeminal ganglion, and the oculomotor nerve. The DPSC displayed neuronal-like morphologies, with bipolar and multi-polar cells observed, consistent with neuronal morphologies of the peripheral nervous system and CNS respectively (1).

The ability of the DPSC to induce changes to endogenous structures was also observed. This consisted of altering the pathway of axonal branches and bifurcation, depending on the location of the DPSC aggregates. Whilst these axonal pathways varied from the physiological patterning, they demonstrated that the DPSC had the capacity to influence axonal growth. From previous research, we know this induced axonal guidance is mediated by the secretion of paracrine factors, including CXCL12 (140). In combination with other mechanisms, the ability to induce neuroplasticity is beneficial in cell-based therapies, stimulating axonal growth and homing of endogenous cells towards the injected cells and the area of injury or disease. In the current study, these changes in pathways were measured but not compared between the experimental and control groups, as the cell numbers and exact location varied between samples. In order to examine samples with similar DPSC numbers and in a similar location, for example between the ophthalmic and maxillary/mandibular branches, the sample size needs to be greatly increased. This would allow for more accurate comparisons between groups, indicating if modified DPSC induce neuroplasticity at similar levels to non-modified DPSC. The levels of secreted factors could be measured *in vitro*, and the profiles compared between groups. Additionally, using explanted chicken embryos, specific neurotrophic factor interactions could be examined (140, 149).

The number of GFP^+ DPSC expressing β-III tubulin were quantitated, which in previous studies was only examined qualitatively (1). The intermediate neuronal marker β-III tubulin clone TUJ1 antibody was able to visualise neurons in the chicken embryo early developmental stages. Expression of β-III tubulin was used as a measure of neuronal differentiation potential. The results showed that a greater number of injected DPSC expressed the neuronal marker in the experimental group (OCT4 over-expression and *in vitro* neural induction), hence possessing greater neuronal differentiation potential. The control groups for the *in vitro* culture conditions and OCT4 over-expression demonstrated that these modifications individually were not as effective as the combination of OCT4 over-expression and neural induction. The control expected to be most similar to non-modified DPSC, was not the lowest with regard to β-III tubulin expression. This was surprising, however this control also had the greatest amount of variation, highlighting the need to increase the sample sizes to clear the ambiguity in relation to the experimental and other control groups. With a greater sample size the combined effect and difference to controls would become more evident.

The efficiency of this assay was observed to be low. In discussion of the efficiency of this model system one may draw the following impressions. Firstly, in a batch of fertilised eggs there will be some unfertilised eggs and some embryos that will be abnormal (undeveloped, delayed development, deformed). This can be due to inherent factors, which may be evident in eggs from a specific flock, or environmental factors, such as temperature, which can be seen in specific batches of eggs. The temperature appeared to be the main factor affecting fertilisation rate and normal development, with fertilisation rate decreasing in cold temperatures (winter) and abnormal development increasing in hot temperatures (summer). This is out of the control of both the breeder and us as the consumer, and is not known until the eggs are opened and the embryos prepared for injection. During development, the temperature and humidity needed to be maintained within the correct range, as slight variations affect viability (131).

It was assumed that the eggs were fertilised only hours before delivery and that they were at the same developmental stage. Realistically, there would be some variation and this was seen when the eggs were opened up and staged. The embryos that were either too young or too old by only a few hours at the time of the cell injections were kept as controls for normal development and handling, but not for injections (i.e. no sham-operated embryos) due to low embryo numbers and assay efficiency. Fifty per cent of these controls did not survive. This may have been due to abnormal development that had not been previously detected, human error, or additionally, there are critical developmental stages at which the natural mortality rate increases (148). The latter is expected to have contributed more; abnormal embryos were detected at fifteen per cent

of the fertilised eggs and most were likely to have been already detected, while human error accosted five per cent of fertilised eggs and a small amount of manipulation was performed prior to cell injection.

Whilst this model allows for a high turnover, the post-injection mortality of the embryos was the principal limiting factor (148). A third of the injected embryos survived. However, the mortality of the injected embryos was not substantially greater than the mortality of the control embryos, which may have been greater if sham-operated controls had been included. Given the procedure performed on the embryos, it seems reasonable that the mortality would be greater than for the controls. GFP^+ DPSC were detected in three quarters of the surviving injected embryos. Reasons for why GFP^+ DPSC were not detected in the remaining embryos is attributed to factors controlled by the experimenter, and these are associated with the injection needle. Penetrating the embryo at the correct position and to the correct depth would ensure cells remain in the embryo, otherwise the cells may have gone through if the vitelline membrane in the deep was pierced by the needle, though this would be expected to result in embryo loss. Alternatively, few cells may have come out of the needle; the needle may have become blocked as cells begin to adhere to one another, the cells may have been depleted, or the pressure may have been insufficient.

Here, the whole tissue samples were used. Tissue sections would be useful for more easily quantitating cell numbers for survival and colocalisation, as well as including multiple stains, however other information regarding interaction with endogenous cells would be lost. Frozen tissue sections were tested but the integrity of the tissues was affected. Due to the small size of the tissues, there were several difficulties faced with using the cryostat to make tissue sections. Furthermore, the method resulted in many sections, of which few contained the injected cells.

Given the considerations involved in using this model for xenotransplantation, the overall outcome of this assay was positive and promising for further work. Whilst there was variation, particularly in the control group, the results are suggestive that OCT4 over-expressing DPSC that have undergone neural induction *in vitro* have enhanced neuronal differentiation capacity, and this is attributed to the combination of OCT4 over-expression and neural induction rather than just one component. The limitations were the small sample size of DPSC and embryos. Future work should increase the number of embryos used in each group to decrease the variation, but also confirm that this result is observed with multiple DPSC samples (different donors). Due to the time required to set up the assay, learn the model with sound, reproducible technique, and perform the assay, in addition to the efficiency considerations, examination of

more DPSC samples could not be accommodated. In conclusion, using the chicken embryo it was demonstrated that the reprogrammed DPSC have the ability to survive, integrate and differentiate *in vivo* during a time of active neurogenesis, with the reprogramming enhancing the neuronal potential of human DPSC.

CHAPTER 8

GENERAL DISCUSSION AND CONCLUSION

8.1 | Discussion

This thesis presents results investigating the reprogramming of human DPSC into NSC. The major outcomes are separated into chapters addressing the *in vitro* analysis of the reprogrammed DPSC, whole-genome transcriptomic analysis by next-generation sequencing, and *in vivo* analysis using the chicken embryo developmental model. This thesis identified a transcription factor and neural conditions suitable for enhancing the neural potential of DPSC by converting them into neuronal progenitor-like cells.

To date, there have been many *in vitro* studies on the neuronal potential of human DPSC, as well as the *in vivo* application of these cells in stroke models (see Chapter 1 review) (36). Previous work from our research group has investigated the neuronal potential of human DPSC, their properties and effects in the nervous system, and their response in a stroke model (1, 8, 140, 150). The ability to differentiate DPSC into neuronal-like cells *in vitro* was demonstrated, with cells expressing neuronal proteins and exhibiting electrical currents that are important for neuronal function (1). Additionally, their ability to induce neuroplasticity and elicit neuroprotection through secretion of paracrine factors has been studied (8, 140, 150). The stroke model provided encouraging results for the use of DPSC in cell-based therapies, with significant neurobehavioural improvement observed (8). That study highlighted that the positive outcome was mediated via paracrine effects and not replacement of neural cells.

The findings of the current study demonstrated that the neural properties of DPSC can be enhanced through the over-expression of the OCT4 transcription factor in combination with a neural-inducing environment. This work examined the response of the DPSC to these changes using gene and protein expression analysis, stem cell assays, and analysis in a developmental model. Combined, the results demonstrated that these reprogrammed DPSC had enhanced neuronal potential, suggesting they may be neuronal progenitor-like cells. There have been limited studies on the reprogramming of DPSC (16, 20, 151). There is no previously published work on the effect of OCT4 over-expression on DPSC from a neural perspective.

The OCT4 transcription factor is associated with pluripotency and is important in the regulation of ESC proliferation and lineage commitment during embryogenesis (10). This transcription factor is one of the key factors for iPSC generation, but has also been extensively used in direct reprogramming studies (11). For direct reprogramming (i.e. bypassing the pluripotent stage), two reprogramming strategies exist (152, 153). The first strategy involves tissue-specific transcription factors, and generally results in post-mitotic cells. The second strategy is focused

on plasticity induction by pioneer transcription factors in combination with specific environmental cues, and allows for production of progenitor cells. This is the strategy adopted in this thesis focusing on the use of OCT4 for reprogramming (11, 152, 153).

Mechanisms by which this OCT4 reprogramming occurs may involve direct non-physiological binding of the transcription factor to lineage-specific target genes or may mimic the role of the transcription factor during embryonic development for normal lineage commitment (154). This depends on the ability of the transcription factor to overcome the existing epigenetic barriers. With high expression levels that are common to reprograming studies, the factor can transiently access the chromatin leading to an open epigenetic state and allow subsequent chromatin remodelling (11, 152-154). Cell proliferation facilitates removal of epigenetic barriers (152, 153). This leaves the cells in a flexible state and subsequent reprogramming down the desired lineage is guided by extracellular signals from chemically defined culture media (11, 12, 152-154).

Several studies have been published on cell conversion using only OCT4 (13-15, 155). The first study achieved conversion of fibroblasts into multi-lineage blood progenitors (155), and in a later study into tri-potent neural progenitors (13). Subsequent research applied this OCT4 reprogramming to convert blood cells into neural cells, since fibroblasts but not blood cells have molecular hallmarks of the neural lineage. Additional small molecule inhibitors were required to overcome lineage restrictions (14, 15). The same research group published on the molecular evidence for this OCT4-induced plasticity, addressing the process of direct reprogramming (12). The transcriptional profile of the OCT4-induced fibroblasts displayed elevated expression levels of developmental genes associated with multiple cell lineages, and then further activated specific cell lineage genes in response to the environment cues (haematopoietic and neural culture media, additional culture components may be required for endodermal conversion). This study highlighted the importance of the environmental conditions, which is often overlooked. They also demonstrated that the plastic state was established by the combined effect of OCT4 over-expression and the short-term exposure to reprogramming medium.

In Chapter 6, the whole-genome transcriptional profile of the OCT4 over-expressing, neural-induced DPSC displayed elevated expression levels of genes associated with the CNS and neurogenesis in response to the OCT4 over-expression and neural inductive environmental signals. This was significantly different to the effect of only the neural inductive conditions. This outcome aligned with the previous research, and indicated that the outcome is in response

to both the transcription factor and the neural inductive conditions (12, 13). While OCT4 over-expressing DPSC cultured in standard DPSC medium were not analysed by RNA-sequencing, previous research suggested that the transcriptome is likely to differ from that of the DPSC in neural inductive conditions only or both components combined (OCT4 over-expression and neural inductive conditions) (12, 16). OCT4 over-expression in DPSC has been shown to enhance odontogenic and adipogenic differentiation under these culture conditions, supporting the concept of OCT4-induced plasticity (16). Hence, it can be presumed that the transcriptome of OCT4 over-expressing DPSC in standard DPSC culture medium would show elevated levels of genes for multiple cell lineages. Meanwhile, under neural inductive environmental conditions some elevated expression of neural genes was detected, and the combined components showed significant neural enhancement.

The reprogramming medium referred to in the study on OCT4-induced plasticity of fibroblasts was highly comparable (higher concentration of bFGF and inclusion of insulin-like growth factor 2) to the pre-inducing medium (step one) used in this thesis by the multi-step neural induction protocol, with the same duration (13, 104). The neural progenitor medium used in that study also corresponded to the NSC medium (step three) reported here, with the exclusion of the β-mercaptoethanol (13, 104). While the current investigation was focused on the endpoint of the multi-step neural induction protocol, additional analysis throughout the protocol would provide insight into the neural stage of the OCT4 over-expressing DPSC at each point. The previous research suggested that after the pre-inducing medium (step one), elevated expression levels of genes important for multiple cell lineages may be observed while the neural genes would be increased following the neural cultures (step two and/or three) or likewise for other specific cell lineage media. Additionally, it would be interesting to see if removal of the pre-inducing medium (step one) would decrease the effect of this OCT4 reprogramming.

The OCT4-induced plasticity in fibroblasts study also showed that reprogramming medium was required to maintain OCT4 expression, while we saw the transgenic OCT4 expression levels remain elevated and consistent in DPSC throughout the neural induction (12). It would be of interest to examine the transgenic OCT4 expression levels beyond the neural induction, to determine if the levels decrease during differentiation as in physiological conditions. Additionally, a transient or inducible vector system could be used to control the over-expression of OCT4 and determine at which stage of the reprogramming the OCT4 expression is crucial. The previous research also showed that the reprogramming medium had a dominant effect over the OCT4 over-expression with regard to the whole-genome transcriptional change (12). Here, the transcriptomic analysis was performed at the completion of the multi-step neural induction

protocol, following both culture in the pre-inducing medium and the neural media. The *in vitro* analysis showed changes in neural gene expression resulting from the culture conditions but with specific effects due to the OCT4 over-expression. The whole-genome transcriptional analysis, however, showed more changes in response to the OCT4 over-expression and neural inductive conditions than just the neural inductive conditions, suggesting that the effect of neural induction was not necessarily greater than the effect of OCT4 over-expression. Understandably, the cells here are different, the culture conditions have some variation, and transcriptomic analysis was not performed at both time-points (i.e. following pre-induction and following neural induction).

A question that is often raised with direct reprogramming is the possibility that the cells are passing through a transient pluripotent stage. This depends on the transcription factors used and the culture conditions. Generation of iPSC typically requires four transcription factors (Yamanaka factors) and the right environmental signals, such as leukaemia inhibitory factor (152). It has been shown that studies indicating direct reprogramming using the four factors for pluripotency induction were in fact passing through a pluripotent stage, suggesting that the use of the four factors stimulates iPSC production even in neural conditions (156, 157). Other studies have reduced the factors needed for iPSC formation but have often needed the addition of epigenetic modulators, suggesting that all the factors are important (158, 159). A recent study demonstrated that OCT4 removal decreased the efficiency of iPSC generation but increased their developmental potential (160). These studies suggest that iPSC production requires multiple factors and the right conditions, and that OCT4 is involved in efficiency. The OCT4-induced plasticity in fibroblasts study also showed that the molecular state of these cells that were undergoing direct reprogramming was different to cells undergoing indirect reprogramming, and no molecular hallmarks of iPSC formation were detected (12). Molecular hallmarks of iPSC include: mesenchymal-to-epithelial transition genes that precede iPSC formation, expression of early (e.g. NANOG) and late (e.g. SOX2) pluripotent regulators, reactivation of the silenced X chromosome as a late and specific indicator, silencing of transgenes for which the machinery is established within a couple of days, and endogenous OCT4 reactivation (12, 156, 157). In this thesis, endogenous OCT4 expression did not increase and expression throughout the protocol remained driven by the CMV promoter in the vector used. Additionally, NANOG protein expression was not detected. Future work could examine more markers of pluripotency. The results shown here, combined with knowledge from previous research suggests that the current conditions investigated are unlikely to produce iPSC.

The overall aim of this thesis was to convert human DPSC into NSC, however the characteristics of the reprogrammed DPSC appeared better matched to neuronal progenitor cells than NSC. While not extensive, there is some research on the electrophysiological properties of NSC, showing that they display voltage-dependent outward and inward rectifying potassium ion currents but not the tetrodotoxin-sensitive voltage-dependent sodium ion currents that are also observed in neurons (161). Here, the electrophysiological analysis, although not complete and only demonstrated in a small number of cells, found both voltage-dependent potassium ion currents in the OCT4 over-expressing, neural-induced DPSC. The inward potassium ion current is typically small in neurons to help maintain the resting membrane potential while being able to be overcome to achieve an action potential (161). The inward potassium ion current was bigger in these reprogrammed DPSC than expected in neurons and would be difficult to be overcome. However, sodium ion currents were also detected in these reprogrammed DPSC, similar in size to the sodium ion currents observed in neurons (1, 161). Additionally, the calcium signalling pathway was enriched, with up-regulation of genes for voltage-gated calcium ion channels. These are typical of neurons at the early developmental stage (162). This was observed in the neural-induced DPSC and further enhanced in the OCT4 over-expressing, neural-induced DPSC, indicating the combined effect and the possibility of existing in different neural states based on the treatment conditions.

The similarity and difference to the electrophysiology of both NSC and neurons suggested that the reprogrammed DPSC may be in an intermediate neuronal progenitor cell state. The previous research by our group on neuronal differentiation of DPSC detected sodium ion currents but not potassium ion current (1). This highlights the potential of reprogramming DPSC using this method or a variation of this method. Further patch-clamp analysis would provide important data on the role of the OCT4 over-expression and the neural inductive conditions. Electrophysiological characterisation of the comparison with NSC, neuronal progenitors and immature neurons would assist in understanding the state of these reprogrammed DPSC. It has also been shown that glial cells may express these voltage-dependent ion channels, therefore further analysis for glial properties would be beneficial (161).

In Chapter 7 of this thesis *in vivo* analysis using the chicken embryo model was presented. This model had previously been established in our group to investigate the response of DPSC injected in proximity to the developing hindbrain. Previous research showed that non-modified DPSC survive and integrate in the developing nervous system of the chicken (1, 140). The cells differentiated into neuronal-like cells and expressed neuronal proteins (1). Furthermore, they induced neuroplasticity of the established endogenous axonal processes and this was mediated

via the chemokine CXCL12 and its receptor CXCR4 (140). Here, the modified DPSC survived and integrated into the developing chicken embryo. Neuronal-like morphologies were observed and the expression of the β-III tubulin neuronal marker was quantified. The OCT4 over-expressing, neural-induced DPSC had greater expression of the neuronal marker. The cells in all groups also induced neuroplasticity, as expected from previous research (1, 140). However, comparisons regarding neuroplasticity were not made as the exact location and number of injected cells varied within each embryo. Similar location and cell number between embryos would indicate whether the reprogrammed DPSC induced greater neuroplasticity. Measurements were made to demonstrate that established endogenous axonal processes could vary from their normal path over distances of several hundred microns, which showed the paracrine effect of the DPSC. Additional neuronal markers could be examined, such as microtubule-associated protein 2 to examine neurite formation.

8.2 | Recommendations for Future Work

8.2.1 *What is the mechanism that drives the change in transcriptional profile in OCT4 over-expressing, neural-induced human DPSC?*

The work presented in this thesis demonstrated that the OCT4 over-expression and neural induction guided the DPSC into a neural phenotype with significant transcriptional changes displayed. This leads to the question of how these conditions cause the change observed. The previous research on OCT4-induced plasticity provided a working definition of the molecular state in fibroblasts (12). Similarly, additional transcriptomic analysis of the empty vector-transduced and OCT4 over-expressing DPSC at each step of the method used here (i.e. in standard DPSC culture medium, at completion of step one, etc.) can be used to deconstruct the process of cellular reprogramming. Based on what has been previously shown, up-regulation of a broader range of developmental genes may be observed after culturing in pre-inducing medium (step one), and neural lineage-specific genes may be highlighted after culturing in the neural media (step two and/or step three). Additionally, inclusion of other cell lineage differentiation media (e.g. adipogenic) following the pre-inducing medium would provide further support for OCT4-induced plasticity with subsequent response to environmental signals. Combined, these results would indicate if OCT4 induces plasticity in DPSC and whether the environmental signals subsequently stimulate an appropriate response. Analysis by chromatin-immunoprecipitation sequencing can then be performed to elucidate the mechanism of OCT4-induced plasticity, by identifying the DNA targets of the OCT4 transcription factor. These targets and their roles can be studied using gene knock-in and knock-out experiments, and small

molecules that can interfere with the relevant pathways. This functional analysis would provide a framework by which OCT4 induces plasticity, highlighting the important downstream components and signalling pathways.

8.2.2 *Do OCT4 over-expressing, neural-induced human DPSC differentiate into different types of neural cells in vivo?*

Previous work has shown that DPSC can survive and differentiate *in vivo* (1). It was shown here that the modified DPSC were detected in the chicken embryo and some cells expressed the β-III tubulin neuronal marker. Using the chicken embryo, modified DPSC can be further analysed for differentiation into specific cell types (e.g. specific neuronal classes, astrocytes, oligodendrocytes, and microglia), by broadening immunostaining for specific cell markers and neurotransmitter phenotypes (e.g. VGLUTs for excitatory glutamatergic neurons, GABA for GABAergic interneurons, peripherin for peripheral neurons, etc.) (87). Additionally, patch-clamp recordings can be performed on cells in tissue slices to assess them for functional neurons (163). Similar to a previous study, this model can be used to examine the factors secreted by these modified DPSC (140). The chicken embryo model system provides a rapid and affordable method to examine the cells. Subsequent research can be conducted using a mammalian model to examine survival and differentiation in the developed brain with greater similarity to humans (e.g. mouse model). (163). Previous research using neuronally pre-differentiated DPSC showed that the cells localised to the endogenous neurogenic niches (163). Thus, these reprogrammed DPSC would be expected to be detected in similar regions. Further to this differentiation analysis, CRISPR gene editing technology can be used to generate reporter cell lines to easily detect certain neural cell types upon differentiation. For example, a recent study published on the generation of a tyrosine hydroxylase reporter iPSC line, used the mOrange fluorescent protein knocked into the tyrosine hydroxylase locus, to detect dopaminergic neurons (164).

8.2.3 *Do OCT4 over-expressing, neural-induced human DPSC enhance functional recovery in a stroke model via cell replacement?*

Previous research in our group demonstrated that non-modified DPSC enhanced neurobehavioural outcomes in a rodent stroke model, highlighting their potential use for cell-based therapies (8). We hypothesised that if DPSC were made more ‘neural’, their capacity to stimulate neurobehavioural improvement via multiple mechanisms, including the ability to replace neural cells, would be enhanced. Similar to the previous study, these OCT4 over-expressing, neural-induced DPSC can be intracerebrally transplanted into a rodent stroke model

24 hours following focal cerebral ischaemia induced via middle cerebral artery occlusion. Functional assessment would be performed to detect and compare neurobehavioural outcomes between the experimental groups. Immunostaining for human cell markers and neural markers would determine cell survival rates and integration of cells, and indicate the neural cell types into which the implanted cells differentiate. The neural-induced DPSC would be expected to have better survival than non-modified DPSC. However, the difference if any between neural-induced DPSC and OCT4 over-expressing, neural-induced DPSC would be interesting. The additional *in vitro* analysis discussed previously would help to better infer the outcomes between groups in a stroke model.

8.3 | Project Significance and Concluding Remarks

The research presented in this thesis identified a transcription factor and neural inductive conditions to guide DPSC into neuronal progenitor cells. While the initial hypothesis and aims of converting the DPSC to NSC was not achieved, the cells were instead directed further along the neuronal lineage. That is not to say that DPSC cannot be converted to NSC, but rather other factors and/or conditions may be required.

This work is the first to examine the effect of OCT4 over-expression in DPSC under neural conditions. These results serve as proof-of-principle that under the appropriate environmental conditions, DPSC neural capacity can be enhanced. OCT4 over-expressing, neural-induced DPSC underwent significant transcriptional changes, displaying elevated expression levels of genes associated with many neural processes, enhancing their neuronal differentiation capacity. Therefore, OCT4 has the capacity to enhance the efficiency of reprogramming and induce plasticity of the DPSC, allowing them to respond to environmental conditions or other factors to determine cell fate. The OCT4 transcription factor showed promise as a plasticity inducer, with the environmental conditions influencing the trajectory of the reprogramming.

There is still much to be investigated with these modified DPSC. They have the potential to provide a therapeutic benefit, and may prove more effective than other stem cells. Their origin, accessibility and proliferation capacity keeps them relevant for use in cell-based therapies of neurological diseases, such as stroke. We have yet to find a way to treat and improve stroke outcomes. There are few clinical trials using neural cells, and as NSC cannot be obtained easily, it may be more efficient to use reprogrammed NSC. Using the right methodology, DPSC may provide positive effects through multiple mechanisms of action that are key to improving stroke outcomes. This thesis has progressed knowledge by identifying conditions to enhance the neural capacity of human DPSC.

APPENDICES

APPENDIX A: PRIMER DESIGN

Primers were designed for the genes of interest (transcription factors, neural genes, RNA-sequencing validation genes), to be used for qPCR with SYBR Green technology. The primers were designed through the Benchling (https://www.benchling.com/, CA, USA) Primer Wizard tool that uses Primer3 software (Wageningen University, Wageningen , the Netherlands) (165). The following table shows the parameters that were used to design the primers. The Nucleotide BLAST suite (National Centre for Biotechnology Information (NCBI), MD, USA) was used to search each primer against the nucleotide collections (using somewhat similar sequences setting). Significant alignments were examined to include high percentage query covers (100%) for the target and lower percentage query covers (e.g. around 70% and less) for non-target alignments with preferably fewer matches on the 3' end. Each primer set was searched in Primer-BLAST (NCBI, MD, USA) to confirm that the primer sets bind to their target only. The OligoAnalyzer tool (Integrated DNA Technologies, IA, USA) was used to assess secondary structures of primers (hairpin, self-dimer and hetero-dimer formations).

Table A Parameters for primer design.

Property	**Details**
Primer Length	22 base pairs (18-27)
Melting Temperature	60°C (57-63), each primer set within 5°C of each other
GC Content	50% (45-55)
Amplicon Size	100 base pairs (75-200)
3' GC Clamp	≥ 1 base pair
Exon Overlap	At least 1 primer if possible (some genes have only one exon)
BLAST	100% target, ≤ 70% for non-targets with fewer matches on the 3' end
Hairpin Formation	< melting temperature
Self-dimer Formation	ΔG > -9kcal/mole
Hetero-dimer Formation	ΔG > -9kcal/mole

To determine if a primer set was efficient and thus suitable to use, at the completion of the qPCR the melting curves were examined. For a good primer set, a single peak above threshold was observed, with no peak observed in the negative control (water) sample. If there was a peak in the water sample, the temperature had to be lower than the temperature in the experimental sample. Where necessary, PCR products were analysed by agarose gel electrophoresis to confirm the presence of only the expected fragment.

APPENDIX B: POSITIVE CONTROLS FOR ANTIBODIES

Immunofluorescence Staining

The SH-SY5Y neuroblastoma cell line was used as a positive control for expression of neural proteins. Primary antibodies detected the proteins of interest (Figure B.A). This indicated that the staining method using these antibodies worked, and that the negative and positive results were valid.

Western Blot

Antibodies were tested on positive samples expected to express the proteins of interest (Figure B.B). The loading control, β-actin, was detected in all samples. The human DPSC transduced with the three vectors carrying the OCT4, SOX2 and HES1 cDNAs along with GFP, confirmed the detection of GFP, as well as the over-expressed OCT4, SOX2 and HES1 proteins. The human ESC expressed the pluripotent markers OCT4, SOX2 and NANOG. The mouse NSC expressed the NSC marker SOX1. The other markers used to identify NSC, which included SOX2, HES1 and nestin, were not detected. The SOX2 and nestin antibodies were human-specific, while HES1 may not be expressed in this NSC sample or may be very low. The SH-SY5Y cell line confirmed the detection of the neuronal markers nestin, β-III tubulin and NF-M. These samples confirmed that the antibodies detected their proteins using this protocol.

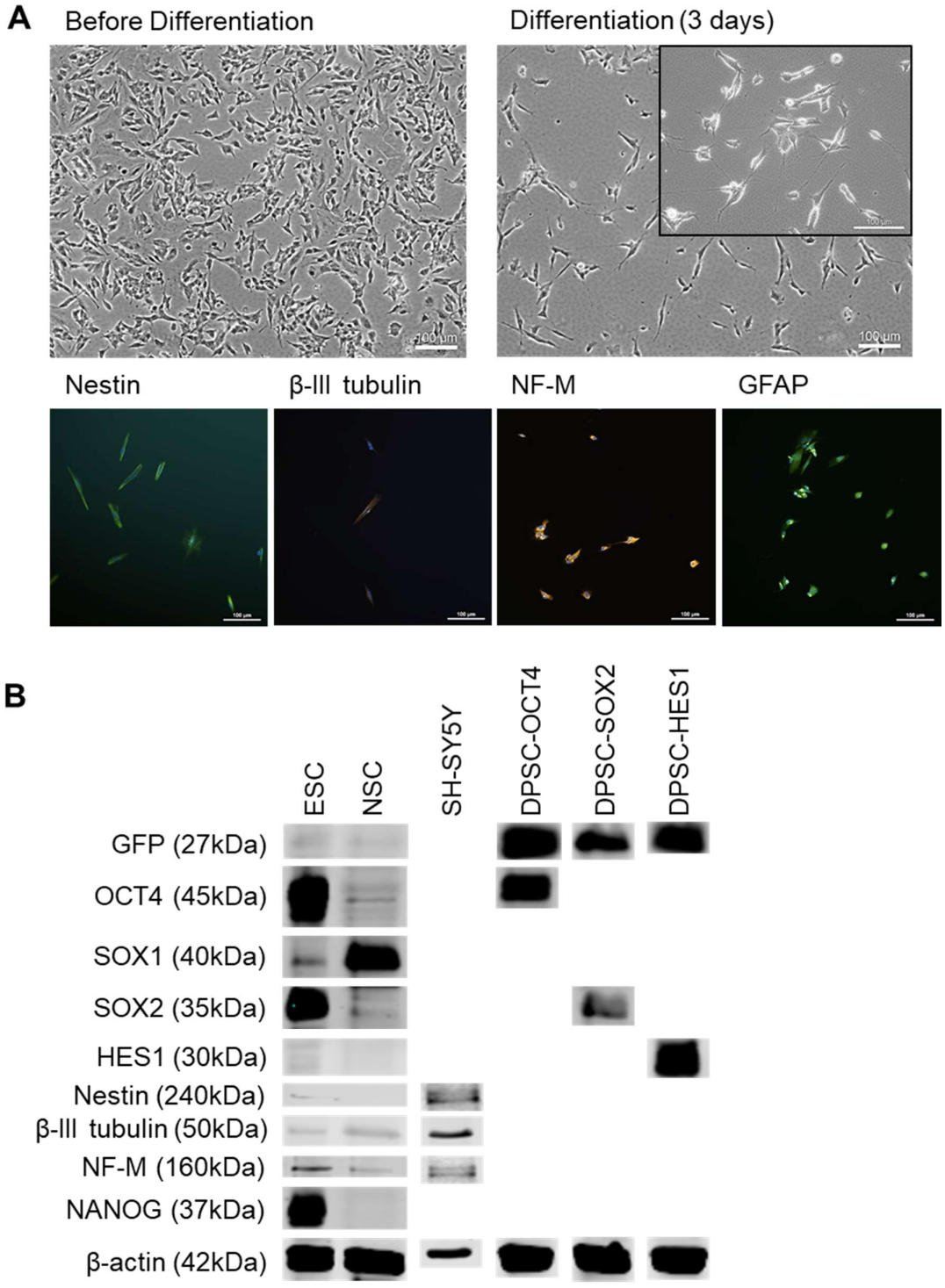

Figure B Positive controls for antibodies using in protein expression analysis. **(A)** SH-SY5Y human neuroblastoma cell line before and after neuronal differentiation. After differentiation, cells were immunostained for neural markers; nestin, β-III tubulin, NF-M, and GFAP. **(B)** Western blot antibodies detecting proteins in whole cell lysates of positive samples; human ESC, mouse NSC, SH-SY5Y cells, and human DPSC over-expressing OCT4, SOX2 and HES1 (DPSC-OCT4, DPSC-SOX2, DPSC-HES1). Note: samples were run on more than one gel and no comparisons were necessary between samples. Representative images, scale bar=100µm.

APPENDIX C: HES1 VECTOR-TRANSDUCED HUMAN DENTAL PULP STEM CELLS

DPSC-HES1 were less spindle-shaped than DPSC-EV (Figure C, parts A and B). HES1 gene and protein were over-expressed (Figure C, parts C and D). Both DPSC-EV and DPSC-HES1 cultured in NSC medium for one week showed up-regulation of the neuronal genes, *NES*, *TUBB3* and *NEFM*, with non-significantly higher levels in DPSC-EV than DPSC-OCT4. There was no difference in the gene expression levels in DPSC-OCT4 between one and two weeks in NSC culture. The neuronal proteins were detected in all the samples. NANOG was not detected.

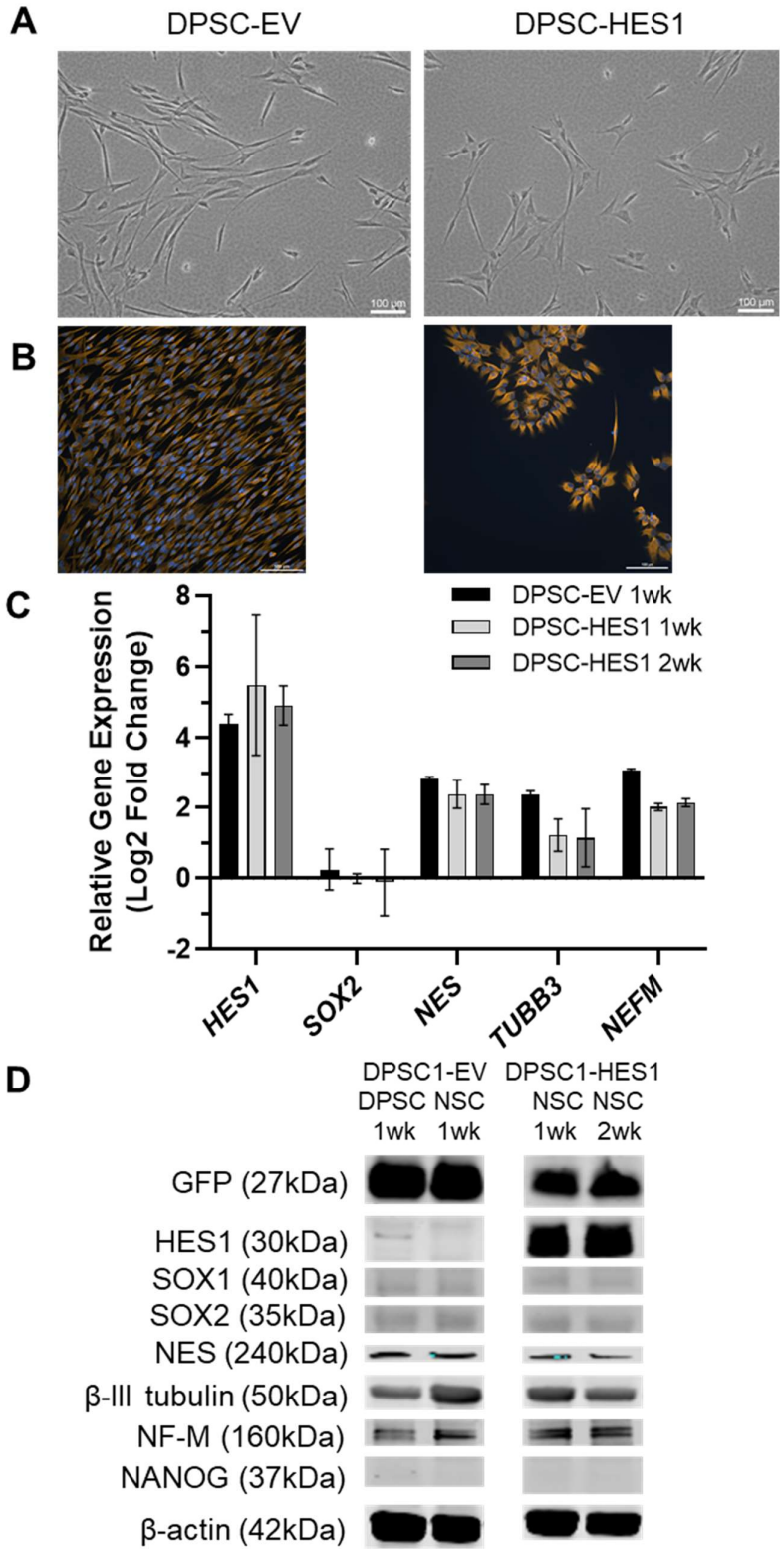

Figure C HES1 over-expression in DPSC. **(A)** DPSC-EV and DPSC-HES1 cultured in NSC medium for 1 week. **(B)** Cell morphology highlighted by immunofluorescence staining (vimentin protein). **(C)** Gene expression levels in samples from 1 and 2 weeks in NSC medium, relative to DPSC-EV in standard DPSC culture medium. **(D)** Protein expression levels; β-actin was the loading control. Representative images, data represents mean±SD, n=2, scale bar=100µm.

APPENDIX D: RNA-SEQUENCING DATA ANALYSIS CODE

output: html_document

```{r setup, include=FALSE}
knitr::opts_chunk$set(echo = TRUE)
```

```{r libraries, echo=FALSE, message=FALSE, warning=FALSE}

library(biomaRt)
library(ngsReports)
library(tidyverse)
library(limma)
library(edgeR)
library(pander)
library(knitr)
library(ggplot2)
library(ggrepel)

baseDir <- "~/projects/SAHMRI/190905_maria_rnaseq/"
binDir <- "~/projects/SAHMRI/190905_maria_rnaseq/bin/"
outdir <- "~/projects/SAHMRI/190905_maria_rnaseq/output/"
panderOptions("table.split.table", Inf)
```

```{r, echo=FALSE, out.width = "20%", out.height="20%"}
include_graphics("https://www.sahmri.org/s/img/sahmri-logo-colour.svg")
```

Analyses conducted by the SAHMRI Bioinformatics Facility:

Jimmy Breen, PhD BSc
Bioinformatics Core Leader,
Computational & Systems Biology Program, Precision Medicine Theme, SAHMRI
Research Lead (Computational Biology), Robinson Research Institute
University of Adelaide Bioinformatics Hub, University of Adelaide

Nader Aryamanesh, PhD MSc BSc
Research Fellow, Bioinformatics Core-Facility, SAHMRI
Computational & Systems Biology Program, Precision Medicine Theme, SAHMRI
Adelaide Health and Medical Sciences, The University of Adelaide

Mobile: 0477 830 366
Email: jimmy.breen@sahmri.com

2019-09-10

Analysis Details

- Data processing (trimming using AdapterRemoval, Alignment using STAR, quantification using featureCounts/R)
- Quality control assessment using FastQC
- Data filtering for low counts and transcriptional profiling (Table of expression levels for all samples)
- Differential gene expression across the two groups
- Functional Annotation: Gene Ontology and KEGG Pathway enrichment analysis

Data processing

Initial raw read processing was performed using an in-house pipeline developed at SAHMRI. Raw single-end FASTQ reads were aligned to the GRCh37 version of the human genome using the transcriptome algorthim `STAR` (https://github.com/alexdobin/STAR). After alignment, mapped sequence reads were summarised to the mm10 gene intervals using the tool `featureCounts`, available through the package `RSubread` (https://bioconductor.org/packages/release/bioc/html/Rsubread.html).

```{r transfer, echo=FALSE, message=FALSE, warning=FALSE, eval=FALSE}

# Transfer data from HPC
#rsync -avP --exclude="*.bam" --exclude="*.fastq.gz"
"sahmri:/cancer/storage/shared/shared_core_projects/190905_Maria_RNAseq/*" .
```

FastQC collation

```{r fig.height = 8}
files <- list.files(paste0(baseDir, "0_qc/"), pattern = "fastqc.zip$", full.names = TRUE)
fdl <- FastqcDataList(files)

reads <- readTotals(fdl)

# tbl_df(reads)

plotSummary(fdl)
plotReadTotals(fdl)
# plotBaseQuals(fdl[1:9], plotType = "boxplot")

plotDupLevels(fdl)
plotGcContent(fdl[1:12], plotType = "line",  theoreticalType = "Transcriptome")
```

Count details

```{r message=FALSE}
countSummary <- read_delim(paste0(baseDir,
                           "3_counts/project_allBams_GRCh37.geneCounts.tsv.summary"),
                      delim = "\t")
colnames(countSummary) <- gsub(".*/2_star/", "", colnames(countSummary))
colnames(countSummary) <- gsub("_GRCh37_Aligned.sortedByCoord.out.bam", "", colnames(countSummary))

# Counts to excel
# pander(countSummary[c(1,7,10,12),])
write_excel_csv(countSummary[c(1,7,10,12),], paste0(outdir,"Mapping_stats.csv"))

countSummaryDe <- read_delim(paste0(baseDir,
                       "3_counts/project_allBams_GRCh37.dedup.geneCounts.tsv.summary"),
                       delim = "\t")
colnames(countSummaryDe) <- gsub(".*/2a_markDupTest/", "", colnames(countSummaryDe))
colnames(countSummaryDe) <- gsub("_GRCh37_Aligned.sortedByCoord.out.dedup.bam", "",
colnames(countSummaryDe))

# Counts to excel
# pander(countSummaryDe[c(1,7,10,12),])
write_excel_csv(countSummaryDe[c(1,7,10,12),], paste0(outdir,"Mapping_stats_de.csv"))
```

Import gene counts

```{r message=FALSE}
# Read in table of counts
counts <- read_delim(paste0(baseDir, "3_counts/countTable.tsv"),
                  delim = "\t", comment = "#")
colnames(counts) <- gsub(".*/2_star/", "", colnames(counts))
colnames(counts) <- gsub("_GRCh37_Aligned.sortedByCoord.out.bam", "", colnames(counts))
counts <- as.data.frame(counts)

rownames(counts) <- counts$Geneid
counts <- counts[, -which(names(counts) %in% "Geneid")]

# head(counts)
```

Group information

```{r}
groupData <- data.frame(Sample = colnames(counts),
                        Group = c(rep("DPSC", 4),
                                  rep("DPSC_Control", 4),
                                  rep("DPSC_OCT4", 4)),
                        Replicate = c(rep(c(1,2,3,4), 3)))
tbl_df(groupData)
```

Gene Annotation

```{r}
# ensembl_gene = useEnsembl(biomart="ENSEMBL_MART_ENSEMBL",
#                 host="grch37.ensembl.org",
#                 dataset = "hsapiens_gene_ensembl")
#
# allGeneSet <- getBM(mart = ensembl_gene,
#       attributes = c("ensembl_gene_id", "external_gene_name", "entrezgene_id", "gene_biotype"),
#       filters = "ensembl_gene_id",
#       values = rownames(counts))
# save(allGeneSet, file = "allGeneSet.RData")
load(paste0(baseDir,"allGeneSet.RData"))
```

DGE List object

```{r}
cds <- DGEList(counts)

dim(cds)
table(rowSums(cds$counts==0)==12)
```

Low gene count QC

```{r}
lcpm <- cpm(cds, log = TRUE)

sampleID <- groupData$Group

library(RColorBrewer)
nsamples <- ncol(cds)
col <- brewer.pal(12, "Paired")
par(mfrow=c(1,2))
plot(density(lcpm[,1]), col=col[1], lwd=2, ylim=c(0,0.21), las=2,
     main="", xlab="")
title(main="A. Raw data", xlab="Log-cpm")
abline(v=0, lty=3)
for (i in 2:nsamples){
 den <- density(lcpm[,i])
 lines(den$x, den$y, col=col[i], lwd=2)
}
```

```{r}
cpm <- cpm(cds)
lcpm <- cpm(cds, log=TRUE)

keep.exprs <- rowSums(cpm>1)>=4
cds <- cds[keep.exprs,, keep.lib.sizes=FALSE]
```

```{r}
lcpm <- cpm(cds, log=TRUE)
plot(density(lcpm[,1]), col=col[1], lwd=2, ylim=c(0,0.21), las=2,
     main="", xlab="")
title(main="B. Filtered data", xlab="Log-cpm")
abline(v=0, lty=3)
for (i in 2:nsamples){
  den <- density(lcpm[,i])
  lines(den$x, den$y, col=col[i], lwd=2)
}
# legend("topright", sampleID, text.col=col, bty="n")
```

Trimmed mean of M-values (TMM) normalization

```{r}
cds <- calcNormFactors(cds, method = "TMM")
```

MDS plot - Sample Clustering

```{r warning = FALSE}
mds <- plotMDS(cds, plot = FALSE)

cbind(as.data.frame(mds$x), as.data.frame(mds$y)) %>%
  tibble::rownames_to_column(var = "Sample") %>%
  inner_join(groupData, by = "Sample") %>%
  ggplot(aes(mds$x,mds$y, label = Sample,
             colour = Group)) +
  geom_point(size = 3) +
  # geom_label(aes(label = Sample)) +
  # scale_x_continuous(limits = c(-4,4)) +
  # scale_y_continuous(limits = c(-0.7,0.7)) +
  xlab("Dimension 1") +
  ylab("Dimension 2") +
  theme_bw()
```

Differential Gene Expression using `limma-voom`

```{r}
design <- model.matrix(~0 + Group, data = groupData)
colnames(design) <- gsub("Group", "", colnames(design))
# design

contr.matrix <- makeContrasts(ControlVsDpsc= DPSC-DPSC_Control,
                              Oct4VsDpsc = DPSC_OCT4-DPSC,
                              ControlVsOct4 = DPSC_OCT4-DPSC_Control,
   levels = colnames(design))

geno <- colnames(contr.matrix)
contr.matrix
```

Information on `limma-voom` fitted models

```{r}
efit <- voom(cds, design, plot=TRUE) %>%
  lmFit(design) %>%
  contrasts.fit(contrasts=contr.matrix) %>%
  eBayes()
```

Summary table for differentially expressed genes

```{r}
summary(decideTests(efit))
```

```{r}
vfit <- voom(cds, design, plot=FALSE) %>%
  lmFit(design) %>%
  contrasts.fit(contrasts=contr.matrix) %>%
  eBayes()

tfit <- treat(vfit, lfc=1)
table(decideTests(tfit))
dt <- decideTests(tfit)

summary <- as.data.frame(dt@.Data)

summary(decideTests(tfit))
```

```{r}
vfit <- voom(cds, design, plot=FALSE) %>%
  lmFit(design) %>%
  contrasts.fit(contrasts=contr.matrix) %>%
  eBayes()

tfit <- treat(vfit, lfc=2)
table(decideTests(tfit))
dt <- decideTests(tfit)

summary <- as.data.frame(dt@.Data)

summary(decideTests(tfit))
```

DE Results Tables and Annotation

```{r}

comps <- c("ControlVsDpsc", "Oct4VsDpsc", "ControlVsOct4")

resultsTblList <- lapply(1:3, function(x){
  topTreat(tfit, coef=x, n=Inf) %>%
    tibble::rownames_to_column(var = "GeneID") %>%
    left_join(allGeneSet, by = c("GeneID" = "ensembl_gene_id")) %>%
    dplyr::select(GeneID,
                  GeneName = external_gene_name,
                  EntrezGeneID = entrezgene_id,
                  logFC, AveExpr, FDR = adj.P.Val) %>%
    arrange(FDR) %>%
    dplyr::filter(FDR < 0.05)
})
names(resultsTblList) <- comps

resultsTblListAll <- lapply(1:3, function(x){
  topTreat(tfit, coef=x, n=Inf) %>%
    tibble::rownames_to_column(var = "GeneID") %>%
    left_join(allGeneSet, by = c("GeneID" = "ensembl_gene_id")) %>%
    dplyr::select(GeneID,
                  GeneName = external_gene_name,
                  EntrezGeneID = entrezgene_id,
                  logFC, AveExpr, FDR = adj.P.Val) %>%
    arrange(FDR)
})
names(resultsTblListAll) <- comps
```

Top Results

```{r}
lapply(resultsTblList, function(x){
  x %>%
    head(n=10)
})
```

Whats up and whats down?

```{r}
comp1 <- head(resultsTblList$ControlVsDpsc, n=5)
comp2 <- head(resultsTblList$ControlVsOct4, n=5)
comp3 <- head(resultsTblList$Oct4VsDpsc, n=5)

# Control vs DPSC
comp1
counts[rownames(counts) %in% comp1$GeneID,][,1:8]

comp2
counts[rownames(counts) %in% comp2$GeneID,][,5:12]

comp3
counts[rownames(counts) %in% comp3$GeneID,][,c(1:4,9:12)]
```

Comparison to deduplicated counts

```{r message=FALSE}

# Read in table of deduplicated gene counts
decounts <- read_delim(paste0(baseDir, "3_counts/dedup_countTable.tsv"), delim = "\t", comment = "#")
colnames(decounts) <- gsub(".*/2a_markDupTest/",
                           "", colnames(decounts))
colnames(decounts) <- gsub("_GRCh37_Aligned.sortedByCoord.out.dedup.bam",
                           "", colnames(decounts))
decounts <- as.data.frame(decounts)
rownames(decounts) <- decounts$Geneid
decounts <- decounts[, -which(names(decounts) %in% c("Geneid", "Undetermined_S0")) ]

# Load into a specific DGEList
cdsDe <- DGEList(decounts)

# Size of the data
dim(cdsDe)
# Eliminating row with zero values for all samples.
table(rowSums(cdsDe$counts==0)==12)

# Filter the same as before
cpmDe <- cpm(cdsDe)
keep.exprs <- rowSums(cpm>1)>=4
cdsDe <- cdsDe[keep.exprs,, keep.lib.sizes=FALSE]
cdsDe <- calcNormFactors(cdsDe, method = "TMM")

# Rerun voom transformation
vfit2 <- voom(cdsDe, design, plot=FALSE) %>%
  lmFit(design) %>%
  contrasts.fit(contrasts=contr.matrix) %>%
  eBayes()

tfit2 <- treat(vfit2, lfc=2)
```

Summary table for differentially expressed genes in deduplicated counts

```{r}
summary(decideTests(tfit2))
```

```{r}
resultsTblListDe <- lapply(1:3, function(x){
  topTreat(tfit2, coef=x, n=Inf) %>%
    tibble::rownames_to_column(var = "GeneID") %>%
    left_join(allGeneSet, by = c("GeneID" = "ensembl_gene_id")) %>%
    dplyr::select(GeneID,
                  GeneName = external_gene_name,
                  EntrezGeneID = entrezgene_id,
                  logFC, AveExpr, FDR = adj.P.Val) %>%
    arrange(FDR) %>%
    dplyr::filter(FDR < 0.05)
})
names(resultsTblListDe) <- comps

resultsTblListDeAll <- lapply(1:3, function(x){
  topTreat(tfit2, coef=x, n=Inf) %>%
    tibble::rownames_to_column(var = "GeneID") %>%
    left_join(allGeneSet, by = c("GeneID" = "ensembl_gene_id")) %>%
    dplyr::select(GeneID,
                  GeneName = external_gene_name,
                  EntrezGeneID = entrezgene_id,
                  logFC, AveExpr, FDR = adj.P.Val) %>%
    arrange(FDR)
})
names(resultsTblListDeAll) <- comps
```

Venn Diagram (Normal vs Deduplicated counts)

```{r}
plot01 <- list(Normal=resultsTblList$ControlVsDpsc$GeneID,
               Deduplicated=resultsTblListDe$ControlVsDpsc$GeneID)

gplots::venn(plot01)
```

Results of all genes and just DE genes

```{r}
# Combine DE gene tables into one dataframe
flatDE <- bind_rows(resultsTblList, .id = "Comparison")
writexl::write_xlsx(flatDE, paste(outdir, "all_diffExpressed_FDR5_genes.xlsx"))

flatAll <- bind_rows(resultsTblListAll, .id = "Comparison")
writexl::write_xlsx(flatDE, paste(outdir, "all_genes.xlsx"))
```

Heatmap of all DE genes in each group

```{r, fig.width=7, fig.height=15}

# Extract genes from DE and subset matrix
cpm <- cpm(cds$counts, log = TRUE)
cpm <- cpm[rownames(cpm) %in% flatDE$GeneID,]

# Make an annotation dataframe
annotation <- groupData %>%
  tibble::column_to_rownames(var = "Sample") %>%
  dplyr::select(-Replicate)
```

```
pheatmap::pheatmap(data.matrix(cpm), show_rownames = FALSE,
                   show_colnames = FALSE,
                   annotation_col = annotation)
```

Heatmap of specific comparisons

First its the Control vs DPSC comparison

```{r echo = FALSE, message=FALSE, fig.width = 7, fig.height = 18}

cpm <- cpm(cds$counts, log = TRUE)

# Control vs DPSC
# We'll take absolute logFC > 6 here
sub <- resultsTblList$ControlVsDpsc[abs(resultsTblList$ControlVsDpsc$logFC) > 6,]

subHeat <- as.data.frame(cpm) %>%
  tibble::rownames_to_column(var = "EnsemblID") %>%
  dplyr::filter(EnsemblID %in% sub$GeneID) %>%
  left_join(allGeneSet, by = c("EnsemblID" = "ensembl_gene_id")) %>%
  dplyr::select(-EnsemblID, -entrezgene_id, -gene_biotype,
                -`09-Sample--SAMPLE-Maria-RNAseq_S9`, -`10-Sample--SAMPLE-Maria-RNAseq_S10`,
                -`11-Sample--SAMPLE-Maria-RNAseq_S11`, -`12-Sample--SAMPLE-Maria-RNAseq_S12`) %>%
  distinct(external_gene_name, .keep_all = TRUE) %>%
  tibble::column_to_rownames(var = "external_gene_name")

pheatmap::pheatmap(data.matrix(subHeat),
                   show_rownames = TRUE,
                   annotation_col = annotation,
                   show_colnames = FALSE)
```

Now the Control vs DPSC-Oct4 comparison

```{r echo = FALSE, message=FALSE, fig.width = 7, fig.height = 18}

cpm <- cpm(cds$counts, log = TRUE)

# Control vs DPSC
# We'll take absolute logFC > 7 here
sub <- resultsTblList$ControlVsOct4[abs(resultsTblList$ControlVsOct4$logFC) > 7,]

subHeat <- as.data.frame(cpm) %>%
  tibble::rownames_to_column(var = "EnsemblID") %>%
  dplyr::filter(EnsemblID %in% sub$GeneID) %>%
  left_join(allGeneSet, by = c("EnsemblID" = "ensembl_gene_id")) %>%
  dplyr::select(-EnsemblID, -entrezgene_id, -gene_biotype,
                -`01-Sample--SAMPLE-Maria-RNAseq_S1`, -`02-Sample--SAMPLE-Maria-RNAseq_S2`,
                -`03-Sample--SAMPLE-Maria-RNAseq_S3`, -`04-Sample--SAMPLE-Maria-RNAseq_S4`) %>%
  distinct(external_gene_name, .keep_all = TRUE) %>%
  tibble::column_to_rownames(var = "external_gene_name")

pheatmap::pheatmap(data.matrix(subHeat),
                   show_rownames = TRUE,
                   annotation_col = annotation,
                   show_colnames = FALSE)
```

And last, the DPSC vs DPSC-Oct4 comparison

```{r echo = FALSE, message=FALSE, fig.width = 7, fig.height = 18}

cpm <- cpm(cds$counts, log = TRUE)
```

```
# Control vs DPSC
# We'll take absolute logFC > 7 here
sub <- resultsTblList$Oct4VsDpsc[abs(resultsTblList$Oct4VsDpsc$logFC) > 7,]

subHeat <- as.data.frame(cpm) %>%
  tibble::rownames_to_column(var = "EnsemblID") %>%
  dplyr::filter(EnsemblID %in% sub$GeneID) %>%
  left_join(allGeneSet, by = c("EnsemblID" = "ensembl_gene_id")) %>%
  dplyr::select(-EnsemblID, -entrezgene_id, -gene_biotype,
                -`05-Sample--SAMPLE-Maria-RNAseq_S5`, -`06-Sample--SAMPLE-Maria-RNAseq_S6`,
                -`07-Sample--SAMPLE-Maria-RNAseq_S7`, -`08-Sample--SAMPLE-Maria-RNAseq_S8`) %>%
  distinct(external_gene_name, .keep_all = TRUE) %>%
  tibble::column_to_rownames(var = "external_gene_name")

pheatmap::pheatmap(data.matrix(subHeat),
                   show_rownames = TRUE,
                   annotation_col = annotation,
                   show_colnames = FALSE)
```

REFERENCES

1. Arthur A, Rychkov G, Shi S, Koblar SA, Gronthos S. Adult human dental pulp stem cells differentiate toward functionally active neurons under appropriate environmental cues. Stem Cells. 2008;26(7):1787-95.
2. Kiraly M, Porcsalmy B, Pataki A, Kadar K, Jelitai M, Molnar B, et al. Simultaneous PKC and cAMP activation induces differentiation of human dental pulp stem cells into functionally active neurons. Neurochemistry International. 2009;55(5):323-32.
3. Gervois P, Struys T, Hilkens P, Bronckaers A, Ratajczak J, Politis C, et al. Neurogenic maturation of human dental pulp stem cells following neurosphere generation induces morphological and electrophysiological characteristics of functional neurons. Stem Cells and Development. 2015;24(3):296-311.
4. Kaukua N, Shahidi MK, Konstantinidou C, Dyachuk V, Kaucka M, Furlan A, et al. Glial origin of mesenchymal stem cells in a tooth model system. Nature. 2014;513(7519):551-4.
5. Janebodin K, Horst OV, Ieronimakis N, Balasundaram G, Reesukumal K, Pratumvinit B, et al. Isolation and characterization of neural crest-derived stem cells from dental pulp of neonatal mice. PLoS One. 2011;6(11):e27526.
6. Chai Y, Jiang X, Ito Y, Bringas P, Jr., Han J, Rowitch DH, et al. Fate of the mammalian cranial neural crest during tooth and mandibular morphogenesis. Development. 2000;127(8):1671-9.
7. Yamazaki H, Tsuneto M, Yoshino M, Yamamura K, Hayashi S. Potential of dental mesenchymal cells in developing teeth. Stem Cells. 2007;25:78-87.
8. Leong WK, Henshall TL, Arthur A, Kremer KL, Lewis MD, Helps SC, et al. Human adult dental pulp stem cells enhance poststroke functional recovery through non-neural replacement mechanisms. Stem Cells Translational Medicine. 2012;1(3):177-87.
9. Nito C, Sowa K, Nakajima M, Sakamoto Y, Suda S, Nishiyama Y, et al. Transplantation of human dental pulp stem cells ameliorates brain damage following acute cerebral ischemia. Biomedicine and Pharmacotherapy. 2018;108:1005-14.
10. Shi G, Jin Y. Role of OCT4 in maintaining and regaining stem cell pluripotency. Stem Cell Research & Therapy. 2010;1(39).
11. Sterneckert J, Hoing S, Scholer HR. Concise review: Oct4 and more: the reprogramming expressway. Stem Cells. 2012;30(1):15-21.
12. Mitchell R, Szabo E, Shapovalova Z, Aslostovar L, Makondo K, Bhatia M. Molecular evidence for OCT4-induced plasticity in adult human fibroblasts required for direct cell fate conversion to lineage specific progenitors. Stem Cells. 2014;32(8):2178-87.

13. Mitchell RR, Szabo E, Benoit YD, Case DT, Mechael R, Alamilla J, et al. Activation of neural cell fate programs toward direct conversion of adult human fibroblasts into tri-potent neural progenitors using OCT-4. Stem Cells and Development. 2014;23(16):1937-46.
14. Lee JH, Mitchell RR, McNicol JD, Shapovalova Z, Laronde S, Tanasijevic B, et al. Single Transcription Factor Conversion of Human Blood Fate to NPCs with CNS and PNS Developmental Capacity. Cell Reports. 2015;11(9):1367-76.
15. Liao W, Huang N, Yu J, Jares A, Yang J, Zieve G, et al. Direct Conversion of Cord Blood CD34+ Cells Into Neural Stem Cells by OCT4. Stem Cells Translational Medicine. 2015;4(7):755-63.
16. Liu L, Wu L, Wei X, Ling J. Induced overexpression of Oct4A in human dental pulp cells enhances pluripotency and multilineage differentiation capability. Stem Cells and Development. 2015;24(8):962-72.
17. Maucksch C, Jones KS, Connor B. Concise review: the involvement of SOX2 in direct reprogramming of induced neural stem/precursor cells. Stem Cells Translational Medicine. 2013;2(8):579-83.
18. Pevny LH, Nicolis SK. Sox2 roles in neural stem cells. The International Journal of Biochemistry and Cell Biology. 2010;42(3):421-4.
19. Ring KL, Tong LM, Balestra ME, Javier R, Andrews-Zwilling Y, Li G, et al. Direct reprogramming of mouse and human fibroblasts into multipotent neural stem cells with a single factor. Cell Stem Cell. 2012;11(1):100-9.
20. Liu P, Cai J, Dong D, Chen Y, Liu X, Wang Y, et al. Effects of SOX2 on proliferation, migration and adhesion of human dental pulp stem cells. PLoS One. 2015;10(10):1-17.
21. Kageyama R, Shimojo H, Imayoshi I. Dynamic expression and roles of Hes factors in neural development. Cell Tissue Research. 2015;359(1):125-33.
22. Imayoshi I, Kageyama R. bHLH factors in self-renewal, multipotency, and fate choice of neural progenitor cells. Neuron. 2014;82(1):9-23.
23. Dhanesh SB, Subashini C, James J. Hes1: the maestro in neurogenesis. Cell and Molecular Life Sciences. 2016;73(21):4019-42.
24. Sheng C, Zheng Q, Wu J, Xu Z, Wang L, Li W, et al. Direct reprogramming of Sertoli cells into multipotent neural stem cells by defined factors. Cell Research. 2012;22(1):208-18.
25. Forster JI, Koglsberger S, Trefois C, Boyd O, Baumuratov AS, Buck L, et al. Characterization of Differentiated SH-SY5Y as Neuronal Screening Model Reveals Increased Oxidative Vulnerability. Journal of Biomolecular Screening. 2016;21(5):496-509.
26. Livak KJ, Schmittgen TD. Analysis of relative gene expression data using real-time quantitative PCR and the 2(-Delta Delta C(T)) Method Methods. 2001;25(4):402-8.

27. Schindelin J, Arganda-Carreras I, Frise E, Kaynig V, Longair M, Pietzsch T, et al. Fiji: an open-source platform for biological-image analysis. Nature Methods. 2012;9(7):676-82.
28. Gronthos S, Mankani M, Brahim J, Robey PG, Shi S. Postnatal human dental pulp stem cells (DPSCs) in vitro and in vivo. Proc Natl Acad Sci U S A. 2000;97(25):13625-30.
29. Gronthos S, Brahim J, Li W, Fisher LW, Cherman N, Boyde A, et al. Stem cell properties of human dental pulp stem cells. Journal of Dental Research. 2002;81(8):531-5.
30. Dominici M, Le Blanc K, Mueller I, Slaper-Cortenbach I, Marini FC, Krause D, et al. Minimal criteria for defining multipotent mesenchymal stromal cells. The International Society for Cellular Therapy position statement. Cytotherapy. 2006;8(4):315-7.
31. Hilkens P, Gervois P, Fanton Y, Vanormelingen J, Martens W, Struys T, et al. Effect of isolation methodology on stem cell properties and multilineage differentiation potential of hDPSCs. Cell Tissue Research. 2013;353:65-78.
32. Quirici N, Soligo D, Bossolasco P, Servida F, Lumini C, Deliliers GL. Isolation of bone marrow mesenchymal stem cells by anti-nerve growth factor receptor antibodies. Experimental Hematology. 2002;30:783-91.
33. Gronthos S, Zannettino ACW, Hay SJ, Shi S, Graves SE, Kortesidis A, et al. Molecular and cellular characterisation of highly purified stromal stem cells derived from human bone marrow. Journal of Cell Science. 2003;116(9):1827-35.
34. Gronthos S, Simmons PJ. The growth factor requirements of STRO-l-positive human bone marrow stromal precursors under serum-deprived conditions in vitro. Blood. 1995;85(4):929-40.
35. Shi S, Gronthos S. Perivascular niche of postnatal mesenchymal stem cells in human bone marrow and dental pulp. Journal of Bone and Mineral Research. 2003;18(4):696-704.
36. Gancheva MR, Kremer KL, Gronthos S, Koblar SA. Using Dental Pulp Stem Cells for Stroke Therapy. Front Neurol. 2019;10:422.
37. Gundle R, Stewart K, Screen J, Beresford JN. Isolation and culture of human bone derived cells. In: Beresford J, Owen M, editors. Marrow Stromal Cell Culture. Cambridge: Cambridge University Press; 1998.
38. Jaiswal N, Haynesworth SE, Caplan AI, Bruder SP. Osteogenic differentiation of purified, culture-expanded human mesenchymal stem cells in vitro. Journal of Cellular Biochemistry. 1997;64(2):295-312.
39. Marrelli M, Paduano F, Tatullo M. Cells isolated from human periapical cysts express mesenchymal stem cell-like properties. International Journal of Biological Sciences. 2013;9(10):1070-8.

40. Yen CY, Wu YW, Hsiung CN, Yeh MI, Lin YM, Lee SY. Cell-based semiquantitative assay for sulfated glycosaminoglycans facilitating the identification of chondrogenesis. Analytical Biochemistry. 2015;486:41-3.
41. Ramirez-Zacarias JL, Castro-Munozledo F, Kuri-Harcuch W. Quantitation of adipose conversion and triglycerides by staining intracytoplasmic lipids with Oil red O. Histochemistry. 1992;97:493-7.
42. Gimble J. Marrow stromal adipocytes. In: Beresford JN, Owen ME, editors. Marrow stromal cell culture. Cambridge: Cambridge University Press; 1998. p. 67-87.
43. Ellis KM, O'Carroll DC, Lewis MD, Rychkov GY, Koblar SA. Neurogenic potential of dental pulp stem cells isolated from murine incisors. Stem Cell Research and Therapy. 2014;5(30).
44. Harkness L, Zaher W, Ditzel N, Isa A, Kassem M. CD146/MCAM defines functionality of human bone marrow stromal stem cell populations. Stem Cell Research and Therapy. 2016;7:4.
45. Russell KC, Phinney DG, Lacey MR, Barrilleaux BL, Meyertholen KE, O'Connor KC. In vitro high-capacity assay to quantify the clonal heterogeneity in trilineage potential of mesenchymal stem cells reveals a complex hierarchy of lineage commitment. Stem Cells. 2010;28(4):788-98.
46. Matsui M, Kobayashi T, Tsutsui TW. CD146 positive human dental pulp stem cells promote regeneration of dentin/pulp-like structures. Human Cell. 2018;31(2):127-38.
47. Sugiyama M, Iohara K, Wakita H, Hattori H, Ueda M, Matsushita K, et al. Dental pulp-derived CD31-/CD146- side population stem/progenitor cells enhance recovery of focal cerebral ischemia in rats.pdf>. Tissue Engineering: Part A. 2011;17(9-10):1303-11.
48. Fitter S, Gronthos S, Ooi SS, Zannettino AC. The Mesenchymal Precursor Cell Marker Antibody STRO-1 Binds to Cell Surface Heat Shock Cognate 70. Stem Cells. 2017;35(4):940-51.
49. Lin G, Liu G, Banie L, Wang G, Ning H, Lue TF, et al. Tissue distribution of mesenchymal stem cell marker Stro-1. Stem Cells and Development. 2011;20(10):1747-52.
50. Zannettino AC, Paton S, Kortesidis A, Khor F, Itescu S, Gronthos S. Human mulipotential mesenchymal/stromal stem cells are derived from a discrete subpopulation of STRO-1bright/CD34 /CD45(-)/glycophorin-A-bone marrow cells. Haematologica. 2007;92(12):1707-8.
51. Dennis JE, Carbillet J-P, Caplan AI, Charbord P. The STRO-1+ marrow cell population is multipotential. Cells Tissues Organs. 2002;170:73-82.

52. Kortesidis A, Zannettino A, Isenmann S, Shi S, Lapidot T, Gronthos S. Stromal-derived factor-1 promotes the growth, survival, and development of human bone marrow stromal stem cells. Blood. 2005;105(10):3793-801.
53. Gronthos S, Zannettino A, Graves S, Ohta S, Hay S, Simmons P. Differential cell surface expression of the STRO-1 and alkaline phosphatase antigens on discrete developmental stages in primary cultures of human bone cells. Journal of Bone and Mineral Research. 1999;14(1):47-56.
54. Alvarez R, Lee HL, Hong C, Wang CY. Single CD271 marker isolates mesenchymal stem cells from human dental pulp. International Journal of Oral Science. 2015;7(4):205-12.
55. Betters E, Liu Y, Kjaeldgaard A, Sundstrom E, Garcia-Castro MI. Analysis of early human neural crest development. Developmental Biology. 2010;344(2):578-92.
56. Pan W, Kremer KL, Kaidonis X, Ludlow VE, Rogers ML, Xie J, et al. Characterization of p75 neurotrophin receptor expression in human dental pulp stem cells. International Journal of Developmental Neuroscience. 2016;53:90-8.
57. Martens W, Sanen K, Georgiou M, Struys T, Bronckaers A, Ameloot M, et al. Human dental pulp stem cells can differentiate into Schwann cells and promote and guide neurite outgrowth in an aligned tissue-engineered collagen construct in vitro. The FASEB Journal. 2014;28(4):1634-43.
58. Solis-Castro OO, Boissonade FM, Rivolta MN. Establishment and neural differentiation of neural crest-derived stem cells (NCSCs) from human dental pulp in serum-free conditions. Stem Cells Translational Medicine. 2020:1-15.
59. Fracaro L, Senegaglia AC, Herai RH, Leitolis A, Boldrini-Leite LM, Rebelatto CLK, et al. The Expression Profile of Dental Pulp-Derived Stromal Cells Supports Their Limited Capacity to Differentiate into Adipogenic Cells. International Journal of Molecular Science. 2020;21(8).
60. D'Aiuto L, Zhi Y, Kumar Das D, Wilcox MR, Johnson JW, McClain L, et al. Large-scale generation of human iPSC-derived neural stem cells/early neural progenitor cells and their neuronal differentiation. Organogenesis. 2014;10(4):365-77.
61. Liu D, Pavathuparambil Abdul Manaph N, Al-Hawwas M, Bobrovskaya L, Xiong LL, Zhou XF. Coating Materials for Neural Stem/Progenitor Cell Culture and Differentiation. Stem Cells and Development. 2020;29(8):463-74.
62. Dottori M, Pera MF. Neural Differentiation of Human Embryonic Stem Cells. In: Weiner LP, editor. Neural Stem Cells: Methods and Protocols. Methods in Molecular Biology. 2 ed. Totowa, NJ: Humana Press; 2008. p. 19-30.
63. Sun Y, Huang Z, Yang K, Wang D, Liu W, Sun K, et al. Surface coating as a key parameter in engineering neuronal network structures in vitro. Biointerphase. 2012;7(29).

64. Ge H, Tan L, Wu P, Yin Y, Liu X, Meng H, et al. Poly-L-ornithine promotes preferred differentiation of neural stem/progenitor cells via ERK signalling pathway. Science Reports. 2015;5:15535.
65. Kim YH, Baek NS, Han YH, Chung MA, Jung SD. Enhancement of neuronal cell adhesion by covalent binding of poly-D-lysine. Journal of Neuroscience Methods. 2011;202(1):38-44.
66. Winkel A, Jaimes Y, Melzer C, Dillschneider P, Hartwig H, Stiesch M, et al. Cell culture media notably influence properties of human mesenchymal stroma/stem-like cells from different tissues. Cytotherapy. 2020:1-16.
67. Milone MC, O'Doherty U. Clinical use of lentiviral vectors. Leukemia. 2018;32(7):1529-41.
68. Ghosh S, Brown AM, Jenkins C, Campbell K. Viral Vector Systems for Gene Therapy: A Comprehensive Literature Review of Progress and Biosafety Challenges. Applied Biosafety. 2020;25(1):7-18.
69. Durand S, Cimarelli A. The inside out of lentiviral vectors. Viruses. 2011;3(2):132-59.
70. Zhao J, Lever AML. Lentivirus-mediated Gene Expression. In: Zhang J, Rokosh G, editors. Cardiac Gene Expression: Methods and Protocols. Methods in Molecular Biology. 366. 1 ed. Totowa, NJ, USA: Humana Press; 2007. p. 343-55.
71. Tolmachov OE, Tolmachova T, Al-Allaf FA. Designing Lentiviral Gene Vectors. In: Xu K, editor. Viral Gene Therapy: Intech Open; 2011. p. 263-84.
72. Dull T, Zufferey R, Kwelly M, Mandel RJ, Nguyen M, Trono D, et al. A Third-Generation Lentivirus Vector with a Conditional Packaging System. Journal of Virology. 1998;72(11):8463-71.
73. Gama-Norton L, Botezatu L, Herrmann S, Schweizer M, Alves PM, Hauser H, et al. Lentivirus production is influenced by SV40 large T-antigen and chromosomal integration of the vector in HEK293 cells. Human Gene Therapy. 2011;22(10):1269-79.
74. Hsu CC, Li HP, Hung YH, Leu YW, Wu WH, Wang FS, et al. Targeted methylation of CMV and E1A viral promoters. Biochemical and Biophysical Research Communications. 2010;402(2):228-34.
75. Wang N, Rajasekaran N, Hou T, Lisowski L, Mellins ED. Comparison of transduction efficiency among various lentiviruses containing GFP reporter in bone marrow hematopoietic stem cell transplantation. Experimental Hematology. 2013;41(11):934-43.
76. Ikeda Y, Collins MK, Radcliffe PA, Mitrophanous KA, Takeuchi Y. Gene transduction efficiency in cells of different species by HIV and EIAV vectors. Gene Therapy. 2002;9(14):932-8.

77. Geraerts M, Willems S, Baekelandt V, Debyser Z, Gijsbers R. Comparison of lentiviral vector titration methods. BMC Biotechnology. 2006;6:34.
78. Hlavaty J, Tonar Z, Renner M, Panitz S, Petznek H, Schweizer M, et al. Tropism, intracerebral distribution, and transduction efficiency of HIV- and SIV-based lentiviral vectors after injection into the mouse brain: a qualitative and quantitative in vivo study. Histochemistry Cell Biology. 2017;148(3):313-29.
79. Takahashi K, Tanabe K, Ohnuki M, Narita M, Ichisaka T, Tomoda K, et al. Induction of pluripotent stem cells from adult human fibroblasts by defined factors. Cell. 2007;131(5):861-72.
80. Yu X, Alder JK, Chun JH, Friedman AD, Heimfeld S, Cheng L, et al. HES1 inhibits cycling of hematopoietic progenitor cells via DNA binding. Stem Cells. 2006;24(4):876-88.
81. Campeau E, Ruhl VE, Rodier F, Smith CL, Rahmberg BL, Fuss JO, et al. A versatile viral system for expression and depletion of proteins in mammalian cells. PLoS One. 2009;4(8):e6529.
82. Cheng Z, Gong Y, Ma Y, Lu K, Lu X, Pierce LA, et al. Inhibition of BET bromodomain targets genetically diverse glioblastoma. Clinical Cancer Research. 2013;19(7):1748-59.
83. Hayer A, Shao L, Chung M, Joubert LM, Yang HW, Tsai FC, et al. Engulfed cadherin fingers are polarized junctional structures between collectively migrating endothelial cells. Nature Cell Biology. 2016;18(12):1311-23.
84. Delenda C, Gaillard C. Real-time quantitative PCR for the design of lentiviral vector analytical assays. Gene Therapy. 2005;12:S36-50.
85. Zhang B, Metharom P, Jullie H, Ellem KA, Cleghorn G, West MJ, et al. The significance of controlled conditions in lentiviral vector titration and in the use of multiplicity of infection (MOI) for predicting gene transfer events. Genetic Vaccines and Therapy. 2004;2(1):6.
86. Takahashi K, Yamanaka S. Induction of pluripotent stem cells from mouse embryonic and adult fibroblast cultures by defined factors. Cell. 2006;126(4):663-76.
87. Vierbuchen T, Ostermeier A, Pang ZP, Kokubu Y, Sudhof TC, Wernig M. Direct conversion of fibroblasts to functional neurons by defined factors. Nature. 2010;463(7284):1035-41.
88. Christodoulou I, Patsali P, Stephanou C, Antoniou M, Kleanthous M, Lederer CW. Measurement of lentiviral vector titre and copy number by cross-species duplex quantitative PCR. Gene Therapy. 2016;23(1):113-8.
89. Santeramo I, Bagnati M, Harvey EJ, Hassan E, Surmacz-Cordle B, Marshall D, et al. Vector Copy Distribution at a Single-Cell Level Enhances Analytical Characterization of

Gene-Modified Cell Therapies. Molecular Therapy Methods and Clinical Development. 2020;17:944-56.
90. Telford WG, Hawley T, Subach F, Verkhusha V, Hawley RG. Flow cytometry of fluorescent proteins. Methods. 2012;57(3):318-30.
91. Carey BW, Markoulaki S, Hanna J, Saha K, Gao Q, Mitalipova M, et al. Reprogramming of murine and human somatic cells using a single polycistronic vector. Proceedings of the National Academy of Sciences. 2009;106(1):157-62.
92. Govindasamy V, Abdullah AN, Ronald VS, Musa S, Ab Aziz ZA, Zain RB, et al. Inherent differential propensity of dental pulp stem cells derived from human deciduous and permanent teeth. Journal of Endodontics. 2010;36(9):1504-15.
93. Liu L, Wei X, Ling J, Wu L, Xiao Y. Expression pattern of Oct-4, Sox2, and c-Myc in the primary culture of human dental pulp derived cells. Journal of Endodontics. 2011;37(4):466-72.
94. Tamaoki N, Takahashi K, Tanaka T, Ichisaka T, Aoki H, Takeda-Kawaguchi T, et al. Dental pulp cells for induced pluripotent stem cell banking. Journal of Dental Research. 2010;89(8):773-8.
95. Tai MH, Chang CC, Kiupel M, Webster JD, Olson LK, Trosko JE. Oct4 expression in adult human stem cells: evidence in support of the stem cell theory of carcinogenesis. Carcinogenesis. 2005;26(2):495-502.
96. Lengner CJ, Camargo FD, Hochedlinger K, Welstead GG, Zaidi S, Gokhale S, et al. Oct4 expression is not required for mouse somatic stem cell self-renewal. Cell Stem Cell. 2007;1(4):403-15.
97. Liedtke S, Enczmann J, Waclawczyk S, Wernet P, Kogler G. Oct4 and its pseudogenes confuse stem cell research. Cell Stem Cell. 2007;1(4):364-6.
98. Ming GL, Song H. Adult neurogenesis in the mammalian brain: significant answers and significant questions. Neuron. 2011;70(4):687-702.
99. Mertens J, Marchetto MC, Bardy C, Gage FH. Evaluating cell reprogramming, differentiation and conversion technologies in neuroscience. Nature Reviews Neuroscience. 2016;17(7):424-37.
100. Jopling C, Boue S, Izpisua Belmonte JC. Dedifferentiation, transdifferentiation and reprogramming: three routes to regeneration. Nature Reviews Molecular Cell Biology. 2011;12(2):79-89.
101. Fusco S, Leone L, Barbati SA, Samengo D, Piacentini R, Maulucci G, et al. A CREB-Sirt1-Hes1 Circuitry Mediates Neural Stem Cell Response to Glucose Availability. Cell Reports. 2016;14(5):1195-205.

102. Bardy C, van den Hurk M, Eames T, Marchand C, Hernandez RV, Kellogg M, et al. Neuronal medium that supports basic synaptic functions and activity of human neurons in vitro. Proc Natl Acad Sci U S A. 2015;112(20):E2725-34.
103. Lujan E, Chanda S, Ahlenius H, Sudhof TC, Wernig M. Direct conversion of mouse fibroblasts to self-renewing, tripotent neural precursor cells. Proc Natl Acad Sci U S A. 2012;109(7):2527-32.
104. Feng N, Han Q, Li J, Wang S, Li H, Yao X, et al. Generation of highly purified neural stem cells from human adipose-derived mesenchymal stem cells by Sox1 activation. Stem Cells and Development. 2014;23(5):515-29.
105. Younsi A, Zheng G, Scherer M, Riemann L, Zhang H, Tail M, et al. Three Growth Factors Induce Proliferation and Differentiation of Neural Precursor Cells In Vitro and Support Cell-Transplantation after Spinal Cord Injury In Vivo. Stem Cells International. 2020;2020:5674921.
106. Denham M, Hasegawa K, Menheniott T, Rollo B, Zhang D, Hough S, et al. Multipotent caudal neural progenitors derived from human pluropotent stem cells that give rise to lineages of the central and peripheral nervous system. Stem Cells. 2015;33(6):1759-70.
107. Hu F, Wang X, Liang G, Lv L, Zhu Y, Sun B, et al. Effects of epidermal growth factor and basic fibroblast growth factor on the proliferation and osteogenic and neural differentiation of adipose-derived stem cells. Cellular Reprogramming. 2013;15(3):224-32.
108. Inui K, Oreffo ROC, Triffitt JT. Effects of beta mercaptoethanol on the proliferation and differentiation of human osteoprogenitor cells. Cell Biology International. 1997;21(7):419-25.
109. He S, Guo Y, Zhang Y, Li Y, Feng C, Li X, et al. Reprogramming somatic cells to cells with neuronal characteristics by defined medium both in vitro and in vivo. Cell Regeneration. 2015;4:12.
110. Denham M, Dottori M. Neural Differentiation of Induced Pluripotent Stem Cells. In: Manfredi G, Kawamata H, editors. Neurodegeneration: Methods and Protocols. Methods in Molecular Biology. Totowa, NJ: Humana Press; 2011. p. 99-110.
111. Andrews S. FastQC: A Quality Control tool for High Throughput Sequence Data. 2010 [Available from: http://www.bioinformatics.babraham.ac.uk/projects/fastqc/.
112. Ward C, To T, Pederson S. ngsReports: An R Package for managing FastQC reports and other NGS related log files. Bioinformatics. 2019.
113. Schubert M, Lindgreen S, Orlando L. AdapterRemoval v2: rapid adapter trimming, identification, and read merging. BMC Research Notes, 12. 2016;9(1):88.
114. Dobin A, Davis CA, Schlesinger F, Drenkow J, Zaleski C, Jha S, et al. STAR: ultrafast universal RNA-seq aligner. Bioinformatics. 2013;29(1):15-21.

115. Liao Y, Smyth GK, Shi W. featureCounts: an efficient general purpose program for assigning sequence reads to genomic features. Bioinformatics. 2013;30(7):923-30.
116. Cunningham F, Achuthan P, Akanni W, Allen J, Amode M R, Armean IM, et al. Ensembl 2019. Nucleic Acids Research. 2018;47(D1):D745-D51.
117. Robinson MD, Oshlack A. A scaling normalization method for differential expression analysis of RNA-seq data. Genome Biology. 2010;11(3):R25.
118. Ritchie ME, Phipson B, Wu D, Hu Y, Law CW, Shi W, et al. limma powers differential expression analyses for RNA-sequencing and microarray studies. Nucleic Acids Research. 2015;43(7):e47.
119. Law CW, Chen Y, Shi W, Smyth GK. voom: precision weights unlock linear model analysis tools for RNA-seq read counts. Genome Biology. 2014;15(2):R29.
120. Kolde R. pheatmap: Pretty Heatmaps. 2019 [R package version 1.0.12:[Available from: https://cran.r-project.org/web/packages/pheatmap/index.html.
121. Ge SX, Jung D. ShinyGO: a graphical enrichment tool for animals and plants. bioRxiv. 2018.
122. Subramanian A, Tamayo P, Mootha VK, Mukherjee S, Ebert BL, Gillette MA, et al. Gene set enrichment analysis: A knowledge-based approach for interpreting genome-wide expression profiles. Proc Natl Acad Sci U S A. 2005;102(43):15545-50.
123. Liberzon A, Subramanian A, Pinchback R, Thorvaldsdóttir H, Tamayo P, Mesirov JP. Molecular signatures database (MSigDB) 3.0. Bioinformatics. 2011;27(12):1739–40.
124. Quality Scores for Next-Generation Sequencing. San Diego, CA, USA: Illumina, Inc.; 2011 [Available from: https://www.illumina.com/documents/products/technotes/technote_Q-Scores.pdf.
125. Conesa A, Madrigal P, Tarazona S, Gomez-Cabrero D, Cervera A, McPherson A, et al. A survey of best practices for RNA-seq data analysis. Genome Biology. 2016;17:13.
126. Sjöstedt E, Zhong W, Fagerberg L, Karlsson M, Mitsios N, Adori C, et al. An atlas of the protein-coding genes in the human, pig, and mouse brain. Science 2020;367(6482).
127. Haslinger A, Schwarz TJ, Covic M, Lie DC. Expression of Sox11 in adult neurogenic niches suggests a stage-specific role in adult neurogenesis. European Journal of Neuroscience. 2009;29(11):2103-14.
128. Zhao C, Deng W, Gage FH. Mechanisms and functional implications of adult neurogenesis. Cell. 2008;132(4):645-60.
129. Louvi A, Artavanis-Tsakonas S. Notch signalling in vertebrate neural development. Nature Reviews Neuroscience. 2006;7(2):93-102.
130. Ables JL, Breunig JJ, Eisch AJ, Rakic P. Not(ch) just development: Notch signalling in the adult brain. Nature Reviews Neuroscience. 2011;12(5):269-83.

131. Hamburger V, Hamilton HL. A series of normal stages in the development of the chick embryo. Journal of Morphology. 1951;88(1):49-92.
132. Glover JC, Boulland J-L, Halasi G, Kasumacic N. Chimeric animal models in human stem cell biology. Institute for Laboratory Animal Research Journal. 2010;51(1):62-73.
133. Guthrie S. Patterning and axon guidance of cranial motor neurons. Nature Reviews Neuroscience. 2007;8(11):859-71.
134. Pochampally RR, Neville BT, Schwarz EJ, Li MM, Prockop DJ. Rat adult stem cells (marrow stromal cells) engraft and differentiate in chick embryos without evidence of cell fusion. Proc Natl Acad Sci U S A. 2004;101(25):9282-5.
135. Sigurjonsson OE, Perreault MC, Egeland T, Glover JC. Adult human hematopoietic stem cells produce neurons efficiently in the regenerating chicken embryo spinal cord. Proc Natl Acad Sci U S A. 2005;102(14):5227-32.
136. Goldstein RS. Transplantation of human embryonic stem cells and derivatives to the chick embryo. In: Turksen K, editor. Human Embryonic Stem Cell Protocols, Methods in Molecular Biology 584: Humana Press; 2010. p. 367-85.
137. Lee G, Kim H, Elkabetz Y, Al Shamy G, Panagiotakos G, Barberi T, et al. Isolation and directed differentiation of neural crest stem cells derived from human embryonic stem cells. Nature Biotechnology. 2007;25(12):1468-75.
138. Jiang X, Gwye Y, McKeown SJ, Bronner-Fraser M, Lutzko C, Lawlor ER. Isolation and characterization of neural crest stem cells derived from in vitro-differentiated human embryonic stem cells. Stem Cells and Development. 2009;18(7):1059-70.
139. Wichterle H, Peljto M, Nedelec S. Xenotransplantation of embryonic stem cell-derived motor neurons into the developing chick spinal cord. In: Audet J, Stanford WL, editors. Stem Cells in Regenerative Medicine: Methods and Protocols. 482: Humana Press; 2009. p. 171-83.
140. Arthur A, Shi S, Zannettino AC, Fujii N, Gronthos S, Koblar SA. Implanted adult human dental pulp stem cells induce endogenous axon guidance. Stem Cells. 2009;27(9):2229-37.
141. Nosrat IV, Smith CA, Mullally P, Olson L, Nosrat CA. Dental pulp cells provide neurotrophic support for dopaminergic neurons and differentiate into neurons in vitro; implications for tissue engineering and repair in the nervous system. European Journal of Neuroscience. 2004;19:2388-98.
142. Nosrat IV, Widenfalk J, Olson L, Nosrat CA. Dental pulp cells produce neurotrophic factors, interact with trigeminal neurons in vitro, and rescue motoneurons after spinal cord injury. Developmental Biology. 2001;238(1):120-32.

143. Lia M, Ransohoff RM. Multiple roles of chemokine CXCL12 in the central nervous system: a migration of immunology to neurobiology. Progressive Neurobiology. 2008;84(2):116-31.
144. Klein RS, Rubin JB. Immune and nervous system CXCL12 and CXCR4: parallel roles in patterning and plasticity. Trends in Immunology. 2004;25(6):306-14.
145. Le Douarin NM. The avian embryo as a model to study the development of the neural crest: a long and still ongoing story. Mechanisms of Development. 2004;121(9):1089-102.
146. Etchevers HC, Dupin E, Le Douarin NM. The diverse neural crest: from embryology to human pathology. Development. 2019;146(5).
147. D'Amico-Martel A, Noden DM. Contributions of placodal and neural crest cells to avian cranial peripheral ganglia. The American Journal of Anatomy. 1983;166:445-68.
148. Boulland JL, Halasi G, Kasumacic N, Glover JC. Xenotransplantation of human stem cells into the chicken embryo. Journal of Visualized Experiments. 2010(41):e2071.
149. Chao MV. Neurotrophins and their receptors: a convergence point for many signalling pathways. Nature Reviews Neuroscience. 2003;4(4):299-309.
150. Winderlich JN, Kremer KL, Koblar SA. Adult human dental pulp stem cells promote blood-brain barrier permeability through vascular endothelial growth factor-a expression. Journal of Cerebral Blood Flow and Metabolism. 2016;36(6):1087-97.
151. Yan X, Qin H, Qu C, Tuan RS, Shi S, Huang GT. iPS cells reprogrammed from human mesenchymal-like stem/progenitor cells of dental tissue origin. Stem Cells and Development. 2010;19(4):469-80.
152. Sancho-Martinez I, Baek SH, Izpisua Belmonte JC. Lineage conversion methodologies meet the reprogramming toolbox. Nature Cell Biology. 2012;14(9):892-9.
153. Vierbuchen T, Wernig M. Molecular roadblocks for cellular reprogramming. Molecular Cell Review. 2012;47(6):827-38.
154. Orkin SH, Hochedlinger K. Chromatin connections to pluripotency and cellular reprogramming. Cell. 2011;145(6):835-50.
155. Szabo E, Rampalli S, Risueno RM, Schnerch A, Mitchell R, Fiebig-Comyn A, et al. Direct conversion of human fibroblasts to multilineage blood progenitors. Nature. 2010;468(7323):521-6.
156. Bar-Nur O, Verheul C, Sommer AG, Brumbaugh J, Schwarz BA, Lipchina I, et al. Lineage conversion induced by pluripotency factors involves transient passage through an iPSC stage. Nature Biotechnology. 2015;33(7):761-8.
157. Maza I, Caspi I, Zviran A, Chomsky E, Rais Y, Viukov S, et al. Transient acquisition of pluripotency during somatic cell transdifferentiation with iPSC reprogramming factors. Nature Biotechnology. 2015;33(7):769-74.

158. Huangfu D, Osafune K, Maehr R, Guo W, Eijkelenboom A, Chen S, et al. Induction of pluripotent stem cells from primary human fibroblasts with only Oct4 and Sox2. Nature Biotechnology. 2008;26(11):1269-75.
159. Shi Y, Desponts C, Do JT, Hahm HS, Scholer HR, Ding S. Induction of pluripotent stem cells from mouse embryonic fibroblasts by Oct4 and Klf4 with small-molecule compounds. Cell Stem Cell. 2008;3(5):568-74.
160. Velychko S, Adachi K, Kim K-P, Hou Y, MacCarthy CM, Wu G, et al. Excluding Oct4 from Yamanaka Cocktail Unleashes the Developmental Potential of iPSCs. Cell Stem Cell. 2019;25(6):737-53.e4.
161. Cho T, Bae JH, Choi HB, Kim SS, McLarnon JG, Suh-Kim H, et al. Human neural stem cells: electrophysiological properties of voltage-gated ion channels. NeuroReport. 2002;13(11):1447-52.
162. Tang F, Dent EW, Kalil K. Spontaneous calcium transients in developing cortical neurons regulate axon outgrowth. The Journal of Neuroscience. 2003;23(3):927-36.
163. Kiraly M, Kadar K, Horvathy DB, Nardai P, Racz GZ, Lacza Z, et al. Integration of neuronally predifferentiated human dental pulp stem cells into rat brain in vivo. Neurochemistry International. 2011;59(3):371-81.
164. Calatayud C, Carola G, Fernandez-Carasa I, Valtorta M, Jimenez-Delgado S, Diaz M, et al. CRISPR/Cas9-mediated generation of a tyrosine hydroxylase reporter iPSC line for live imaging and isolation of dopaminergic neurons. Scientific Reports. 2019;9(1):6811.
165. Untergasser A, Nijveen H, Rao X, Bisseling T, Geurts R, Leunissen JAM. Primer3Plus, an enhanced web interface to Primer3. Nucleic Acids Research. 2007;35(Sup2):W71-4.